POLITECNICO DI MILANO

Department of Civil and Environmental Engineering

EFFECTS OF HYDRAULIC REPEATED LOADS ON THE HYDROMECHNICAL RESPONSE OF AN UNSATURATED SILTY SOIL

Supervisors:

Prof. Cristina Jommi

Prof. Guido Musso

PhD candidate:

Arash Azizi

March 2016

Arash Azizi
Effects of repeated hydraulic loads on the hydromechanical response of an unsaturated silty soil –
e-mail: arashazizi@polimi.it

Effects of repeated hydraulic loads on the hydromechanical response of an unsaturated silty soil

A Thesis
Presented to
The Academic Faculty
by
Arash Azizi
In Partial Fulfillment
of the Requirements for the
Doctorate
in
Civil and Environmental Engineering

March 2016

ABSTRACT

Soils used in earth constructions are mostly unsaturated, and they undergo frequent wetting-drying cycles due to changes in the climatic conditions, particularly at shallow depths. Repeated hydraulic loads are also induced in levees and dykes by changes in the water height, which affect the extent of the unsaturated zone. Changes in water content significantly influence the hydromechanical behaviour of the construction material, which therefore has to be assessed for repeated hydraulic loads. This research work investigated the coupled hydromechanical behaviour of a silt, typically used in the construction of dykes, with the aim of providing a better understanding of the consequences of wetting-drying cycles in the field on the overall response of the material.

The soil was studied in the laboratory by means of a comprehensive series of complementary experimental tests. The first series involved wetting-drying and loading-unloading stress paths applied in suction-controlled oedometer. Irreversible changes in the degree of saturation implied that hysteresis of water retention is induced by changes in the suction and volume of soil samples. A rate form of the water retention curve (WRC) model was proposed to simulate the hysteresis, in which the contact angle was used to express the dependence of the response on non-monotonic changes in suction and void ratio. A constitutive hypo-plastic model was then proposed and coupled with the contact angle-WRC model to account for the coupling between the hydraulic and the mechanical behaviours. The model was then employed to simulate the experimental hydromechanical response observed in laboratory tests.

The second series of experimental tests was performed to study the impact of wetting-drying cycles on microstructural features and hydraulic properties of as-compacted samples. When as-compacted samples were subjected to wetting-drying cycles, fabric changes took place due to interactions between different structural levels even though no significant total volumetric strain occurred. Accordingly, the water retention behaviour detected for such samples was different from the as-compacted one. The new WRC model was proposed accounting for different structure levels and an evolving pore size distribution of the tested materials.

Eventually, the effects of repeated hydraulic loads on the mechanical behaviour of the silt were studied using constant water content triaxial tests. The hydraulic repeated loads changed the soil fabric by forming larger pores, resulting in fundamental changes in their hydromechanical response. The hydraulic repeated

loads increased the compressibility of the soil at low-stress levels. Since samples subjected to repeated hydraulic loads experienced more volumetric contraction during compression, they became slightly denser than the as-compacted one being subjected to the same stress level. Moreover, when such samples subjected to the same suction, their hydraulic state changed with respect to their corresponding water retention curves, where samples subjected to repeated hydraulic loads expelled more water than the as-compacted one, and hence, such samples became stiffer and exhibited higher strength associated with dilative behaviour during subsequent shear loading.

ACKNOWLEDGEMENTS

First and foremost, I would like to acknowledge my supervisor Prof. Cristina Jommi for her constant motivation, encouragement, and support.

I would also like to thank my co-supervisor Prof. Guido Musso for his unlimited support. He always provides me with crucial guidance as well as detailed instructions on my research projects.

I also like to thank Prof. Gabriele Della Vecchia for his helpful advices.

My sincere thanks to Renato, Oronzo and Giampiero and other current members of Geomechanics laboratory of Politecnico di Torino.

I also want to acknowledge the wonderful friends I've made in the over the past three years, Gianluca, Giacomo, Hossein…

Finally, I would like to thank my parents and sibling for their love and encouragement over the years. Most importantly, I want to thank my wife, Niloofar, for her sympathy, her honesty and her love, that helped me to go beyond every problem.

TABLE OF CONTENTS

CHAPTER 3
Water retention model accounting for hysteresis of hydraulic and mechanical drying-wetting cycles

CHAPTER 4
Coupled hydromechanical model for the compression behaviour of unsaturated silty soils

CHAPTER 5

Effect of repeated hydraulic loads on the water retention behaviour and microstructure of a silty soil

CHAPTER 6

Effect of repeated hydraulic loads on the hydromechanical behavoiur of a silty soil

1

INTRODUCTION

1.1 OVERVIEW

It has been generally recognized that saturated soil mechanics is not always the realistic approach to use in many geotechnical engineering applications, whereas unsaturated soils are widely encountered in engineering practice, particularly at shallow depths of the earth. Many structures are commonly constructed in contact with unsaturated soils, such as retaining walls, shallow foundations, dykes and embankments, soil slopes, landfill liners, tunnels, earth dams and etc. These constructions are frequently subjected to drying-wetting cycles due to climate changes, resulted in continuous variation of the soil water content. The hydraulic and mechanical (hydromechanical) beaviours of unsaturated soils are significantly influenced by the variation of water content. Hence, it is essential to study the effect of drying-wetting cycles, which is also referred as “repeated hydraulic loads”, in order to understand the comprehensive description of the unsaturated soil behaviour.

Despite ample existence of soils at the unsaturated condition, unsaturated soil mechanics is a relatively new area of study, and only in recent years, many of the theoretical derivations in this discipline have become thoroughly and readily

available to engineers. One of the reasons for the lack of research in unsaturated soil is probably due to the fact that the laboratory and field testing of unsaturated soil has proven to be relatively costly, time-consuming, and difficult to conduct.

In addition, considerable attention has been paid to develop models that rationalize the constitutive behaviour of unsaturated soil. Previously proposed models incorporated many features of unsaturated soil behaviour. However, there are still some rooms for model enhancements, further elaboration, and an inclusion of other features of unsaturated soils.

The present dissertation work was motivated by these research needs. As a result, experimental program and their thorough analysis in addition to the enhancement of existing constitutive models that provide a good representation of unsaturated soil behaviour were organized in order to investigate some aspect of unsaturated soil mechanics, i.e. hysteresis of hydraulic behaviour, coupling hydromechanical behaviour and effects of drying-wetting cycles on unsaturated soil responses.

1.2 PROBLEM STATEMENT

Many destructive geotechnical and geo-environmental problems in engineering practice have been reported in past years, involving unsaturated soils where civil infrastructures were constructed on or in soils above the groundwater table. Some examples of such problems can be found in the constructions of dykes and embankments or earth dams, earth retaining structures, slope stability and landslides, excavations, etc. Expansive clays, collapsible soils and residual soils are known as problematic types of unsaturated soils, responsible for many geohazards such as landslides. These landslides may be triggered by the shrinkage and swelling of unsaturated soils, caused by the continuous variation of the soil water content. Therefore, many of the aforementioned problems require the comprehension of the hydraulic relationship between soil water content and matric suction as well as the volumetric behaviour, yielding and shear strength.

It is essential to understand various aspects of unsaturated soils and predict its behaviour using the proper constitutive models in order to reduce the damage caused by geohazards and prevent them from happening.

Previously proposed models tackled many of these features but they are not complete regarding the fact that the hysteresis of water retention, water content variation and its effect on hydromechanical behaviour have not been thoroughly detected, and moreover, the majority of these models provide no information on the unsaturated soil behaviour under repeated loadings.

1.3 BACKGROUND

The main difference between saturated and unsaturated soils resulted from the existence of pore air and interactions of pore air and pore water. The matric suction is negative pore pressure induced by the difference between the air pressure and water pressure within the soil mass, which plays a complex role in unsaturated soil behaviour. This complexity may result from the fact that suction generates inter-particle forces normal to particle contacts, but pore pressures generate isotropic stresses around soil particles.

The essential hydraulic peculiarity of unsaturated soil is the relationship between suction and the amount of water stored in the soil, known as a water retention curve. Early formulations of water retention curve (WRC) models defined a unique relationship between the stored water and suction, but further experimental results showed that the water retention behaviour is different along wetting and drying paths. The hysteretic nature of water retention is known as hydraulic hysteresis. Many researchers have studied the water retention, and many models have been proposed to reproduce this hysteresis behaviour. In addition, many experimental results showed the water retention behaviour is also influenced by mechanical properties, e.g. the initial density or applied net stress (Vanapalli et al., 1999; Gallipoli et al., 2003b; Tarantino, 2009).

The mechanical properties of the unsaturated soil, such as volumetric behaviour, yielding, compressibility and shear strength, are extremely influenced by suction. One of the distinct features of the volumetric behaviour of unsaturated soil is the wetting-induced collapse potential. The shrinkage or swelling behaviour of unsaturated soil during wetting has been reported to depend on the initial dry density and confining stress (Alonso et al., 1995; Sivakumar et al., 2006). The experimental results showed that expansive clay has been experienced irreversible accumulation of volumetric strain when subjected to the cycles of drying-wetting. This irreversible volumetric change was reported to be a function of the history of compaction pressure and the subsequent variation of net stress and suction (Alonso et al., 1995; Sharma, 1998). The suction increases the preconsolidation stress and the shear strength as the soil becomes stiffer. However, the compressibility of unsaturated soil is believed not to be only dependent on suction but also on compaction history, wetting-induced change of fabric and hydraulic history.

Further experimental results showed the effect of hydraulic history and hydraulic hysteresis on the mechanical behaviour of unsaturated soil. It is commonly recognised the hydromechanical behaviour of unsaturated soil are coupled. Many experimental results were presented, studying the effect of drying-wetting cycles on its isotropic compression behaviour (e.g. Sharma, 1998; Barrera et al., 2002;

Wheeler et al, 2003b; Sivakumar et al., 2006; Tarantino 2009; Sun et al., 2007). Although the hydromechanical behaviour of unsaturated soil has been widely studied in the literature, there is still a lack of water retention experimental data and the hydromechanical test results due to the long time required for testing of unsaturated soils.

Most of existing proposed constitutive models for unsaturated soil have been developed in the elasto-plastic framework. The pioneer framework for unsaturated soil was introduced by Basic Barcelona Model (BBM). Alonso et al. (1990) proposed the first critical state constitutive model using two independent stress variables. The net stress and matric suction were adopted to reproduce the unsaturated behaviour in a three-dimensional stress space. Although the model provided no data on hydraulic behaviour but it was able to account for most mechanical features of unsaturated soil behaviour. The same framework and stress variables were subsequently adopted in numbers of unsaturated constitutive models (Wheeler and Sivakumar 1995, Cui and Delage 1996, Loret and Khalili 2002).

Jommi (2000) introduced the average soil skeleton stress by adopting the Bishop effective stress and substituting the Bishop parameter with the degree of saturation. Incorporation of the degree of saturation as an internal variable allowed the model accounting the hydraulic state of the unsaturated soil. The same effective stress variables were used by numerous researchers (e.g. Nuth and Laloui 2008; Romero and Jommi, 2008; Buscarnera and Nova, 2009; Della Vecchia et al., 2012).

A few models were proposed to couple hydraulic hysteresis and mechanical behaviour. They were mostly proposed accounting for both plastic volumetric strain and irreversible change of the degree of saturation considering as hardening laws for both hydraulic and mechanical behaviour. Consequently, the coupling between hydraulic hysteresis and mechanical behaviour and their interactions could be captured (e.g. Vaunat, 2000; Wheeler et al., 2003; Tamagnini, 2004).

Since both air and water are present in the pores of the unsaturated soil, comprehension of soil mechanics at the microscopic level is believed to be a valuable tool for studying the hydromechaical behaviour of unsaturated soils. Many attentions have been paid to study the microstructure of unsaturated soils since efficient experimental tools and techniques were introduced providing high resolution and good interpretation of the size, shape, arrangement and distribution of particles and aggregates (e.g. Delage and Lefebvre, 1984; Al-Mukhtar et al., 1996; Sivakumar and Wheeler, 2000; Simms and Yanful, 2002; Cui et al., 2002; Cuisinier and Laloui, 2004; Koliji et al., 2006; Romero and Simms, 2008; Koliji et al., 2010; Casini et al., 2012). Some advanced approaches was introduced accounting for microstructural features of unsaturated soils regarding the hydraulic

and mechanical behaviours, in which coupling functions between the different structural levels were implemented (e.g., Alonso et al. 1999; Loret and Khalili 2000; Alonso et al. 2005; Romero et al., 2011; and Della Vecchia et al. 2012 and 2015).

Various robust alternative frameworks have been proposed to the classical elastic-plastic framework for constitutive modelling of saturated soil, such as hyperplasticity, hypoplasticity, bounding surface and etc. However, a few numbers of these frameworks were extended to model the unsaturated state of the soil (e.g. Sánchez et al. 2005; Wong 2010; Mašín and Khalili 2008). In general, the excessive nonlinearity of the behaviour and irreversible change of hydromechanical properties of unsaturated soil observed in experimental studies, are difficult to be captured using the models conceived in the framework of elastoplasticity and this may be more easily tackled by models conceived in alternative frameworks.

1.4 OBJECTIVE

The experimental studies and development of constitutive models in unsaturated soil mechanics have mostly focused on clays and sands only. The main objective of the current research was to investigate the effect of repeated hydraulic loads on unsaturated silt behaviour, which is a typical material used in dykes and embankments all over the world and propose a relevant hydraulic and mechanical constitutive models being able to reproduce the observed experimental results. The principal objectives of the present research included:

1) Study the hydraulic behaviour and irreversible change of the degree of saturation due to repeated loadings, including the hydraulic drying-wetting cycles (variation of suction) and loading-unloading cycles (mechanical drying-wetting).
2) Study the coupling between hydromechanical behaviour in unsaturated silt.
3) Develop a new constitutive model for simulating the hydromechanical behaviour of unsaturated silt incorporating coupling hydromechanical mechanism, which allows the model to describe the hysteresis observed in hydraulic behaviour.
4) Study the influence of repeated loads on the microstructure and water retention properties of the silty soil.

5) Develop a new hydraulic model considering the microstructure features of unsaturated silt, which allows reproducing the effect of repeated hydraulic loads on microstructure, and in turn on water retention behaviour.
6) Provide new information on the effects of repeated hydraulic loads on the mechanical and shearing behaviour of unsaturated silt.

1.5 OUTLINE OF THE DISSERTATION

This dissertation is presented in seven chapters, as briefly described in this session.

The first chapter presents the overview of the research program and the general description of the layout of this thesis. The relevant existing problems in unsaturated soil are mentioned and the objectives of the present research program are listed. The background of experimental studies and constitutive modeling of unsaturated soils are briefly described.

Next, the layouts of the apparatuses and experimental techniques used in the experimental work are discussed in chapter 2. First, the properties of tested material are displayed and sample preparation techniques are introduced. Next, the techniques used for measuring and controlling the suction, are explained. Then experimental methods used to study the microstructure (ESEM and MIP) are described. Moreover, the suction controlled oedometer and triaxial apparatuses located in the laboratory of Politecnico di Torino, are described. Lastly, the calibrations techniques used and the considerations paid to minimize the experimental errors and to obtain more reliable experimental results are explained.

Chapter 3 presents an extensive literature review on the existing models of water retention, incorporating the mechanical aspect and hysteretic behaviour. After the literature review, the following session discusses the physical mechanisms behind the hysteresis of WRC, and the physical parameter is introduced, which is selected to account for hysteresis of water retention behaviour. Then a simple rate form model based on contact angle-dependent water retention model is proposed to simulate the hysteresis in water retention behaviour. Water retention data covering clayey silt used to evaluate the performance of the model. In the experimental work, the laboratory testing was carried out to generate the experimental database. Water retention tests were conducted to obtain series of WRC with hysteresis under different stress path history (drying-wetting and loading-unloading paths).

In chapter 4, the constitutive modeling of soil in a hypoplastic framework is introduced and the previous hypoplastic models are reviewed. The clay

hypoplastic model is presented. The new constitutive hypoplastic model is then proposed for unsaturated soils accounting for the coupling effects between the hydraulic and mechanical behaviours of unsaturated soils. The proposed model fully incorporates the hydraulic state of the soil by means of coupling with the hysteretic WRC model introduced in Chapter 3. The proposed hypoplastic model is validated comparing the model predictions to the results of the tests performed in this research.

Chapter 5 presents experimental results of microstructure study on the behaviour of unsaturated silt. The effect of repeated hydraulic loads on the microstructure is investigated and water retention behaviour of the sample subjected to repeated hydraulic loads are detected. The new approach is proposed accounting the evolution of microstructure due to drying-wetting cycles. This allows reproducing the effect of these repeated hydraulic loads on water retention behaviour.

In chapter 6, the triaxial test results are presented. These tests were carried out on as-compacted samples and samples subjected to cycles of drying-wetting. The effect of these repeated hydraulic loads on the hydromechanical behaviour of unsaturated silt is studied. The compressibility and shearing behaviour are influenced by these repeated hydraulic loads as well as the hydraulic behaviour.

Finally, the summary of conclusions is presented in chapter 7, and the recommendations for future work are proposed.

References

[1] Al-Mukhtar, M., Belanteur, N., Tessier, D., Vanapalli, S.K., 1996. The fabric of a clay soil under controlled mechanical and hydraulic stress states. Applied Clay Science 11, 99–115.

[2] Alonso, E.E. , A. Gens & A. Josa 1990. A constitutive model for partially saturated soils. Géotechnique, 40(3): 405-430.

[3] Alonso, E. E., Lloret, A., Gens, A. & Yang, D. Q. (1995). Experimental behaviour of highly expansive double-structure clay. Proc. of 1st International Conference on Unsaturated Soils, Paris, Vol. 1: 11-18.

[4] Alonso, E. E., Romero, E., Hoffmann, C., & García-Escudero, E. (2005). Expansive bentonite–sand mixtures in cyclic controlled-suction drying and wetting. Engineering Geology 81: 213–226.

[5] Alonso, E. E., Vaunat, J. & Gens, A. (1999). Modelling the mechanical behaviour of expansive clays. Engineering Geology, 54: 173-183.

[6] Buscarnera G, Nova R. An elastoplastic strain hardening model for soil allowing for hydraulic bonding-debonding effects. Int J Numer Anal Methods Geomech 2009;33:1055–86.

[7] Casini, F., Vaunat, J., Romero, E., Desideri, A., 2012. Consequences on water retention properties of double-porosity features in a compacted silt. Acta Geotechnica 7 (2), 139–150.

[8] Cui, Y. J. & Delage, P. (1996). Yielding and plastic behaviour of an unsaturated compacted silt. Géotechnique 46, No.2: 291-311.

[9] Cui, Y.J., Loiseau, C., Delage, P., 2002. Microstructure changes of a confined swelling soil due to suction controlled hydration. In: Jucá, J.F.T., de Campos, T.M.P., Marinho, F.A.M. (Eds.), Unsaturated Soils, 2. A.A. Balkema Publishers, Lisse, pp. 593–598.

[10] Cuisinier, O., Laloui, L., 2004. Fabric evolution during hydromechanical loading of a compacted silt. International Journal for Numerical and Analytical Methods in Geomechanics 28 (6), 483 499.

[11] Delage, P., Lefebvre, G., 1984. Study of the structure of a sensitive Champlain clay and its evolution during consolidation. Canadian Geotechnical Journal 21, 21–35.

[12] Della Vecchia G. Coupled hydro-mechanical behaviour of compacted clayey soil. PhD Thesis, Politecnico diMilano 2009.

[13] Della Vecchia, G., A.C. Dieudonne, C. Jommi, R. Charlier, 2015. Accounting for evolving pore size distribution in water retention models for compacted clays. International Journal for Numerical and Analytical Methods in Geomechanics 39 (7), 702-723.

[14] Della Vecchia G, Jommi C, Romero E. A fully coupled elastic–plastic hydromechanical model for compacted soils accounting for clay activity. International Journal for Numerical and Analytical Methods in Geomechanics 2013; 37 (5):503–535.

[15] Gallipoli, D., Wheeler, S. & Karstunen, M. (2003b). Modelling the variation of degree of saturation in a deformable unsaturated soil. Géotechnique 53, No. 1, 105–112.

[16] Gens, A. & Alonso, E. E. (1992). A framework for the behaviour of unsaturated expansive clays. Can. Geotech. J. 29: 1013-1032.

[17] Gens A, Sánchez M & Sheng D. 2006. On constitutive modeling of unsaturated soils', Acta Geotechnica, 1: 137-147.

[18] Griffiths, F.J., Joshi, R.C., 1989. Changes in pore size distribution due to consolidation of clays. Geotechnique 39 (1), 159–167.

[19] Jommi, C. (2000). Remarks on the constitutive modelling of unsaturated soils. In Experimental evidence and theoretical approaches in unsaturated soils: Proceedings of an international workshop (eds A. Tarantino and C. Mancuso), pp. 139–153. Rotterdam: A. A. Balkema.

[20] Khalili, N., Habte, M. A. & Zargarbashi, S. (2008). A fully coupled flow deformation model for cyclic analysis of unsaturated soils including hydraulic and mechanical hysteresis. Comput. Geotech. 35, No. 6, 872–889.

[21] Koliji, A., Laloui, L., Cuisinier, O., Vulliet, L., 2006. Suction induced effects on the fabric of a structured soil. Transport in Porous Media 64, 261–278.

[22] Koliji, A., Vulliet, L., Laloui, L., 2010. Structural characterization of unsaturated aggregated soil. Canadian Geotechnical Journal 47, 297–311. http://dx.doi.org/10.1139/ T09-089.

[23] Mašín D, Khalili N. A hypoplastic model for mechanical response of unsaturated soils. International Journal for Numerical and Analytical Methods in Geomechanics 2008; 32:1903–1926.

[24] Nuth, M. & Laloui, L. (2008). Advances in modelling hysteretic water retention curve in deformable soils. Comput. Geotech. 35, No. 6, 835–844.

[25] Nuth M, Laloui L. Effective stress concept in unsaturated soils: clarification and validation of a unified framework. Int J Numer Anal Meth Geomech 2008;32(7):771 801.

[26] Romero, E., Della Vecchia, G. & Jommi, C. (2011). An insight into the water retention properties of compacted clayey soils. Géotechnique 61.

[27] Romero E, Jommi C. An insight into the role of hydraulic history on the volume changes of anisotropic clayey soils. Water Resources Research 2008; 44:W12412:1–W12412:16.

[28] Romero, E., Simms, P., 2008. Microstructure investigation in unsaturated soils: a review with special attention to contribution of mercury intrusion porosimetry and environmental scanning electron microscopy. Geotechnical and Geological Engineering 26 (6), 705–727.

[29] Sánchez M, Gens A, Guimaraes L, Olivella S. A double structure generalized plasticity model for expansive materials. International Journal for Numerical and Analytical Methods in Geomechanics 2005; 29:751‐787.

[30] Sharma, R. S. (1998). Mechanical behaviour of unsaturated highly expansive clays. PhD Thesis, Oxford University.

[31] Sheng D, Fredlund DG, Gens A. A new modelling approach for unsaturated soils using independent stress variables. Can Geotech J 2008;45(4):511–34.

[32] Sivakumar, V., Tan, W. C., Murray, E. J. & McKinley, J. D. (2006). Wetting, drying and compression characteristics of compacted clay. Géotechnique 56, No. 1: 57– 62.

[33] Sivakumar, V., Wheeler, S., 2000. Influence of compaction procedure on the mechanical behaviour of an unsaturated compacted clay. Part 1: Wetting and isotropic compression. Geotechnique 50 (4), 359–368.

[34] Sun DA, Cui HB, Matsuoka H, Sheng D. A three-dimensional elastoplastic model for unsaturated compacted soils with hydraulic hysteresis. Soils and Foundation 2007;47(2):253–64.

[35] Tamagnini, R. An extended Cam-clay model for unsaturated soils with hydraulic Hysteresis. Géotechnique, 2004, 54(3): 223-228.

[36] Tarantino, A. (2009). A water retention model for deformable soils. Géotechnique 59, No. 9, 751–762.

[37] Vanapalli, S. K., Fredlund, D. G. & Pufhal, D. E. (1999). The influence of soil structure and stress history on the soil-water characteristics of a compacted till. Géotechnique 49, No. 2, 143–159.

[38] Vaunat J, Jommi C, Gens A. A strategy for numerical analysis of the transition between saturated and unsaturated flow conditions. In Proc. NUMOG VI, Pietruszczak S, Pande G (eds.). AA. Balkema: Rotterdam, 1997; 297–302.

[39] Vaunat, J., Romero, E., and Jommi, C. (2000). An elastoplastic hydro-mechanical model for unsaturated soils. proc. int. workshop on unsaturated soils. In Tarantino, A. and Mancuso, C., editors, Experimental Evidence and Theoretical Approaches in Unsaturated Soils, pages 21–38, Trento, Italy. AA. Balkema, Rotterdam. 5.1

[40] Wheeler, S. J. & Karube, D. (1996). Constitutive modelling. Proc. 1st Int. Conf. Unsat. Soils, Paris, Vol.3: 1323-1356.

[41] Wheeler SJ, Sharma RS, Buisson MSR. Coupling of hydraulic hysteresis and stress-strain behaviour in unsaturated soils. Géotechnique 2003;53(1): 41–54.

[42] Wheeler, S. J. & Sivakumar, V. (1995). An elasto-plastic critical state framework for unsaturated soil. Géotechnique 45: 35-53.

[43] Wong H, Morvan M, Branque D. A 13-parameter model for unsaturated soil based on a bounding surface plasticity. Journal of Rock Mechanics and Geotechnical Engineering 2010; 2(2):135‑142.

[44] Zhou, A. (2013). A contact angle-dependent hysteresis model for soil-water retention behaviour Computer and Geotechnics, 49, 36 – 42.

2

EXPERIMENTAL TECHNIQUES AND APPARATUSES

2.1 Tested material and sample preparation

The material used in this research was used to construct dykes on the flood plain of the Po River at Viadana, located in the north of Italy, as shown in Figure 2.1. The material was taken at depths between ground level and 1 meter. The tested material, which is placed in sub-soils between the dyke and the river, is above ground water level, but continuously subjected to variation of moist content due to change of relative humidity and ground water level (seasonal variation).

2.1.1 Viadana silt

The soil used in the experimental study is mostly silt with poor fractions of sand and clay, named as “Viadana silt”. The Viadana silt was first air-dried and mechanically grinded, and then, the sand fraction of the original soil (19.1%) was removed by passing the soil through a sieve #200, because the investigation on behaviour of silty soil was of interest in the present work.

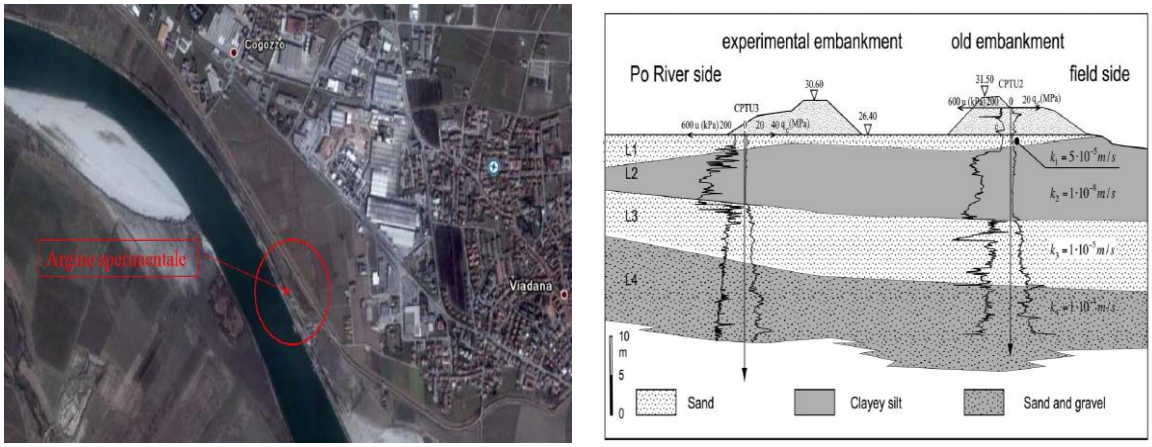

(a) (b)

Figure 2.1. a) Map of the Po River course and Viadana site b) Vertical section crossing the embankments and the foundation layers (Calabresi et al., 2013).

The soil was characterized by performing tests to obtain Atterberg limits, grain specific gravity and grain size distribution. The grain size distribution of the soil before and after removing the sand fraction is presented in Figure 2.2. The grain size distribution of the tested material showed that the silt and clay fractions are 79.6% and 20.4%, respectively. The grain specific gravity at 20℃ was G_s=2.735, obtained according to ASTM B854. The activity (A) of the tested material was measured to be 0.4, which indicates an inactive soil with typical Kaolinite behaviour.

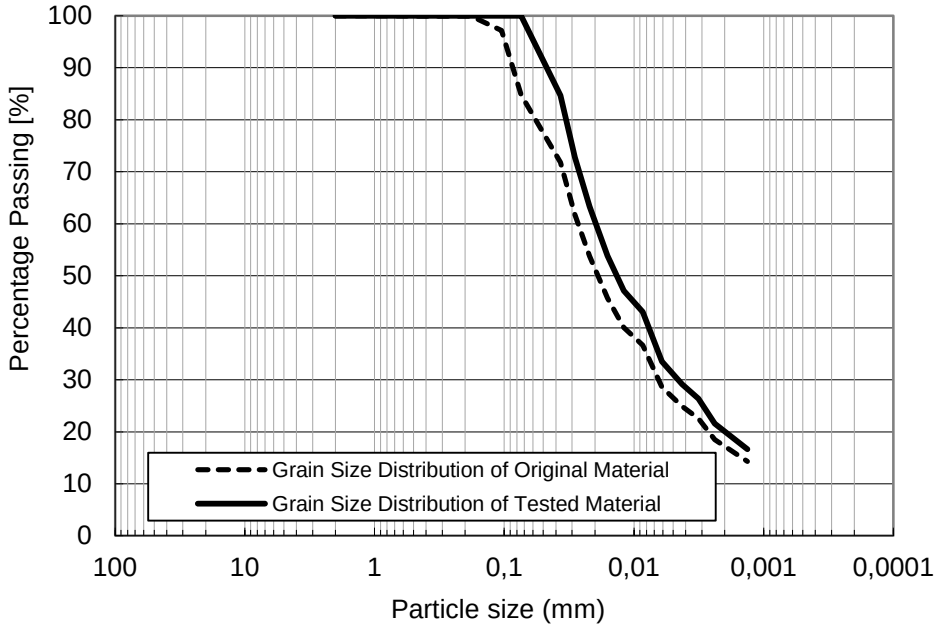

Figure 2.2. Grain size distributions of the original and tested material.

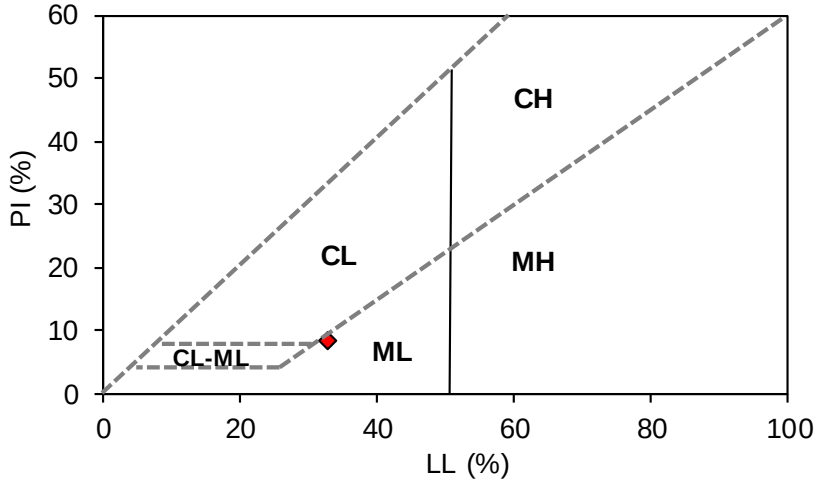

Figure 2.3. Plasticity chart and the characterization of Viadana silt.

Table 2.1. Properties of the tested material.

Variables	Value
LL	32.6
PL	24.3
PI	8.3
G_s	2.735
%d < 2μm	20.4
$CaCo_3$ content	17.3

The Atterberg limits of the Viadana silt were found to be 32.6% for liquid limit (LL), 40.9% for plastic limit (PL), and hence, the plastic index (PI) was 8.3%. It can be classified as low plasticity silt (ML) according to ASTM D2487, as shown in plastic chart of Figure 2.3. The properties of the tested soil are listed in Table 2.1.

2.1.2 Static compaction technique

The dry density and water content of the samples were selected corresponding to the points represented in the proctor plane in Figure 2.4. The main compaction curve was obtained by Vassallo (2003) for the same material, whereas two hypothetical curves are also plotted for lower and higher compaction energy. The samples were mostly compacted at dry side of optimum proctor (Tx referred to all triaxial tests and WR referred to water retention tests), having a dry density very close to the proctor optimum one. These samples may generate a soil fabric analogous to in-situ compacted material used to construct the dykes. Moreover,

they show less tendency of wetting-induced collapse, resulted in preventing an undesirable accumulation of deformation when they are subjected to drying-wetting cycles. However, a few samples were prepared at low dry densities and compacted at water contents corresponding to dry side of the proctor curve (Oe-LU referred to oedometer loading-unloading test, Oe-DW referred to oedometer drying-wetting test, and Oe-LU-CW referred to loading-unloading oedometer test at constant water content) to study the collapse and compressibility of loose samples.

The required amount of dry soil powder was initially sprayed and hand-mixed with a specific amount of demineralized water in order to achieve the target dry density and water content. It was sealed in a plastic bag and placed in a humid container for 48 hours allowing the water content equilibration. It was then placed in rigid hermetic mould. Figure 2.5 (a) and (b) show the cylindrical moulds used for preparation of compacted samples of oedometer and triaxial tests, respectively. The axial force was gradually applied to the soil mass, confined in the mould, using Wykeham Farrance loading framework (Figure 2.6) until the specified volume was achieved under controlled water content. The compaction was performed, in which the axial displacement was controlled, at a low rate of 0.15 mm/min to ensure good homogeneity. The size of the samples prepared for oedometer tests was 50 mm of diameter and 20 mm of height and for triaxial tests was 76 mm of height, 38 mm of diameter. The samples were then removed and covered in plastic bags and held in a sealed humid container for 24 hours.

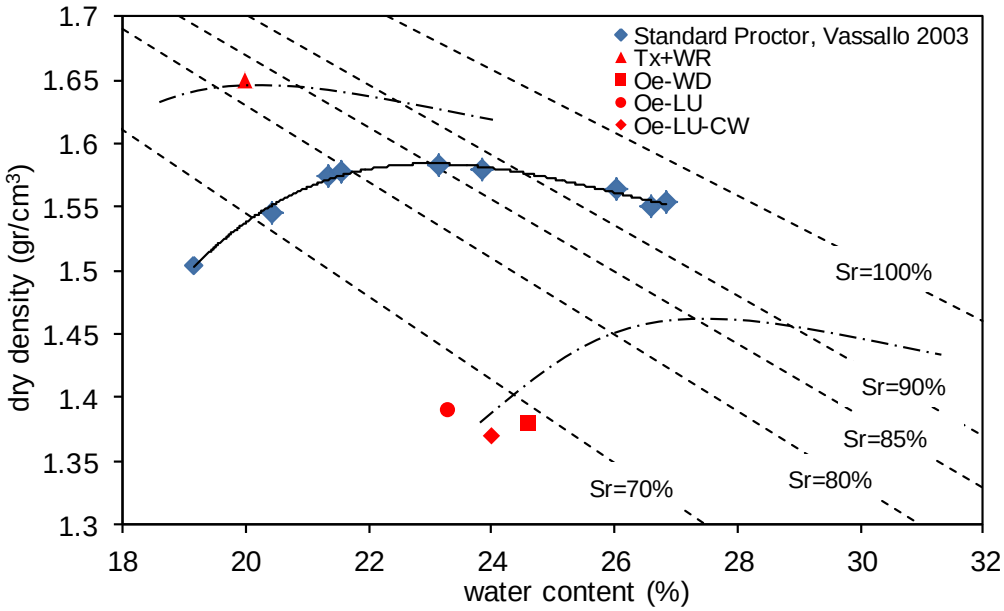

Figure 2.4. Proctor plane and the position of the as-compacted samples.

(a) (b)

Figure 2.5. Hermetic mould for preparation of compacted sample a) Oedometer test b) Triaxial test.

Figure 2.6. Wykeham Farrance loading frame.

The dimensions of every sample were directly measured by a caliper for the height and by a PI-tape gauge for the diameter. The as-compacted properties of the prepared samples are listed in the Table 2.2.

Table 2.2. Properties of as-compacted samples.

Type of tests	γ_d (gr/cm^3)	e_0	w_0	Sr_0
Tx and WR	1.65	0.657	20	0.83
Oe-LU	1.392	0.965	23.3	0.66
Oe-DW	1.381	0.98	24.6	0.69
Oe-LU-CW	1.37	0.996	24	0.659

2.1.3 Drying-wetting cyclic sample

In order to study the effect of repeated loads on the hydromechanical behaviour of the unsaturated soil, 15 as-compacted samples were selected and subjected to cycles of drying-wetting. These samples are named as “D/W cyclic” in this dissertation. These samples were subjected to 3 or 6 cycles, which are denoted as “3 D/W” and “6 D/W” samples in the following, respectively.

In former experimental works, the soil samples have been commonly subjected to drying-wetting cycles by changing the suction acting within soil samples (e.g. Alonso et al., 2005; Lloret et al., 2003; Cuisinier and Masrouri, 2005; Nowamooz andMasrouri, 2008), while the samples were placed in the relevant suction-controlled apparatuses. In the present research program, a different technique was used in which the samples were subjected to cycles of drying-wetting before the positioning in suction-controlled apparatuses. After being subjected to the cycles, the samples were then placed in oedometer or triaxial apparatus for the following tests. The size of the sample tested by oedometer and triaxial was different. Therefore, similar techniques but different equipment were employed to apply the repeated hydraulic loads, which are explained in the following chapters, see details in chapter 5 for oedometer samples and chapter 6 for triaxial samples.
The repeated hydraulic repeated loads were applied by means of controlling the moisture content of samples. The weight of the samples was sequentially monitored to track the water volume of the samples, as represented for a triaxial sample in Figure 2.7. It shows that the water volume of the sample decreased from 28.5 to 0.96 cm^3 during drying (Figure 2.7 (a)), whereas the initial water volume (28.5 cm^3) was recovered during wetting (Figure 2.7 (b)).

2.2 Techniques for controlling and measuring suction

It is essential to understand the theoretical definition of suction before discussing the techniques used for controlling and measuring suction. Total soil suction is composed of two components: matric component and osmotic component.

The osmotic suction is related to the existence of dissolved salts in the pore water present in unsaturated soil. The osmotic suction can affect the mechanical behaviour of unsaturated soil if the salt content in the soil changes. However, the chemistry of the pore water remains unchanged in most geotechnical application and then osmotic suction appears not to be sensitive to changes in soil water content, particularly in the soil with macrostructure prevailed. In this dissertation, the matric component principally involves in following discussions.

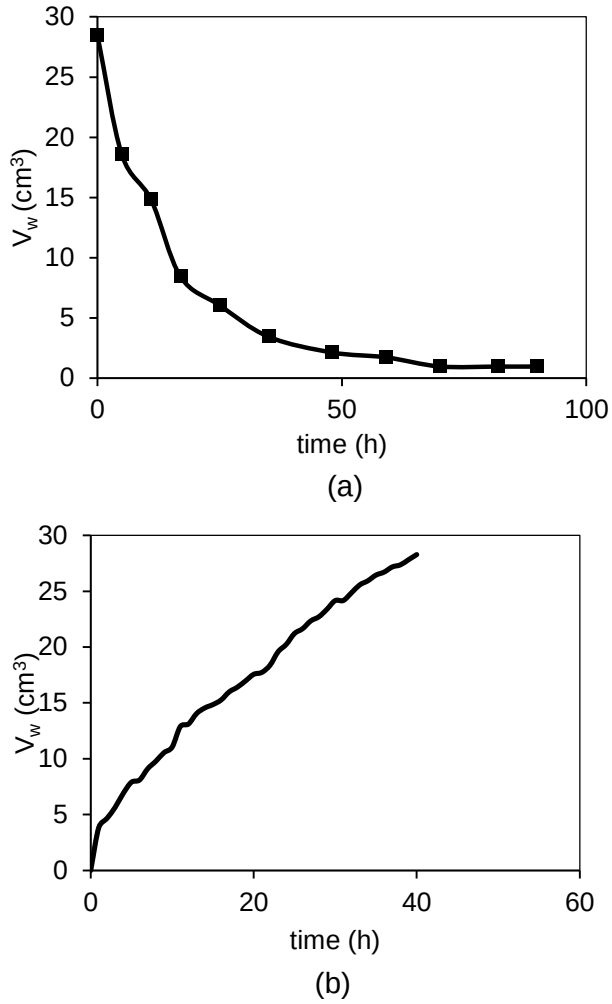

Figure 2.7. Water volume of sample subjected to drying-wetting path (triaxial sample): a) wetting path b) drying path.

The matric suction is related to the capillary action of water associated with air-water menisci in unsaturated soil pores. The interaction between soil particle, air and water generates the contractile skin, forms as a curve meniscus due to the surface tension (σ) and the difference between pressures of air and water along contractile skin. The matric suction (s) is then defined as the difference between the air pressure (u_a) and the water pressure (u_a), and can be defined by the Laplace equation,

$$s = u_a - u_w = \frac{2\sigma\, cos\theta}{R} \tag{2.1}$$

where θ and R are contact angle and pore radius, respectively.

The measurement and control of the matric suction is an important issue in experimental study of unsaturated soil. In past few years, numbers of techniques have been discussed in the literatures. The axis translation, humidity control technique and filter paper methods were used in the present experimental work. These methods are briefly introduced in the following.

2.2.1 Axis-translation technique

The axis translation is the most common method widely used in in experimental study of unsaturated soil due to its easy measurement and control of suction. This technique was developed and employed by Hilf (1956). The method is applied by controlling the total stress, pore water pressure and pore air pressure independently. The total stress and the pore air pressure increase at the same amount caused that the net stress (σ_{tot}-u_a) remains constant. The target suction is imposed by controlling the difference between the applied air pressure and water pressure. In the present experimental work, the different suction steps were imposed by applying different water gauge pressures while the air gauge pressure was kept constant. On the other hand, the matric suction was measured by continuous measurement of water pressure while the air pressure remained unchanged.

In principle, the axis translation controls separately the pressure of air and water phases in the soil. It can be understand that the rise in the air pressure allows increasing the water pressure, implying that the positive pressure prevents cavitation in water drainage system. The water within the soil sample and the water in the measuring system are connected by high air entry value (HAEV) ceramic discs. These ceramic discs with air entry value greater than the maximum applied matric suction are used to avoid free passage of the air into the water lines. Hence, the maximum air entry value of the ceramic disc as well as the maximum value of the cell pressure limits the maximum value of the suction that can be applied using the axis translation technique. In this study, the axis translation was used for suction values smaller than 400 kPa. However, this technique has been frequently used for the suction values up to 1.5 MPa (e.g. Sivakumar, 1993; Romero, 1999).

The selection of the relevant HAEV ceramic disc is important in order to minimize the required time for equalisation of the pore water pressure since the higher the entry value, the lower the pressure ability of porous stone. Ceramic discs with air entry value of 0.1, 0.55 and 1.5 MPa were frequently used in oedometer and triaxal tests depending on the maximum applied or measured matric suction. The time required for equalisation of water content, observed in the water retention tests performed in the oedometer apparatus, is plotted in Figure 2.8. The axis translation technique was employed for three steps of suction increment.

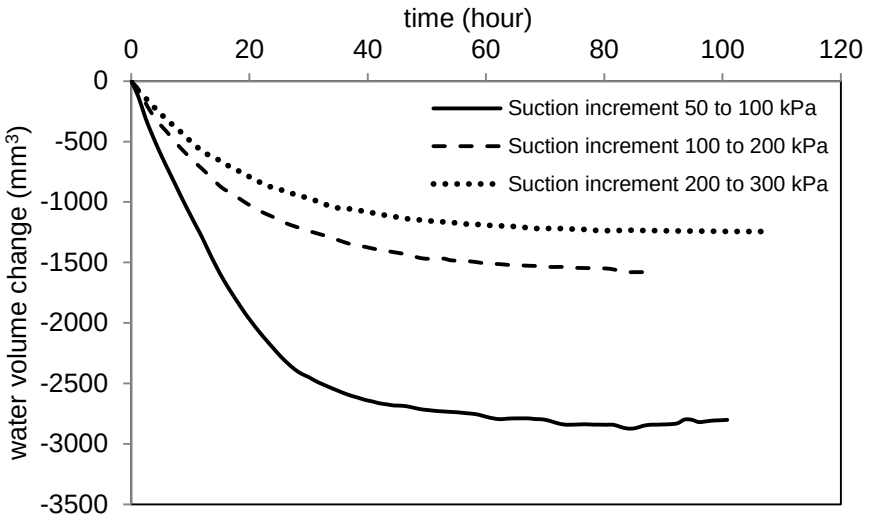

Figure 2.8. Equalization of the water content within the soil mass using the axis translation technique (Oe-WR test).

2.2.2 Vapour equilibrium technique

The control of suction using vapour equilibrium technique involves controlling the relative humidity of the atmosphere surrounding the soil sample. This method first used in the experimental study of unsaturated soil by Esteban & Saez (1988).

In order to impose the desired suction using the vapour equilibrium technique, the oedometer samples were placed in a closed desiccator, as shown in Figure 2.9 (a) and (b). The samples were supported by a rigid wire above the saturated salt solution. Relative humidity of the air inside a closed desiccator was maintained constant through contact with salt solutions, and under isothermal equilibrium conditions, water vapour in the chamber came into equilibrium with the salt solution. Water exchanges occurred by vapour transfer between the solution and the sample, and the given suction was applied to the sample when vapour equilibrium was achieved. The relative humidity and the corresponding imposed suction depend on concentration and molality of the solutions. Moreover, the activity of the solutions is very sensitive to variation of temperature. This means that the temperature must be strictly controlled during testing.

Therefore, different saturated salt solutions were used to control the relative humidity (RH) of air, and in turn imposed suction in the closed desiccator. The RH and suction corresponding to the saturated solutions are listed in Table 2.4, as reported by Romero (2001). The saturated solutions used in the experiments are marked by red boxes.

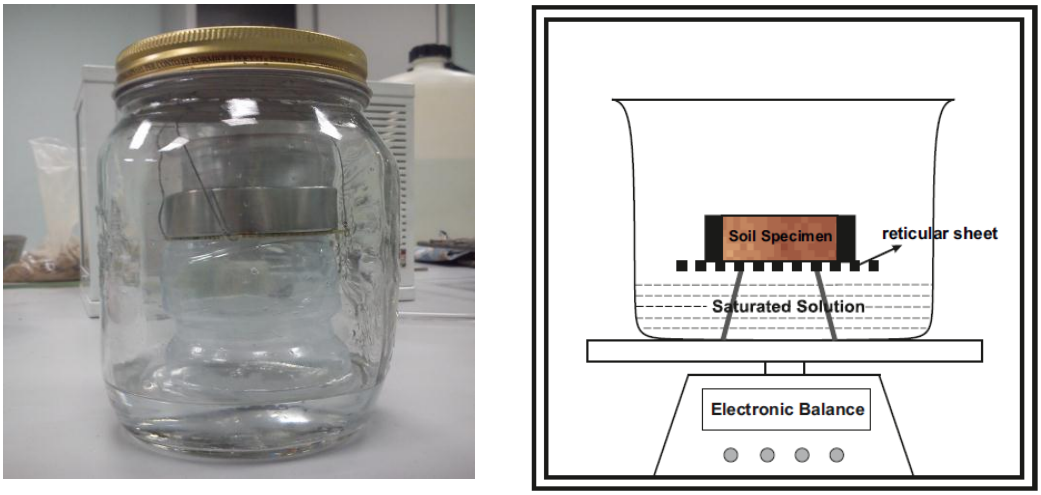

(a) (b)

Figure 2.9. a) Vapour equilibrium equipment b) schematic section of the technique.

Table 2.3. Salt solutions and corresponding suction (Reported by Romero, 2001)

Compound	T (°C)	A (%)	B (K)	u_v/u_{vo}(%) a 25 °C	ψ (MPa) a 25 °C	Solubility (g/100 g H_2O) 30 °C
$NaOH·H_2O$	15-60	5.48	27	6	386	113
$LiBr·2H_2O$	10-30	0.23	996	6	386	193
$ZnBr_2·2H_2O$	5-30	1.69	455	8	347	529
$KOH·2H_2O$	5-30	0.014	1924	9	330	128
$LiCl·H_2O$	20-65	14.53	-75	11	303	86
$CaBr_2·6H_2O$	11-22	0.17	1360	16	251	170*
$LiI·3H_2O$	15-65	0.15	1424	18	235	170
$CaCl_2·6H_2O$	15-25	0.11	1653	29	170	97*
$MgCl_2·6H_2O$	5-45	29.26	34	33	152	57*
$NaI·2H_2O$	5-45	3.62	702	38	133	192
$K_2CO_3·2H_2O$	20			44	112	113
$Ca(NO_3)_2·4H_2O$	10-30	1.89	981	51	92	156
$Mg(NO_3)_2·6H_2O$	5-35	25.28	220	53	87	74*
$NaBr·2H_2O$	0-35	20.49	308	58	75	98
$NaNO_2$	20			66	57	88
KI	5-30	29.35	254	69	51	153
$SrCl_2·6H_2O$	5-30	31.58	241	71	47	57*
$NaNO_3$	10-40	26.94	302	74	41	95
NaCl	10-40	69.20	25	75	39	36
NH_4Cl	10-40	35.67	235	79	32	41
KBr	5-25	40.98	203	81	29	71
$(NH_4)_2SO_4$	10-40	62.06	79	81	29	78
KCl	5-25	49.38	159	84	24	37
$Sr(NO_3)_2·4H_2O$	5-25	28.34	328	85	22	89
$BaCl_2·2H_2O$	5-25	69.99	75	90	14	38
$ZnSO_4·7H_2O$	20			91	13	62*
CsI	5-25	70.77	75	91	13	95
KNO_3	0-50	43.22	225	92	11	46
$CuSO_4·5H_2O$	20			97	4	24*
K_2SO_4	10-50	86.75	34	97	4	13

The vapour equilibrium technique allows applying high values of suction because it maintains the negative pore water pressure in soil samples. However, some difficulty was reported for controlling the humidity at low values of relative humidity. It suggested to be used for the suction values greater than 3 MPa (Romero, 2001).

In the present work, the vapour equilibrium technique was used to study the water retention behaviour of Viadana silt when the samples were subjected to suction greater than 4 MPa.

The control of suction by this technique is much slower than the axis-translation due to the very low kinetics of vapour transfer. The sample was kept in contact with each solution more than one month to achieve the equilibrium. The equilibrium time observed in the experiments is plotted in Figure 2.10. The weight and the size of sample were frequently measured.

This method is based on the relationship between the relative humidity and suction, which can mathematically represents by equation 2.2, as proposed by Fredlund and Raharadjo (1993),

$$\psi = \frac{\rho_w RT}{M_w} \ln\left(\frac{RH\%}{100}\right) \tag{2.2}$$

where ψ is total suction, ρ_w is the volumetric mass of water (kg/m^3), R is molar gas constant (J/mol.K), T is the absolute temperature, M_w is the molecular mass of water vapour (g/mol) and RH is the relative humidity.

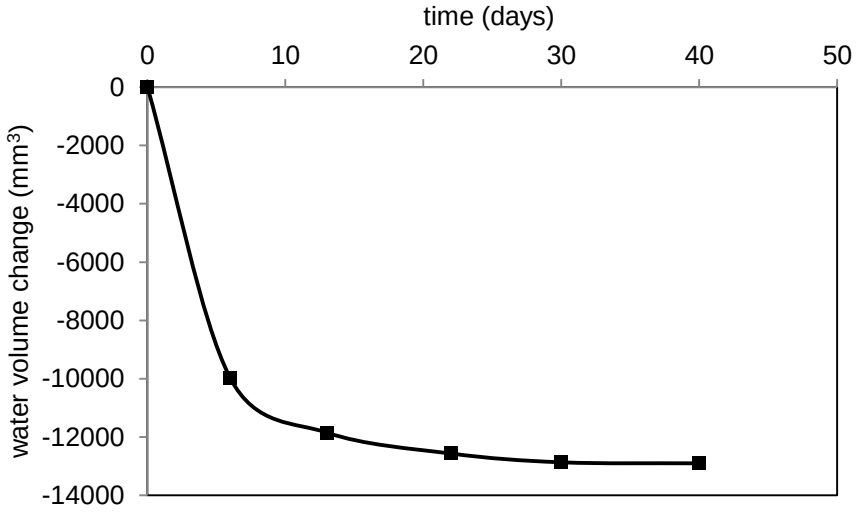

Figure 2.10. Equalization of the water content within the soil mass using the vapour equilibrium technique (WR tests).

As formerly explained, the D/W cyclic samples were maintained in the room environment at temperature of 21℃ to be dried. The RH of the room was measured to be 38.5%. This implies that the suction imposed during drying the D/W cyclic samples can be computed, considering $\rho_w = 1$, $T = 273.16 + 21$, $R = 8.31432$ and $M_w = 18.016$,

$$\psi = 135022 \times \ln(0.385) = 128.8\ (MPa) \tag{2.3}$$

2.2.3 Filter Paper technique

The filter paper method has been commonly used to measure total and matric suction in geotechnical engineering field (e.g. McKeen, 1980; Fredlund et al., 1995, Leong et al., 2002). It has been widely used because it is as inexpensive and easy method to be carried out in the laboratory. In-contact filter paper technique is used to measure the matric suction where the filter paper comes to equilibrium with the soil through liquid, whereas the non-contact filter paper technique is used to measure the total suction where the filter paper comes to equilibrium with the soil through vapour.

The in-contact filter paper method was used in the present experimental work to measure the initial matric suction of two as-compacted samples after preparation for triaxial tests, and two other samples prepared with the same properties but subjected to 6 cycles of drying-wetting (D/W cyclic samples). The Whatman no. 42 filter paper was placed between two larger protective filter papers. All 3 filter papers were formerly cut to diameter smaller than 38mm. The samples were precisely cut to two pieces ensuring the smooth surfaces provide an intimate contact between the soil and filter papers. The sandwiched filter papers were placed in between two pieces of sample (Figure 2.11). The two pieces were taped together and wrapped up in the plastic cover. The sample and the embedded filter papers were then put in the jar container sealed tightly with plastic tape to prevent any moisture exchange between the air inside and outside of the jar. They were kept in a controlled temperature room for two weeks for the equilibrium. At equilibrium, the suction value of the filter paper and the soil is equal. After equilibrium was established, the middle filter paper was removed and its water content was measured.

The calibration curve of the filter paper water content-suction is used to obtain the corresponding suction value. Different calibration curves have been proposed in the literatures (e.g Harrison and Blight, 1998; Leong et al., 2002, Chao, 2007).

The proposed calibration curves differ in low suction ranges, starting to converge after about 300 kPa. The calibration curve proposed by Caruso et al. (2011) was selected to obtain the corresponding suction of moist filter paper. The values of suction of four samples measured using the filter paper are plotted in Figure 2.12, where the utilized calibration curve is also drawn. The average initial suction of the as-compacted samples after preparation was 33 kPa, whereas average measured suction of D/W cyclic samples after subjecting to 6 cycles of drying-wetting was about 5 kPa.

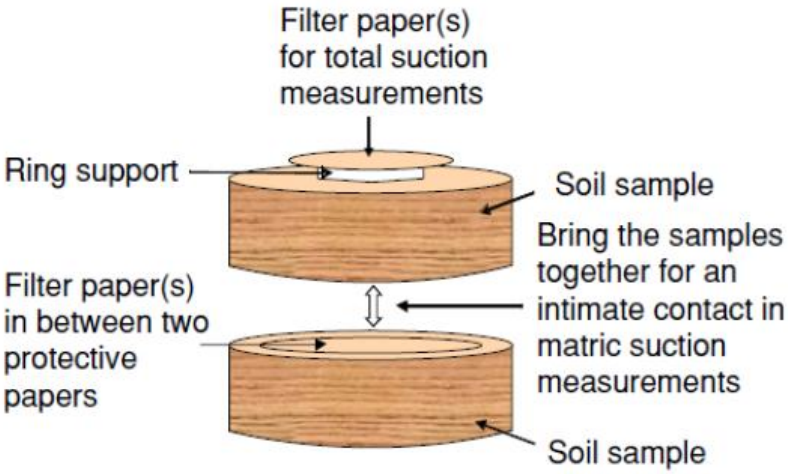

Figure 2.11. Placing filter papers to measure suction.

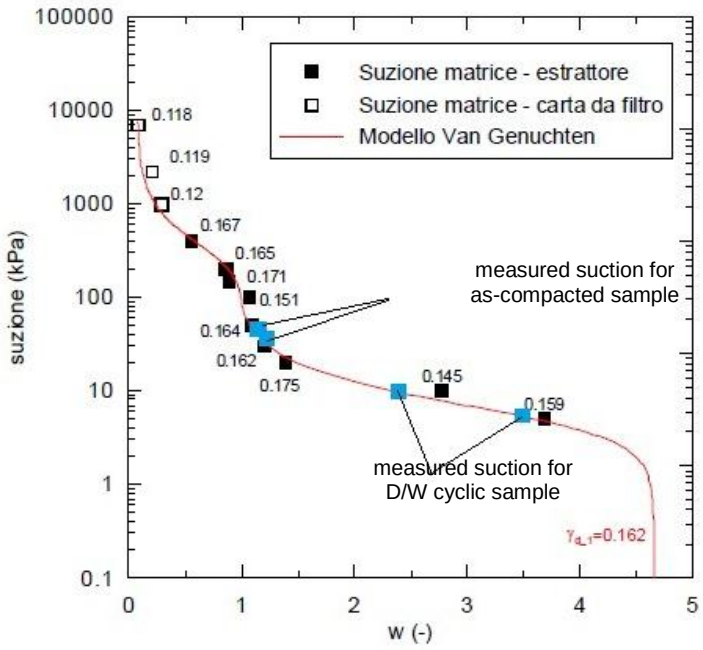

Figure 2.12. Calibration curve (Caruso et al, 2011) and suction measured by filter paper.

2.3 Microstructural study

Many attentions have been recently paid to microstructure study of the soil. There are various methods to study the fabric of the geomaterials such as scanning electron microscopy (SEM), Environmental scanning electron microscopy (ESEM), nitrogen adsorption and mercury intrusion porosimetry (MIP). In principle, the results obtained from these experiments allow evaluating and characterizing the soil fabric and providing useful information about geometry of soil particles and pores.

The MIP and ESEM tests were performed in this research to investigate the microstructure of unsaturated samples. The combination of results of the MIP test and the images of soil pores and particles (ESEM and SEM) was commonly used to study soil fabric (e.g. Delage and Lefebvre, 1984; Romero, 1999; Simms and Yanful, 2001; Musso et al., 2003; Cuisinier and Laloui, 2004; Romero et al, 2011, Della Vecchia et al, 2012). The testing equipment and procedures using the MIP and ESEM techniques are described in the following.

2.3.1 MIP equipment and testing procedures

Pore size distribution (PSD) is related to the soil grain size distribution on mineralogy, and fabric, and it can be obtained by MIP test. This information can be interpreted to understand the influence of mechanical and hydraulic loading on the soil fabric, and provide information about the properties of the soil dependent on its fabric. It has been reported that many features of soil behaviour are related to the PSD such as water, air, and heat conductivity, capillary phenomena, volumetric deformation (Romero, 1999).

As shown in Figure 2.13, the MIP test is carried out by injecting the mercury through a porous medium, placed in a penetrometer under the vacuum condition. The injection is performed by changing the applied pressure allows penetrating pores with different sizes. The diameter of the pores filled by mercury can be computed for each pressure increment.

The relationship between the absolute applied pressure (p) in MIP tests and the apparent pore diameter (d) is obtained using Washburn equation (Washburn, 1921).

$$p = -\frac{4\sigma^{Hg} cos\theta_{nw}}{d} \tag{2.4}$$

where σ^{Hg} is the surface tension of the mercury, θ_{nw} is the contact angle between the mercury and the pore wall. This equation establishes the mechanical equilibrium across an interface of a non-wetting liquid and its vapour in a pore. Assuming pores of cylindrical shapes, it can be represent as an equivalent form to the Laplace equation, see details in Romero (1999).

As explained by Diamond (1970), there are several assumptions and sources of errors for the MIP test, which provide some limitations using this technique. This implies that the pore size distribution obtained from the MIP test can be different from the real pore size distribution of the tested material, in which the measured diameter is the apparent one. Among these limitations are: the hysteresis of the MIP technique mostly caused by the variation of the contact angle between mercury and the soil particle, and the geometry of the pores known as “ink-bottle effect”; the pores constricted with smaller pores cannot be detected unless the smaller ones are penetrated; isolated pores enclosed by surrounding solids are not detected; the apparatus may not have the capacity to enter the smallest pores of the samples; and the high applied pressure may result in fabric change (Romero 1999).

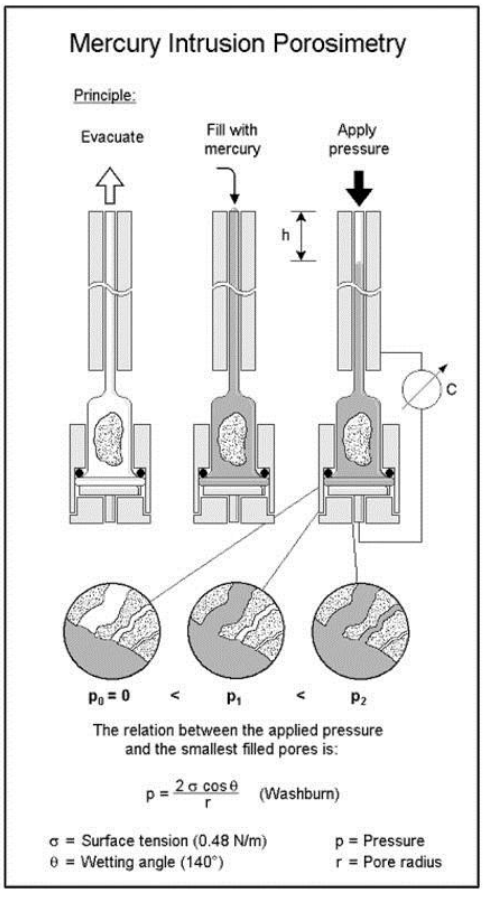

Figure 2.13. Schematic of MIP test to study microstructure of porous media.

The MIP tests were performed using the Micromeritics AutoPore IV 9500. Two different operating systems were used depending on the range of applied pressure and intruded pore diameter. The first system was employed for the low-pressure range, between 0 and 345 kPa. The second operating system involved applying the high pressure from atmospheric pressure up to 228 MPa. These operating systems allow intruding the pores with diameter range between 400 and 0.007 µm.

The MIP apparatus requires a small dehydrated cubical or cylindrical sample. Therefore, the MIP sample extracted from the core of analysed samples trimmed into cylindrical sample with height and diameter of about 10 mm. In order to remain the fabric of the compacted sample unchanged and prevent shrinkage during drying, the MIP samples were dehydrated using the freeze-drying technique (Delage and Pellerin, 1984). The freeze-drying was chosen because it involves temperature and pressure conditions that eliminate the surface tension forces caused by air-water interfaces. This technique was applied by rapidly freezing the sample to cryogenic temperatures, followed by subjecting to the vacuum leading to remove of water by sublimation, i.e. the change of the moisture, which was formed as an ice, to the vapour phase.

After the sample was freeze dried, it was weighted and placed in the penetrometer, followed by evacuation of the gas from chamber to generate the vacuum condition. The tests began at low pressure, in which the big pores were initially intruded by mercury. The low pressure operating system of the penetrometer was installed at the beginning. The penetrometer was removed and installed in high pressure port when the low pressure analysis was completed. Consequently, the smaller pores were intruded using the high pressure system. The amount of pressure and the volume of mercury were monitored during the test. The volume of mercury remaining in the penetrometer stem is measured by determining the penetrometer electrical capacitance, in which mercury empty and fill the penetrometer stem in intrusion and extrusion phases, respectively (Romero, 1999).

2.3.2 Computation of required variables from MIP test results

The analytical elaboration of the MIP results to obtain pore volume parameters are described by Romero (1999) and Della Vecchia (2009). The results of MIP test are presented as incremental, differential or cumulative intrusion and extrusion volume normalized by dry weight of the sample. The ratio between the cumulative volume (V) and the total volume of the sample (V_{TOT}) is defined as cumulative porosity n_{cu},

$$n_{cu} = \frac{V}{V_{TOT}} \tag{2.5}$$

Pores having sizes smaller than 7 nm would require injection pressures greater than the one of the penetrometer, therefore this fraction of pores is not explored by MIP, which is not intruded upon mercury intrusion. If n_{cu0} is the normalized total volume of pores, the degree of saturation of the non-wetting mercury Sr_{nw} (Prapaharan et al., 1985; Romero, 1999) can be defined as

$$Sr_{nw} = \frac{n_{cu}}{n_{cu0}} \tag{2.6}$$

Obviously, if all pores are filled with intruded mercury, $Sr_{nw} = 1$.
The data are elaborated in order to obtain the pore size density function $f(x)$. If $F(x)$ denotes the fraction of the pore space having a pore diameter between x and ∞, $f(x)dx$ is the fraction of the pore volume constituted by pores with diameters between x and $x + dx$ and $f(x)$ is, therefore, the density of pore volume corresponding to diameter x. The volumetric pore size density introduced by Juang and Holtz (1986) is,

$$f(x) = \frac{1}{V_0}\left(-\frac{d(V_0 - V)}{dx}\right) \tag{2.7}$$

where V_0 is the total volume of pores in the sample and $V_0 - V$ is the volume of intruded mercury or the volume of pores with diameter equal or greater than x. In this way

$$F(x) = \int_x^{\infty} f(x)dx = \frac{(V_0 - V)}{V_0} = Sr_{nw} \tag{2.8}$$

And therefore,

$$f(x) = \frac{dSr_{nw}}{dx} = Sr_{nw} \tag{2.9}$$

Assuming constant surface tension and contact angle, a relation between the absolute pressure and the intruded pore diameter can be obtained

$$f(x) = \frac{p}{x}\frac{dSr_{nw}}{dp} \tag{2.10}$$

To overcome the distortions due to the fact that the pore size x extends over several order of magnitude and that the class width dx reported by intrusion record is not constant (emphasising the smaller pores), the pore size density function at $\log x$ can be defined as

$$f(\log x_m) = -\frac{dSr_{nw}}{d(\log x)} \tag{2.11}$$

$$f(\log x_m) = \frac{dSr_{nw}}{d(\log p)} = \frac{p}{\log e}\frac{dSr_{nw}}{dp} \tag{2.12}$$

In the literature the pore size density is usually represented in finite terms by the quantity

$$f(\log x_m) = \frac{\Delta e}{\Delta log\ x} \tag{2.13}$$

2.3.3 Environmental scanning electron microscopy (ESEM)

The direct observation of the soil fabric provides remarkable information about the arrangement and geometry of pores and soil particles, which can be a supplementary to MIP analysis to systematically investigate the microstructure of the soil. The scanning electron microscopy (SEM) is a common method widely used in the research works (e.g. Collins and McGown, 1974; Al Mukhtar et al., 1996; Delage et al., 1996; Romero et al., 2011).

As shown in Figure 2.14, the conventional SEM technique involves scanning across the surface of the sample by emitting an electron beam through electron gun. When the electron beam strikes the surfaces in high vacuum condition, a variety of signals are released which are subsequently detected and amplified to produce high quality image and element composition. The secondary electrons are type of signals emitted from the top surface of the samples, and they contribute to produce readily image of the surface. The resolution of the image can increase by

employing the smaller diameter of the emitted primary electron beam and also conductive coating of the sample. The vacuum ensures unimpeded travel of the electrons within the instrument.

The preparation of the sample for the SEM test requires a considerable attention. In general, providing undisturbed surface, surface replicas or conductive ultrathin coating is problematic. This limitation becomes more dramatic if the sample exhibits high volume of pores and water content. Moreover, the SEM equipment does not able to provide an image for wet surface since the wet sample produce vapour when placed in vacuum chamber. Therefore, the SEM test can be carried out on sample who is formerly dehydrated, and no variation on the sample condition is allowed during the observation.

The environmental scanning electron microscopy (ESEM) is the advanced version of SEM with the primary advantage of imaging the hydrate sample at its natural state and preserving its original characteristics for further testing (Donald, 2003; Stokes, 2003; Mitchell and Soga, 2005; Romero and Simms, 2008). This technique allows controlling the relative humidity of the environment of the sample through pressure, temperature and gas composition. In principal, overcharging of the surface of sample due to the presence of the water vapour in the chamber, results in the loss of the image quality. This discrepancy has been overcome in ESEM technique by separating the pressure limits surrounding the electron gun and the sample chamber. This ensures high vacuum condition surrounding the electron gun whereas relative humidity around the sample can maintain relatively high. Furthermore, the sample prepared for the ESEM tests do not require any conductive coating.

The variation of the relative humidity in the ESEM chamber and in turn within the soil sample induces by controlling the pressure and temperature value in the chamber. The control of relative humidity inside the chamber is based on the transition between separated regions, including the region in which the vapour pressure at equilibrium is saturated and the region where vapour pressure at equilibrium is not saturated. This implies that the possibility of water condensation in the sample or evaporation from the sample allows studying the dynamic changes within the samples, such as drying, wetting, corrosion and melting.
In order to provide additional information to MIP data for studying the fabric of the as-compacted Viadana sample, the ESEM sample was trimmed into cylindrical sample measuring the height and diameter of about 10mm. The moisture content of the ESEM sample was strictly preserved before placing in the chamber and starting the ESEM analysis in order to produce the image of sample fabric at its real as-compacted moisture content.

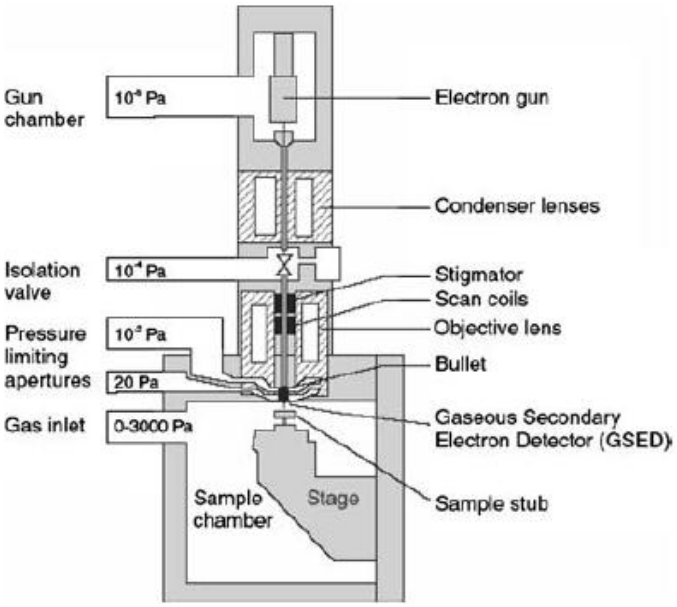

Figure 2.14. Schematic cross section of ESEM (Danilatos, 1993).

2.4 Oedometer testing system

2.4.1 General layout

The suction controlled oedometer apparatus were used in this work to study the water retention, effect of repeated loads and also the variation of void ratio on the water retention behaviour, and hydromechnical behaviour of Viadana silt during loading-unloading cycles. The characteristics of the apparatus are briefly described in following session. The similar equipment is described in detail by Romero (1999).

2.4.2 Suction controlled Oedometer

The basic of suction controlled oedometer is similar to conventional oedometer with some alterations in the geometry of the loading platen. Both vapour equilibrium and axis translation techniques can be applied in the equipment, but only the latter was employed in the present experiments.

The size of the oedometer sample is 50 mm of diameter and 20mm of height. This size minimises the effect of side friction and equalisation time, and provide sufficient height for precise measurement of the axial train. The axial displacement

is measured using the linear variable differential transformer (LVDT) assembled above the equipment and connected to top platen displacement. The HAEV ceramic disk is placed at the bottom of suction controlled oedometer, where the water pressure is applied. The air pressure is applied to the upper coarse porous stone through a conduit in the loading cap which is separated by a thick rubber membrane from the vertical loading platen. An air trap is installed in the air pressure line to protect pressure regulator from water condensation. The axial load is applied by pressurized air acting on the loading platen. The maximum applied diaphragm pressure is limited to 1.6 MPa due to the capacity of the equipment. The apparatus used in this study and the schematic layout of the apparatus are presented in Figure 2.15 (a) and (b).

The tests were performed using the HAEV porous stone with nominal 0.5 MPa, however, the real air entry value was measured to be slightly smaller. The maximum suction imposed in tests was 400 kPa, which was sufficiently smaller than the air entry value of the used porous stone.

Water volume meter with the capacity of 50 cc is connected to the HAEV porous stone and water within the sample. The variation of the water content of the sample results in the variation of the deaired water inside the water volume meter and in turn the movement of the indicator connected to the LVDT, which allows measuring the water volume change of the sample during absorption and desorption of water. The additional water channel is also placed at the basement of the equipment connected to the water unit which is used to remove any air bubbles, accumulated in the water unit, due to the air diffusion. This is employed by opening the water outlet and allowing the flow of water, leading to the flushing the accumulated air.

2.4.3 Modification to measure suction

The pressure transducer is connected to the water unit to control the water pressure in the suction controlled oedometer equipment. This transducer is placed between the water volume meter and sample, and connected to data acquisition system. In order to measure the suction in constant water content test, a valve was assembled between the water volume meter and the water pressure transducer. When this valve turns to close, the test remains at undrained condition, in which the water within the sample is connected to the water pressure transducer. This allows measuring the water pressure while the air pressure and the water content of the sample remain constant. As a consequence, the variation of suction within the sample can be computed as a difference between the imposed air pressure and measured water pressure. It has to be pointed out that the constant water content tests were carried out in a very small loading rate

ensuring the water pressure measured by pressure transducer was in equilibrium with the water pressure of the HAEV porous stone and soil sample.

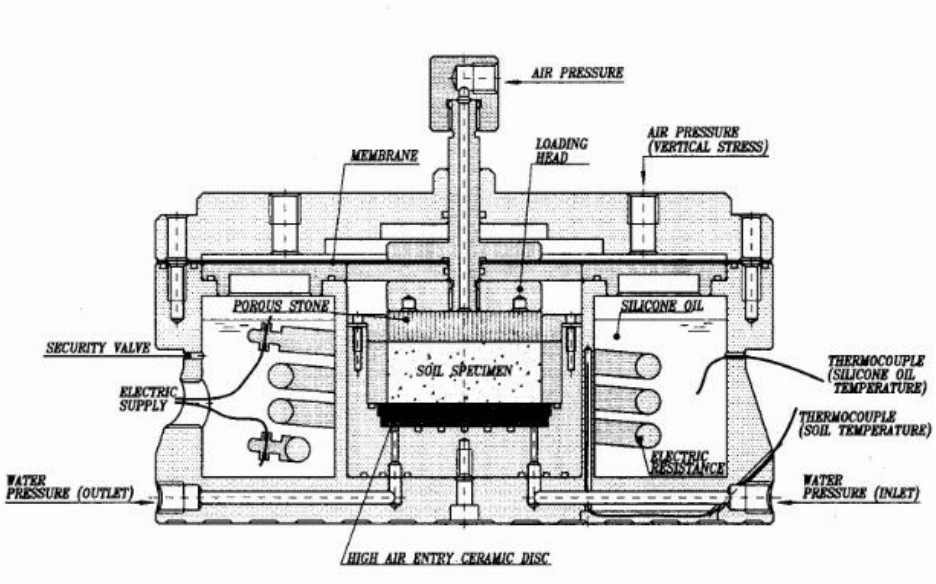

(a)

(b)

Figure 2.15. a) Schematic section of suction controlled oedometer (Romero, 1999) b) Suction-controlled apparatus used in the experimental tests.

2.4.4 Computation of required variables from oedometer test results

The relevant geomechanical variables can be computed from the data of the oedometer test. The axial displacement (Δh) is the only deformation variable which is measured in the oedometer test since the lateral deformation is prevented. Hence, the axial strain (ε_a) can be calculated,

$$\varepsilon_a = \frac{\Delta h}{h_0} \tag{2.14}$$

where h_0 is the initial height of the sample.

The volumetric strain (ε_v) is equal to axial strain due to null radial strain,

$$\varepsilon_v = \varepsilon_a \tag{2.15}$$

The current value of the void ratio can be computed, assuming the positive value for compression deformation,

$$e = e_0 - \varepsilon_v(1 + e_0) \tag{2.16}$$

where e_0 is the initial void ratio.

The water content of the soil (w) can be computed using the volume of solid $(V_s)$and the current value of the volume of water (V_w) of the sample,

$$w = \frac{V_w}{V_s} \tag{2.17}$$

and hence, the degree of saturation (Sr) is calculated,

$$Sr = \frac{wG_s}{e} \tag{2.18}$$

where G_s is the grain specific gravity.

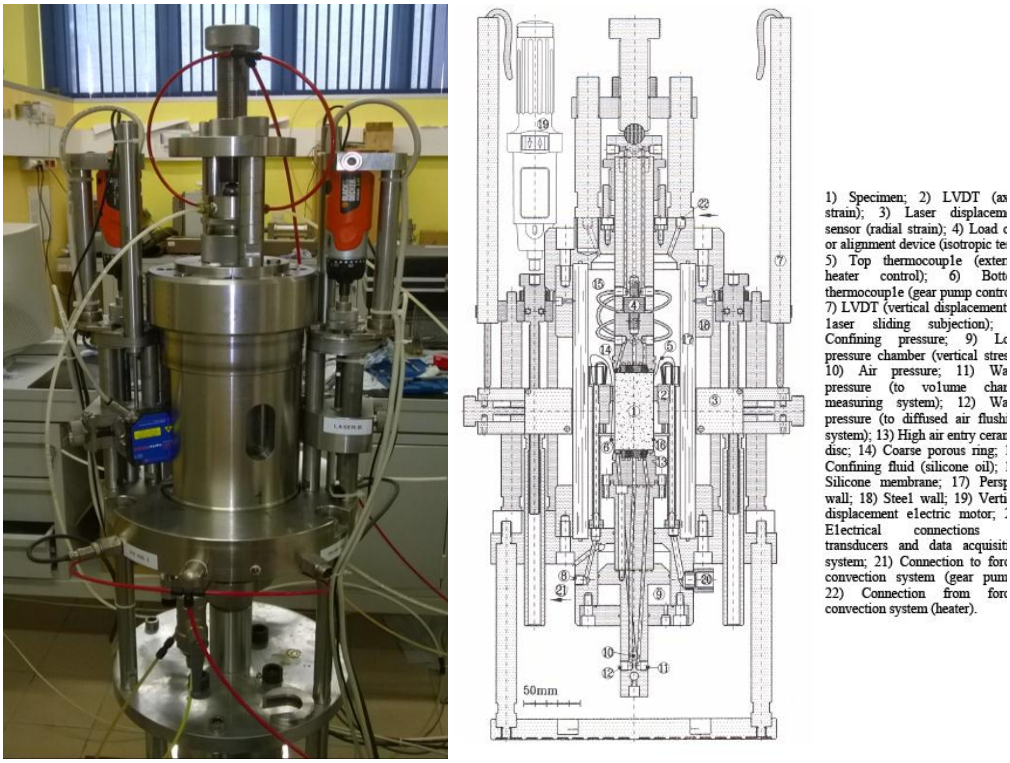

(a) (b)

Figure 2.16. a) Suction-controlled triaxial apparatus used in the present study b) Schematic cross section (Romero, 1999).

2.5 Triaxial testing system

2.5.1 General layout

The conventional triaxial cell requires further development to be used in unsaturated soil testing. This development mainly involves the adoption of the method to control the suction and monitor the volume change of the sample. The suction controlled triaxial apparatus used in this research was able to employ the osmotic, vapour equilibrium and axis translation techniques to control the suction value. The fundamental features of the triaxial cell are similar to the Bishop and Wesley (1975) hydraulic triaxial cell for controlled stress path testing. The apparatus designed to perform compression and extension tests under either strain controlled or stress controlled conditions. The relevant size of the unsaturated sample is 76 mm of height and 38 mm of diameter. The sample is placed inside 15mm thick perspex wall cell externally enclosed by a stainless steel AISI 316 cylinder. The apparatus used in this study and the schematic layout of the apparatus are presented in Figure 2.16 (a) and (b).

The control of the pressure in the loading chamber, which is mounted at the bottom of the apparatus and filled with deaired water, allows pushing the piston placed inside the chamber. This piston transfers the pressure of the chamber to loading ram and in turn to the sample acting as the axial load on the lower base of the sample. The top cap is assembled at top of the sample and connected to adjustable rod precisely aligned with the piston in the loading chamber. This rod is passed through the top of the triaxial cell, in which it is maintained in the fixed position. These arrangements allow pushing or pulling the sample at the bottom against stationary top cap as well as preventing top cap rotation. The loading cell is mounted between the top cap and the rod, where it can measure the axial force.

The main difference between the conventional and suction controlled triaxial apparatuses is the ability of independent control of the air and water pressure within the sample in the latter case. This capability is facilitated at both end sides of the sample. The top and bottom caps are equipped with two types of porous stone appropriate for the fluid of concern (air or water) fluid pressures. The HAEV porous stone connected to water pressure, surrounded by coarse porous stainless steel connected to the air pressure. Applying both fluid pressures at both sides of the sample considerably minimises the time required for equalisation.

2.5.2 Water volume change measuring device

The water volume change of the sample is measured using a single glass burette enclosed in a perspex cylinder, which is filled with two immisicible fluids, namely, deaired water and kerosene. The kerosene stays above the water inside and outside of the burette. The water in the burette is connected to both ends of the sample on one side, and it is connected to the separation system, which transforms the generated pneumatic pressure to water pressure, on the other side. The interface of two fluids inside the burette moves only because of change of volume of water within the sample whereas it is not influenced by variation of the water pressure. The differential diaphragm pressure transducer connected to inside and outside of the burette measures the water volume changes due to different of hydraulic head as the fluid interface moves. The capacity of the water volume change measuring device is limited to 7 cm^3. The change of water links, connected to the burettes, by means of inverting relevant valves permits to connect the water either inside or outside of burette to the sample. This implies that the direction of water flow in the burette can be reversed during the test, which can be applied as the water volume change approaches to the limitation value.

2.5.3 Calibration of water volume change

The precise calibration of the water volume measuring device, and also accounting the effect of air diffusion and water evaporation are essential to obtain authentic values for the water volume change of the unsaturated sample.

The change of deaired water volume inside the burette was measured by visual monitoring of the variation of the interface of the fluids, and also weighting the amount of water expelled from the burette. The calibration data for both measurement methods and interpolated calibration lines and corresponding error distributions are plotted in Figure 2.17 (a) and (b). The average value of calibration lines was employed in the acquisition system.

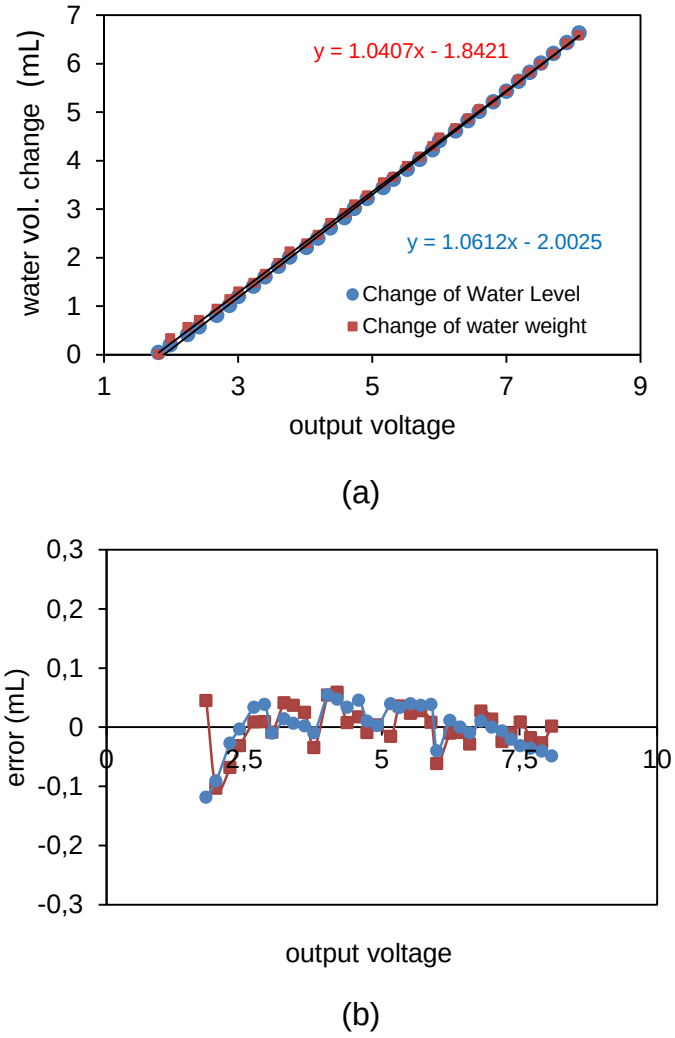

Figure 2.17. *a) Calibration of water volume change measuring system b) Offset error.*

2.5.4 Correction due to air diffusion and water evaporation

As formerly explained, the HAEV ceramic porous stone was used to prevent free passage of the air to the water drainage unit of the triaxial apparatus. However, air bubbles may appear due to diffusion of the air through the water in the porous stone. This diffused air is accumulated beneath the porous stones by means of grooves with openings at both extremities. The accumulation of air, particularly in long-term tests, can lead to obtain incorrect measurement of water volume change or water pressure.

An air trap was placed in the circuit of water lines, which was periodically used to flush the accumulated diffused air beneath the porous stone. Assuming the concentration of the dissolved air is the driving mechanism, the rate of the air diffusion ($\frac{dV_d}{dt}$) can be computed as it was suggested by Fredlund and Rahardjo (1993),

$$\frac{dV_d}{dt} = \frac{nADh(u_a - u_w)}{(u_a + u_{atm})t_c} \tag{2.18}$$

where n is the porosity, A is the cross sectional area of the porous stone, D is the diffusion coefficient, h is the solubility of the dissolved air in water, u_{atm} is the absolute atmospheric pressure, and t_c is the thickness of the porous stone.

On the other hand, the vapour pressure at the surface of the sample is different from the vapour pressure in the air unit of the triaxial apparatus. This resulted in the transfer of the vapour from the sample to the surrounding air. This evapourative flux can affect the measurement of the water volume change of the sample. Consequently, the readings of water volume change have to be corrected by means of quantifying the influence of water evaporation as well as the impact of air diffusion.

In triaxial tests performed in this research, all samples were subjected to drying because of the imposed suction at first stage of the tests. As a result, the moist content of the samples at this stage decreased while the water volume increases in the burette. As the water volume change was approached to the equilibrium state, it had to tend toward a horizontal plateau with time, but instead, it tended toward a linear asymptotic, as the results obtained from tests 3 shown in Figure 2.18. It implied that the external effect including the air diffusion and water evaporation was involved. The combination of these two factors represented as a originate line with the same slope of the asymptotic line, implying that the rate of the water evaporation was constant as well as the rate of air diffusion.

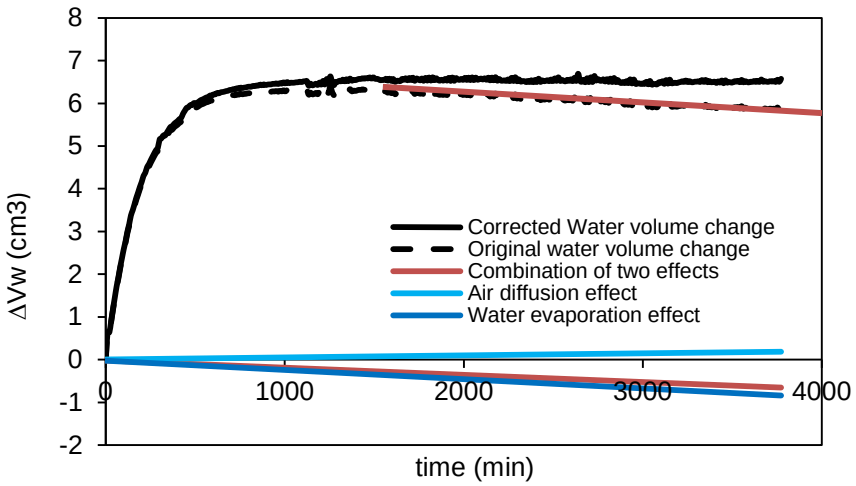

Figure 2.18.Correction applied to the measured water volume change due to the water evaporation and air diffusion at suction equalisation (50 kPa) phase of triaxial test,TxS50P200).

The corrected curve was obtained by subtracting the measured data (original curve) from this line, in which the air diffusion and water evaporation effects were applied simultaneously.

Although using this technique was sufficient to correct the water volume change in experimental point of view, but further computation was performed to quantify the rate of the water evaporation. These two factors have opposite effects on the water volume change readings, i.e. the evaporation decreases the amount of water volume (a line with a negative slope), whereas the diffusion increases the amount of water volume (a line with a positive slope). The rate of water evaporation was computed to be 3.6×10^{-6} cm^3/s, by means of subtracting the rate of diffusion (0.8×10^{-5} was obtained from the equation 2.18) from the rate of the combined effect (from the curve plotted in Figure 2.19 for combined effect). As it can be observed, the evaporation is a dominant effect.

2.5.5 Axial deformation measuring devices

Three LVDTs are used to measure the axial displacement of the sample in different ranges. The local axial displacement is measured using two miniature LVDTs. These local LVDTs are stuck to opposite sides of the sample using two pedestals. The upper pedestal holds the top segment of the LVDT at fixed position, and the lower pedestal makes a basement for the bottom segment, which moves into the top segment during the compression of the sample. Considerable attention is needed to provide a perfect adhesion between the pedestals and the membrane at the center of the sample (Figure 2.19). The nominal working range of these LVDTs is ±3 mm and the initial length assumed 35 mm.

Figure 2.19. Miniature LVDT stuck to the sample measuring local axial strain.

However, the initial length is altered during assemble of LVDTs, and it has to be measured after the assemblage. The limit range of the miniature LVDTs and the fact that they can dismantle due to the large deformation of the sample, confirm the need for the external measurement of the axial deformation as well as the local one. Therefore, the external LVDT contrasted to loading ram is used for a large displacement.
These LVDTs were calibrated by monitoring the variation of voltage corresponding to the applied axial displacement using the micrometer. The calibration lines and the errors are plotted in the Figure 2.20. These LVDTs were used in their linear ranges at all the experiments.

2.5.6 Radial deformation measuring laser system

The radial deformation of the sample was directly measured using the electro-optical laser sensors. The laser system has important advantages which make it remarkable among other different electrical methods developed for measurement of local radial displacement. The laser sensors are mounted on the opposite sides of the sample and outside of the cell implying that they are not influenced by changes of the pressure and temperature inside the triaxial cell.

Moreover, sensors are not affected upon deformation of the sample, and do not restrain or load the sample. The support system held the laser sensors are connected to electric motors allows vertical displacement of the sensors. As a consequence, the whole profile of the sample from the bottom pedestal to top cap can be monitored in approximately 30 s. The vertical displacement of sensors is measured using two LVDTs fixed outside of the cell.

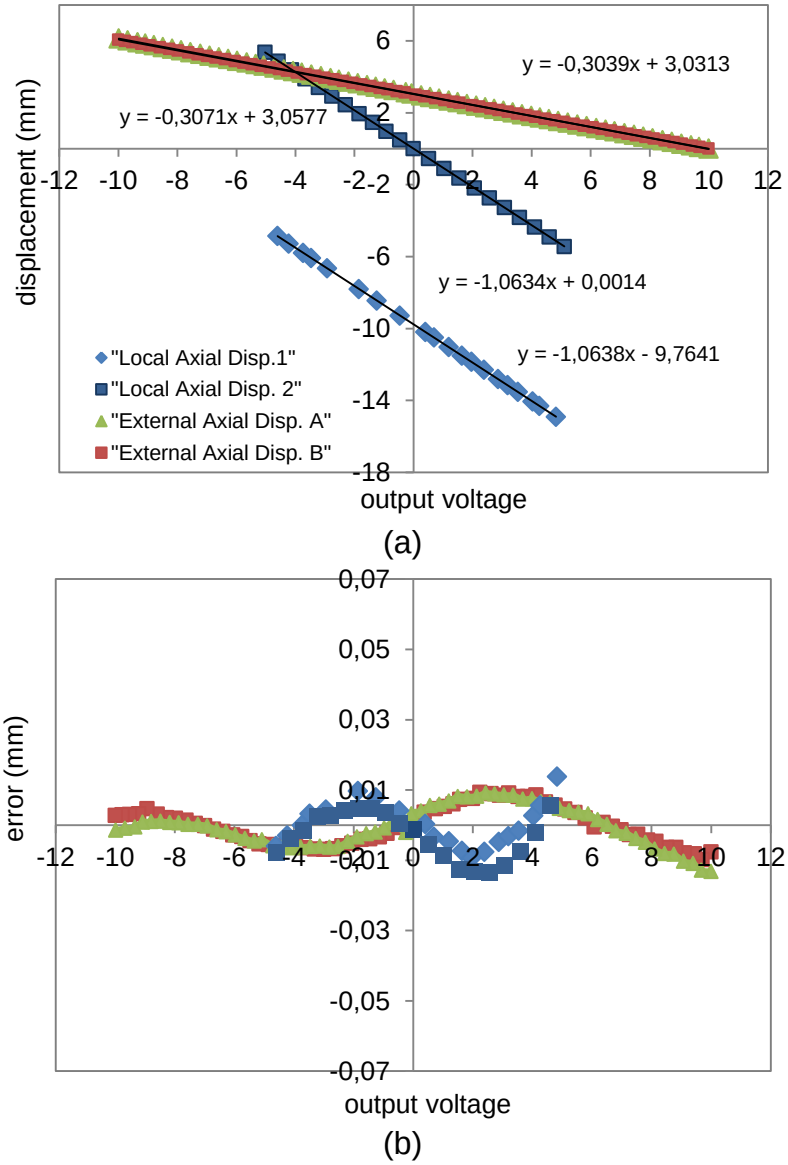

Figure 2.20. a) Calibration of LVDTs for axial displacement measurement b) Offset error.

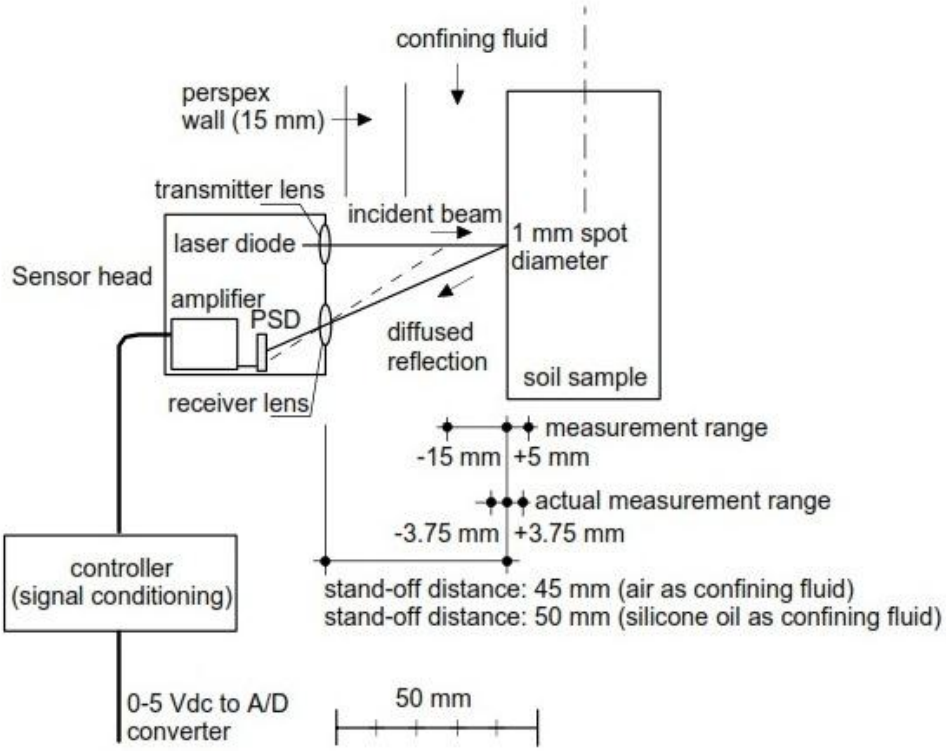

Figure 2.21. Schematic of laser system measuring the radial displacement of the sample (Romero, 1999).

The operation principles and the configuration of the laser sensors are explained in details by Romero (1999). The laser-based positioning system uses the principle of optical triangulation. Laser triangulation sensors contain a solid-state laser light source and a PSD detector. A laser beam is projected on the target being measured, and a portion of the beam is reflected through focusing optics onto a detector. As the target moves, the laser beam proportionally moves on the detector. The signal from the detector is used to determine the relative distance to the target. This information is then typically available through an analog output, a digital (binary) interface or a digital display for processing. The sensing system utilizes the light quantity distribution of the entire beam spot that is focused on the system, to determine the target position (center of the beam spot distribution).

Soil samples must be then covered by latex membrane, where two opposite sides of the membrane were coated by white acrylic painting. These white vertical bars were painted along the height of the sample. This white bars are scanned by the optical laser sensors. This painting prevents the discrepancy which occurs in laser readings due to change of colour of the membrane during long term test. After placing the sample and assemblage of the triaxial cell, the position of the laser sensors were adjusted, whose front faces were positioned at a distance of 45 mm from the lateral surface of the sample.

This distance consists of 15mm transparent perspex wall, 25 mm of the confining air filling inside of the triaxial cell chamber and 5mm of air gap between the perspex wall and the sensor front face. At this position, laser sensors were able to measure the lateral displacement from +5 to -15 mm (Figure 2.20), ensuring the resolution of 2 µm at a response time of 60 ms. The metallic cell that surrounds the perspex window acts as a protective cover minimizing ambient light effects arriving to the sensors lens.

A careful attention was paid to calibrate the laser system and minimise the errors, which affect the output signals. It is essential to calibrate the sensor output using the same layout as the testing setup since the output signal is affected by refraction in diffusive reflectance crossing different transparent medium, and also by the presence of any object that reflects or change the light intensity. A dummy stainless steel sample was placed and the latex membrane was coated with white painting. The triaxial cell was assembled and the laser sensors were adjusted to the relevant position (at the same height of the center of the sample and at the distance of 45 mm from the surface of the sample). The laser sensors were then moved forward and backward while the output voltage was monitored by acquisition system and the displacement of the sensors were measured using the micrometer placed in contact with sensors. This is equivalent to the radial displacement of the surface of the sample when the positions of the laser sensors are fixed. The calibration was carried out for measurement of the displacement at different constant cell pressures.

The perspex wall may move outward if the cell pressure increases. Therefore, further calibration was carried out to investigate the effect of variation of the output signal when the pressure within the triaxial cell chamber varies. The positions of the laser sensors were kept unchanged and the cell pressure increased to 800 kPa, following by decreasing to zero. The results of the calibration tests in terms of the displacement and output voltage are plotted in the Figure 2.22.

The effect of pressure on radial displacement Δr can be accounted for each laser sensor,

$$\Delta r = \alpha_1(\Delta V + \alpha_2 \Delta\sigma_3) \tag{2.19}$$

where α_1, α_2 are the slope of linear calibration of displacement-output voltage and output voltage-cell pressure (σ_3) relationship, respectively.

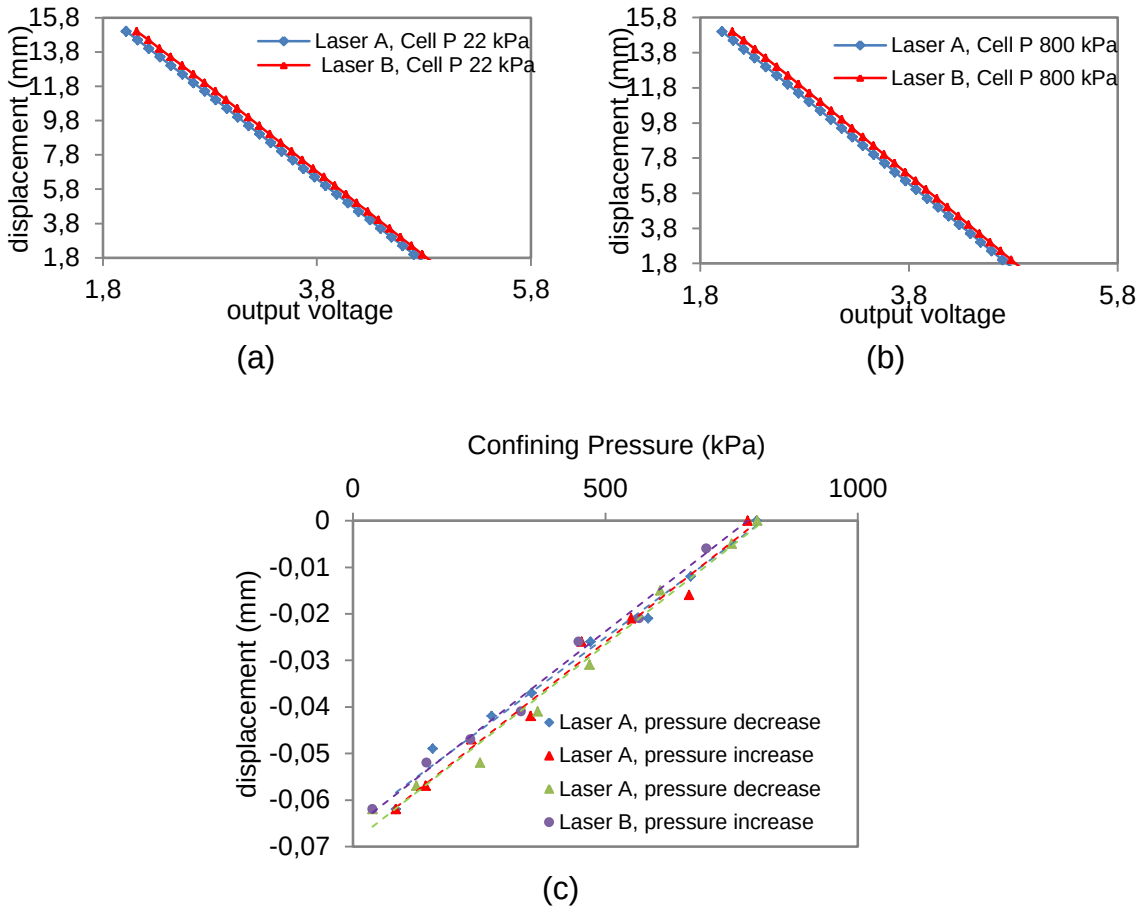

Figure 2.22. Calibration of the laser sensor readings a) Displacement-output voltage at constant confining pressure of 22 kPa b) Displacement-output voltage at constant confining pressure of 800 kPa c) Displacement-confining pressure at fixed position of laser sensors.

2.5.7 Calibration of the measured volume change and the axial stress during shearing phase

Using the laser sensors to monitor the radial displacement, and also scan and measure the whole profile along the height of the sample, allows not only detecting the volume change but also detecting irregular and inhomogeneous deformation of the sample.

When the sample is subjected to shearing paths it approaches to the failure, deforming in a barrel shape. The positions of the laser sensors are fixed, measuring the radius at the middle of the sample.

The inhomogeneous deformation implies that the classical small-strain definition of the volumetric strain ε_v is not valid at shearing stage of the triaxial test as,

$$\varepsilon_v = \varepsilon_a + 2\varepsilon_r \tag{2.20}$$

where ε_a and ε_r are axial and radial strain measured at the center of the sample.

As a result, a different approach was used to obtain the volumetric strain of the sample at shearing stage. The entire height of the sample was sequentially scanned every few hours. The loading was not influenced by the scanning processes since the laser sensors were travelled the whole height of the sample in 30 seconds. The volume of the sample where then measured at different time intervals by means of the integration of the radius with respect to the height of the scanned profiles. Being the middle of the scanned profile as the originate of the coordinate,

$$V_i = \int_{-\frac{h_i}{2}}^{\frac{h_i}{2}} \pi {r_i}^2 \, dr \tag{2.21}$$

where V_i, h_i and r_i are the volume, height and the radius at i-th scanned profile.

The radius of the equivalent cylindrical sample $(\bar{r}_i)$ can be computed,

$$\bar{r}_i = \sqrt{\frac{V_i}{\pi h_i}} \tag{2.22}$$

Being r_0 the initial radius of the sample the equivalent radial strain $\bar{\varepsilon}_{ri}$ is,

$$\bar{\varepsilon}_{ri} = \frac{\bar{r}_i - r_0}{r_0} \tag{2.23}$$

If ε_r is the radial strain obtained from laser reading at fixed position and at the time of the i-th scnnaing, the correction parameter (C_i) is defined as,

$$C_i = \frac{\bar{\varepsilon}_{ri}}{\varepsilon_r} \tag{2.24}$$

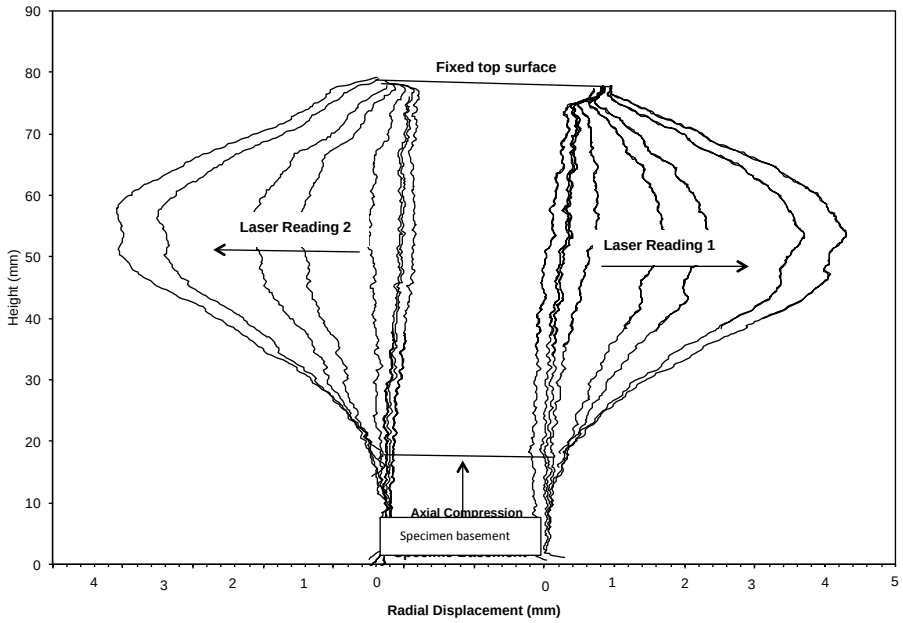

Figure 2.23. Scanned profiles of the sample at shearing stage of triaxial test (TxS50P200).

Accordingly, if the correction parameter obtained from different scanning profile plotted with respect to time, the time dependent correction parameter (C_t) can be obtained by fitting a curve to data points, as shown in Figure 2.24.

Consequently, the corrected volumetric strain (ε_{vol}) at shearing stage of the triaxial test is computed using the classical small strain equation, in which the radial strain is multiplied by correction factor,

$$\varepsilon_{vol} = \varepsilon_a + 2C_t\varepsilon_r \tag{2.25}$$

The area of the sample where the axial load is applied changes during shearing loading. Therefore, the axial stress has to be corrected by means of the current area of the sample. The equivalent area (A_{eq}) is computed as,

$$V_{eq} = \varepsilon_{vol}V_0 + V_0 \tag{2.26}$$

where V_{eq} is the current equivalent volume of the sample.

$$A_{eq} = \frac{V_{eq}}{h} \tag{2.27}$$

where h is the height of the sample.

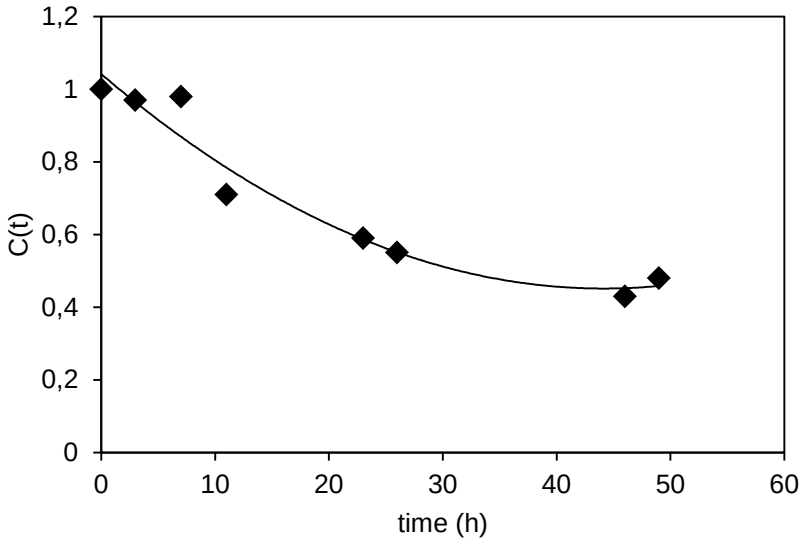

Figure 2.24. Evolution of the correction parameter with time (triaxial test TxS50P200).

And the axial stress is evaluated upon dividing the axial load by the equivalent area,

$$\sigma_a = \frac{F}{A_{eq}} \tag{2.28}$$

2.5.8 Calibration of pressure transducers and loading cell

Four pressure compressors were employed in for independent control of the air, water, cell and axial pressures. The pressure compressors of air pressure and cell pressure are pneumatic compressors whereas the axial pressure is controlled by hydraulic pressure compressor. The water pressure is also generated by pneumatic pressure but it the separation system transform the pneumatic to hydraulic one. This separation system involves a thick latex membrane located inside a small cell. The pneumatic unit is connected to the inside of the membrane, and the space between the membrane and the cell is filled with de-aired water, which is connected to the hydraulic unit (burette) of the triaxial equipment. Therefore, the pneumatic pressure is applied inside the membrane and transfer to the de-aired water through the membrane.

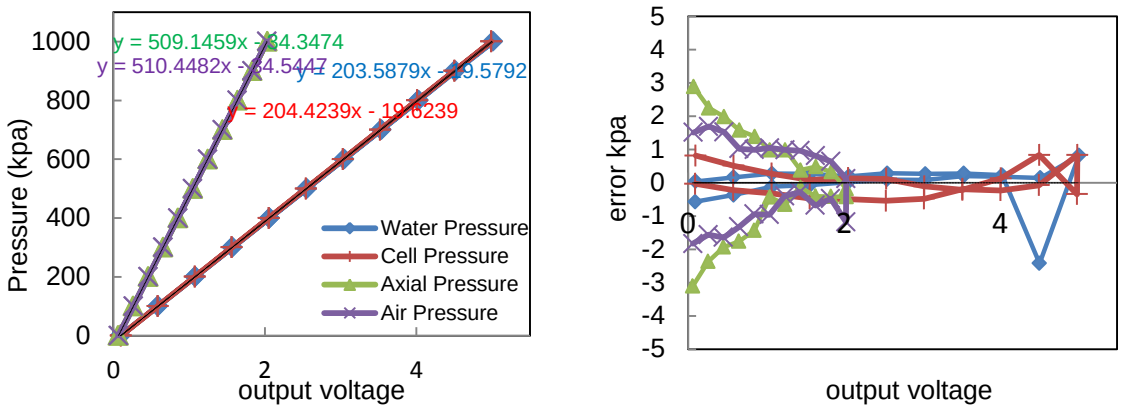

Figure 2.25. a) Calibration of water pressure transducers b) Offset error.

Accordingly, four pressure transducers were connected to these pressure compressors as well as data acquisition system. All transducers were calibrated using the Budenberg gauge equipment. This equipment allows applying the target pneumatic pressure to the transducer by means of equivalent dead weight. The calibration of transducers and the errors are plotted in the Figure 2.25 (a) and (b).

The Load cell is placed above the top cap of the sample and used to measure the applied axial force. The maximum capacity of the load cell was 22 KN, although the range of maximum axial force measured during the present experimental tests was substantially smaller. The load cell was calibrated using the certified load cell with high accuracy Figure (2.26).

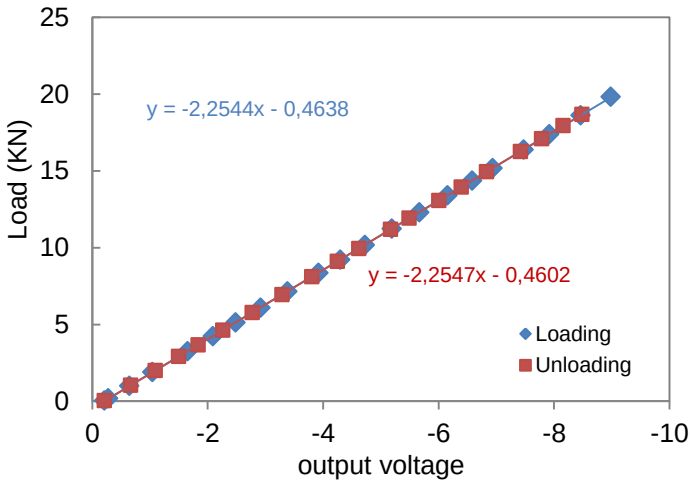

Figure 2.26. Calibration of load cell during loading and unloading

2.5.9 Measuring matric suction

All triaxial tests were performed using the axis translation technique, i.e. controlling the suction by means of independent control of air and water pressures. The axis translation technique was also employed to measure the suction for the triaxial tests performed at constant water content. The additional transducer was mounted at the same level of the sample and as close as possible to the sample to minimise the difference in hydraulic head of sample and transducer, and also, to shorten the water lines connected these two components. As previously mentioned, both ends of the sample are connected to burette. Two extra water lines, diverged from top cap and pedestal, extended the water circuit to air trap and the following three-ways valve, connected to the open atmosphere on one direction and the transducer on the other one. The valve turns to connect the transducer to the open atmosphere to regulate the pressure of transducer to zero at atmospheric pressure, whereas it turns to connect the transducer to the sample to measure the water pressure during the test. Providing the latter case in the water content tests, the water pressure was measured while the air pressure was kept constant, allowing to compute the suction by means of a difference between the imposed air and the measured water pressures.

2.5.10 Computation of required variables from triaxial test results

As previously explained, the confining pressure within the cell, air pressure and the water pressure are independently controlled during the experimental testing. The net axial stress (${\sigma_a}^{net}$) and net radial stress (${\sigma_r}^{net}$) variables are defined as,

$${\sigma_a}^{net} = \sigma_a - u_a \tag{2.29}$$

$${\sigma_r}^{net} = \sigma_r - u_a \tag{2.30}$$

The net mean stress (p^{net}) and deviatoric stress (q) are computed as,

$$p^{net} = \frac{{\sigma_a}^{net} + 2{\sigma_r}^{net}}{3} = p - u_a \tag{2.31}$$

$$q = {\sigma_a}^{net} - {\sigma_r}^{net} = \sigma_a - \sigma_r \tag{2.32}$$

The local axial strain is computed using the average value of axial strains measured by two miniature LVDTs,

$$\varepsilon_a = \frac{1}{2}(\varepsilon_{a1} + \varepsilon_{a2}) \tag{2.33}$$

being ε_{a1} and ε_{a2} are the local strain measured by each LVDTs.

The external axial strain (ε_{aEx}) is also computed measuring the axial displacement (Δh_{Ex}) by means of external LVDT,

$$\varepsilon_{aEx} = \frac{\Delta h_{Ex}}{h_0} \tag{2.34}$$

where h_0 is the initial height of the sample

Comparing the local axial strain and external axial strain showed that the difference between measured strains is negligible except for very small strain at the beginning of the shearing loading. In principal, local axial strains are more reliable for studying the properties of the soil, such as stiffness, at small strain.

The deviatoric strain is computed as,

$$\varepsilon_d = \frac{2}{3}(\varepsilon_a - \varepsilon_r) \tag{2.35}$$

The water content of the sample during constant water content shearing triaxial test remains unchanged. Therefore, the degree of saturation can be computed with respect to its initial value (S_{r0}) and volumetric strain,

$$S_r = S_{r0}(1 + \varepsilon_{vol}) \tag{2.36}$$

References

[1] Al Mukhtar, G., Belanteur, Tessier, and Vanapalli (1996). The fabric of a clay soil under controlled mechanical and hydraulic stress states. Applied Clay Sciences, 11:99–115.

[2] Alonso, E.E., Romero, E., Hoffmann, C., García-Escudero, E., 2005. Expansive bentonite–sand mixtures in cyclic controlled-suction drying and wetting. Eng. Geol. 81, 213–226.

[3] CARUSO M., STERPI D. (2011), Ritenzione idrica di un geomateriale a doppia porosità, Incontro Annuale dei Ricercatori di Geotecnica, IARG 2011, Torino

[4] Chao K.C., 2007, *Design principles for foundations on expansive soils*, Ph.D. Thesis, Colorado State University.

[5] Collins K, McGown A (1974) The form and function of microfabric features in a variety of natural soils. Ge´otechnique 24(2):223–254

[5] Cuisinier, O. and Laloui, L. (2004). Fabric evolution during hydromechanical loading of a compacted silt. International Journal for Numerical and Analytical Methods in Geomechanics, 28:483–499.

[6] Cuisinier, O., Masrouri, F., 2005. Hydromechanical behavior of a compacted swelling soil over a wide suction range. Eng. Geol. 81, 204–212.

[7] Danilatos GD (1993) Introduction to the ESEM instrument. Microsc Res Tech 25:354–361

[8] Delage, P., Audiguier, M., Cui, Y., and Howat, M. (1996). Miscrostructure of a compacted silt. Canadian Geotechnical Journal, 33:150–158.

[9] Delage, P. and Lefebvre, G. (1984). Study of the structure of a sensitive champlain clay and of its evolution during consolidation. Canadian Geotechnical Journal, 21:21–35.

[10] Delage P, Pellerin M (1984) Influence de la lyophilisation sur la structure d'une argile sensible du Quebec. Clay Miner 19:151–160

[11] Della Vecchia G. Coupled hydro-mechanical behaviour of compacted clayey soil. PhD Thesis, Politecnico diMilano 2009.

[12] Della Vecchia G, Jommi C, Romero E. A fully coupled elastic–plastic hydromechanical model for compacted soils accounting for clay activity. International Journal for Numerical and Analytical Methods in Geomechanics 2013; 37 (5):503–535

[13] Diamond, S. (1970). Pore size distributions in clays. Clays and Clay Minerals, 18:7–23.

[14] Donald, A.M. (2003). The use of environmental scanning electron microscopy

[15] Esteban, V. & Saez, J. (1988). A device to measure the swelling characteristics of rock samples with control of the suction up to very high values. Proc. ISRM Symposium on Rock Mechanics and Power Plants, Madrid, Vol.2.

[16] Fredlund, D. G. (1975). A diffused air volume indicator for unsaturated soils. CanadianGeotechnical Journal, 12: 533-539.

[17] Fredlund, D.G. and Rahardjo, H. (1993). Soil Mechanics for Unsaturated Soils, John Wiley and Sons, Inc., New York, NY.

[18] Harrison, B. & Blight, G. 1998. The Effect of Filter Paper and Psychrometer Calibration Techniques on Soil Suction Measurements. *Proceedings of the Second International Conference on Unsaturated Soils* 1, Beijing: International Academic Publishers: 362–367.

[19] Hilf, J. W. (1956). An investigation of pore water pressure in compacted cohesive soils. Technical Memo 654, Denver, Bureau of Reclamation.

[20] Juang CH, Holtz RD (1986a) Fabric, pore size distribution and permeability of sandy soils. J Geotech Eng ASCE 112(9): 855–868

[21] Leong, E., He, L. & Rahardjo, H. 2002. Factors Affecting the Filter Paper Method for Total and Matric Suction Measurements. *Geotechnical Testing Journal* 25(3): 322-333.

[22] Lloret, A., Villar, M.V., Sanchez, M., Gens, A., Pintado, X., Alonso, E.E., 2003. Mechanical behaviour of HAEVily compacted bentonite under high suction changes. Geotechnique 53 (1), 27–40.

[23] McKeen, R. G. (1980). "Field Studies of Airport Pavement on Expansive Clay," *Proceedings 4th International Conference on Expansive Soils,* Vol. 1, pp.242-261, ASCE, Denver, Colorado.

[24] Mitchell JK, Soga K (2005) Fundamentals of soil behaviour, 3rd edn. John Wiley, Sons, Inc, New Jersey

[25] Musso G, Romero E, Gens A, Castellanos E (2003). The role of structure in the chemically induced deformations of Febex bentonite. Appl Clay Sci 23:229–237

[26] Nowamooz, H., Masrouri, F., 2008. Hydromechanical behaviour of an expansive bentonite–silt mixture in cyclic suction-controlled drying and wetting tests. Eng. Geol. 101, 154–164.

[27] Prapaharan, S., Altschaeffl, A., and Dempsey, B. (1985). Moisture curve of a compacted clay: Mercury intrusion method. Journal of Geotechnical Engineering, 111(9):1139–1143.

[28] Romero, E. (1999). Thermo-hydro-mechanical behaviour of unsaturated Boom clay: an experimental study. PhD thesis, Universidad Politècnica de Catalunya, Barcelona, Spain.

[29] Romero, E., Della Vecchia, G. & Jommi, C. (2011). An insight into the water retention properties of compacted clayey soils. Ge´otechnique 61.

[30] Romero, E. and Simms, P. (2008). Microstructure investigation in unsaturated soils: A review with special attention to contribution of mercury intrusion porosimetry and environmental scanning electron microscopy. Geotechnical and Geological Engineering, 26:705–722.

[31] Simms, P. and Yanful, E. (2001). Measurement and estimation of pore shrinkage and pore distribution in a clayey till during soil-water characteristic curve tests. Canadian Geotechnical Journal, 38:741–754.

[32] Sivakumar, V. (1993). A critical state framework for unsaturated soils. PhD Thesis, University of Sheffield.

[33] Stokes, D.J. (2003). Recent advances in electron imaging, image interpretation and applications: environmental scanning electron microscopy. Phil. Trans. R. Soc. Lond. A 361, 2771–2787

[34] Vassallo, R. 2003. Comportamento di terreni costipati non saturi a piccole, medie e grandi deformazioni. Ph.D. thesis, University of Napoli Federico II, Naples, Italy.

[35] Washburn, E.W., 1921. The dynamics of capillary flow. Phys. Rev., 17, 273-283.

3

WATER RETENTION MODEL ACCOUNTING FOR HYSTERESIS OF HYDRAULIC AND MECHANICAL DRYING-WETTING CYCLES

3.1 Introduction

The behaviour of unsaturated soils and its constitutive modelling, is more complicated than the one of saturated soils not only because of the complex role of suction in mechanical and hydraulic behaviour, but also due to the fact that the hydraulic and mechanical behaviours of unsaturated soil are coupled. Many attempts have been paid to model accurately the hydraulic behaviour of unsaturated soils since its essential role to understand the comprehensive description of the hydromechanical behaviour was discovered, particularly, after adopting to be used instead of bishop parameter to introduce effective stress for modeling hydromechanical behaviour of unsaturated soil (e.g. Jommi, 2000; Nuth and Laloui 2008; Romero and Jommi, 2008; Buscarnera and Nova, 2009; Della Vecchia et al., 2012). In the present work, previously proposed models for hydraulic behaviour of unsaturated soil are briefly reviewed, and then, the effects of hysteresis of contact angle with respect to variation of suction and volume of soil is described.

Next, the water retention curve model accounting for the hysteresis of mechanical and hydraulic wetting-drying cycles was proposed. The experimental tests results were then presented to investigate the hysteresis of retention behaviour of clayey silt while subjected to hydraulic and mechanical wetting-drying cycles, and the results are compared to model predictions.

3.2 Soil Water Retention Curve

The relationship between the amount of water stored within the pores of an unsaturated soil, and suction is known as water retention curve (WRC). Different choices are possible to describe the quantity of stored water: e.g. gravimetric water content (w), volumetric water content (θ), degree of saturation (S_r).

Old WRC models (e.g. Gardner, 1958; Brooks & Corey, 1964; Campbell, 1974; van Genuchten, 1980; Fredlund and Xing, 1994) introduced a unique relationship between degree of saturation (for instance) and suction, which can be written as,

$$S_r = F(s) \tag{3.1}$$

These models were defined as simple but well applicable empirical equations which were easy to best fit the experimental data by employing few numbers of parameters. The experimental results showed that the hydraulic behaviour of unsaturated soil is influenced by its pore structure, which in turn also depends on mechanical variables. Changing in the mechanical variables influence the amount of water stored in pores at low suction range, for instance resulting in changing the air entry value in drying and air occlusion in wetting branches of water retention curves. Various models proposed accounting this aspect of WRC using different mechanical variables. These models may be written in a form:

$$S_r = F(s, \xi) \tag{3.2}$$

where ξ is the mechanical variable.

Different mechanical variables were proposed to incorporate in WRC models, i.e. soil volume, soil density or void ratio, volumetric strain, stress variable (e.g. Vanapalli et al., 1999; Gallipoli et al., 2003b; Sun et al., 2007; Nuth and Laloui, 2008; Tarantino, 2009; Maśin, 2010).

It indicates that main drying and main wetting branches in deformable soils can be then characterized by two surfaces, namely, the main drying and main wetting surfaces, in the S_r-s- ξ space, as shown in Figure 3.1. The intersection of the main drying and wetting surfaces with S_r- ξ plane at constant suction represent the main compression and the main swelling curves, respectively. On the other hand, their intersections with S_r-s plane at constant ξ represent the main wetting and the main drying curves.

The hysteresis associated with drying and wetting of soil ascertained that there is no unique soil WRC. There are numbers of transitional drying and wetting scanning curves bounded between main drying and main wetting surfaces, in which these scanning curves become asymptotic to the main bounding curves. Numerous models have been developed incorporating the hysteresis of soil WRC using the one-dimensional elastoplastic framework in a sense that the elastic (scanning) domain bounded within main curves employed as a yielding branches in S_r-s plane (e.g. Vaunat et al., 2000; Wheeler et al., 2003; Tamagnini, 2004; Sheng and Zhou, 2011).
The recent WRC models formulated with differential equations, which provide more capability to capture smooth nonlinear hydraulic hysteresis in scanning domain without distinction between elastic and plastic zones (e.g. Li X., 2005; Pedroso and Williams, 2010; Zhou et al., 2012). These models may be formulated in a rate form:

$$\dot{S_r} = F(s, \dot{s}) \tag{3.3}$$

Generally, the rate form of WRC model incorporating the mechanical dependency and hydraulic hysteresis may be represented as:

$$\dot{S_r} = F(s, \dot{s}, \xi) \tag{3.4}$$

It should be also noticed most above-mentioned rate form soil WRC models were proposed in which the scanning curves are computed by data-fitting methodology using the interpolation between the projections of suction (or degree of saturation) on main branches. Zhou (2013) proposed the contact angle-dependent hysteresis model interpreting the hydraulic wetting-drying hysteresis in terms of contact angle variation. The van Genuchten (1980) model was adopted to model the main drying curve, however, the scanning and the main wetting curves were simulated depending on the variation of contact angle due to hydraulic wetting and drying process.

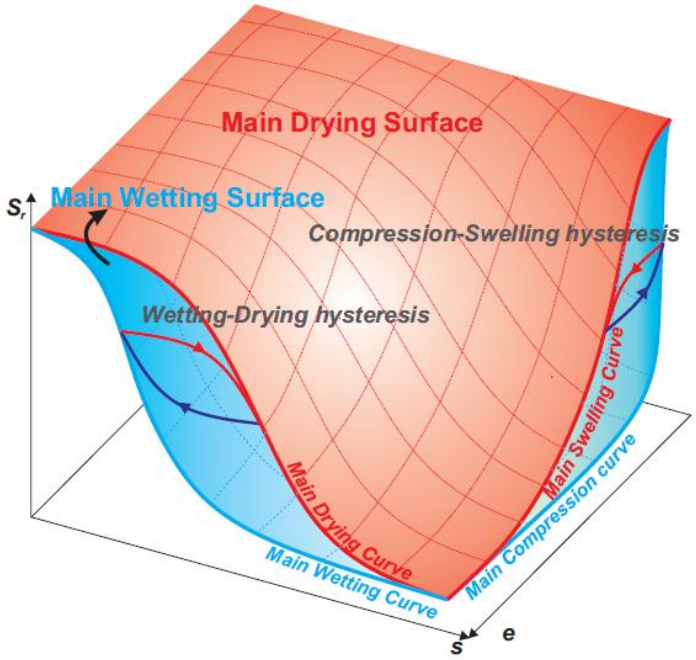

Figure 3.1. Main drying and Main wetting surfaces and hysteresis of hydraulic and mechanical wetting-drying cycles.

When suction is kept constant, loading and unloading induce irreversible change of degree of saturation. This implies that the hysteresis of degree of saturation is not only related to the change of suction, but also associated with the soil volume changes. Therefore, the soil WRC model needs to be able to take into account the hydraulic hysteresis caused by both wetting-drying cycles at constant void ratio (as an example of mechanical variable) and compression-swelling cycles at constant suction. However, only a few models have considered the hysteresis of mechanical wetting-drying (Khalili et al., 2008; Nuth & Laloui, 2008; Tarantino, 2009; Gallipoli, 2012).

3.3 Contact Angle Hysteresis

The hysteresis of hydraulic behaviour may be induced by several reasons as discussed by (e.g. Hillel 1998): “ink bottle” phenomena, i.e. the non-uniform geometry of pores; the entrapment of air in irregular shaped pores; swelling and shrinkage, and variation of the liquid-solid contact angle. The latter effect is adopted in this research to be only responsible for the hysteresis of WRC. In fact, the dominant reason induces hysteresis in the water retention behaviour of unsaturated soil has not been thoroughly recognized yet and it is reasonable to ascribe the hysteresis behaviour to a single effect for the aim of simplicity and decrease of WRC model parameters.

The contact angle (θ) is defined as the angle formed by the intersection of the liquid-solid and the liquid-vapour interfaces. As explained by Gao and McCarthy (2006), the contact angle takes place between the maximum (Advancing, θ_A) and minimum (Receding, θ_R) contact angles $\theta_R \leq \theta \leq \theta_A$, and the difference between θ_A and θ_R is defined as the contact angle hysteresis. The contact angle hysteresis consists of two components: static and dynamic. The static hysteresis of contact angle, which arises from surface roughness and heterogeneity (Johnson and Dettre, 1964), is dominant for slow-moving liquid on rough solid surfaces and the dynamic hysteresis can be neglected (Rotenberg et al., 1984). This implies that the advancing and receding contact angles can be assumed to be remained constant for the liquid-solid interface in unsaturated soil.

Figure 3.2 shows two assumed spherical soil particles connected by a liquid bridge. The hydraulic wetting-drying is displayed in which the position of the soil particles remains unchanged, implying the total volume of the soil remains constant. When the amount of water and the volume of the liquid bridge increase during wetting, the position of the meniscus curvature remains constant and the contact angle increases. Once the contact angle reaches the advancing contact angle, the meniscus curvature starts to move upward while the contact angle ($\theta=\theta_A$) remains constant. In contrast, when the amount of water and the volume of the liquid bridge decrease during drying, the contact angle reduced to the receding contact angle. For further drying, it remains constant ($\theta=\theta_A$) and the meniscus curvature starts to move backward (Figure 3.2 (a) and (b)). The process in which position of the meniscus curvature remains constant is called pinning, whereas the process in which the contact angle remains constant is called slipping.

The contact angle hysteresis does not only occur during hydraulic drying and wetting, but it also occurs when the total volume of the soil is changing. The contact angle variation during compression and swelling of the soil can be resembled by moving toward (Figure 3.2 (c)) and backward (Figure 3.2 (d)) of the soil particles, respectively. When the soil volume decreases (mechanical wetting), the pinning occurs (θ increases to θ_A) and then it is followed by slipping ($\theta=\theta_A$ remains constant) similar to hydraulic wetting.

On the other hand, when the soil volume increases (mechanical drying) the pinning occurs (θ decreases to θ_R), and it is then followed by slipping ($\theta=\theta_R$ remains constant) similar to hydraulic drying.

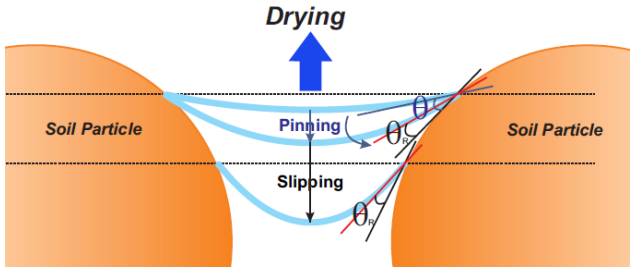

(a)

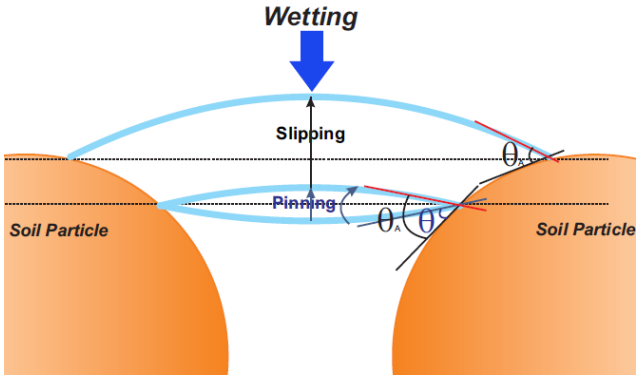

(b)

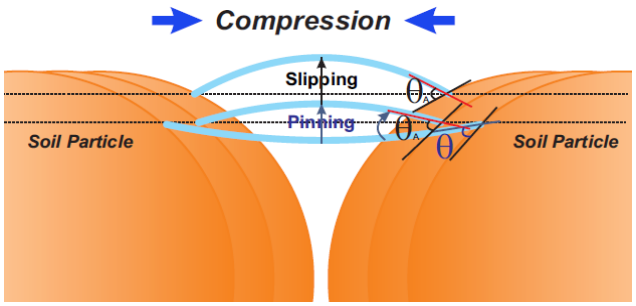

(c)

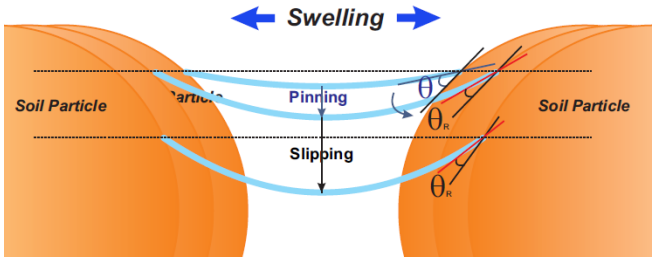

(d)

Figure 3.2. Contact angle variation due to a) drying b) wetting and c) compression d) swelling.

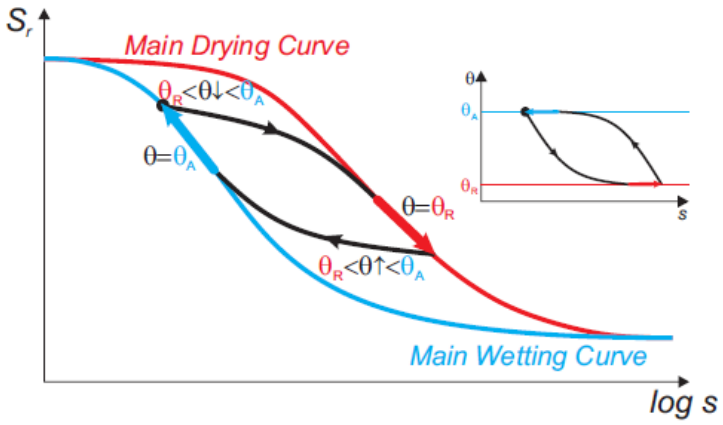

(a)

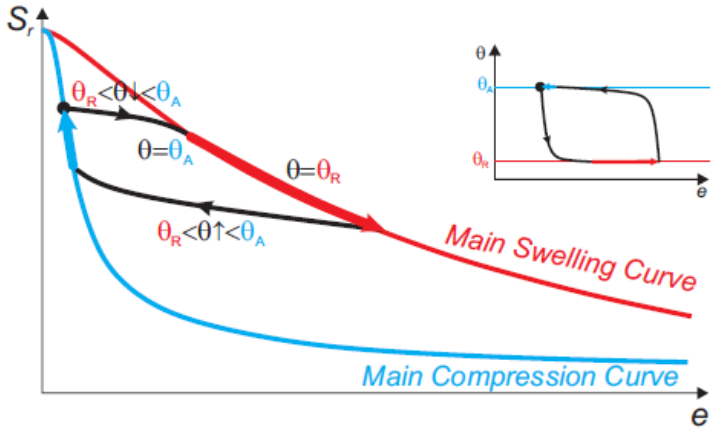

(b)

Figure 3.3. (a) Main drying and wetting curves in S_r-log(s) plane (b) Main swelling and compression curves S_r-e plane.

As shown in Figure 3.3 (a) and (b), the contact angle varies between the advancing and receding contact angles (pinning) during hydraulic and mechanical wetting-drying in a scanning domain, but it remains constant at θ_A for further wetting or compression for main wetting surface, and at θ_R for further drying or swelling for main drying surface.

In the present work, the contact angle-dependent hysteresis WRC model proposed by Zhou (2013) was enhanced incorporating the dependency of contact angle and the WRC on mechanical behaviour of the soil. The contact angle approach is integrated in Galipolli's WRC model (2003b), which is adopted as a reference model to reproduce the main drying branch. The incremental equation is derived introducing the hysteresis functions, which control the hysteresis of WRC induced by wetting-drying and compression-swelling cycles.

3.4 Contact Angle-Dependent Water Retention Model for Deformable Soils

As proposed by Zhou (2013), a relationship between the arbitrary suction (s) and the suction on the main drying branch (s_d) of WRC can be derived from the integration of the pore size distribution function ($f(r)$) of soil. The integration of relative frequency of the pores, whose sizes bound between minimum radius (R_{min}) and maximum radius (R_{max}) gives,

$$\int_0^{\infty} f(r)dr = \int_{R_{min}}^{R_{max}} f(r)dr = 1 \tag{3.5}$$

Hence, the cumulative function $F(R)$ measures the amount of pores, whose radius is smaller than R, and, by definition,

$$F(R) = \int_{R_{min}}^{R} f(r)dr \tag{3.6}$$

Different classes of pores can be assumed being sequentially filled starting from smallest one during the wetting process. This is true if the pores characterized by a bundle of different sized cylindrical tubes disregard the connectivity between the pores. The current degree of saturation ($Sr(R)$) can be then identified if the pores between R_{min} and any arbitrary radius R are filled with water,

$$S_r(R) = \int_{R_{min}}^{R} f(r)dr = F(R) \tag{3.7}$$

The arbitrary pore radius R can be calculated using the inverse of cumulative function of soil pores,

$$R = F^{-1}(S_r(R)) \tag{3.8}$$

If degree of saturation is assumed to be equal for the arbitrary suction (s) and the suction on the main drying branch (s_d), they can be computed using the capillary law, in which the contact angles for (s) and (s_d) are θ and θ_R, respectively,

$$s = \frac{2\sigma\, cos\theta}{R} = \frac{2\sigma\, cos\theta}{F^{-1}(S_r(R))} \tag{3.9}$$

$$s_d = \frac{2\sigma cos\theta_R}{R} = \frac{2\sigma cos\theta_R}{F^{-1}(S_r(R))} \tag{3.10}$$

As a result, the relationship between (s_d) and (s) depends on contact angles at arbitrary suction θ and main drying suction θ_R,

$$s_d = \frac{scos\theta_R}{cos\theta} \tag{3.11}$$

The derived equation for main drying suction is integrated to the WRC model proposed by Galipolli (2003b); i.e., the modified van Genuchten (1980) WRC model incorporating the effect of mechanical variable by introducing the dependence of the air entry value parameter on void ratio,

$$S_r = \left[1 + (\frac{e^{\alpha} s_d}{\omega})^n\right]^{-m} \tag{3.12}$$

where n, m, α and ω are model parameters.

Replacing the s_d according to equation (3.11) yields to,

$$S_r = \left[1 + (\frac{e^{\alpha} scos\theta_R}{\omega cos\theta})^n\right]^{-m} \tag{3.13}$$

The incremental formulation of equation (3.13) can be obtained by differentiation with respect to s, e and θ due to the fact that the $\dot{S_r}$ is caused by changes in suction, void ratio and contact angle,

$$\dot{S_r} = \frac{\partial S_r}{\partial s}\dot{s} + \frac{\partial S_r}{\partial e}\dot{e} + \frac{\partial S_r}{\partial \theta}\dot{\theta} \tag{3.14}$$

The differentiation of equation (3.12) gives,

$$\frac{\partial S_r}{\partial s} = -\frac{mn}{s}\left(\frac{e^{\alpha}scos\theta_R}{\omega cos\theta}\right)^n \left[1 + \left(\frac{e^{\alpha}scos\theta_R}{\omega cos\theta}\right)^n\right]^{-m-1} = \frac{\phi}{s} \tag{3.15}$$

$$\frac{\partial S_r}{\partial e} = -\frac{mn\alpha}{e}\left(\frac{e^{\alpha}scos\theta_R}{\omega cos\theta}\right)^n \left[1 + \left(\frac{e^{\alpha}scos\theta_R}{\omega cos\theta}\right)^n\right]^{-m-1} = \alpha\frac{\phi}{e} \tag{3.16}$$

$$\frac{\partial S_r}{\partial \theta} = -mn\tan\theta\left(\frac{e^{\alpha}scos\theta_R}{\omega cos\theta}\right)^n \left[1 + \left(\frac{e^{\alpha}scos\theta_R}{\omega cos\theta}\right)^n\right]^{-m-1} = \phi\, tan\theta \tag{3.17}$$

where ϕ defines as $\phi = -mn(\frac{e^{\alpha}s\, cos\theta_R}{\omega\, cos\theta})^n \left[1 + (\frac{e^{\alpha}s\, cos\theta_R}{\omega\, cos\theta})^n\right]^{-m-1}$ for simplification. Hence, the incremental formulation of degree of saturation can be rewritten as,

$$\dot{S_r} = \frac{\phi}{s}\dot{s} + \alpha\frac{\phi}{e}\dot{e} + \phi\, tan\theta\, \dot{\theta} \tag{3.18}$$

The contact angle can change with suction and void ratio,

$$\dot{\theta} = \frac{\partial \theta}{\partial s}\dot{s} + \frac{\partial \theta}{\partial e}\dot{e} \tag{3.19}$$

Equation (3.14) can be rearranged to

$$\dot{S_r} = (\frac{\partial S_r}{\partial s} + \frac{\partial S_r}{\partial \theta}\frac{\partial \theta}{\partial s})\dot{s} + (\frac{\partial S_r}{\partial e} + \frac{\partial S_r}{\partial \theta}\frac{\partial \theta}{\partial e})\dot{e} \tag{3.20}$$

$$\dot{S_r} = \frac{\phi}{s}\left[1 + \frac{\partial\theta}{\partial s} s \tan\theta\right]\dot{s} + \alpha\frac{\phi}{e}\left[1 + \frac{\partial\theta}{\partial e}\frac{e\tan\theta}{\alpha}\right]\dot{e} \tag{3.21}$$

Comparing equation (3.21) with equation (3.15) and (3.16) implies that the first part of equation (3.21) contributes in change of degree of saturation when the suction changes, in which the term $(\frac{\partial\theta}{\partial s} s \tan\theta)$ is employed to generate the hysteresis of hydraulic behaviour for wetting-drying cycles and it takes a form similar to the reference contact-angle model.

On the other hand, the second part contributes when the void ratio changes, whereas the hysteresis due to compression-swelling cycles is introduced in terms of $(\frac{\partial\theta}{\partial e}\frac{e\tan\theta}{\alpha})$. If the differential of contact angle with respect to suction and void ratio represents as follow,

$$\frac{\partial\theta}{\partial s} = -{H_\theta}^s\left(\frac{1}{s\tan\theta}\right) \tag{3.22}$$

$$\frac{\partial\theta}{\partial e} = {H_\theta}^e\left(\frac{\alpha}{e\tan\theta}\right) \tag{3.23}$$

The equation (3.21) can be rewritten as,

$$\dot{S_r} = \frac{\phi}{s}[1 - {H_\theta}^s]\dot{s} + \alpha\frac{\phi}{e}[1 - {H_\theta}^e]\dot{e} \tag{3.24}$$

The represented hydraulic hysteresis function ${H_\theta}^s$ is assigned to the portion of degree of saturation and it corresponds to hysteresis of soil water retention behaviour due to suction variation, while the mechanical hysteresis function ${H_\theta}^e$ corresponds to hysteresis of soil water retention behaviour due to void ratio variation. These hysteresis functions obey the same restrictions to resemble the hysteresis behaviour. When ${H_\theta}^s$ and ${H_\theta}^e$ are equal to 1, there is no change in degree of saturation and the entire changes in degree of saturation consumed by contact angle variation.

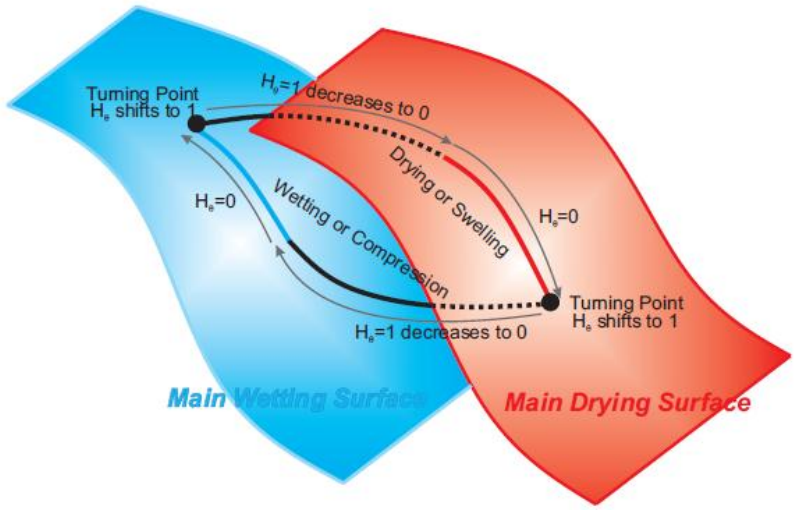

Figure 3.4. Evolution of Hysteresis function during wetting-drying and swelling-compression

This generates the straight horizontal scanning line in which the degree of saturation remains constant whereas the suction or void ratio changes. However, when they are equal to zero, the contact angle does not contribute in variation of degree of saturation and the WRC follows the main wetting-drying branches according to equation (3.12); i.e., where the contact angle is equal to the receding or advancing contact angle. Therefore, variation of degree of saturation consumes partially by changing of contact angle as the hysteresis functions moves from 1 to 0 during wetting-drying or compression-swelling processes (Figure 3.4). It means that the hysteresis functions have to be defined in such a way that their value remains zero at main wetting-drying or compression-swelling branches, whereas they shift to 1 at any turning point, where the drying turns to wetting or compression turns to swelling, and vice versa. It can also be understood that when the contact angle is equal to receding contact angle at main drying branch, it remains at main drying surface for following swelling process since the swelling affect the contact angle in the same way as the drying process, so the hysteresis function is not needed to turn. However, it moves toward main wetting surface if it follows the compression as the compression cause that the contact angle varies from receding to advancing contact angle so the hysteresis function is needed to turn. The opposite process can also be justified for the main wetting branch. As a result, the hysteresis functions can take the same mathematical form for drying and swelling or wetting and compression. The logarithmic equations are proposed hereby in the same format for drying and swelling or wetting and compression for the aim of simplicity. However, it is worthwhile to obtain physical model for hysteresis functions based on geometrical mechanic relationship between soil particles and connecting liquid bridges.

$$H_\theta = {H_\theta}^s = {H_\theta}^e = \left[\frac{\log\left(\frac{cos\theta}{cos\theta_R}\right)}{\log\left(\frac{cos\theta_A}{cos\theta_R}\right)}\right]^\beta \quad \dot{s} > 0\,, \dot{e} > 0 \tag{3.25}$$

$$H_\theta = {H_\theta}^s = {H_\theta}^e = \left[\frac{\log\left(\frac{cos\theta_A}{cos\theta}\right)}{\log\left(\frac{cos\theta_A}{cos\theta_R}\right)}\right]^\beta \quad \dot{s} < 0\,, \dot{e} < 0 \tag{3.26}$$

where β is the parameter of the model.

By trial and error, it was experienced that the logarithmic equation allows using the same exponent (β) for hydraulic and mechanical hysteresis. However, using different parameters are suggested to be used for the hydraulic and mechanical hysteresis functions if the hydraulic and mechanical hysteresis behaviours are considerably different.

It is also can be cited that such a model can be represented in a rate form as,

$$\dot{S_r} = F(s, e, \theta, \dot{\theta}) \tag{3.27}$$

where changing in contact angle depends on changing of suction and voids ratio,

$$\dot{\theta} = f(\dot{s}, \dot{e}) \tag{3.28}$$

3.5 Calibration of Parameters

Considering equation (3.22) and (3.23), it can be understood that the contact angle varies in a domain between two horizontal planes created by θ_A and θ_R in a θ-s-e space. The contact angle remains at upper plane $(\theta = \theta_A)$ when the soil is at main wetting surface, and it remains at lower plane $(\theta = \theta_R)$ when the soil is at main drying surface. The contact angle varies accordingly between these two planes corresponding to scanning curves of water retention behaviour. The receding contact angle is assumed to be zero, as suggested by the reference contact-angle model, because it is very low in most soils. The main drying surface is modeled using the parameters of the adopted reference model (Galipolli, 2003b)

calibrated with respect to the main drying curve and compression line (n,m,α,ω). Therefore, the proposed model employs two additional parameters (θ_A, β). Although these two parameters are similar to parameters of the reference contact-angle model, but they are employed to predict the soil water retention behaviour in S_r-s-e space including the main surfaces, nonlinear scanning curves and hysteresis of mechanical wetting-drying cycles as well as the hydraulic hysteresis in scanning domain. These parameters can be calibrated providing the best fitting least-square procedure in S_r-s-e. The advancing contact angle (θ_A) can be calibrated using the wetting surface, incorporating the result of compression test (mechanical wetting) and hydraulic wetting. It controls the position of main wetting surface, which can be displayed as the main wetting and the main compression curves in S_r-s and S_r-e planes, respectively. If the advancing contact angle is the only parameter employed to reproduce main wetting surface, the model is more applicable where the main wetting and main drying curves follow similar trends. If the slope of the main wetting and main drying curves are different, independent n parameters proposed to be adopted for drying (n_d) and wetting (n_w), as it was used in the present work.

If the θ_R is assumed to be zero and $\theta = \theta_A$ at wetting surface, equation (3.13) for wetting curve can be rewritten,

$$S_r = \left[1 + \left(\frac{e^{\alpha} s}{\omega cos\theta_A}\right)^n\right]^{-m} \tag{3.29}$$

It implies that the wetting branch is predicted incorporating the effect of contact angle on air entry value of drying branch. Therefore, the air entry and air occlusion values can be used to initially estimate the advancing contact angle, and it can be then improved by best fitting approach,

$$\theta_A = Arccos\left(\frac{\omega_{ao}}{\omega_{ae}}\right) \tag{3.30}$$

where ω_{ao} and ω_{ae} are air occlusion and air entry values, respectively. The water retention behaviour of Viadana silt was investigated in the present research, and the resulting experimental behaviour was predicted by the proposed model. The air entry and air occlusion values for Viadana silt were obtained to be 44 kPa and 5 kPa for drying and wetting curves obtained from water retention test. Therefore, equation 3.30 gives θ_A equal to 83.5 degree, which can be used as a first

assumption. The advancing contact angle θ_A was obtained to be 85.6 after fitting the predicted wetting curve of the model to the experimental wetting trend.

The parameter β controls the rate of the contact angle variation, and as a result, governs the curvature of the scanning curve in S_r-s and S_r-e planes. A single parameter is employed to account for hydraulic and mechanical hysteresis so this parameter (β) can be calibrated using a scanning curve due to either change of suction while the void ratio is kept constant or change of void ratio while the suction is kept constant.

As proposed by van Genuchten (1980), parameter m can be considered dependent on parameter n,

$$m = 1 - \frac{1}{n} \tag{3.31}$$

The parameters in Table 3.1 are used in this work to simulate the water retention behaviour of tested material.

Table 3.1. Parameters of the proposed model for Viadana silt

Parameters	n_d	n_w	ω	α	θ_A	β
Viadana silt	1.41	1.23	5.11	6.51	84.2	0.46

3.6 Experimental Work

3.6.1 Tested Material and Sample Preparation

The soil used in the experimental study was clayey silt, called “Viadana silt”. The pore size distribution showed the silt fraction is 77.6%, whereas the clay fraction is 22.4%. Moreover, grain specific gravity (G_s), liquid limit (w_l) and plasticity index (PI) were found to be 2.735, 32.6% and 8.3%, respectively.

All samples were prepared using the static compaction technique. First, the dry soil powder was hand-mixed with demineralized water to reach the target water content. It was then sealed in a plastic bag and placed in a humid container for 48 hours allowing the water content equilibration. Next, the moist powder was placed in a hermetic mould, being the dimensions of cylindrical oedometric sample (50 mm of height and 20 mm of diameter).

It was then compacted using Farrance Wykeham loading frame, in which the static force was gradually applied to the sample until the desired volume, corresponding to the size of oedometer sample, was achieved, under controlled water content.

3.6.2 Experimental Equipment and Techniques

The suction controlled oedometer apparatus and axis translation technique were used to perform tests in which the imposed and measured suction was smaller than 400 kPa. As shown in Figure 3.5 (a), the HAEV ceramic disk is placed at the bottom of suction controlled oedometer, where the water pressure is applied. The air pressure is applied to the upper coarse porous stone through a conduit in the loading cap which is separated by a thick rubber membrane from the vertical loading platen. In order to measure the suction in constant water content test, the valve, placed between the water volume meter and the water pressure transducer, turns to close. This allows measuring the water pressure while the air pressure remains constant.

The vapour equilibrium technique was also used to study the water retention behaviour of Viadana silt when the samples were subjected to suction greater than 4 MPa (Figure 3.5(b)). The samples were removed from oedometer apparatus and placed in a closed desiccator, where the samples supported by a rigid wire above a saturated solution. Different saturated solutions were used to control the relative humidity (RH) of air in the closed desiccator. The weight and the size of sample were frequently measured. The sample was kept in contact in each solution about one month to achieve the equilibrium. The RH and suction corresponding to the saturated solutions are listed in Table 3.2, as reported by Romero (2001).

Table 3.2. Saturated solution and corresponding suction at temperature at 25 °C (Romero, 2001)

Compound	RH(%)	Total suction (MPa)
K_2SO_4	97	4
KNO_3	92	11
KCl	84	24
$NaNO_3$	74	41
$Ca(NO_3).4H_2O$	51	92

3.6.3 List of Tests

Oedometer tests were carried out in the present research to study the hysteresis of water retention behaviour and evaluate the capability of the proposed model. Characterizations of these tests are represented in Table 3.3. Test Oe-WR and test Oe-LU were performed to obtain main drying and main wetting curves by means of changing suction at the constant axial net stress, and detect the main compression curve where axial net stress increased at constant suction, respectively. The scanning curves were also detected for cycles of wetting-drying and loading-unloading. Parameters of the model were calibrated using the experimental behaviour observed in these two tests. Two other tests were performed (Oe-DW and Oe-LU-CW) in which the experimental results compared to predictions of the model employing the same parameters previously calibrated. The specimen of test Oe-DW was prepared at lower density (higher porosity) compared to the specimen of test Oe-WR in order to evaluate the capability of the model to predict the water retention behaviour while the volume change (void ratio change) also considerably contributes in wetting-drying cycles. The last test (Oe-LU-CW) was performed in which the specimen were subjected to the cycles of loading-unloading at constant water content while the suction was measured. The model was then employed to predict suction values with respect to the variation of void ratio, and in turn degree of saturation, while the water content remained unchanged.

Table 3.3. List of tests

Test Title	Preparation		Initial Condition		Loading Path		
	γ_d gr/cm^3	w %	s kPa	$\sigma_{1\ net}$ kPa	s kPa	$\sigma_{1\ net}$ kPa	Water Drainage
Oe-WR	1.65	20.2	10	20	10→350→50 →92000→10	Constant	Open
Oe-LU	1.39	23.3	50	10	Constant	10→600→10 →1600→10	Open
Oe-DW	1.38	24.6	400	10	400→10→400→5	Constant	Open
Oe-LU-CW	1.37	24	200	10	Measured	10→150→10 →500 →10→1500 →10	Close (Constant w)

3.7 Experimental Results and Model Validation

3.7.1 Test Oe-WR and Model Prediction

Figure 3.5 shows result of suction controlled test performed to study the water retention behaviour of Viadana silt. Test Oe-WR was carried out on a sample compacted at water content of 20.2% and dry density of 16.5 KN/m^3. The sample was placed in oedometer and subjected to axial net stress of 50 kPa while the imposed suction was 10 kPa. The water retention was obtained by increasing suction to 350 kPa, followed by wetting-drying cycle where suction decreased to 50 kPa and then increased to 400 kPa.

The sample was then removed from the odometer and placed in the desiccator with relevant saturated solutions in order to study the water retention behaviour of Viadana silt for greater values of suction in both drying and wetting paths. The wetting path was continued by placing back the sample in oedometer and decreasing suction from 400 kPa to 10 kPa. Applied wetting-drying path is shown in Figure 3.5 (a). The main drying and wetting branches and also scanning curves associated with hydraulic hysteresis were obtained, as shown in Figure 3.5 (b).

As shown in Figure 3.5 (b), the proposed model was used to predict the values of degree of saturation corresponding to the imposed suction where experimental void ratio was adopted in numerical computation for the same experimental water retention path. Moreover, Figure 3.5 (c) shows the evolution of the contact angle with suction and void ratio during wetting-drying paths. However, the volume change of the sample was inconsiderable and the variation of contact angle and irreversible change of degree of saturation in turn, was mostly resulted from variation of suction.

It can be observed the contact angle was equal to receding contact angle for the initial drying process (lower plane), but wetting-drying hysteresis in scanning domain resulted from an increment and reduction of contact angle. Its value then decreased to lower plane for further drying. As the sample was subjected to wetting, the contact angle increased to advancing contact angle (upper plane) and it remained constant for the main wetting curve. The model was able to consistently predict the main wetting curve and the hysteresis of water retention regarding to the variation of contact angle.

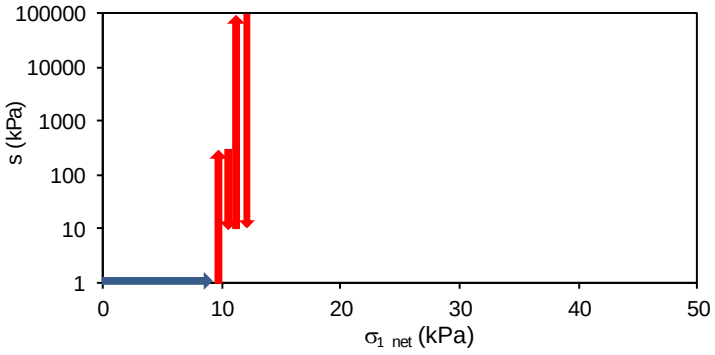

(a)

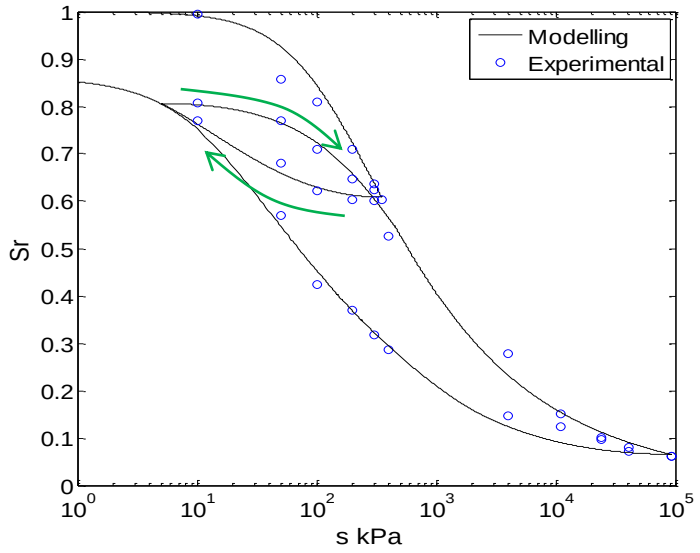

(b)

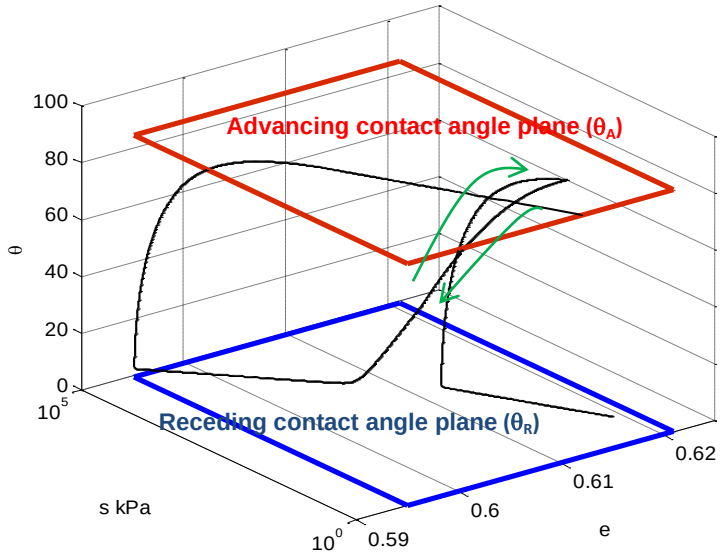

(c)

Figure 3.5. Computed and experimental behaviour during wetting–drying cycles (a) Applied stress path (b) S_r–log(s) (c) Evolution of contact angle with suction and void ratio

3.7.2 Test Oe-LU and Model Prediction

Figure 3.6 illustrates the test result of loading-unloading cycles at constant suction of 50 kPa (Oe-LU). The sample was prepared at low dry density (1.392 gr/cm^3) and water content (23.3%). First, the sample was subjected to suction of 50 kPa while the initial axial net stress was 10 kPa. The sample was dried and contracted due to initial drying path resulted from the increase of initial suction at preparation to the imposed suction of 50 kPa.

The first cycle of loading-unloading was then applied by increasing the axial net stress to 600 kPa followed by decreasing to 10 kPa. Next, the sample was reloaded by increasing the axial net stress to 1600 kPa, and lastly, unloaded by decreasing the axial net stress to 10 kPa. The suction was kept constant at 50 kPa when the loading-unloading cycles were applied (Figure 3.6 (a)). The void ratio decreased during loading as the axial net stress increased (Figure 3.6 (b)), and resulted in the rise of degree of saturation implying the sample was mechanically wetted.

The rate of increase of degree of saturation was smaller at the beginning where the water retention was in scanning domain, but it increased as it followed the main wetting surface for further volume reduction. The degree of saturation gently decreased due to volume expansion during unloading, implying the mechanical drying. The mechanical hysteresis and irreversible change of degree of saturation can be observed when the sample was subjected to compression-swelling cycle (Figure 3.6 (c)).

Figure 3.6 (c) shows also the computed degree of saturation using the proposed WRC model, where the void ratio corresponding to the applied axial net stress, was adopted. The experimental results and model prediction are also plotted in S_r-e plane, as shown in Figure 3.6 (d). It can be observed that the water retention took place in scanning domain during unloading-reloading cycle, which was predicted by the model regarding the change of contact angle (Figure 3.6 (e)).

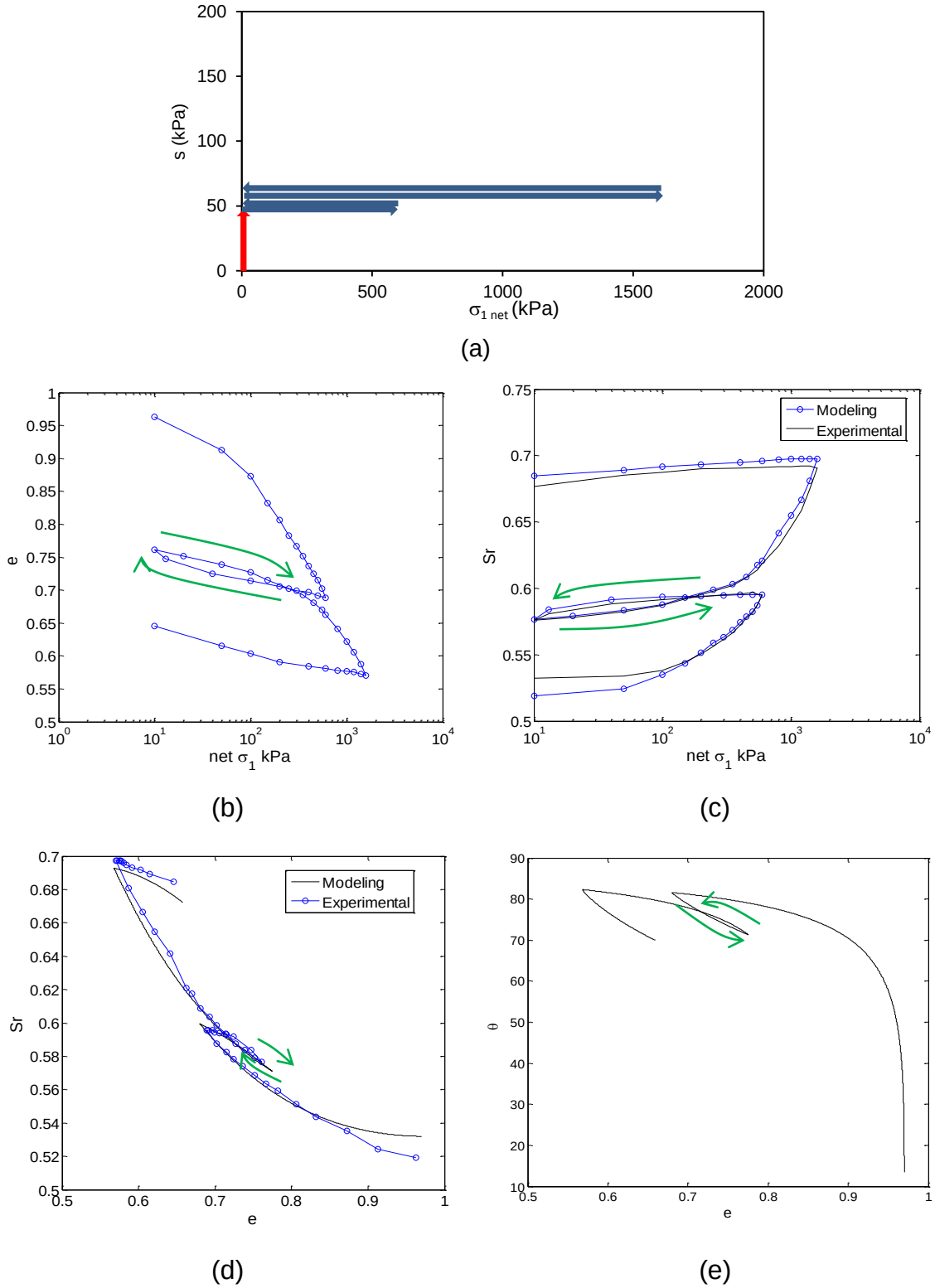

Figure 3.6. Loading–unloading cycles at constant suction of 50 kpa (a) Applied stress path (b) Experimental behaviour in e–σ_{1net} plane Comparing experimental and modelling results in (c) S_r–σ_{1net} plane (d) S_r–e plane (e) Evolution of contact angle with void ratio

3.7.3 Test Oe-DW and Model Prediction

In order to study the experimental behaviour and the model performance where both mechanical and hydraulic hysteresis contributes in water retention behaviour, two cycles of wetting-drying were applied to the loose sample of Viadana silt while the axial net stress was kept constant at 10 kPa (test Oe-DW). The sample was prepared at dry density of 1.381 gr/cm^3 and water content of 24.6%. It was placed in oedometer and subjected suction of 400 kPa in order to establish the initial condition of the test. The first cycle included wetting, i.e., decreasing suction from 400 kPa to 10 kPa, followed by increasing suction to 400 kPa. The second cycle included decreasing suction to 5 kPa and then increasing to 400 kPa. The applied stress path is plotted in Figure 3.7 (a).

Figure 3.7 (b) shows the measured and computed variation of degree of saturation with suction and void ratio. The main drying and wetting curves varied during wetting-drying cycles because of the continuous change of void ratio.

The degree of saturation increased in scanning domain, approaching to the main wetting surface while the sample showed volume collapse during the first wetting path. The hydraulic state was moved to scanning domain as the sample subjected to drying process. The degree of saturation increased earlier for the second wetting path because the sample experienced smaller void ratio leading to shift of main wetting curve to an upper position in the main wetting surface. Consequently, the contact angle also reached the advancing contact angle earlier. Figure 3.7 (c) shows the evolution of contact angle in θ-s-e space, indicating that the irreversible change of contact angle allowed the model to properly capture the transition between scanning domain and main wetting surface, which was consistent to the experimental results.

3.7.4 Test Oe-LU-CW and Model Prediction

The last test was performed where the sample was subjected to loading-unloading cycles at constant water content (Oe-LU-CW). The dry density and the water content of the sample at preparation was 1.37 gr/cm^3 and 24%, respectively. The sample was placed in oedometer and the suction increased to 200 kPa while the axial net stress was 10 kPa. After the equilibrium of the imposed suction, the water drainage was closed and the water pressure was measured using the transducer connected to the water within the sample.

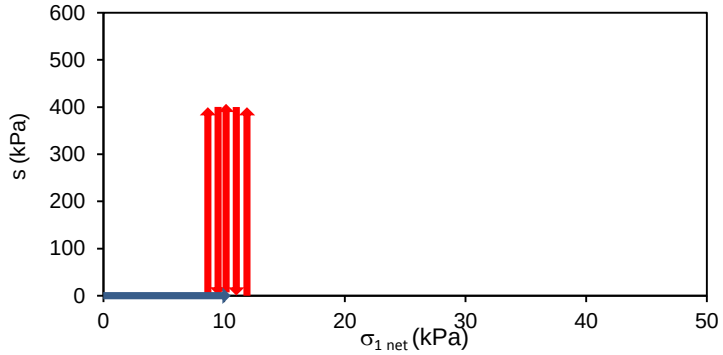

(a)

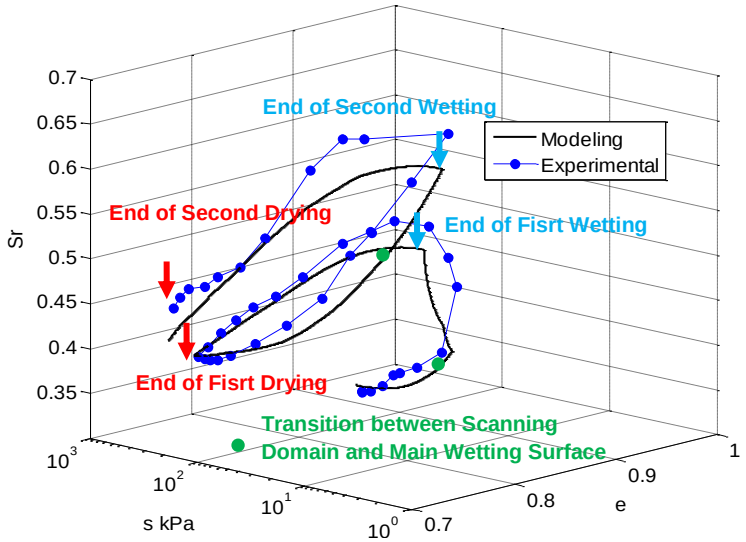

(b)

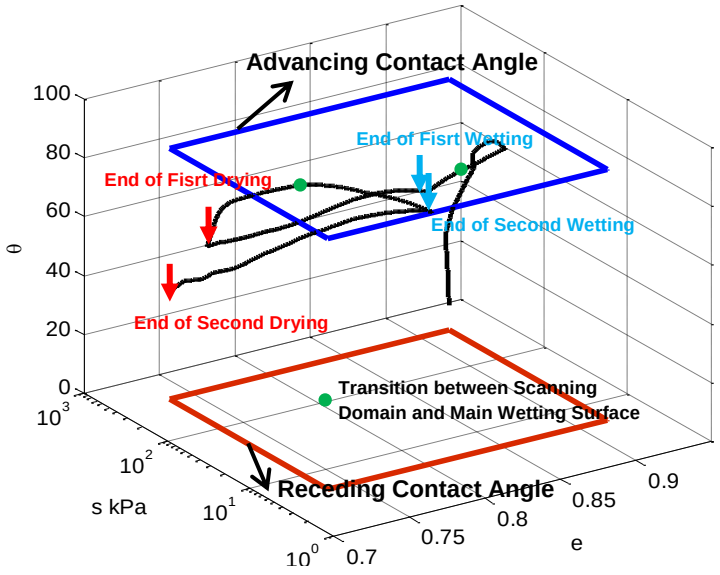

(c)

Figure 3.7. Comparing experimental behaviour and modelling prediction during drying–wetting cycles at constant axial net stress (a) Applied stress path (b) S_r–s-e space (c) θ–s-e space

Then the sample was subjected to loading-unloading cycles of 150, 500, 1500 kPa, where the water content remains constant at 11.8%, as shown in Figure 3.8 (a). The air pressure remained constant and the suction were computed from the difference between the imposed air pressure and measured water pressure. The load increment and reduction was applied very slowly to guarantee that the measured water pressure was in equilibrium with the water pressure of the porous stone and water pressure within the soil sample.

As shown in Figure 3.8 (b) and 8 (c), the suction was increased within the soil as the sample was mechanically wetted during the increase of axial net stress. The sample was initially in main drying surface so it was wetted moving in the scanning domain, and then it reached to the main wetting surface where the degree of saturation was increased rapidly for further loading.

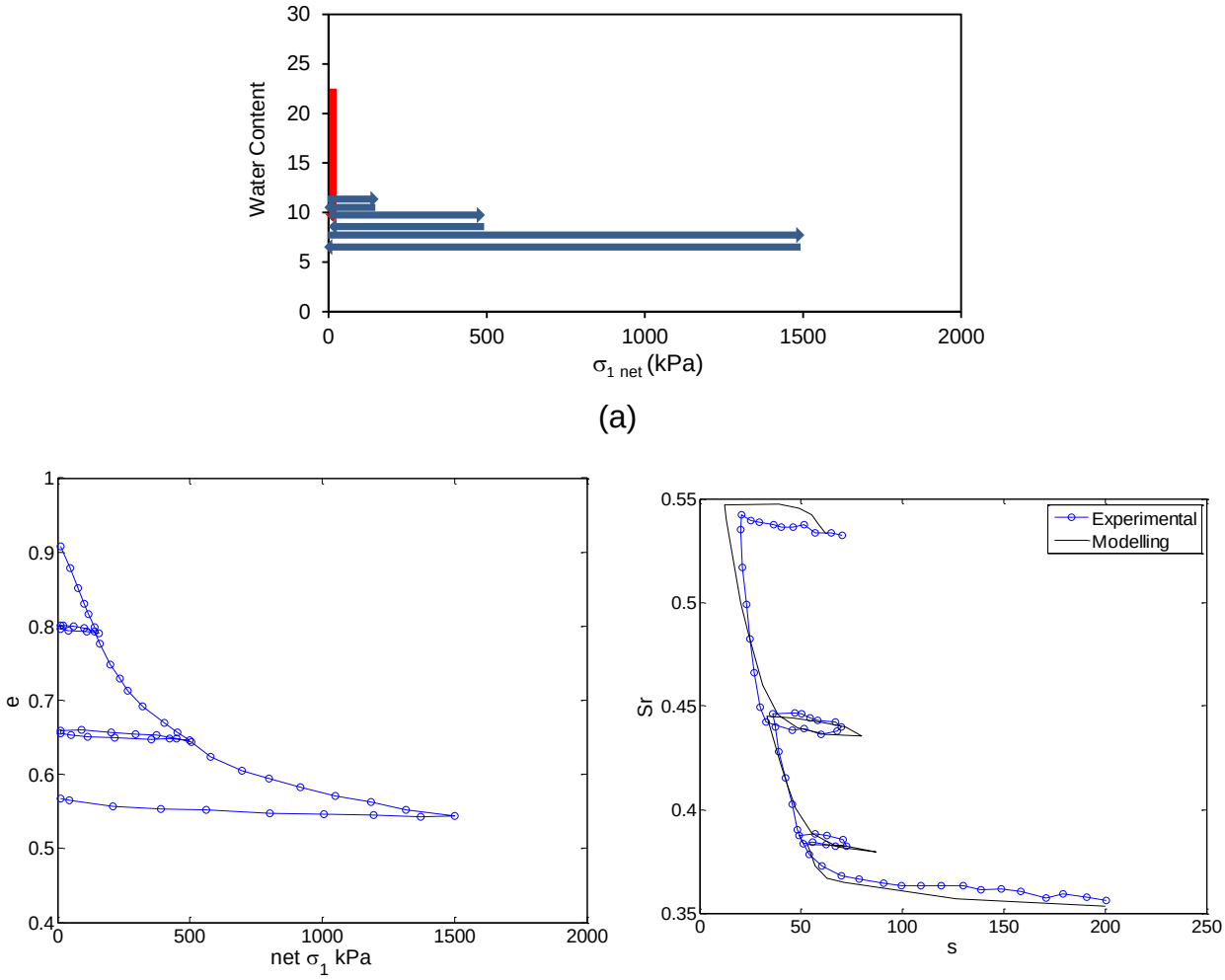

Figure 3.8. *Computed and experimental behaviour for loading-unloading cycles at constant water content. (a) Applied stress path (b) e-$\sigma_{1\ net}$ plane (c) S_r-s plane*

The unloading-reloading path changed the degree of saturation along the scanning domain, but these scanning paths are reversible as they approached to main wetting surface during further loading.

The measured void ratio changes adopted and the suction is predicted by proposed WRC model in which the degree of saturation was computed regarding to the fact that the water content remained constant. As it is shown in Figure 3.8 (c), the predicted suction shows good agreement to experimental values as well as the capability of the model in resembling the hysteresis loops induced by mechanical wetting-drying paths.

3.8 Conclusion

The irreversible change of degree of saturation during mechanical and hydraulic wetting-drying draw attention to hysteresis of water retention behaviour, and it has to be taken into account to properly model the hydromechanical behaviour of unsaturated soil. The new approach was introduced in this work by enhancing the contact angle hysteresis framework proposed by Zhou (2015) and adopting Gallipoli's model (2003b), accounting for the mechanical effect on WRC and the hysteresis of water retention behaviour induced by both loading-unloading and wetting-drying cycles.

The contact angle in unsaturated soil varies with volume and suction changes. Its value remains at maximum contact angle (Advancing contact angle, θ_A) and minimum contact angle (Receding contact angle, θ_R) at main wetting and main drying surfaces, respectively.

The contact angle varies between the advancing and receding contact angles along the scanning domain. The proposed model was introduced as a differential equation, and it is able to model the main drying and main wetting surfaces, and also to simulate the hysteresis behaviour in scanning domain during wetting-drying and compression-swelling cycles, using the variation of contact angle with suction and void ratio. The hysteresis functions were introduced contributing in modeling the hysteresis of water retention. The hysteresis function similar to reference model was proposed to account for mechanical hysteresis for the aim of simplification. However, the proposed framework is open to improve by introducing a different mechanical and hydraulic hysteresis functions obtained from geomechanical and geometrical features of soil-liquid interface relationships.

The proposed model introduces two additional parameters. The main drying surface was used to calibrate the reference model and the additional parameters can be easily calibrated by best fitting least-square procedure using the scanning

hydraulic or mechanical wetting curves. It has to be pointed out the proposed approach can be applied to any rate form water retention model.

The series of tests were carried out to study the water retention behaviour of clayey silt and the hysteresis induced by wetting-drying and compression-swelling cycles. The model predictions showed good consistency to experimental results, by reproducing the hysteresis of water retention with respect to the variation of contact angle.

References

[1] Brooks R, Corey A. Hydraulic properties of porous media. Hydrology Paper, No. 3. Fort Collins, Colorado: Colorado State University; 1964.

[2] Buscarnera G, Nova R. An elastoplastic strainhardening model for soil allowing for hydraulic bonding-debonding effects. Int J Numer Anal Methods Geomech 2009;33:1055 86.

[3] Campbell, G.S., 1974. A simple method for determining unsaturated conductivity from moisture retentiondata, Soil Sci. 117(6):311-314.

[4] Della Vecchia, G., A.C. Dieudonne, C. Jommi, R. Charlier, 2015. Accounting for evolving pore size distribution in water retention models for compacted clays. International Journal for Numerical and Analytical Methods in Geomechanics 39 (7), 702-723.

[5] Della Vecchia G, Jommi C, Romero E. A fully coupled elastic–plastic hydromechanical model for compacted soils accounting for clay activity. International Journal for Numerical and Analytical Methods in Geomechanics 2013; 37 (5):503–535.

[6] Fredlund DG, Xing A. Equations for the soil-water characteristic curve. Can Geotech J 1994;31(3):521–32.

[7] D. Gallipoli (2012). A hysteretic soil-water retention model accounting for cyclic variations of suction and void ratio. Géotechnique, 62(7): 605–616.

[8] Gallipoli, D., Wheeler, S. & Karstunen, M. (2003b). Modelling the variation of degree of saturation in a deformable unsaturated soil. Ge´otechnique 53, No. 1, 105–112.

[9] Gao, L. and McCarthy, T. J. 2006. Contact angle hysteresis explained. Langmuir. 22(14): 6234–6237.

[10] Gardner, W. R., Some steady state solutions of unsaturated moisture flow equations with application to evaporation from a water table, Soil Sci., 85, 228-232, 1958

[11] Hillel, D., 1998. Environmental Soil Physics, Academic Press, San Diego.

[12] Johnson, R.E., Dettre, R.H., 1964. Contact angle hysteresis. In contact angle wettability and adhesion. Adv. Chem. 43, 112–143. Letey, J., Osborn, J., Pelishek, R.P., 1962.

[13] Jommi, C. (2000). Remarks on the constitutive modelling of unsaturated soils. In Experimental evidence and theoretical approaches in unsaturated soils: Proceedings of an international workshop (eds A. Tarantino and C. Mancuso), pp. 139–153. Rotterdam: A. A. Balkema.

[14] Khalili, N., Habte, M. A. & Zargarbashi, S. (2008). A fully coupled flow deformation model for cyclic analysis of unsaturated soils including hydraulic and mechanical hysteresis. Comput. Geotech. 35, No. 6, 872–889.

[15] Li XS. Modelling of hysteresis response for arbitrary wetting/drying paths.ComputGeotech 2005;32(2):133–7.

[16] Maśin, D. (2010). Predicting the dependency of a degree of saturation on void ratio and suction using effective stress principle for unsaturated soils. Int. J. Numer. Anal. Methods Geomech. 34, No. 1, 73–90.

[17] Miller, G.A., Khoury, C.N., Muraleetharan, K.K., Liu, C., and Kibbey, T.C.G. 2008. Effects of soil skeleton deformations on hysteretic soil water characteristic curves: experiments and simulations. Water Resources Research, 44: W00C06. doi:10. 1029/2007WR006492. PMID:19081782.

[18] Nuth, M. & Laloui, L. (2008). Advances in modelling hysteretic water retention curve in deformable soils. Comput. Geotech. 35, No. 6, 835–844.

[19] Pedroso, D. M. & Williams, D. J. (2010). A novel approach for modelling soil–water characteristic curves with hysteresis. Comput. Geotech. 37, No. 3, 374–380.

[20] Romero, E., Della Vecchia, G. & Jommi, C. (2011). An insight into the water retention properties of compacted clayey soils. Ge´otechnique 61.

[21] Romero, E. & Jommi, C. (2008). An insight into the role of hydraulic history on the volume changes of anisotropic clayey soils. Water Resources Res. 44, No. W00C06, 1–16. doi: 10.1029/2007WR006558.

[22] Romero, E. & Simms, P. (2008). Microstructure investigation in unsaturated soils: A review with special attention to contribution of mercury intrusion porosimetry and environmental scanning electron microscopy. Geotech. Geol. Engng 26, No. 6, 705–722.

[23] Rotenberg, Y., Boruvka, L., Neumann, 1984. The shape of nonaxisymmetric drops on inclined planar surfaces. J. Colloid Interface Sci. 102, 424–434.

[24] Simms, P. H. & Yanful, E. K. (2002). Predicting soil-water characteristic curves of compacted plastic soils from measured poresize distributions. Ge´otechnique 52, No. 4, 269–278.

[25] Sheng D, Fredlund DG, Gens A. A new modelling approach for unsaturated soils using independent stress variables. Can Geotech J 2008;45(4):511–34.

[26] Sun DA, Cui HB, Matsuoka H, Sheng D. A three-dimensional elastoplasticmodel for unsaturated compacted soils with hydraulic hysteresis.Soils Found2007;47(2):253–64.

[27] Tamagnini, R. An extended Cam-clay model for unsaturated soils with hydraulicHysteresis. Géotechnique, 2004, 54(3): 223-228.

[28] Tarantino, A. (2009). A water retention model for deformable soils. Ge´otechnique 59, No. 9, 751–762,

[29] van Genuchten MT. A closed-form equation for predicting the hydraulic conductivity of unsaturated soils. Soil SciSoc Am J 1980;44:892–8.

[30] Vanapalli, S. K., Fredlund, D. G. & Pufhal, D. E. (1999). The influence of soil structure and stress history on the soil-water characteristics of a compacted till. Ge´otechnique 49, No. 2, 143–159.

[31] Vaunat J, Romero E, Jommi C. An elastoplastic hydromechanical model for unsaturated soils.Experimental evidence and theoretical approaches in unsaturated soils.

In: Tarantino A, Mancuso C, editors. Proceedings of international workshop on unsaturated soil. Rotterdam: Balkema; 2000. p. 121–138.

[32] Wheeler SJ, Sharma RS, Buisson MSR. Coupling of hydraulic hysteresis and stress-strainbehaviour in unsaturated soils.Geotechnique 2003;53(1): 41–54.

[33] Zhou, A. (2013). A contact angle-dependent hysteresis model for soil-water retention behaviour In: Computer and Geotechnics, 49, 36 - 42

[34] Zhou AN, Sheng D, Scott SW, Gens A. Interpretation of unsaturated soil behaviour in the stress-saturation space. II: Constitutive relationships and validations. Comput Geotech 2012;43:111–23.

4

COUPLED HYDROMECHANICAL MODEL FOR THE COMPRESSION BEHAVIOUR OF UNSATURATED SILTY SOILS

4.1 Introduction

The constitutive equations are an inevitable supplement to the balance continuum mechanics laws, initial and boundary conditions. Nowadays, advancement of numerical calculation methods allows using more refined constitutive laws which permit to solve any boundary value problems. Constitutive equations define a relationship between the stress and strain in addition to introducing properties of a particular material in terms of material constants.

In soil mechanics, the development of the constitutive models is mainly based on features of the soil behaviour observed in experimental tests. One important feature is that the soil behaviour is not only nonlinear but also irreversible, and the plastic deformations are accumulated under mechanical repeated loads. Moreover, the soil behaviour can significantly depend on deformation history. The stress tensor (σ) can be described as a nonlinear and non-differentiable function of strain history in order to account the irreversibility and history-dependency (Owen & Williams, 1969).

Consequently, the constitutive equation can generally expressed in a rate form function (G), which allows providing the stress rate ($\dot{\sigma}$) associated with the current state and strain rate ($\dot{\varepsilon}$) as,

$$\dot{\sigma} = G(\sigma, q, \dot{\varepsilon}) \tag{4.1}$$

where q is a set of internal state variables.

Assuming the behaviour of soils is rate-independent, the function G has to be positively homogenous with respect to $\dot{\varepsilon}$,

$$G(\sigma, q, \lambda\dot{\varepsilon}) = \lambda G(\sigma, q, \dot{\varepsilon}) \quad \lambda > 0 \tag{4.2}$$

where λ is a scalar value.

If the strain rate direction defines as $\vec{\eta} = \frac{\dot{\varepsilon}}{\|\dot{\varepsilon}\|}$ and the second order stiffness tangent denoted by $\boldsymbol{S}$, the constitutive equation can alternatively be rewritten due to Euler's theorem,

$$\dot{\sigma} = \boldsymbol{S}(\sigma, q, \vec{\eta})\ \dot{\varepsilon} \tag{4.3}$$

This implies that the constitutive equation is incrementally linear when stiffness tangent tensor is independent of the strain rate direction. This class of constitutive equation is known as an elastic model. If two stiffness tensors are introduced, in which one represents the reversible behaviour, and the second one associated with the irreversible behaviour, the incrementally bi-linear constitutive equation of elasto-plastic models are characterised. Following, hypoplastic models are classified as nonlinear constitutive equations, where the elastic stiffness tensor depends on the direction of the strain rate.

There is no distinction between the elastic and plastic deformation in the hypoplastic framework, and irreversible deformations are predicted by a single nonlinear constitutive equation from the beginning of the loading process. This may introduce the hypoplastic equation as a simple but robust tool to reproduce the non-linearity of the soil behaviour. Using advanced techniques to investigate the soil behaviour in small strain range showed that the elastic range for deformation of soil is very trivial, and the corresponding tangent stiffness non-linearly depends on the strain and history of deformation (e.g. Richardson, 1988; Atkinson et al., 1990; Gasparre, 2005; Kuwano and Jardine, 2007). Moreover, the hypoplastic model provides competent predictions comparing to other advanced constitutive models, while it employs fewer parameters (Tamagnini C. et al., 2005; Mašin D. et al., 2006).

The present work involves developing a constitutive model for unsaturated soil using the hypoplastic framework, incorporating the hydraulic state and accounting the hydromechanical aspect of the unsaturated soil behaviour. The nonlinearity and irreversibility of the soil behaviour in an unsaturated state are more evident. This may be induced by the complicated contribution of two fluids in unsaturated soil behaviour, and not only due to mechanical loading but also by hydraulic loading (wetting-drying cycles). In principal, wetting paths are commonly modelled as elastic unloading paths in the elastoplastic framework, which leads to underestimating the irreversible swelling strains upon wetting paths at low-stress levels. This drawback can analytically overcome using the hypoplastic framework which can be more validated also from a quantitative viewpoint, where the unsaturated soil behaviour can be reproduced under hydromechanical paths in a wide range of stress and suction at a comparable number of model parameters.

First, a brief review on previously proposed hypoplastic models and general aspects of hypoplastic constitutive equations are described. Next, the hypoplasic model proposed by Mašin (2005) and its extended version reproducing the unsaturated soil behaviour are introduced. The new hypoplastic constitutive equations are then formulated and the coupling mechanism incorporating the hydromechanical behaviour of unsaturated soil is presented. Finally, the model is validated against experimental results.

4.2 Background

Preliminary rate-form constitutive equations proposed where other state variables rather than stress were disregarded. The general rate form of these equations were formulated as,

$$\dot{\boldsymbol{T}} = G(\sigma, D) \tag{4.4}$$

$\dot{\boldsymbol{T}}$ is the objective co-rotational (Jaumann) stress rate expressed as,

$$\dot{\boldsymbol{T}} = \dot{T} - WT + WT \tag{4.5}$$

where $\dot{T}$ is the time derivative of stress T. The spin tensor W is the axisymmetric part of the velocity gradient and the stretching tensor D is the corresponding symmetric part.

Kolymbas (1991) derived a general form of a constitutive equation by means of accounting some restrictions, such as homogeneity on T and D, and non-linearity. The derived equation consisted of tensorial terms and scalar values, denoted by tensor generators and material parameters, respectively. Then he examined the capability of the equation employing different generators and select the minimal set of generators by trial and error procedure to reproduce satisfactorily different aspects of soil behaviour including response envelopes, proportional strain paths, drained tests and limit surface. Eventually, the proposed constitutive equation consisted of four terms, two linear terms and two nonlinear terms as following,

$$\dot{T} = C_1(T.D + D.\sigma) + C_2\sigma{:}D + (C_3 + C_4\frac{\sigma.\sigma}{tr\ \sigma})\sqrt{D{:}D} \tag{4.6}$$

where C_1, C_2, C_3 and C_4 are material parameters.

Some drawbacks of the primary hypoplastic constitutive equation, such as the improper prediction of tangential stiffness in axial compression, were overcome in an equation proposed by Wu (1992).

The hypoplastic constitutive equation can be rewritten in an alternative expression, in which the linear and nonlinear terms are identified. By introducing the fourth order tensor L and second order tensor N (Lanier et al, 2004), the constitutive equation represented as,

$$\dot{T} = L{:}D + N\|D\| \tag{4.7}$$

where $\dot{T} = \frac{T}{tr(T)}$ and $\|D\|=\sqrt{tr(D^2)}$.

The two terms represented in equation (4.7) account for the reversible and irreversible behaviours of the soil, where L is linear and N is nonlinear in D.

Following the early versions of hypoplastic models, many attempts have been paid to integrate the internal variables and the critical state concept into the constitutive equation (e.g. Wu, 1992; Kolymbas et al. 1995; Gudehus, 1996; Bauer, 1996). The volumetric strain rate $(tr(D))$ and stress rate (T) are zero at a critical state. At the critical state, the rate of the stress tensor is zero,

$$L{:}\frac{D}{\|D\|} + N = 0 \tag{4.8}$$

And the direction of the stretching tensor is obtained by

$$\vec{D} = \frac{D}{\|D\|} = -L^{-1}{:}\,N = -B \tag{4.9}$$

The following equations can be then obtained for the critical state by taking the norm and trace of D. Using the critical state condition $tr(D) = 0$,

$$tr(B) = 0 \tag{4.10}$$

This condition describes a surface in the stress space for all critical state ratios, for which isochoric flow takes place.

The state boundary surface, which is defined as the entire state of soil that can exist in stress-void ratio space, was incorporated as well as the critical state. Gudehus (1996) characterised the state boundary surface for granular material by introducing limiting void ratios: e_i (maximum void ratio corresponds to isotropic normal compression), e_c (critical state void ratio) and e_d (minimum void ratio corresponding to maximum density). The limiting void ratios were incorporated into constitutive equation by means of scalar factors (f_b and f_d), which are represented as following (Gudehus, 1996),

$$\dot{T} = f_b f_e (L{:}\,D + f_d N \|D\|) \tag{4.12}$$

f_b incorporates the dependency of the response on the mean stress level, it is thus named barotropy factor. Factors f_d and f_e incorporate the dependency of the response on the void ratio (relative density), they are thus named pyknotropy factors.

The most important drawback of the model proposed by Bauer and Gudehus (1996) was their failure in predicting the proper shape for the critical state locus in an octahedral plane. This drawback was tackled by adopting the Matsuoka-Nakai failure criterion (1977) as the limit surface in the octahedral plane (von Wolffersdorff, 1996). This failure criterion employs a critical state friction angle and it coincides with Mohr-coulomb surface at triaxial compression and extension (Figure 4.1).

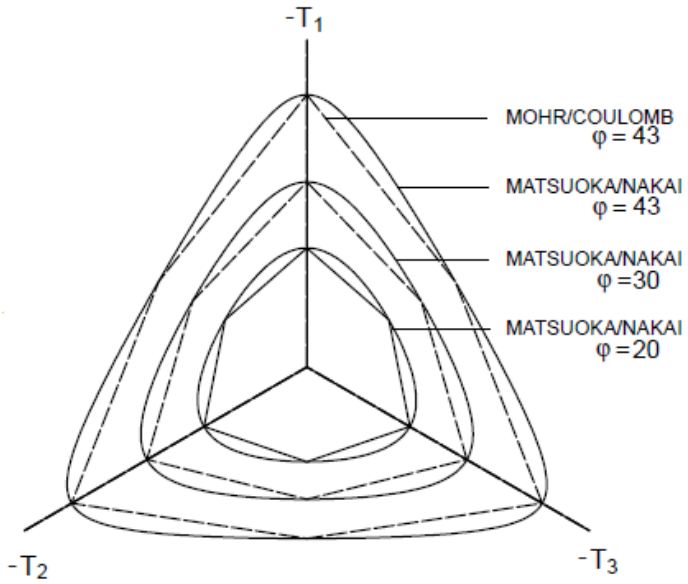

Figure 4.1. Matsuoka-Nakai failure criterion integrated in hypoplastic constitutive equation (von Wolffersdorff, 1996).

The critical state friction angles in cohesive materials are smaller than granular materials. Therefore, von Wolffersdorff (1996) hypoplastic model predicts very low shear stiffness for cohesive material. Herle and Kolymbas (2004) proposed a new hypoplastic model for low friction angle materials. The bulk stiffness was controlled similar to von Wolffersdorff model, whereas the shear stiffness was controlled by a new parameter, which is integrated into modified tensor L. However, modification of the tensor L thus modifies also the yield locus in an undesirable way (Mašin, 2005).

Mašín (2005) developed a hypoplastic model for clays involving the tensor L from the model by Herle and Kolymbas (2004), whereas the yield locus was independently formulated as proposed by Niemunis (2002). The clay hypoplastic model employs the yield locus of Matsuoka-Nakai and flow rule of von Wolffersdorff model. The clay hypoplastic model (Mašín, 2005) is adopted in the present work as the reference hypoplastic constitutive equation.

4.3 General aspects of hypoplasticity

4.3.1 Asymptotic states and proportional paths

Gudehus et al. (1977) defined the asymptotic states as an important feature of soil behaviour. Following its definition, experimental results justified the existence of

asymptotic states of the soil behaviour (e.g. Goldscheider, 1982; Topolnicki et al., 1990; Chu and Lo, 1994). The asymptotic state concept is actually a generalisation of the critical state concept for arbitrary strain path direction. It is believed that along any proportional strain path at a constant strain rate $\vec{D}$, the resulting stress path tends towards a straight line with a constant stress ratio, regardless of the initial state. Since the material behaves regardless of its past history, it is also known as a swept out memory (SOM) behaviour (Gudehus et al., 1977). As shown in Figure 4.2, there are inaccessible stress states and proportional stress paths must be limited within a fan. Two well-known asymptotic states are isotropic compression ($\dot{\varepsilon}_a = \dot{\varepsilon}_r$) and oedometric compression ($\dot{\varepsilon}_r = 0 \; and \; \sigma_r = K_0 \sigma_a$).

Moreover, any direction of strain rate is associated with a unique asymptotic curve in the e-log(p′) plane, denoted as a normal compression lines. The asymptotic curves associated with compressive and isochoric deformations are denoted as a critical state line (e_c) and isotropic compression line (e_i), respectively. Gudehus (1996) proposed the asymptotic curves of granular material are bound between maximum and minimum limiting void ratios (Figure 4.3 (a)), whereas the minimum limiting void ratio is not needed for clay, as suggested by Mašin (2005) (Figure 4.3 (b)).

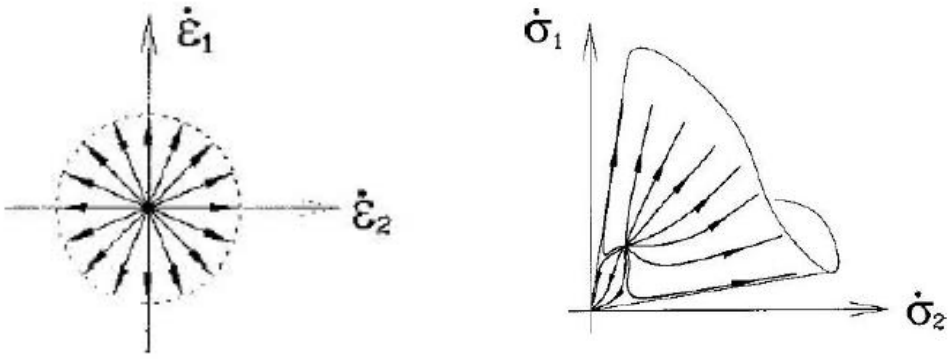

(a) (b)

Figure 4.2. a) Strain path directions b) corresponding stress paths (Kolymbas, 1991).

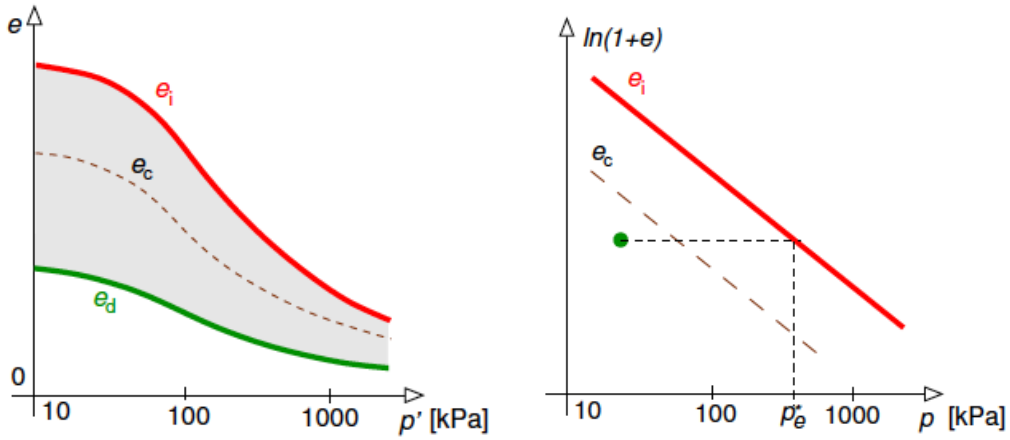

(a) (b)

Figure 4.3. Asymptotic normal compression lines for a) granular material b) clay (Mašin, 2005)

4.3.2 Yield surface and flow rule

It can be pointed out that the yield surface and the flow rule in plasticity theory are prescribed a priori whereas in hypoplastic framework they are derived from the constitutive equation. Considering equation (4.12), the equivalent yield surface and flow rule can be driven (Niemunis, 2002),

$$\|B\| = \|L^{-1}{:}\,N\| = 1 = Y \tag{4.13}$$

Therefore, the strain rate direction can be obtained by

$$\vec{D} = -\frac{L^{-1}{:}\,N}{\|L^{-1}{:}\,N\|} = -\vec{B} = \vec{m} \tag{4.14}$$

As a result, Y may be seen as an equivalent of the yield surface in elasto-plasticity, $\vec{m}$ may be seen as an equivalent of the flow rule. The second order tensor N can be calculated,

$$N = L{:}\,(-Y\vec{m}) \tag{4.15}$$

The tensor N can be replaced, and hypoplastic constitutive equation (4.12) can be rearranged, where yield surface and flow rule explicitly contribute,

$$\dot{T} = f_b f_e L : (D - f_d Y \vec{m} \|D\|) \tag{4.16}$$

4.4 Reference hypoplastic model for clay (Mašin, 2005)

The hypoplastic constitutive equation proposed by Mašin (2005) is commonly accepted as the hypoplastic model for simulating clay behaviour. The formulation of isotropic compression and critical state lines is adopted corresponding to the Modified Cam clay model (Roscoe et al., 1968). The limit surface (SOM) was defined as the failure surface of Matsuoka and Nakai (1977) depending only on the critical friction angle (φ_c). The general formulation takes form as below,

$$\dot{T} = f_s L : D + f_s f_d L : (-Y \frac{m}{\|m\|}) \|D\| \tag{4.17}$$

The fourth order tensor L is the one proposed by Herle and Kolymbas (1997). The second order tensor N (degree of nonlinearity) is given with respect to the yield limit function Y and flow rule m. The function Y is then derived as an interpolation between the minimum value at the isotropic compression $Y = Y_i$ and the maximum value at limit state (at critical state $Y = 1$).The barotropy factor f_s is employed in hypoplastic constitutive equation to incorporate the effect of mean stress on the soil behaviour. The barotropy factor f_s is thus calculated with respect to formulation of isotropic normal compression line, which is predefined. The pyknotropy factor f_d is introduced accounting for the influence of density on the soil behaviour. The factor f_d is formulated considering it has to be 0 at the critical state whereas it remains constant along any normal compression line.

The clay hypoplastic model was further enhanced accounting for mechanical response of unsaturated soil (Mašin and Khalili, 2008). The new formulation combines mathematically the hypoplastic model by Mašin (2005) with the effective stress equation proposed by Khalili and Khabbaz (1998). Attention is given to the stiffening effect of suction on the mechanical response of unsaturated soils and the phenomenon of wetting-induced collapse.

The existing hypoplastic model for unsaturated soils was formulated based on the effective stress depending only on suction. Therefore, the model provided no

information on the hydraulic state of the unsaturated soil so it fails in coupled hydromechanical problems. Accordingly, the effect of water retention and its hysteresis was ignored. In the following, the effective stress adopted in the present research is presented and a new equation is introduced to model the normal compression line of unsaturated soil. The new hypoplastic model is then proposed, which is formulated using the same approach proposed by Mašin and Khalili (2008), but accounting for adopted effective stress and normal compression line model. Moreover, the new mechanism is then proposed coupling the contact angle-water retention curve model (presented in chapter 3) and the hypoplastic model. The new model allows incorporating the hydraulic state and accounting for the hydromechanical behaviour of unsaturated soils.

4.5 Effective stress variable

Numerous attempts have been made to extend the effective stress concept of the saturated soil (Terzaghi 1936) to the unsaturated state, particularly at the early stage of consideration on the unsaturated soil (e.g. Croney et al., 1958; Aitchison, 1961; Jennings, 1961). Bishop (1959) defined the following equation as the effective stress (σ'_{ij}) for unsaturated soil mechanics,

$$\sigma'_{ij} = \sigma_{ij} - u_a\delta_{ij} - \chi(u_a - u_w)\delta_{ij} \tag{4.18}$$

where σ_{ij} is the total stress tensor and δ_{ij} is the Kronecker delta (δ_{ij}=1 if $i= j$ and δ_{ij}=0 if $i \neq j$), and χ is generally assumed to be a function of the degree of saturation, and the difference between air and water pressures $(u_a - u_w)$ is matric suction (s). The main difficulty in using a single effective stress stemmed from limitation in reproducing the volume collapse of unsaturated soils induced by wetting.

Difficulties in describing different features of unsaturated soil behaviour led to the adoption of two stress variables. For instance, net stress ($\bar{\sigma}_{ij} = \sigma_{ij} - u_a\delta_{ij}$) and the matric suction were adopted in many constitutive models proposed for unsaturated soil (e.g. Alonso et al., 1990; Cui and Delage, 1996; Thu et al., 2007). However, experimental results showed that the unsaturated soil behaviour is significantly affected by the hydraulic state whereas such stress variables provide no information on the variation of the hydraulic state (Wheeler, 1996). Therefore, such models cannot be used in the solution of coupled hydromechanical behaviour of unsaturated soils.

Houlsby introduced $\hat{\sigma}_{ij}$ as the average soil skeleton stress tensor and declared that the average stress becomes the Terzaghi effective stress when the soil becomes saturated, therefore, the average soil skeleton stress can be used consistently for both saturated and unsaturated states. An equation emerged from the analysis which had a form similar to equation (4.18) but with χ replaced by the degree of saturation S_r:

$$\hat{\sigma}_{ij} = \sigma_{ij} - u_a\delta_{ij} - S_r(u_a - u_w)\delta_{ij} \tag{4.19}$$

The average soil skeleton stress has been widely adopted as the effective stress and used as one of the stress variables in many unsaturated soils constitutive models (e.g. Jommi, 2000; Tamagnini et al., 2004; Romero and Jommi, 2008; Della Vecchia 2013).

The effective stress adopted in clay hypoplastic model was the one proposed by Khalili and Khabbaz (1998). This effective stress takes form similar to equation (4.18), where the bishop parameter χ is defined as a function of suction:

$$\chi = \begin{cases} 1 & s \leq s_e \\ \left(\frac{s_e}{s}\right)^{\gamma} & s > s_e \end{cases} \tag{4.20}$$

Where s_e is the suction value separating saturated from unsaturated states. It is equal to the air entry value for the main drying path or the air expulsion value for the main wetting path, and γ is an empirical parameter equal to 0.55. Therefore, this model provided no information on the hydraulic state of the unsaturated soil. In the present work, the effective stress equivalent to equation (4.19) is adopted and the proposed hypoplastic equation is developed incorporating the degree of saturation.

4.6 Modelling normal compression behaviour of unsaturated soils

The volume collapse induced by wetting is one of the important features of the unsaturated soil that has to be taken into account for modelling the volumetric behaviour of soils at unsaturated states.

The volume change behaviour of normally consolidated soil in isotropic stress state is known as normal compression line (NCL) and characterised by the

compression index (λ) and reference void ratio (N) at p=p_{ref}. If the current unsaturated NCL places above the saturated NCL, the collapse potential defined as a distance between the current position and the saturated NCL.

The preliminary constitutive models of unsaturated soil were proposed using net stress and suction as stress variables, in which the compressibility of the soil was mostly postulated to only be a function of the suction. For instance, Alonso et al. (1990) assumed that the compression index decrease with suction. Consequently, the collapse potential predicted by this model increases with the mean stress (Figure 4.4).

On the contrary, Wheeler et al. (1995) observed the compressibility of the soil increases with suction since larger pores formed during drying. The compression index was assumed to increases with suction. This assumption resulted in a reduction of collapse potential with the mean stress, as represented in Figure 4.4 (b).

Jommi (2000) used the average soil skeleton stress as an effective stress to interpret the unsaturated soil behaviour in which the compression law was established in the specific volume and effective stress plane. The compression index was assumed to be constant whereas the N decreases with suction. It is of interest to point out that the projection of the NCL in specific volume and mean net stress was no more linear, as shown in Figure 4.5. The compression index decreased with suction but increased with net stress. Although the compression index of the unsaturated soil for any value of suction increased with net stress, but it always remained smaller than saturated compression index, leading to an ever increasing collapse volume with increasing stress.

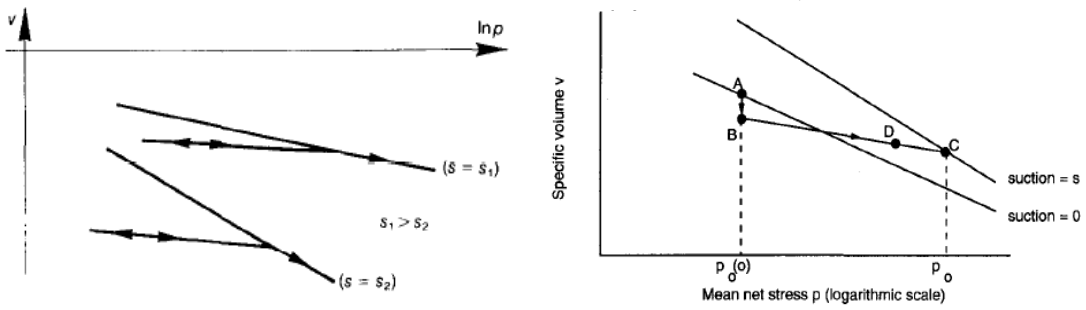

(a) (b)

Figure 4.4. The volume change behaviour and compressibility of soil depending on suction: a) BBM (Alonso et al., 1990) b) Wheeler et al. (1995).

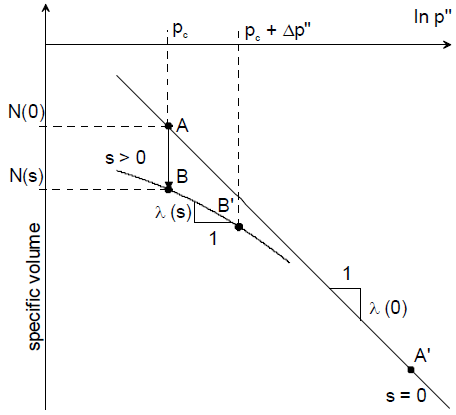

Figure 4.5. The volume change behaviour and compressibility of soil projected in specific volume and net mean stress plane (Jommi, 2000).

The collapse potential predicted in the aforementioned models always increased or decreased with increasing stress which may not be consistent with many experimental results. The experimental results showed that the collapse potential of unsaturated soils may initially increase with increasing the stress and it then starts to decrease for higher values until it reaches to the saturated state, in which it follows the saturated normal compression line (Jotisankasa, 2005; Sun et al., 2007; Kikumoto, 2011).

Zhou et al. (2012) proposed a new compression law assuming that the position of the N remains constant and λ is only a function of an effective degree of saturation (Figure 4.6). The compressibility increases with increase in the mean effective stress and degree of saturation while the collapse potential decreases. On the other hand, the collapse potential increases with a decrease in the degree of saturation resulted from drying. However, the proposed compression law cannot predict the behaviour of very loose sample where their void ratio can place above N.

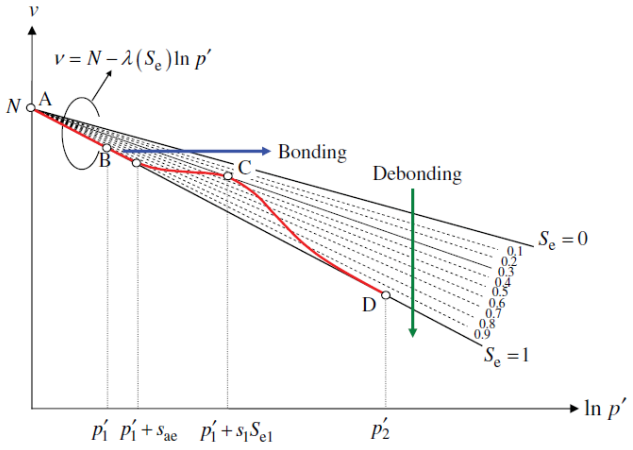

Figure 4.6. Normal compression lines and bonding-debonding of unsaturated soil (Zhou et al. 2012).

Gallipoli et al. (2003) proposed to use a new constitutive variable, named as a bonding factor (ζ). The model was developed considering that the effect of suction on the mechanical behaviour of unsaturated soils is not only because of changing the average stress acting on soil particles but also because of additional force acting at the particle contacts created by water menisci. The bonding factor was (ξ) then introduced as:

$$\xi = f(s).(1 - S_r) \tag{4.21}$$

where function $f(s)$ expresses the ratio of the stabilizing normal force exerted by the inter-particle contacts for a given suction (s) and suction of zero, and term $(1 - S_r)$ accounts for the number of water menisci per unit volume of solid fraction. Gallipoli et al. (2003) suggested using the analytical solution proposed by Fisher (1926) for function $f(s)$. This function varies between 1 and 1.5 assuming that the bonding forces corresponded to the ideal case of a water meniscus located at the contact between two identical spheres, regardless of dimensions and physical properties of particles, as shown in Figure 4.7.
The definition of equation (4.21) implied that the bonding factor, and in turn, the unsaturated compression index and N increases with suction in the space of logarithmic mean effective stress versus specific volume whereas an increase in the stress resulted in an increase of S_r and decrease in the bonding factor, leading to a reduction in the collapse potential.

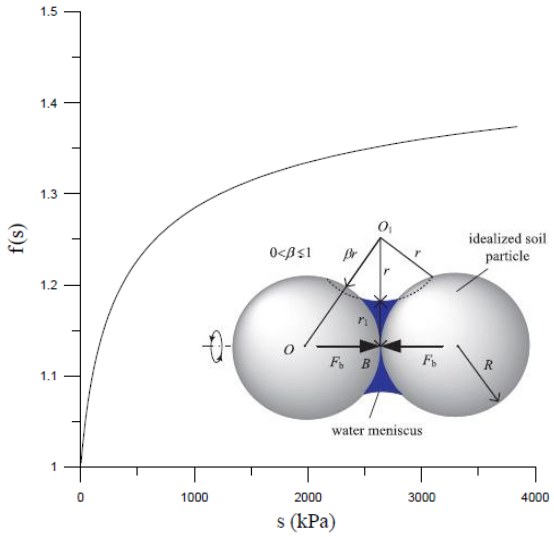

Figure 4.7. Bonding force between two identical spheres generated by water menisci (Gallipoli et al. 2003).

In the present work, a new function is proposed to develop a compression law for unsaturated soils. It takes form similar to equation (4.21) in which the second term $(1 - S_r)$ is used, but the first term $f(s)$ replaced by a new variable, which can be graphically obtained. This new function is defined as the logarithmic ratio between the current mean effective stress and its equivalent stress at saturated normal compression line (p_{sat}) (Figure 4.9). The new function f_ξ is introduced as,

$$f_\xi = log\left(\frac{p'}{p_{sat}}\right)(1 - S_r) \tag{4.22}$$

In which equivalent stress at saturated normal compression line can be obtained by

$$p_{sat} = \exp(\frac{N_{sat} - e}{\lambda_{sat}}) \tag{4.23}$$

where N_{sat}, λ_{sat} are parameters that determine the position and the slope of saturated normal compression line, respectively. Using a methodology similar to that reported by Gallipoli et al. (2003), the following empirical relationship is proposed to describe the normal compression line at unsaturated states based on experimental observation

$$\frac{e}{\mathrm{e}_{sat}} = 1 + \alpha {f_\xi}^\beta \tag{4.24}$$

where α and β are material constants.

As a result, the proposed compression law for unsaturated states takes form as:

$$e = N_{sat}\left(1 + \alpha {f_\xi}^\beta\right) - \lambda_{sat}(1 + \alpha {f_\xi}^\beta) ln\frac{p'}{p_{ref}} \tag{4.25}$$

It is evident that f_ξ becomes 1 at saturated state (s=0 kPa). When suction increases the ratio increases leading to increase of f_ξ. It is of interest to say that f_ξ is also depends on current void ratio. It implies that $f_\xi$increases as the void ratio decreases. The capability of the compression law was evaluated against different experimental results involving behavior of different soil types under isotropic compression, as shown in Figure 4.8.

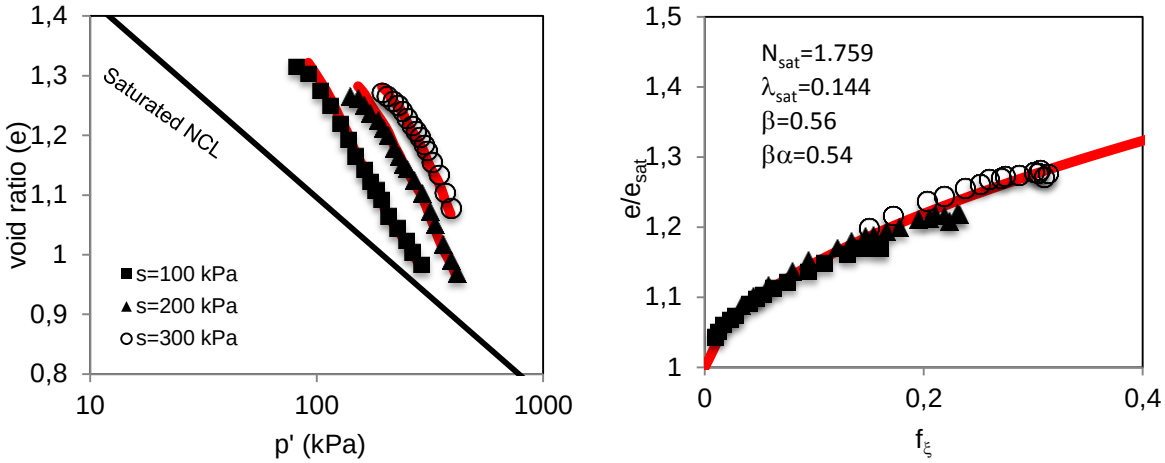
Saturated NCL
s=100 kPa
s=200 kPa
s=300 kPa
void ratio (e)
p' (kPa)
N_sat=1.759
λ_sat=0.144
β=0.56
βα=0.54
e/e_sat
f_ξ

(a)

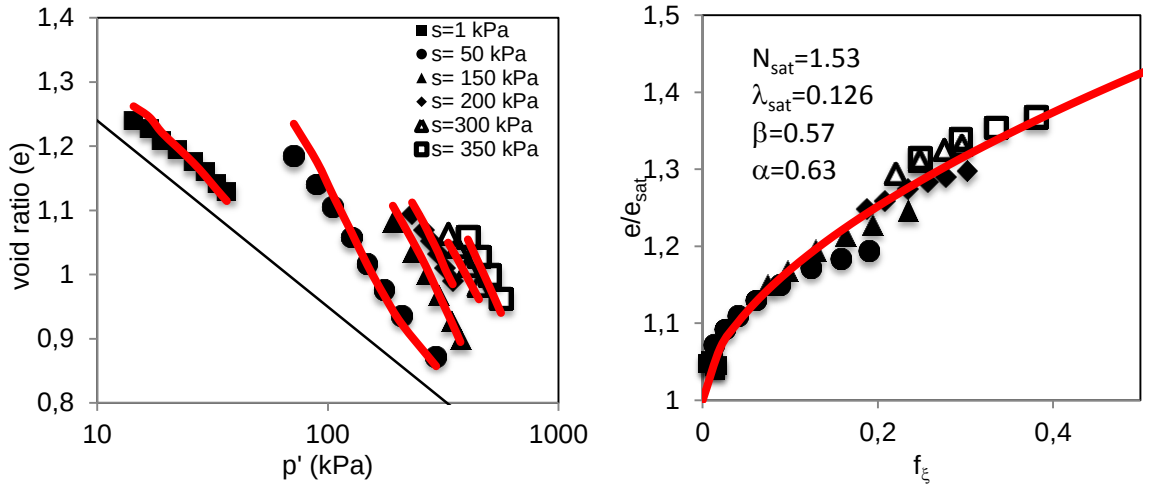
s=1 kPa
s= 50 kPa
s= 150 kPa
s= 200 kPa
s=300 kPa
s= 350 kPa
void ratio (e)
p' (kPa)
N_sat=1.53
λ_sat=0.126
β=0.57
α=0.63
e/e_sat
f_ξ

(b)

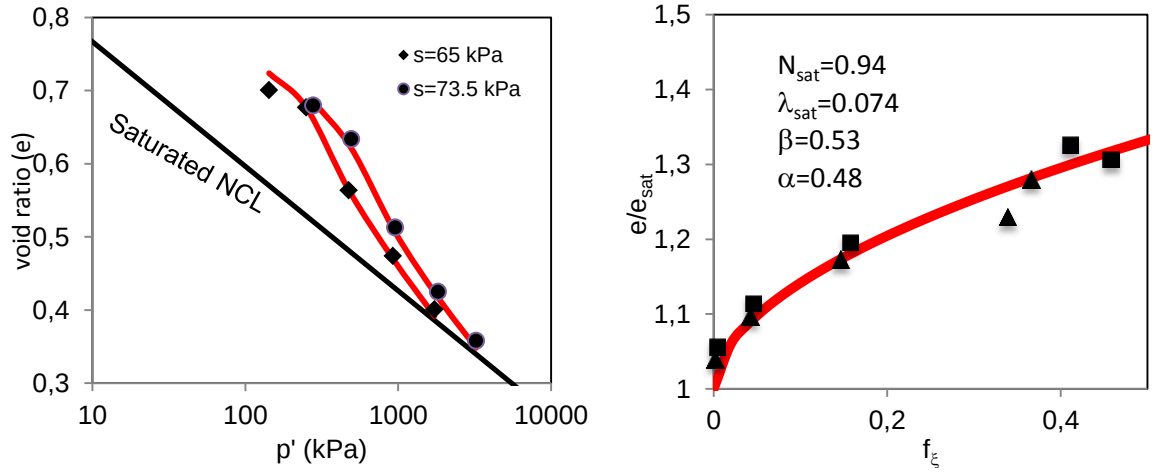
s=65 kPa
s=73.5 kPa
Saturated NCL
void ratio (e)
p' (kPa)
N_sat=0.94
λ_sat=0.074
β=0.53
α=0.48
e/e_sat
f_ξ

(c)

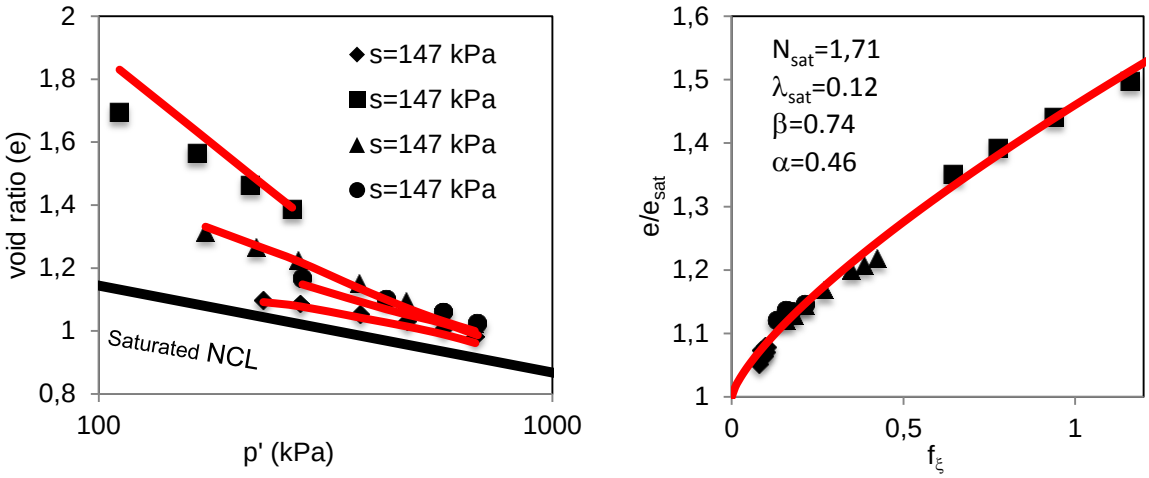

(d)

Figure 4.8. Fitting of Equation (4.25) (right Fig.-red line) to experimental data for different soils and predicting normal compression lines(left-Fig red lines): (a) bentonite/kaolin mixture, data from Sharma, 1998 b) speswhite kaolin, data from Raveendiraraj, 2009 c) silty clay, Jotisankasa, 2005 d) compacted clay, Sun et al., 2007

4.7 Proposed hypoplastic model for unsaturated soil

In the proposed model, the average soil skeleton stress is adopted as an effective stress and the effective stress tensor T' can be defined as

$$T' = T^{net} + S_r s \tag{4.26}$$

where T^{net} is the net stress tensor and formulated as the difference between total stress T^{total} and air pressure ($T^{net} = T^{total} - \mathbf{1}u_a$).

The hypoplasic constitutive equation is written in a rate form and time differentiation of equation (4.26) yields to

$$\dot{T}' = \dot{T}^{net} + \dot{S}_r s + S_r \dot{s} \tag{4.27}$$

The general form of a hypoplastic constitutive equation excluding the barotropy and pyknotropy and accounting for the yield locus function Y and flow rule direction tensor $\vec{m}$ can be represented as

$$\dot{T}' = L(D - Y\vec{m}\|D\|) \tag{4.28}$$

where the tensorial function $\vec{m}$ is defined as

$$\vec{m} = \frac{m}{\|m\|} \tag{4.29}$$

The proposed hypoplastic model is formulated under the isotropic condition and hence, variables and functions of the hypoplastic constitutive equation should be introduced at isotropic stress state. In the following, different components of equation (4.28) are formulated under the isotropic condition. The tensorial function $\vec{m}$ should have purely volumetric direction at isotropic stress state and its value according to the reference clay hypoplastic model is

$$\vec{m} = -\frac{1}{\sqrt{3}} \tag{4.30}$$

The stretch tensor D can be then written in terms of the rate of void ratio $\dot{e}$,

$$D = \frac{\dot{e}}{3(1+e)} \tag{4.31}$$

and as a result, the norm of stretch tensor is derived as

$$\|D\| = \frac{|\dot{e}|}{3(1+e)}\sqrt{3} \tag{4.32}$$

If functions of equation (4.28) replaced by their equivalent isotropic quantities and the stress tensor is presented by mean effective stress $p' = -\frac{1}{3}tr(T)$, the isotropic constitutive equation can be represented as,

$$\dot{p}' = -\frac{L}{(1+e)}(\dot{e} + Y|\dot{e}|) \tag{4.33}$$

Equation (4.33) takes a simple form of classical hypoplastic formulation where the function L is responsible for linear change in mean effective stress with respect to the variation of void ratio, and the product of L and Y determines the degree of nonlinearity.

If equation (4.33) is rewritten for loading ($\dot{e} \leq 0$) under isotropic condition, it takes form as,

$$\dot{p}' = -\frac{L(1 - Y_i)}{(1 + e)}\dot{e} \tag{4.34}$$

where function $Y = Y_i$ at isotropic state.

The normal compression line of the soil behaviour is modelled using a common equation, where parameter N and λ controls the position and the slope of the normal compression line at unsaturated state, respectively. The normal compression line can be simulated by

$$e = N - \lambda\, ln\frac{p'}{p_{ref}} \tag{4.35}$$

where p_{ref}=1 kPa is the reference mean stress and N is the void ratio when $p = p_{ref}$. Differentiation of equation (4.35) yields to

$$\dot{p}' = -\frac{p'}{\lambda}\dot{e} \tag{4.36}$$

If we assume that the normal compression line predicted by hypoplastic constitutive equation coincides with the normal compression line at unsaturated state obtained by equation (4.35), function L can be driven by comparing eqaution (4.34) and (4.36)

$$L = \frac{(1 + e)p'}{\lambda\,(1 - Y_i)} \tag{4.37}$$

Replacing the function L in equation (4.33), the hypoplastic constitutive equation can be rewritten as,

$$\dot{p}' = -\frac{p'}{\lambda\,(1 - Y_i)}(\dot{e} + Y|\dot{e}|) \tag{4.38}$$

Equation (4.38) can be represented for unloading ($\dot{e} > 0$), where function $Y = Y_i$

$$\dot{p}' = \frac{p'}{\lambda}\frac{(1+Y_i)}{(1-Y_i)}\dot{e} \tag{4.39}$$

Equation (4.39) may also coincide with the classical equation reproducing elastic loading-unloading line, which can be written in a rate form as,

$$\dot{p}' = \frac{p'}{k}\dot{e} \tag{4.40}$$

Comparing equation (4.39) and (4.40) yields to

$$\lambda\,\frac{(1-Y_i)}{(1+Y_i)} = k \tag{4.41}$$

Therefore, the nonlinearity function at isotropic state Y_i can be obtained as,

$$Y_i = \frac{\lambda - k}{\lambda + k} \tag{4.42}$$

The pyknotropy factor f_d should be introduced in order to incorporate the influence of overconsolidation ratio. It can be interpolated between $Y = 0$ at $p' = 0$ and $Y = Y_i$ at $p' = p'_i$. This factor is introduced by Mašin (2005),

$$f_d = \left(\frac{p'}{p'_i}\right)^a \tag{4.43}$$

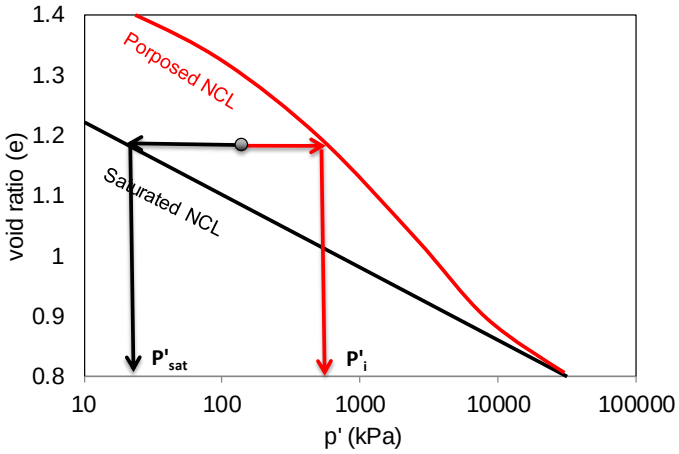

Figure 4.9. Definition of normal compression line and equivalent mean effective stresses

where p'_i is the mean effective stress at normal compression line at unsaturated state equivalent to the current mean effective stress (Figure 4.9) and it can be obtained by

$$p'_i = exp\left(\frac{N - e}{\lambda}\right) \tag{4.44}$$

where N and λ define the position and slope of normal compression line at unsaturated state.

Finally, the isotropic hypoplastic constitutive equation can be written as

$$\dot{p}' = -\frac{L}{(1+e)}(\dot{e} + f_d Y|\dot{e}|) \tag{4.45}$$

where functions L and Y take form as equations (4.37) and (4.42), respectively.

It has to be pointed out that the isotropic hypoplastic constitutive equation was obtained using the same framework proposed by Mašin (2005) and Mašin and Khalili (2008), but the average soil skeleton is adopted as the effective stress. Moreover, the normal compression line at unsaturated state is simulated by the model proposed in the present work (equation (4.25)). The normal compression line at unsaturated state is the asymptotic curve and it depends not only on suction but also on degree of saturation according to the proposed model.

Therefore, the compressibility λ with respect to equation (4.25) can be defined as

$$\lambda = \lambda_{sat}(1 + af_b{}^b) \tag{4.46}$$

And therefore, the mean effective stress at normal compression line at unsaturated state equivalent to the current mean effective stress (p'_i) should be obtained by

$$p'_i = exp\left(\frac{N_{sat}\left(1 + af_b{}^b\right) - e}{\lambda_{sat}(1 + af_b{}^b)}\right) \tag{4.47}$$

In the following, the function H_w is introduced in the hypoplastic constitutive equation reproducing the collapse induced by wetting with reference to the new mechanism accounting for coupling the hydromechanical behaviour of unsaturated soil.

Equation (4.45) cannot predict any straining when the mean effective stress remains constant. Hence, the left side of equation (4.45) needs additional terms reproducing the required changes in the mean effective stress corresponding to the volumetric collapse induced by wetting. As proposed by Mašin and Khalili (2008), this additional term can take form as,

$$\dot{p}' - H_w\langle -\dot{s}\rangle = \frac{L}{(1+e)}(\dot{e} + f_d Y_i|\dot{e}|) \tag{4.48}$$

where $\langle -\dot{s}\rangle = -\dot{s}$ when $\dot{s} < 0$ and $-\dot{s}=0$ otherwise. This implied that the additional term $H_w\langle -\dot{s}\rangle$ takes value only during the wetting. It is believed that the collapse potential of the unsaturated soil is defined by the difference between the current normal compression line at unsaturated state and the one at saturated state. Function H_w is obtained considering that the hypoplastic constitutive equation should have predict the variation of maximum void ratio ($\dot{e}_i$) at current normal compression line. Equation (4.68) can be represented by

$$\dot{p}' - H_w\langle -\dot{s}\rangle = \frac{L}{(1+e)}(\dot{e}_i + f_d Y_i|\dot{e}_i|) \tag{4.49}$$

And if it is rearranged considering $h_w = \frac{(1+e)H_w}{L}$,

$$\dot{p}' = -\frac{L}{(1+e)}(\dot{e}_i + Y_i|\dot{e}_i| + h_w\langle -\dot{s}\rangle) \tag{4.50}$$

When $\dot{s} < 0$ and $\dot{e}_i < 0$, then function h_w can be obtained by

$$h_w = \frac{(1+e)\dot{p}'}{L\dot{s}} + \frac{\dot{e}_i}{\dot{s}}(1 - f_d Y_i) \tag{4.51}$$

The normal compression line in the proposed hypoplastic model coincide with equation (4.25), where the void ratio depends on the degree of saturation, current mean effective stress and equivalent mean stress at saturated normal compression line $e = e_i(S_r, p', p_{sat})$. Therefore, differentiation of equation (4.25) yields to

$$\dot{e}_i = \frac{\partial e_i}{\partial S_r}\dot{S}_r + \frac{\partial e_i}{\partial p'}\dot{p}' + \frac{\partial e_i}{\partial p_{sat}}\dot{p}'_{sat} \tag{4.52}$$

where $\dot{p}_{sat}$ is the rate of the equivalent saturated mean stress.

The rate of the degree of saturation can be obtained with respect to the water retention proposed in chapter 3:

$$\dot{S}_r = \left(\frac{\partial S_r}{\partial s} + \frac{\partial \theta}{\partial s}\right)\dot{s} + \left(\frac{\partial S_r}{\partial e} + \frac{\partial \theta}{\partial e}\right)\dot{e} \tag{4.53}$$

Also rate of the mean effective stresses is

$$\dot{p}' = \dot{p}^{net} + \dot{S}_r s + S_r \dot{s} \tag{4.54}$$

And rate of equivalent saturated mean stress can be obtained by

$$\dot{p}'_{sat} = -\exp\left(\frac{N_{sat} - e}{\lambda_{sat}}\right)\dot{e} \tag{4.55}$$

The derivative of the proposed compression law (equation (4.25)) has to be computed with respect to the degree of saturation, mean effective stress and equivalent saturated mean stress to solve the equation (4.52). Because of the particular definition of equation (4.25), and the fact that the void ratio appears on both sides of the equation, the numerical implementation of the proposed model can be simplified assuming that the void ratio and the effective stress on the right-hand side of equation (4.25) are known and equal to the value calculated in the previous substep of the simulation. This is acceptable as long as the size of each substep is small enough.

It is also needed to incorporate the overconsolidation ratio to predict the collapse potential of the unsaturated soil. The factor f_w is then introduced which has to be unity for states at normal compression line and it should decrease to zero when $\frac{p'_i}{p'}$ tends to infinity (no collapse occurs due to wetting in highly overconsolidated soil).

The constrains are matched with function f_d, therefore, similar function with different power parameter are proposed

$$f_w = \left(\frac{p'}{p'_i}\right)^b \tag{4.56}$$

The general proposed isotropic hypoplastic constitutive equation takes form as:

$$\dot{p}' = \frac{L}{(1+e)}(\dot{e} + f_d Y|\dot{e}| + f_w h_w \langle -\dot{s} \rangle) \tag{4.57}$$

It is coupled with the contact angle water retention curve model (proposed in chapter 3), which was formulated as:

$$\dot{S_r} = \frac{\phi}{s}[1 - {H_\theta}^s]\dot{s} + \alpha\frac{\phi}{e}[1 - {H_\theta}^e]\dot{e} \tag{4.58}$$

Functions ϕ, ${H_\theta}^s$, ${H_\theta}^e$ and parameter α were introduced in chapter 3.

4.8 Tackling ratcheting problem for unsaturated state

One of the well-known deficiencies of the hypoplastic constitutive equation is ratcheting, i.e. the excessive accumulation of strain or stress predicted as a response to cyclic loading (Figure 4.10). The constitutive hypoplastic equation possesses no memory variable to remember the history of deformation and the hypoplastic model can predict the response depending only on the current state.

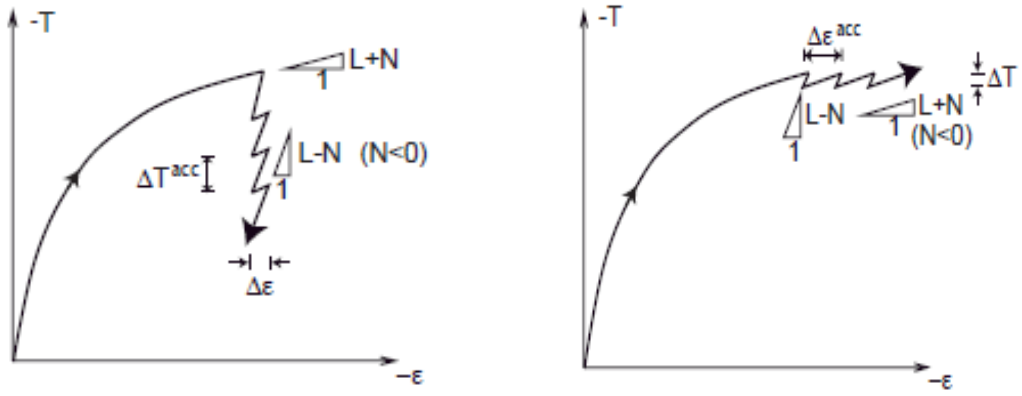

(a) (b)

Figure 4.10. Excessive stress (a) and strain (b) accumulation during stress and strain cycles (Niemunis and Herle,1997).

The intergranular small strain concept (Niemunis and Herle, 1997) is the only granted approach to overcome the ratcheting deficiency. The intergranular layer was introduced in which the reversible deformation of grains takes a place at very small initial displacements during loading. The irreversible deformation occurs due to the grain rearrangement for further loading process. Niemunis and Herle (1997) then proposed the enhanced hypoplastic model incorporating two modes of deformation: the hypoplastic equation associated with grain rearrangements and elastic equation associated with deformations of an intergranular layer. The general form of the model was formulated as the interpolation between the aforementioned two modes.

Despite the physical concepts and its application, the intergranular strain concept assumes a small elastic strain region which is against the general concept of the hypoplastic framework and it makes the equation relatively more complicated as it takes form as the interpolation between the elastic and hypoplastic components. Moreover, it requires 5 additional parameters, which are not easy to be calibrated.

In the present work, we introduce a new mechanism to overcome ratcheting problem for the unsaturated state. The proposed mechanism is rather easier than intergranular strain concept and it needs just one additional parameter comparing to the parameters of the proposed isotropic hydromechanical hypoplastic model. However, it is applicable as long as the soil is at unsaturated state. Since the proposed isotropic mechanical hypoplastic model is coupled with contact angle WRC model, this allows incorporating a contact angle θ, which is a physical parameter, in the formulation of the hypoplastic model. In fact, the contact angle was described that changes with void ratio and its value take place between the advancing θ_A and receding θ_R contact angles. This allows employing the contact

angle as a memory parameter, which decreases with increasing of the void ratio during unloading and increases with decreasing of void ratio during loading. The rate of the effective stress during loading-unloading at constant suction is

$$\dot{p}' = \dot{p}^{net} + \dot{S}_r s \tag{4.59}$$

Since the mechanical model is coupled with the contact angle WRC model, the rate of degree of saturation is a function of the rate of void ratio while $\dot{s}$=0,

$$\dot{S}_r = \frac{\partial S_r}{\partial e}\dot{e} + \frac{\partial S_r}{\partial \theta}\frac{\partial \theta}{\partial e}\dot{e} \tag{4.60}$$

The rate of contact angle was defined changing with suction and void ratio and the latter component contributes in loading-unloading at constant suction:

$$\dot{\theta} = \frac{\partial \theta}{\partial e}\dot{e} \tag{4.61}$$

Now, function f_R can be introduced as below

$$f_R = \left(\frac{\cos\theta}{\cos\theta_A}\right)^c \tag{4.62}$$

f_R is equal to 1 at normal compression line if the hydraulic state placed at main wetting curve since θ=θ_A, whereas θ decreases during unloading to the receding contact angle θ_R, f_R=$\left(\frac{\cos\theta_R}{\cos\theta_A}\right)^c$. This implies that f_R takes value as

$$\left(\frac{\cos\theta_R}{\cos\theta_A}\right)^c \leq f_R \leq 1 \tag{4.63}$$

The compressibility of the soil is then introduced by,

$$\lambda = f_R\lambda_{sat}(1 + a{f_b}^b) \tag{4.64}$$

The function f_R decreases during unloading and contributes in reloading where it decreases the rate of increase in compressibility. The prediction of the original proposed model and the enhanced one accounting for f_R is represented in Figure 4.11. The original model predicts an accumulation of the strain when used to simulate loading-unloading cycles (red curve in Figure 4.10 (a)). As shown in Figure 4.11 (b), the contact angle remains at its maximum value θ_A at normal compression line whereas it decreased during unloading. This reduction and subsequent increasing to θ_A during reloading caused that the enhanced model predicts no accumulation (blue line in Figure 4.11 (a)). The importance of tackling the ratcheting problem may be more realised comparing the predictions of the original and enhanced proposed models when number of loading-unloading cycles increases significantly, as shown in Figure 4.10 (c). The proposed approach to tackle the unsaturated soil is very simple and it needs only one additional parameter c. However, this approach depends on the variation of the contact angle and it cannot be extended to saturated state.

4.9 Calibration of parameters

In this section, parameters of the proposed coupled hydromechanical model are briefly described and appropriate procedures to calibrate these parameters are introduced. Parameters of the hydraulic model were introduced in chapter 3. The contact angle WRC model requires six parameters to simulate the main drying and wetting branches as well as the hysteresis induced by drying-wetting and loading-unloading cycles. The proposed WRC model needs the water retention test including one cycle of drying-wetting as well as a compression test at constant suction. The calibration of the parameters of the contact angle WRC was described in chapter 3 and the same values were used in the present simulations, as presented in Table 4.1.

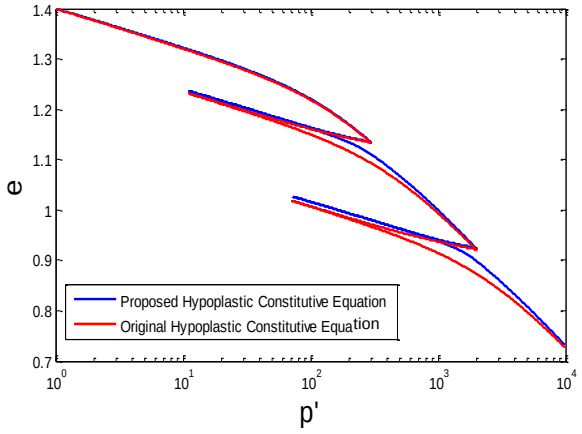

(a)

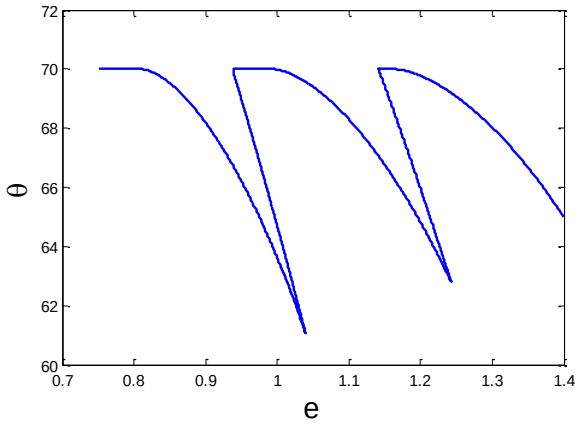

(b)

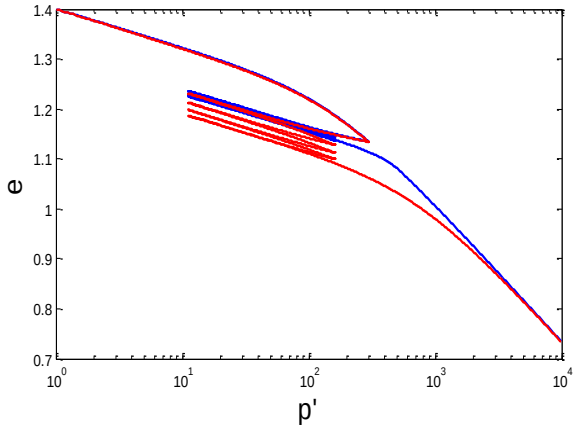

(c)

Figure 4.11. Enhancement of the proposed model tackling the ratcheting of the hypoplastic equation for unsaturated states:
a) Loading-unloading cycles at isotropic states
b)variation of the contact angle with void ratio
c) no accumulation of strains predicted upon loading-unloading cycles

The proposed hypoplastic model was formulated under isotropic condition whereas the experimental results presented in chapter 3 were carried out under oedometer condition. Since the soil behaviour shows similar pattern under oedometer and isotropic condition, the hypoplastic model can be used to reproduce the 1-dimensional behaviour of Viadana silt by replacing the mean effective stress p' with vertical one σ'_v. Obviously, the same modification should be applied to the rate of stress in the hypoplastic equation as well as stresses in the proposed compression law.

The mechanical model requires seven parameters. For the mechanical model, the parameters can be calibrated using compression tests with controlled suction or water content. An additional compression test with a saturated sample is also needed to calibrate parameter associated with the saturated state including λ_{sat} and N_{1D-sat}. The experimental results presented by Nocilla et al. (2008), involving oedometer tests on Viadana silt with the same properties of the material tested in the present work, were used to obtain λ_{sat} and N_{1D-sat} and resulting values are reported in Table 4.1. Parameter κ is obtained from Oe-LU (loading- unloading cycles at constant suction) test with respect to the slope of unloading curve.

Parameters α and β are calibrated with respect to 1-dimensional compression behaviour using the same procedure explained in section 4.6 and parameter α and β were obtained from fitting equation 4.24 with respect to the result of tests Oe-LU aamd Oe-LU-CW.

The parameter b should be calibrated with overconsolidated samples subjected to wetting $\dot{s} < 0$ upon constant net stress $\dot{p}_{net} = 0$. Very high values of b allows volumetric contraction just for normal consolidated sample. Finally, parameters c, which contributes in tackling the ratcheting problem in unsaturated state, should be calibrated upon loading-unlaoding cycles. Generally, the range of 1 to 1.5 for c parameter found to result in preventing accumulation of strains due to loading-unloading cycles.

The parameters of the proposed hydromechanical model for Viadana silt are listed in Table 4.1.

Table 4.1. Parameters of the proposed model for Viadana silt

Hydraulic model	n_d	n_w	ω	α	θ_A	β
Variables	1.41	1.23	5.11	6.51	84.2	0.46

Mechanical Model	α	β	N_{1D-sat}	λ_{sat}	κ	a	b	c
Variables	0.27	0.86	0.879	0.06	0.16	2.2	4.8	1.5

4.10 Model validation

The capability of the proposed coupled hydromechanical model was evaluated by comparing the predictions of the model and results of oedometer tests, see details of the tests in chapter 3.

Figure 4.12 shows the result of test Oe-LU in which the as-compacted sample subjected to loading-unloading cycles at the constant suction of 50 kPa. The results of the test Oe-LU (Figure 4.12 (a) and (b)) show that the degree of saturation rises when the sample contracts. This behavior is satisfactorily captured due to the coupling of the hydraulic model with the void ratio, which also affects the current value of the compressibility index λ. Moreover, no accumulated strain was predicted by the model upon unloading-reloading cycles (ratcheting). However, this sample experienced a reduction of the degree of saturation upon unloading which was not reproduced by the proposed model. It resulted from the fact that the loop observed in the experimental behaviour (change of the void ratio) induced by unloading-reloading cannot be simulated by the hypoplastic model.

Figure 4.13 (a) and (b) shows the experimental behaviour and model predictions when the soil sample is subjected to loading-unloading cycles at constant water content, where changes in suction and void ratio was computed by the proposed hydromechanical model. Suction increased within the soil as the sample was mechanically wetted during the increase of the axial net stress. The prediction of the model is not as precise of test Oe-LU but the trends of variation of void ratio and suction were acceptably reproduced.

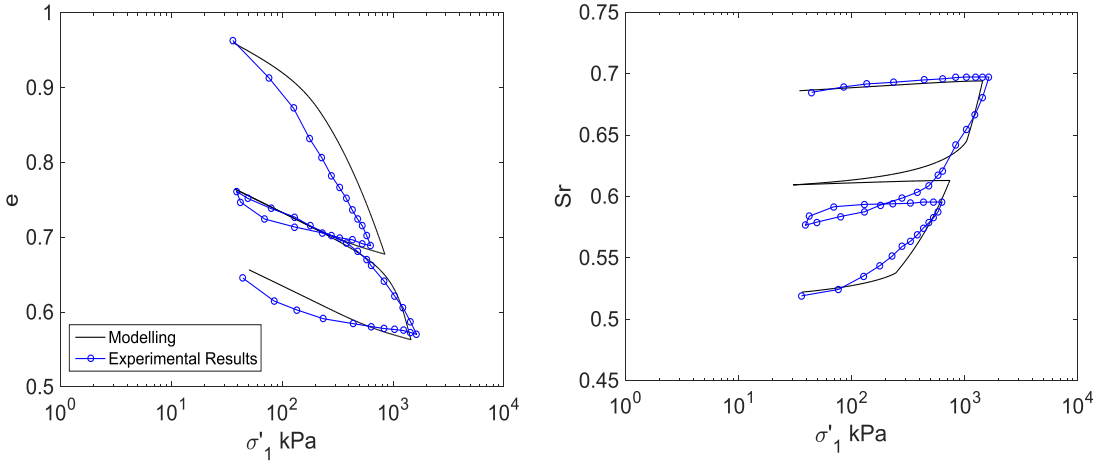

(a) (b)

Figure 4.12. Experimental result of test Oe-LU and prediction of the proposed model a) e-log (σ'_1) b) S_r-log (σ'_1)

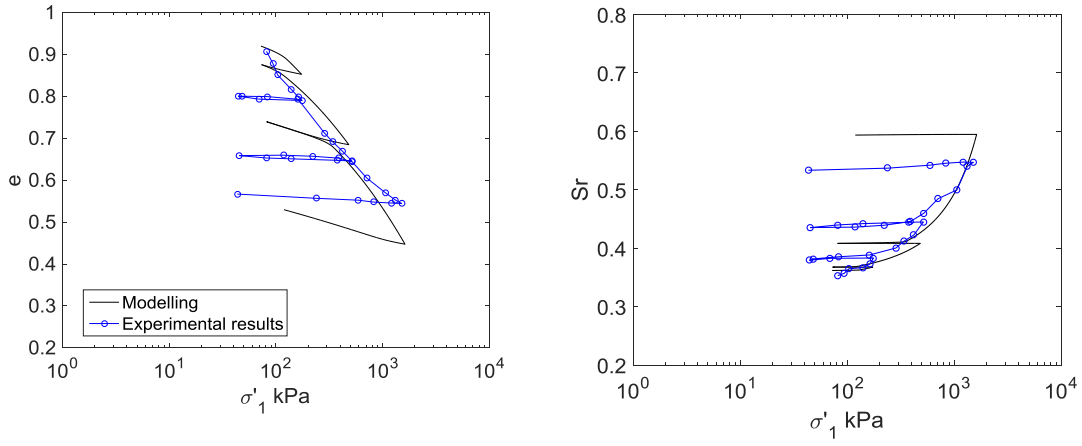

(a) (b)

Figure 4.13. Experimental result of test Oe-LU-CW and prediction of the proposed model a) e-log (σ'_1) b) S_r-log (σ'_1)

Fig. 4.14 (a) and (b) shows the behavior of low-porosity sample when subjected to drying-wetting at constant mean net stress, in which suction increased to 400 kPa, followed by decreasing to 10 kPa. The second drying path was then applied by increasing suction to 400 kPa. The sample was dried and contracted due to initial drying path resulted from the increase of initial suction. Since the sample was dense and its current void ratio was placed below the saturated normal compression line, no collapse was predicted. The variation of the degree of saturation in scanning domain, as well as the reversible volumetric changes upon first wetting and second drying, were also well predicted.

Figure 4.15 (a) and (b) shows the behaviour of high-porosity sample when subjected to drying-wetting cycles. Upon first wetting path, the sample experienced volumetric collapse, and in turn, its degree of saturation exhibited a sudden increase due to the significant decrease in the void ratio. The model was able to capture the collapse induced by wetting and also the shift of the WRC. Water retention behavior of this sample as well as the reversible volume change being subjected to the subsequent cycles was also predicted by the proposed model.

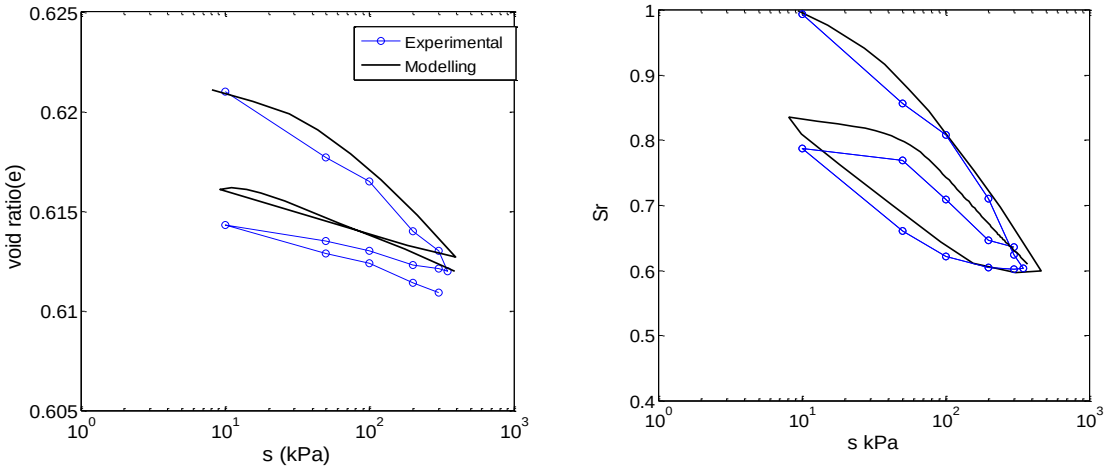

(a) (b)

Figure 4.14. Experimental result of test Oe-WR (Scanning path) and prediction of the proposed model
a) e-log (σ'_1) b) S_r-log (σ'_1)

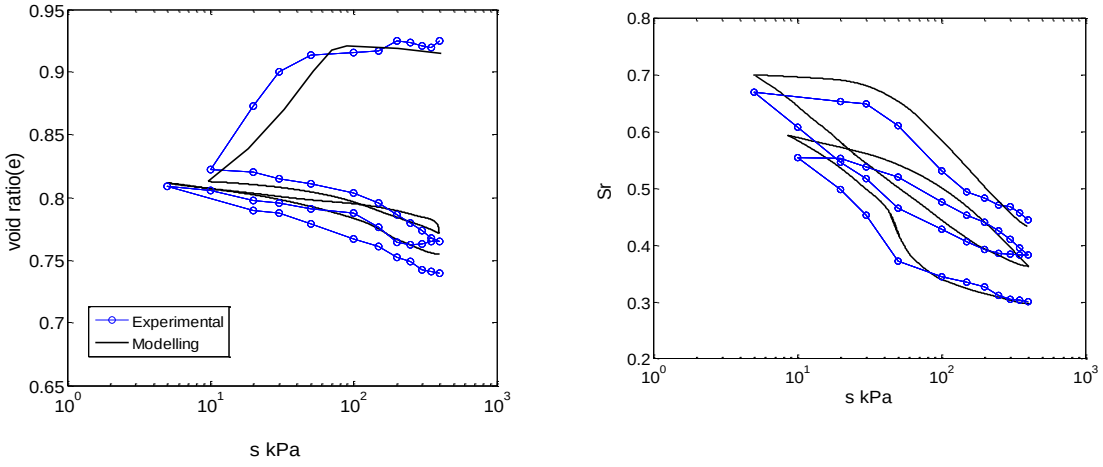

(a) (b)

Figure 4.15. Experimental result of test Oe-DW and prediction of the proposed model
a) e-log (σ'_1) b) S_r-log (σ'_1)

4.11 Conclusion

In the present work, the mechanical model was proposed for unsaturated soils developed under the hypoplastic framework. The model was formulated in the isotropic state in which the average soil skeleton stress and a new compression law were adopted. Therefore, the model allows incorporating the hydraulic state of the soil where the hydromechanical behavior and the effect of hysteresis of WRC can be reproduced.

Besides developing the mechanical model, the new mechanism is proposed which allows coupling the contact angle-water retention curve model (presented in chapter 3) and the proposed hypoplastic model. It can be also pointed out that both the proposed hydraulic and mechanical model formulated in a single rate form equation, which may simplify the implementation of these models in the numerical calculation.

Moreover, the ratcheting problem of the hypoplastic model was tackled in unsaturated state. This was implemented by employing the contact angle as a memory parameter, which decreases with increasing of the void ratio upon unloading and increases with decreasing of the void ratio during loading. The proposed mechanism is simple and needs just one additional parameter.

The proposed hydromechanical hypoplastic model was then validated comparing the predictions of the model and experimental behaviour of Viadana silt. The model was able to capture the effect of hydraulic state on the compressibility of the soil upon loading as well as the effect of changing void ratio on the water retention behaviour and the degree of saturation.

Reference

[1] Aitchison G.D. (1961). Relationship of moisture and effective stress functions in unsaturated soils, Proc. Conf. on Pore Pressure and Suction in Soils. Butterworths, London, pp. 47–52.

[2] Alonso E., Gens A., and Josa A. (1990). A constitutive model for partially saturated soils. Gèotechnique, 40:405–430. 5.1.

[3] Atkinson J.H., Richardson D., Stallebrass S.E. (1990). Effect of recent stress history on the stiffness of overconsolidated soil. Géotechnique 40(4): 531-540

[4] Bauer E. (1996). Calibration of a comprehensive hypoplastic model for granular materials. Soils and Foundations, 36(1):13–26.

[5] Bishop A.W. (1959). The principle of effective stress. Teknisk Ukeblad,106(39):859–63.

[6] Chu J., Lo S.C.R. (1994). Asymptotic behaviour of a granular soil in strain path testing. Géotechnique, 44(1), 65–82.

[7] Corey A.T. (1957). Measurement of water and air permeability in unsaturated soil. Proc. Soil Sci. Amer., 21(1), 7–10.

[8] Cui Y. and Delage P. (1996). Yielding and plastic behaviour of an unsaturated compacted silt. Gèotechnique, 46(2):291–311.

[9] Della Vecchia G., Jommi C., Romero E. (2013). A fully coupled elastic–plastic hydromechanical model for compacted soils accounting for clay activity. International Journal for Numerical and Analytical Methods in Geomechanics, 37 (5):503–535.

[10] Fisher R.A. (1926). On the capillary forces in an ideal soil; correction of formulae given by W.B. Haines. *Journal Agric. Science* 16(3): 492-505.

[11] Gallipoli D., Gens A., Sharma R., Vaunat J. (2003). An elasto-plastic model for unsaturated soil incorporating the effects of suction and degree of saturation on mechanical behaviour. Géotechnique, 53(1):123–135.

[12] Gasparre A. (2005) . Advanced laboratory characterisation of London Clay. Ph.D. thesis, Imperial College, London.

[13] Goldscheider M. (1982). True triaxial tests on dense sand. In: G. Gudehus (ed.) Constitutive relations for soils, pp. 11– 54. Workshop Grenoble, Balkema.

[14] Gudehus G. (1996). A comprehensive constitutive equation for granular materials. Soils and Foundations, 36(1):1–12.

[15] Gudehus G. (1979). A comparison of some constitutive laws for soils under radially symmetric loading and unloading. Proceedings of the Third International Conference on Numerical Methods in Geomechanics, Aachen,1309–1323.

[16] Herle I., Kolymbas D. (2004).Hypoplasticity for soils with low friction angles. Computers and Geotechnics, 31:365–373.

[17] Houlsby, G.T. (1997). The work input to an unsaturated granular material. Géotechnique, 47(1), 193–196.

[18] Jennings J.E.B., Burland J.B. (1962). Limitations to the use of effective stresses in saturated soils. Géotechnique, 12(2):125–144.

[19] Jommi C. (2000). Remarks on the constitutive modelling of unsaturated soils. In Experimental Evidence and Theoretical Approches in Unsaturated Soils: Proceeding of an International Workshop, Trento, Italy. Balkelma, Rotterdam. 5.1, 5.4.2.

[20] Jotisankasa A. (2005). Collapse behaviour of a compacted silty clay. PhD thesis. London: Imperial College London.

[21] Khalili N., Khabbaz M.H. (1998). A unique relationship for _ for the determination of the shear strength of unsaturated soils. Géotechnique; 48(2):1–7.

[22] Kolymbas D. (1991). An outline of hypoplasticity. Archive of Applied Mechanics, 61:143 151.

[23] Kolymbas D., Herle I.(2004). Shear and objective stress rates in hypoplasticity. International Journal for Numerical and Analytical Methods in Geomechanics; 27:733–744.

[24] Kikumoto M, Kyokawa H, Nakai T, Shahin HM. (2011). A simple elasto-plastic model for unsaturated soils and interpretations of collapse and compaction behaviors. In: Alonso EE, Gens A, editors. Unsaturated soils, vol. 2. Barcelona, Spain: CRC Press, p. 849–55.

[25] Kuwano R, Jardine R.J. (2007). A triaxial investigation of kinematic yielding in sand Géotechnique, 57 (7), pp. 563–579.

[26] Mašín D, Herle I. State boundary surface of a hypoplastic model for clays. Computers and Geotechnics 2005, Submitted for publication.

[27] Mašín D, Khalili N. (2008). A hypoplastic model for mechanical response of unsaturated soils. International Journal for Numerical and Analytical Methods in Geomechanics 32, No. 15, 1903-1926.

[28] Mašín D, Tamagnini C, Viggiani G, Costanzo D. Directional response of a reconstituted fine grained soil. Part II: performance of different constitutive models. International Journal for Numerical and Analytical Methods in Geomechanics 2006; 30(13):1303–1336.

[29] Niemunis A. Extended hypoplastic models for soils. Habilitation Thesis, Ruhr-University, Bochum, 2002.

[30] Niemunis A, Herle I. Hypoplastic model for cohesionless soils with elastic strain range. Mechanics of Cohesive- Frictional Materials 1997; 2:279–299.

[31] Nocilla A, Coop. M.R. The behaviour of sub-soils from the Po River Embankments: an example of transitional behaviour in natural soils Italian Geotechnical Journal, 42 (1) (2008), pp. 49–58.

[32] Owen D. R, Williams W. O., On the time derivatives of equilibrated response functions, *Arch. Rational Mech. Anal.*, 33 (1969), 288–306.

[33] Raveendiraraj A. Coupling of mechanical behaviour and water retention behaviour in unsaturated soils. Ph.D. thesis. UK: University of Glasgow; 2009.

[34] Richardson, D. 1988. Investigations of threshold effects in soil deformations. Ph.D. thesis, City University, London.

[35] Sharma R. Mechanical behaviour of unsaturated highly expansive clays. Ph.D. thesis. UK: University of Oxford; 1998.

[36] Sun DA, Sheng D, Xu YF. Collapse behaviour of unsaturated compacted soil with different initial densities. Canadian Geotechnical Journal 2007; 44(6):673–686.

[37] Tamagnini C, Maˇs´ın D, Costanzo D, Viggiani G. An evaluation of different constitutive models to predict the directional response of a reconstituted fine-grained soils. In Proceedings of the International Workshop on Modern Trends in Geomechanics, Vienna, Austria, Wu W, Yu HS (eds). Springer: Berlin, 2005; 143–157.

[38] Terzaghi, K. (1936). The shear resistance of saturated soils. Proc. 1st Int.Conf. Soil Mech. & Fdn. Engrg., Cambridge, Mass., Harvard University, (1), 54–56.

[39] Thu TM, Rahardjo H, Leong EC. Critical state behaviour of a compacted silt specimen. Soils Found 2007;47:749–55.

[40] Topolnicki, M., Gudehus, G., Mazurkiewicz, B.K.: Observed stress-strain behaviour of remoulded saturated clays under plane strain conditions. Géotechnique 40(2), 155 187 (1990).

[41] von Wolffersdorff PA. A hypoplastic relation for granular materials with a predefined limit state surface. Mechanics of Cohesive-Frictional Materials 1996; 1:251–271.

[42] Wu W. Hypoplastizit .at als mathematisches Modell zum mechanischen Verhalten granularer Stoffe. Ph.D. Thesis, University of Karlsruhe, 1992.

[43] Wheeler S. (1996). Inclusion of specific water volume within an elastoplastic model for unsaturated soils. Canadian Geotechnical Journal, 33:42–57. 5.1

[44] Wheeler S, Sivakumar V. An elasto-plastic critical state framework for unsaturated soils. Géotechnique1995; 45(1):35–53

5

EFFECT OF REPEATED HYDRAULIC LOADS ON WATER RETENTION BEHAVIOUR AND MICROSTRUCTURE OF A SILTY SILT

5. 1 Introduction

5.1.1 Repeated hydraulic loads

Dykes and embankments of Po rivers are frequently subjected to atmospheric changes and also changes in the water level of the main river (repeated hydraulic loads), which may induce landslides and soil failures associated with severe damages and causalities. The hydraulic behaviour of dykes and embankments has been widely investigated to provide experimental evidence and analytical tools for the assessment and design of geotechnical structures at unsaturated conditions. The water retention behaviour of unsaturated soils can be affected by repeated hydraulic loads as well as the mechanical properties. Many researchers have been studied the effect of repeated hydraulic loads (drying-wetting cycles) on hydromechanical behaviour of unsaturated soil (e.g. Sharma, 1998; Alshihabi et al., 2002; Lloret et al., 2003; Alonso et al., 2005; Cuisinier and Masrouri, 2005; Sivakumar et al., 2006; Nowamooz and Masrouri, 2008).

The steady state flow associated with the present river water level may not be a realistic approach for the analysis of river embankments consisting of the fine-grained material. The poor penetration of the water into the embankment may prevent the change of saturation line corresponding to the change of the river water level (Colombo, 1965). As a result, a part of soil within the embankment is at the unsaturated condition and subjected to changes in water content or suction. However, the soil embankment at shallow depth is widely exposed to atmospheric changes. The embankment-atmosphere interactions involve precipitation, air relative humidity, air temperature and water level, which change due to seasonal variation, rainfall, flooding, etc. The variation of these indexes may lead to the substantial changes in the water content and suction acting in the soil, particularly at shallow depths of the embankment.

Figure 5.1 shows the evolution of hydraulic boundary conditions used to investigate the hydraulic behaviour of the fine-grained embankment built along the Po River in Viadana located in the north of Italy, as reported by Calabresi et al. (2013). The old and experimental embankments formed a pond, which was filled with water to reproduce the effects induced by past flooding. Figure 5.1 (a) shows the trend in water levels of Po River and towards the old embankment (field) and experimental one (pond) from 25 April to 15 October 2001. Figure 5.1 (b) shows the time course of common climate change variables (daily precipitation, air relative humidity, temperature, daily potential and actual evaporation) during the same time span. The pore water pressure measurements were also reported, being measured at different positions within the embankment (As represented in Figure 5.1 (c)).

During the first impounding, where the pond was being filled with water, suction within the embankments decreased to very low values, as represented by points T3B, T5B, and T6B. The decrease in suction is caused by a seepage process developing through the shallowest previous layer of the subsoil, resulting in the penetration of the wetting front from the embankment bottom up to the deepest measurement points. These points positioned mainly at the bottom of the embankment have not shown significant suction changes due to climate changes or variation of river water level. However, points positioned at shallower depths (T1B and T2B) showed higher suction variation due to being closer to the atmosphere and subjected to repeated hydraulic loads. The evaporation accelerated the desaturation processes in a way that suction increased more rapidly at those points that were closer to the boundaries, as represented by drops in the water pressures measured at points T1B and T2B.

In the present work, the as-compacted samples of Viadana silt were subjected to drying-wetting cycles in order to study the effect of repeated hydraulic loads on water retention properties of silty soil.

The experimental procedures were developed to reproduce drying-wetting cycles resembling the field condition at shallow depths of soil embankment.
The severity of changes in water content or suction of soil embankment depends on the distance of measurement points from the embankment surface, the soil type and its permeability, the downward seepage process driven by gravity, climate change variables, etc. Figure 5.1 (b) shows that the air relative humidity experienced the minimum and the maximum values of about 30 and 100%, respectively. This can induce significant changes in water content and corresponding suction acting in soil at very shallow depths of the embankment.

5.1.2 Microstructural features of unsaturated soils

The comprehension of hydromechanical behaviour (multiphase coupling) requires studying unsaturated soil mechanics at microscopic levels and accounting for microstructural features in the evolution laws of soil materials (multiscale coupling). The pore network of unsaturated soils is filled with two fluids (air and water), and each fluid may distinctly contribute to different classes of pores. As a result, microstructural levels of unsaturated soils can respond differently to hydraulic or mechanical loading.

Mercury intrusion porosimetry (MIP) and scanning electron microscopic techniques (SEM or ESEM) have been widely used to provide a quantitative interpretation of the microstructure and fabric of soils involving the arrangement and assemblage of particles, and formation, connectivity and size distribution of pores.

The work presented by Diamond (1970) was the pioneer attempt to study the microstructure features of soils, in which MIP analysis was used to study the evolution of pore size distribution after being subjected to different hydraulic and mechanical loading.

The bimodal pore size distribution was reported in MIP analysis of compacted clayey soil presented by Sridharan et al. (1971), Ahmed et al. (1974) and Garcia-Bengochea et al. (1979). The results proposed that clayey soil compacted at a dry side of optimum possesses a bimodal pore size distribution whereas it possesses a single pore size distribution if compacted at a wet side of optimum. Following, similar bimodal pore size distribution including the aggregates structure with inter-aggregate porosity was also reported for silt compacted at dry side of optimum by Delage et al. (1996).

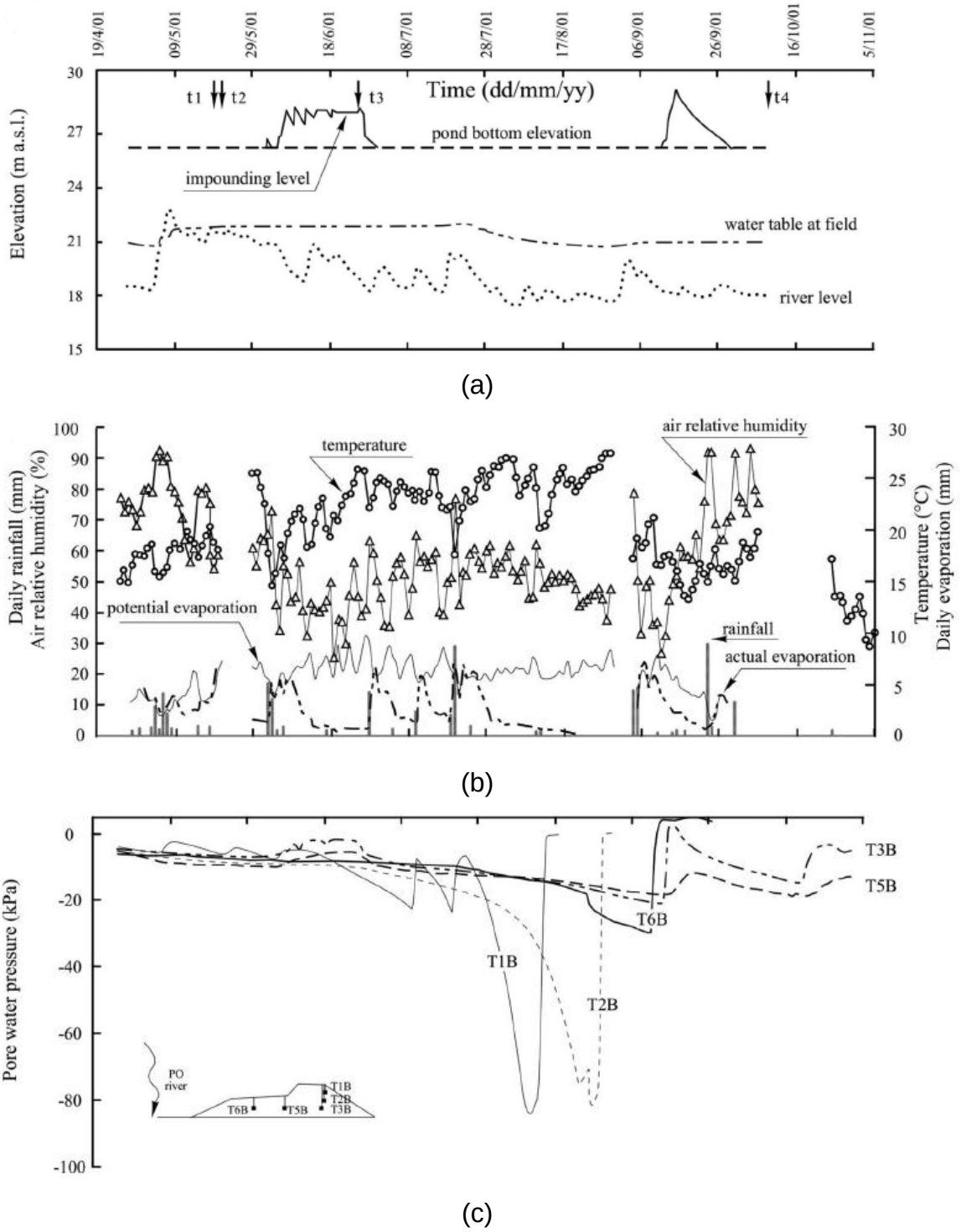

Figure 5.1. Evolution of water levels, atmospheric variables, and water flow: (a) water table levels at field and PO River levels; (b) evolution of daily rainfall, temperature, and relative humidity averaged over a day, daily potential, and actual evaporation; (c) suction measured within the embankment (Calabresi et al., 2013).

Delage and Lefebvre (1984) and Griffiths and Joshi (1989) studied the fabric change of different clays during consolidation, and experimental results demonstrated that the decrease in the volume of large pores was responsible for irreversible volume contraction of clay during consolidation, while very small pores within clay aggregates remained unchanged when subjected to external loading. Koliji et al. (2006) proposed that fabric modification can take place when the soil specimen is subjected to suction changes even though no significant volumetric strain occurs. The evolution of the soil fabric due to hydraulic and mechanical loadings was further studied by different authors (e.g. Al Mukhtar et al., 1996; Cuisinier and Laloui, 2004; Monroy et al. 2010 and Romero et al., 2011, Wang et al., 2012).

The intra-aggregate pores are classified as micropores inside aggregates whereas the inter-aggregate pores are macropores formed between aggregates. The characteristic behaviour of these pores, when subjected to hydraulic and mechanical paths, was reported to be different. For example, the response of the soil fabric can be studied by the results presented by Romero et al. (2011), where the pore size density (PSD) functions of the as-compacted sample is compared to those of samples subjected to loading at constant water content, drying after saturation, wetting at constant volume or wetting at null vertical stress (free saturation), as shown in Figure 5.2. Loading the as-compacted sample of Boom clay shifted the size of the dominant peak of the macropores towards a slightly smaller value, while the volume of the micropores and the pore size of its dominant peak were not affected. However, two saturation paths expanded the micropores and reduced the volume of the macropores (Figure 5.2 (a)). The dominant peak observed in the PSD of saturated samples was proposed as a threshold pore size separating the inter-aggregate and intra-aggregate pores. Also, it can be observed that the inter-aggregate porosity (macropores) experienced a significant volume reduction when being dried after saturation, whereas the intra-aggregate porosity (micropores) was almost completely recovered (Figure 5.2 (b)).

Many approaches were proposed accounting for multiscale coupling in which coupling functions correspondng to different microstructural levels were introduced (e.g., Alonso et al. 1999; LIoret and Khalili 2000; Alonso et al. 2005; Romero et al., 2011; and Della Vecchia et al. 2012 and 2015).

Many attempts have been made to investigate the effect of mechanical variable on the water retention behaviour including experimental and modeling studies (e.g. Vanapalli et al., 1999; Kawai et al., 2000; Ng and Pang, 2000; Benson et al., 2007 and Tarantino and Col, 2008), but experimental results considering the effect of fabric evolution on water retention properties are limited.

The link between the pore size distribution of soils (typically bimodal in the case of dry of optimum compacted clays) and different regions of the water retention curve was suggested by Romero et al. (1999). Romero and Vaunat (2000) detected two regions in water retention curves, namely, inter-aggregate and intra-aggregate water regions. An inter-aggregate water region was introduced when the water ratio was high enough to fill the inter-aggregate while the intra-aggregate were fully saturated, and an intra-aggregate water region was detected where the water ratio was high enough to partially fill the inter-aggregate voids. Romero et al. (2011) proposed bimodal water retention curve model, in which water retention regions of inter-aggregate and intra-aggregate pores were predicted using different formulations (Figure 5.3).

The inter-aggregate region presents a prevalent storage mechanism, which is dependent on the void ratio, and therefore, is sensitive to mechanical actions. Vice versa, at low water contents the influence of the initial and current dry density is found to be negligible, signifying that the suction-water content relationship is mainly dependent on the mineralogical composition of clay (specific surface) and is controlled by the soil intra-aggregate microstructure (Romero and Vaunat, 2000; Aubertin et al., 2003). Figure 5.3 shows predictions of WRC model (proposed by Romero et al., 2009) and the experimental behaviour of compacted clay, in which the effect of the void ratio on the water retention behaviour is found to be negligible for water ratio smaller than 0.35, and two main curves obtained for two different void ratios (either drying or wetting) converged to the same value (Della Vecchia, 2009).

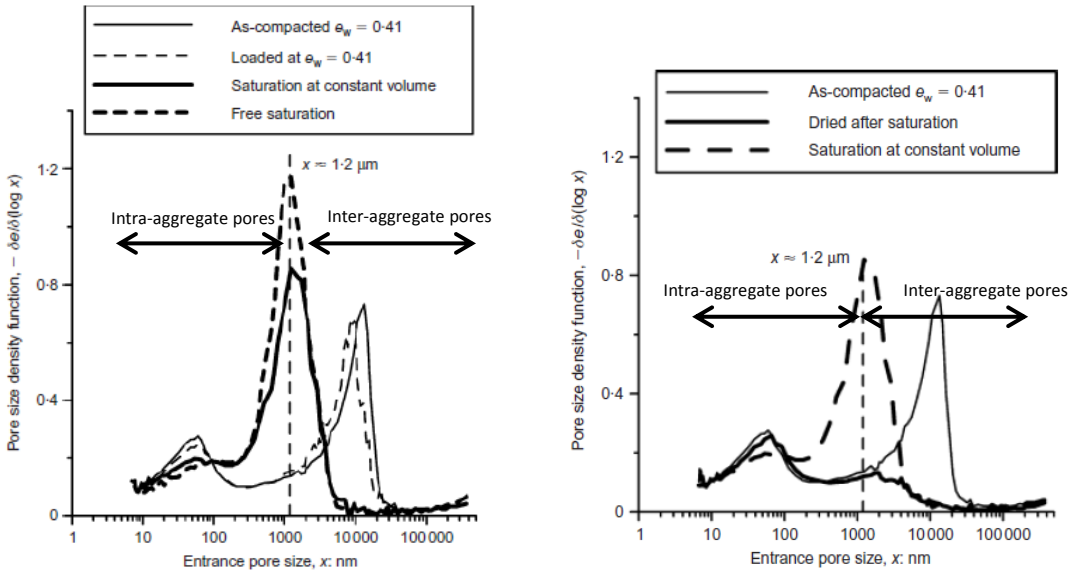

(a) (b)

Figure 5.2. Evolution of PSD function of compacted Boom Clay subjected to different (a) hydromechanical paths (b) hydraulic paths (Romero et al., 2011).

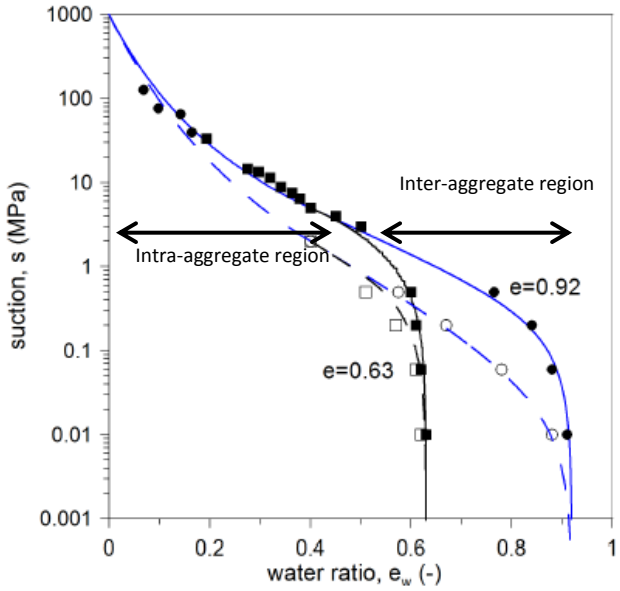

Figure 5.3. WRC model accounting for inter-aggregate and intra-aggregate regions (Della Vecchia, 2009).

The relationship between water retention properties and pore size distribution of soils has been considered since early stages of water retention models (e.g., Brooks and Corey, 1964; van Genuchten, 1980 and Fredlund and Xing, 1994). However, this relationship was assumed to be phenomenological and the role of soil fabric incorporated by means of fitting parameters calibrated regarding the experimental hydraulic behaviour.

Hu et al. (2013) proposed the hysteretic water retention model introducing the role of evolving pore size distribution for deformable soils. The authors assumed that the shape and the distribution pattern of the PSD function are not significantly altered during deformation processes, and they neglected the change in intra-aggregate pore size distribution. However, along hydro-chemo-mechanical loading paths, changes in the intra-aggregate porosity are not negligible when variations of water content and/or chemical composition of the pore fluid are involved.

Della Vecchia et al. (2015) proposed a framework accounting for evolving pore size distribution, in which different pore modes contributed individually in modelling the water retention behaviour considering their corresponding PSD functions. The pore size distribution data was quantified using MIP tests and its implications were employed to introduce physically based evolution laws for the parameters of water retention models.

In the present research work, the effects of drying-wetting cycles on the water retention behaviour of the as-compacted samples of Viadana silt were studied.

Following, the link between changes in the water retention behaviour and soil fabric was examined, providing MIP analyses and interpreting the effects of drying-wetting cycles on the pore network of the as-compacted samples. The WRC model was then proposed accounting for evolving pore size distribution, which allowed quantifying the contributions of different pore modes with reference to PSD functions of the as-compacted samples before and after being subjected to repeated hydraulic loads.

5. 2 Sample preparation

Six samples of Viadana silt were prepared in the present research, where they were statically compacted at a dry side of the optimum proctor, having the same dry densities very close to the proctor optimum one. Such as-compacted samples may generate soil fabrics analogous to the one of in-situ materials compacted in the field and used to construct the embankment. Moreover, they show less tendency to collapse induced by wetting. This ensures that an excessive accumulation of deformation during drying-wetting cycles is prevented. Having size of 20 mm of height and 50 mm of diameter, samples were compacted at a dry density of 16.5 KN/m^3 and water content of 20 %.

The properties of the as-compacted samples are summarised in table 5.1, where γ_d is the dry unit weight, e_0 is the corresponding initial void ratio, w_0 and Sr_0 are the compaction water content and initial degree of saturation, respectively. Three samples were used for water retention test, MIP and ESEM analyses directly after being prepared by static compaction (as-compacted samples) whereas three other samples were subjected to drying-wetting cycles, and their water retention behaviour and microstructure were then investigated (3 and 6 D/W cyclic samples).

Table 5.1. Properties of as-compacted samples.

Type of tests	γ_d (KN/m^3)	e_0	w_0 (%)	Sr_0
Water retention and MIP	16.5±0.008	0.657	20±0.6	0.83

5.2.1 Applying repeated hydraulic loads

In order to study the effects of repeated hydraulic loads on water retention and microstructure properties of Viadana silt, three as-compacted samples were

selected and subjected to cycles of drying-wetting, in which two of them were subsequently used for water retention tests and the other one was analysed by MIP test. Samples subjected to 3 and 6 cycles of drying-wetting are respectively named as “3 D/W cyclic” and “6 D/W cyclic” in the following (or generally “D/W cyclic”). Despite the most preceding experimental works in which drying-wetting cycles were applied to soil samples by means of changing imposed suction in suction-controlled apparatuses, repeated hydraulic loads in the present study were applied by controlling the water content of samples before placing in suction-controlled oedometer.

As-compacted samples were dehydrated while being exposed to laboratory room conditions (temperature (T)=21℃, relative humidity (RH)=38.5%). The corresponding suction computed to be about 128.8 MPa. As shown in Figure 5.4 (a), the sample inside the holder ring was placed above the reticular rigid sheet, and being subjected to 10 kPa of axial stress. The axial stress was applied by means of the dead weight held at the top of the sample. Therefore, the water content of the sample was mainly evaporated from the basement, where it was in contact with the atmosphere through the reticular sheet. Under this condition, the shrinkage of the sample mostly occurred upon the axial deformation, and the excessive decrease of the sample’s diameter was prevented during drying. The weight of the sample was sequentially monitored to track changes in the water content. The water volume change decreased during drying process until equilibrium was established after about 120 hours. At the end of drying, the height and diameter of the sample were measured.

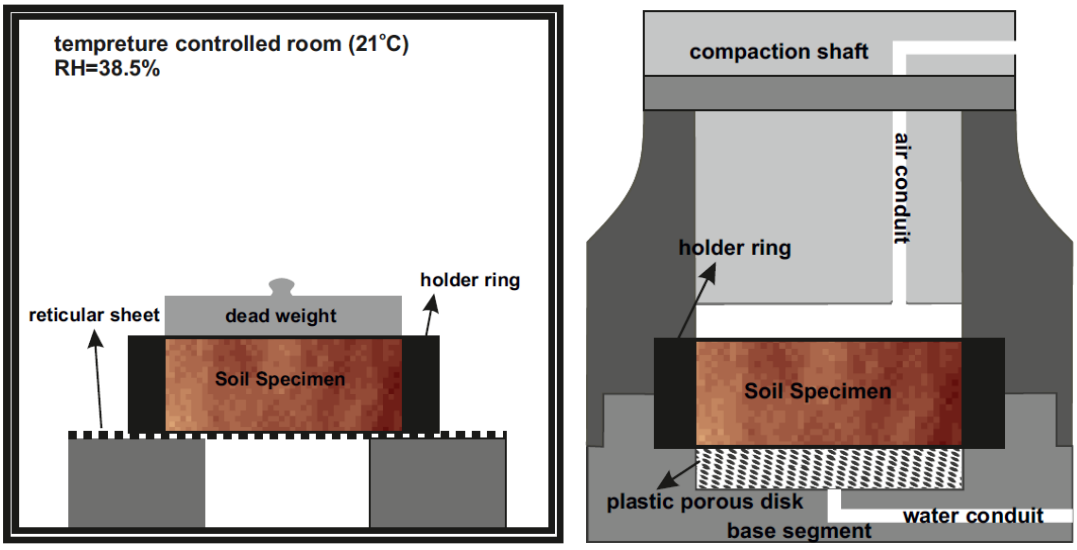

(a) (b)

Figure 5.4. Schematic plot of equipment and technique used to apply repeated hydraulic loads (oedometer sample) a) Drying process b) Wetting process.

For the wetting process, the dry sample was placed in the same hermetic mould previously used for compaction, whereas the base segment replaced by the new one equipped with the plastic porous disc and water conduit (Figure 5.4 (b)). The compaction shaft was inserted into the mould to prevent the evaporation during wetting while it was held above the top surface of the sample. This caused that the vertical deformation occurred during wetting while the radial deformation was constrained using the holder ring.

The water was injected into the sample passing through the base segment and plastic porous disc with the injection rate of 0.5 cm^3/h. This low injection rate ensured that the water flow did not apply significant pressure to the soil fabric, and a microstructure modification thus resulted from the response of pore modes to the presence and absence of water. The plastic porous disc ensured that the injected water is well distributed at the basement of the sample. The water gradually filled the pores of the sample while the air was leaving through a tiny passage conduit within the compaction shaft. The amount of the injected water was continuously measured using a water volume meter. The wetting process was stopped when the inserted water volume corresponding to the initial water content of the as-compacted sample (20%) was achieved. At the end of the wetting process, the sample was dismantled and wrapped up in a plastic cover and held in a sealed humid container for at least 5 days to ensure equalisation of the water within the entire volume of the sample. The height and diameter of the sample were measured after the equalisation was established.

As shown in Figure 5.5, the water was inserted into the soil samples in 28 hours (followed by 5 days of equalisation) whereas the drying process lasted 120 hours until the desired dried condition was achieved.

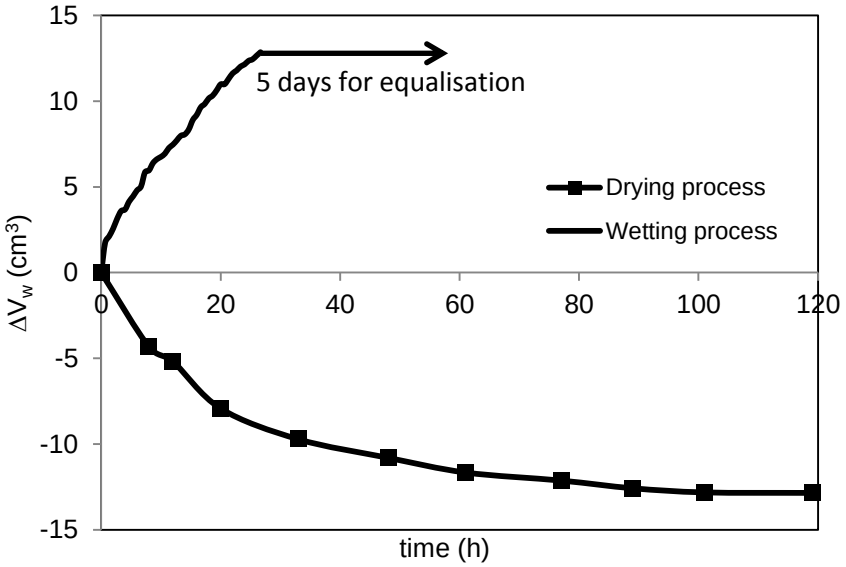

Figure 5.5. Water volume change of samples during wetting and drying.

It has to be pointed out that the technique used in the present research can accelerate the process of wetting and drying of the samples, in which the specimen can be subjected to numbers of cycles within few weeks. Moreover, the variation of the moist content of the sample in the laboratory scale can be a more realistic reproduction of the changes in the moist content of the unsaturated soil in geotechnical engineering practice, when subjected to drying-wetting cycles due to seasonal variations.

5.2.2 Volumetric change of samples being subjected to repeated hydraulic loads

Figure 5.6 shows the volume change of 3 D/W cyclic and 6 D/W cyclic samples in terms of volumetric strain (ε_v) and water content (w). The average residual water content of samples was measured to be 0.38 % at the end of drying processes while the water content, similar to one that samples were compacted at preparation (20%), was recovered at the end of wetting processes.

The volume contractions occurred while the samples were dried. The samples experienced contractive volumetric strains between 1.32 and 1.76 % at the end of drying paths. On the contrary, samples experienced volume expansion during wetting processes, where gentle swelling volumetric strains (maximum value of -0.17%, where the negative sign selected for swelling deformation) can be observed at the end of wetting processes.

As shown in Figure 5.7 (a), the volumetric behaviour of the sample subjected to 3 cycles of drying-wetting was similar to the volumetric response of the 6 D/W cyclic sample up to the same number of drying-wetting cycles.

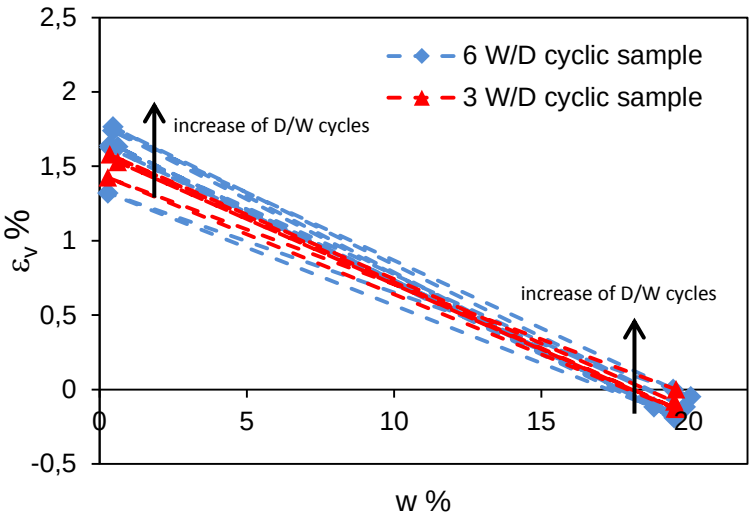

Figure 5.6. Volume change of samples subjected to repeated hydraulic loads.

Both samples experienced the minimum shrinkage at the end of the first drying process (1.42% and 1.33% of ε_v for 3 and 6 D/W cyclic samples, respectively). At the end of the first wetting process, they experienced a small swelling about 0.17%. This may partially result from the fact that these samples experienced a smaller value of suction at the end of wetting process comparing to one equilibrated after preparation (post-compaction), since their water retention state changed from the scanning domain (initial state) to the main wetting branch due to the wetting process of the last cycle. The contractive volumetric strains measured at the end of the subsequent drying processes were greater than the first cycle and they increased gently as the number of cycles increased whereas the expansion volumetric strains correspondingly decreased. Figure 5.7 (b) shows the volumetric strain change ($d\varepsilon_v$) at the end of the drying process of each cycle, implying that samples exhibited irreversible volumetric changes up to the 3rd cycle of drying-wetting, but they displayed sort of reversible volumetric changes upon following cycles of repeated hydraulic loads.

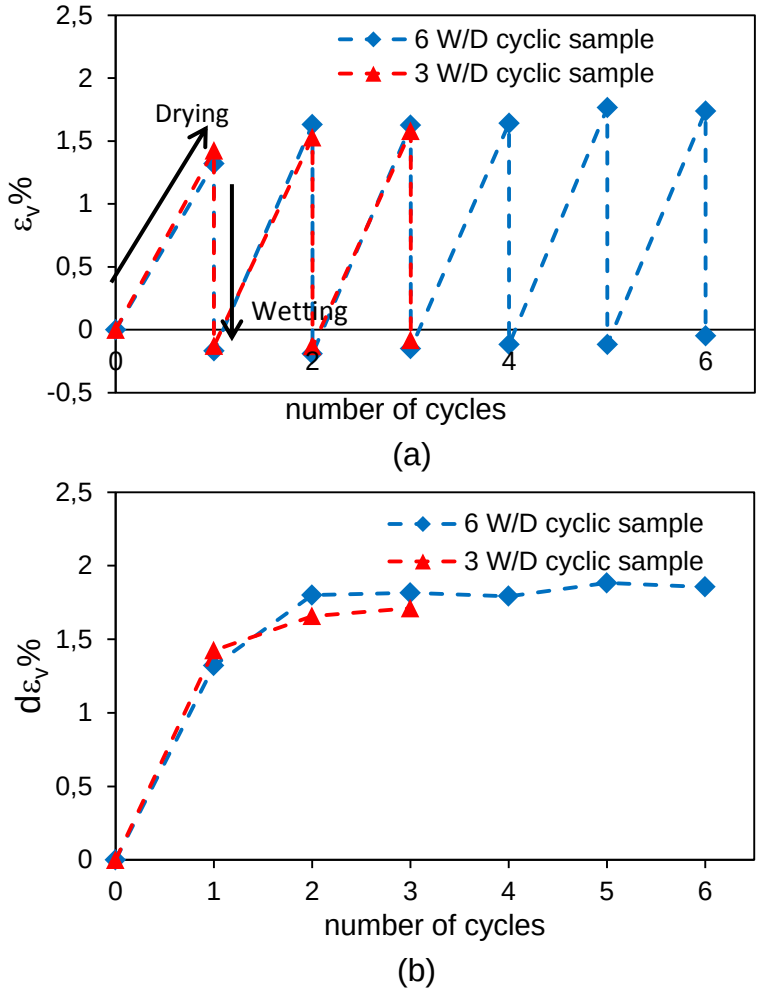

Figure 5.7. Volumetric behaviour of samples subjected to repeated hydraulic loads: (a) Volumetric strain with number of cycles (b) Volumetric strain change at the end of drying process of each cycle.

5.3 Water retention behaviour

5.3.1 Experimental procedure used to study the water retention

The water retention behaviour of Viadana silt was studied using the axis translation and vapour equilibrium techniques to control the suction within the soil samples. The suction controlled oedometer was used to detect the water retention curves at suction values smaller than 400 kPa, in which suction was controlled by the axis translation. The vapour equilibrium technique was also used to study the water retention behaviour of Viadana silt when samples subjected to suction greater than 4 MPa. Samples were removed from oedometer and placed in a closed desiccator, where different saturated salt solutions were used to control the relative humidity (RH) of air, see details in chapter 2.

5.3.2 Water retention behaviour of the as-compacted sample

The sample was placed in suction-controlled oedometer and axial net stress of 50 kPa and suction of 10 kPa were applied to the sample. The volume of the sample slightly decreased at the beginning, where the void ratio decreased from 0.65 to 0.62, but the sample subsequently absorbed water until it was fully saturated. The imposed suction (10 kPa) was smaller than the post-compaction suction acting within the sample, resulted in the water absorption.

The water retention test began by increasing suction to 400 kPa. The test was carried out by increasing the air pressure from 60 to 100, 150, 250, 350, 400 and 450 kPa while the water pressure and axial net stress were kept constant at 50 kPa. This allowed detecting the main drying water retention behaviour at suction levels of 10, 50, 200, 300, 350 and 400 kPa.

The sample was then removed from the oedometer and placed in the desiccator with saturated solutions corresponding to suction values of 4, 11, 24, 41 and 92 MPa while the axial net stress of 10 kPa was applied by means of the dead weight held at the top of the sample. The sample was held in the desiccator for each saturated solution more than 40 days until the equilibrium was established. The weight and the volume of the sample were sequentially measured and the main drying water retention behaviour, in the suction range between 4 and 92 MPa, was then detected regarding the applied suction levels and resulting water contents at the equilibrium.

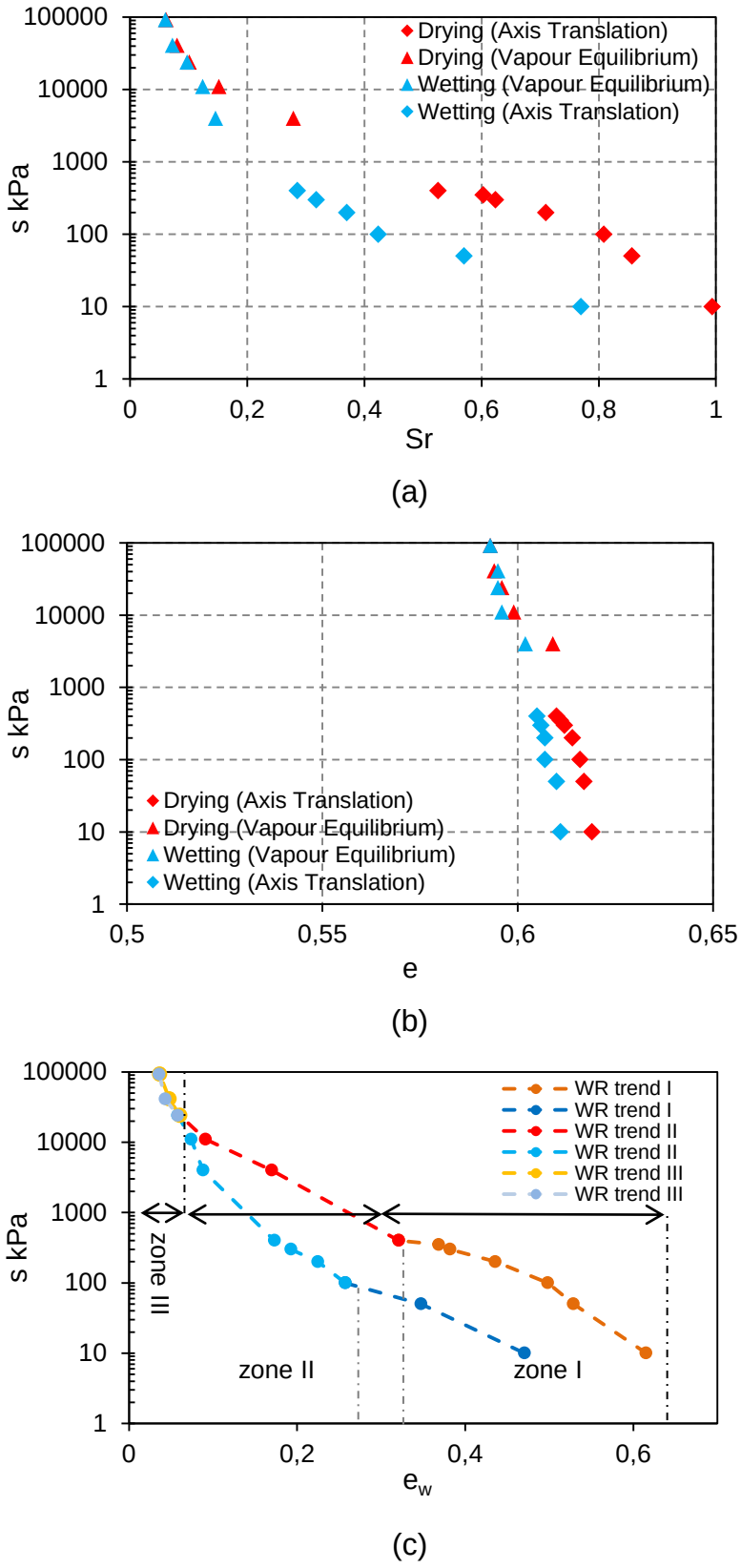

Figure 5.8. Water retention behaviour of the as-compacted sample: a) Sr-log(s) b) e-log(s) c) e_w-log(s)

After the equilibrium was established for the maximum suction level (92 Mpa), the wetting path was applied by placing back the sample in the desiccator with saturated solutions while corresponding suction sequentially decreased to the same suction levels of drying path. The imposed suction decreased until the water content corresponding to the suction value of 4 MPa reached to the equilibrium. The sample was then placed in oedometer, where suction values of 400, 300, 200, 100, 50 and 10 kPa were applied step-by-step using the axis translation technique.

The imposed suction levels and measured degree of saturations (Sr), void ratios (e) and water ratios (e_w) at equilibrium are plotted in Figure 5.8. The entire path for main drying and wetting curves was detected, as represented in Figure 5.8 (a) in terms of Sr- $\log(s)$. The air entry and air occlusion values were obtained to be 44 kPa and 5 kPa for drying and wetting curves, respectively. The volume change of the sample was very small during drying and wetting processes, as shown in Figure 5.8 (b). The void ratio obtained at the end of the wetting path was slightly smaller (0.612) but very close to the initial one. Since the volume of the sample changed insignificantly during drying-wetting paths, water retention shows relatively the same trends in terms of e_w- $\log(s)$ and Sr- $\log(s)$, as shown in Figure 5.8 (a) and 5.8 (c).

It can also be identified that the water retention trend apparently changed at suction values greater than 300 kPa for drying path and suction value greater than 100 kPa for wetting path, as indicated in Figure 5.8 (c). These threshold suction levels correspond to water ratios (e_w) of 0.33 and 0.26 for drying and wetting paths, respectively. It can also be realized that the drying and wetting curves converged to the same values at suction levels greater than 10 MPa (at the water ratio lower than 0.07), where they tended to be linear. Based on the aforementioned observation, the water retention curves of the as-compacted sample of Viadana silt was categorized into 3 trends, as labeled by zone I, II and III in Figure 5.8 (c). The different trends can result from the contribution of different classes of pores in wetting and drying processes. Accordingly, three pore modes can be classified as macropores, mesopores and micropores corresponding to zone I, II and III, respectively, in which the smaller the water ratio the smaller the size of the pores.

5.3.3 Effect of repeated hydraulic loads on WR behaviour

The water retention behaviour of the as-compacted samples subjected to 3 and 6 cycles of drying-wetting (3 and 6 D/W cyclic samples) was also studied using the same experimental procedures previously explained. The water retention behaviour of D/W cyclic samples was compared to as-compacted sample, as shown in Figure 5.9.

Figure 5.9 (a) displays the drying water retention curves obtained for 3 and 6 D/W cyclic samples were mainly similar but different from the one of the as-compacted sample. It is believed that the effects of repeated hydraulic loads on water retention properties have not been further developed with the subsequent cycles leading to detecting the same drying water retention curves for 3 and 6 D/W cyclic samples. This may be consistent with the volumetric behaviour of the samples being subjected to drying-wetting cycles, where the volumetric strain changes became reversible after 2 or 3 cycles (Figure 5.7 (b)). Since no difference was expected in main wetting curves of 3 and 6 D/W cyclic samples, the wetting path was only applied to 6 D/W cyclic sample.

It has to be pointed out that the initial void ratio of samples at the beginning of tests was very close and their volume changes were also insignificant during water retention tests, as shown in Figure 5.9 (b). The resulting water retention curves can be assumed under constant volume condition. This implies that the effect of repeated hydraulic loads observed in water retention behaviour of D/W cyclic sample resulted purely from changes in the soil fabric rather than changes in the global volume of sample.

As shown in Figure 5.9 (a) and 5.9 (c), the main drying and wetting curves for 6 D/W cyclic samples were positioned at the lower level of degree of saturation and water ratio comparing to the ones of the as-compacted sample. During drying, the water desorption for 6 D/W cyclic sample occurred faster than the as-compacted sample up to the suction value of 300 kPa whereas its desorption rate decreased for further suction increments, where the water ratio was lower than 0.22. On the other hand, 6 D/W cyclic sample absorbed water gentler than the as-compacted one when suction decreased to 100 kPa, and then, its water absorption rate increased for further suction reductions (where the water ratio was greater than 0.2).

It is worth noting that the 3 trends of water retention behaviour can also be recognized for the water retention curves of 6 D/W cyclic sample, which was more evident for its main wetting behaviour. It can be understood that the threshold water ratio separating the zone I and II decreased from the drying to wetting water retention behaviour of the as-compacted sample (from 0.33 to 0.26), whereas it remained relatively constant at lower water ratio (0.2) for those of 6 D/W cyclic sample. This may imply that the fabric changes were established after preliminary drying-wetting cycles (2 or 3 cycles) and it remained unchanged for further repeated hydraulic loads. It can also be detected that all water retention curves converged to the same level of water ratio at suction values greater than about 10 MPa ($e_w = 0.07$), implying that the zone III was not influenced by drying-wetting cycles. The zone trend III can relate to the micropores formed inside the aggregates.

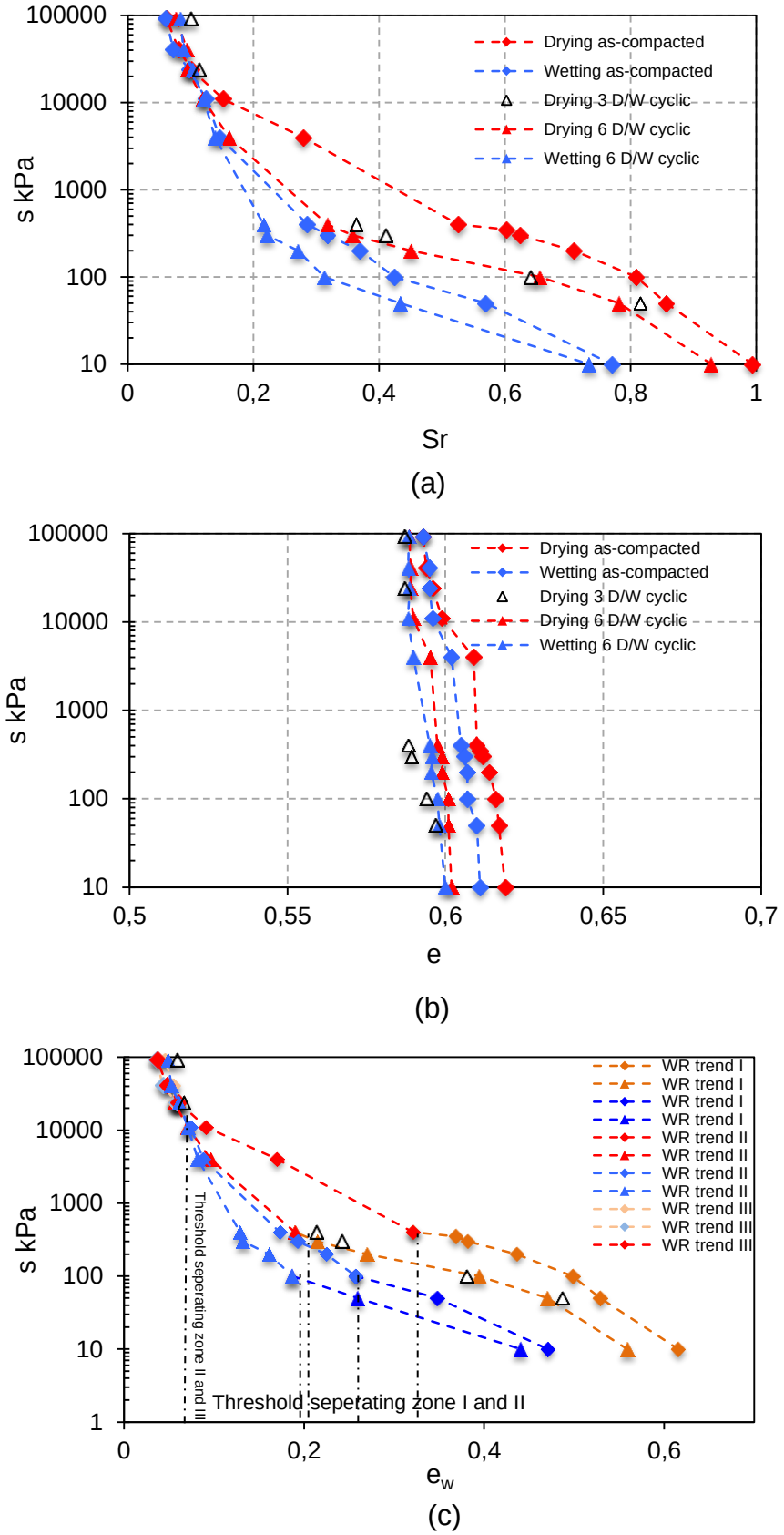

Figure 5.9. Effect of repeated hydraulic loads on the water retention behaviour: a) Sr-log(s) b) e-log(s) c) e_w-log(s)

5.4 Microstructural study

5.4.1 MIP Test

In order to study the microstructure of the as-compacted sample of Viadana silt and quantify the effects of repeated hydraulic loads on the pore size distribution of the as-compacted sample, MIP analysis was employed. Alternative as-compacted and 6 D/W cyclic samples with the same properties of those used for water retention tests were trimmed into small cylindrical samples. They were dehydrated using the freeze-drying technique to preserve the natural fabric of samples and then used for MIP analysis.

5.4.1.1 Interpretation of MIP results

Figure 5.10 (a) and (b) show the result of the MIP analysis for the as-compacted and 6 D/W cyclic samples, plotted in terms of void ratio (intruded)-pore size radius (logarithmic scale) and PSD function-pore size radius (logarithmic scale), respectively. As shown in Figure 5.10 (a), mercury filled pore network of the 6 D/W cyclic sample earlier than those of the as-compacted sample up to the pore size radius of 8300 A, i.e. very close to the position where two curves intercepted. The intruded void ratio corresponding to this point is 0.28. For further increase of intrusion pressure, while pores smaller than 8300 A being filled by mercury, the rate of the intrusion of mercury for 6 D/W cyclic sample decreased more and the intruded void ratio of this sample took place at values smaller than the ones of the as-compacted sample.

The evolution of intruded void ratio due to the effect of repeated hydraulic loads is consistent with the effects of such loads on the water retention behaviour. The change in the trends of intruded void ratio is comparable to the change in the water retention trends of zone I and II. The threshold water ratio separating macropores and mesopores of 6 W/D cyclic sample was found to be 0.2, as mentioned in previous section. Water retention curves showed that drying-wetting cycles cause a shift of the threshold between zone I and II from e_w=0.33 (as-compacted sample, drying branch) to e_w=0.2 (6 D/W cyclic sample, both drying and wetting branch). This shift suggests that drying-wetting cycles induce an increase of the volume of the bigger size pores, which is confirmed by the MIP results. Conversely, the volume of the water associated with the water retention curves at zone II, decreases upon cycling, as confirmed by the smaller volume of intruded pores, having radius of size between 20 and 8300 A.

Figure 5.10 (b) shows the PSD function of the as-compacted and 6 D/W cyclic samples. The bimodal pore size distributions of these samples were evident. Based on the PSD functions of the as-compacted and 6 D/W cyclic samples and their corresponding water retention behaviour, 3 pore modes can be identified in the pore structure.

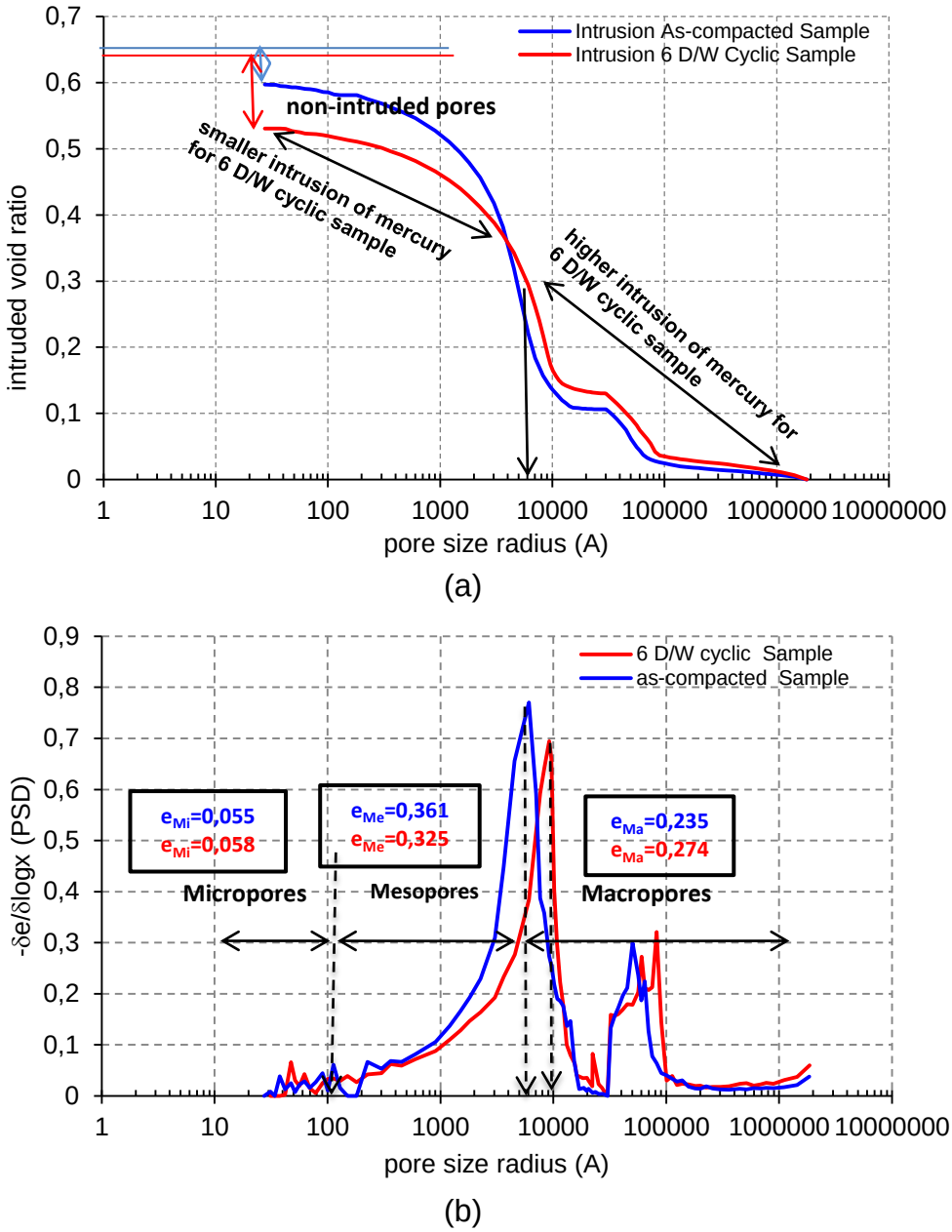

Figure 5.10. Effect of repeated hydraulic loads on MIP results
a) Evolution of intruded void ratio
b) Evolution of pore size density function

As shown in Figure 5.10 (b), 3 pore modes are introduced including micropores with the pore size radius smaller than 150 A, mesopores with the pore size radius between 150 A and 6094 A, and macropores with the pore size radius greater than 6094 A. The pore size radius of 6094 A corresponding to the dominant peak of the PSD of the as-compacted sample was selected as the threshold separating macropores and mesopores. The selected threshold is similar to the one proposed by Romero et al. (2011). The authors used the pore size corresponding to the dominant peak of PSD function of the saturated sample to discriminate the inter-aggregate and intra-aggregate voids in compacted clay. This pore size was consistent with the threshold water ratios responsible for different water retention trends observed in the present experimental results. Moreover, the PSD functions obtained for the loaded samples showed that pores having the size greater than the proposed threshold were affected by the mechanical loading (the results are presented in chapter 6). It is generally accepted that intra-aggregate pores are not much influenced by mechanical loading. This may justify that the mesopores and micropores (having size radius smaller than 6094 A) are both intra-aggregate voids whereas macropores (having size radius greater than 6094 A) are inter-aggregate ones. These pore modes are believed to be responsible for different water retention trends of the as-compacted and 6 D/W cyclic samples. It has to be pointed out that because of a particular structure of the aggregates formed in as-compacted samples of Viadana silt (based on the observation by ESEM images, which will be explained in section 5.4.2), they are denoted as “peds” from now on in the present research.

Micropores are classified as intra-peds pores formed inside peds. The part of PSD functions associated with the micropores was mainly similar for the as-compacted and 6 D/W cyclic samples (having size smaller than 150 A). The corresponding water ratio obtained from the MIP analysis is about 0.06, which is consistent with threshold water ratio separating micropores and mesopores (0.07). The micropores contribute in the water retention behaviour when the water ratio decreased to the values smaller than 0.07. The water retention curve corresponding to this zone remained unchanged during drying-wetting cycles. The clear dominant peak cannot be detected for the micropores, but micro-void ratio (e_{Mi}) of the as-compacted sample was obtained to be 0.056, which was not significantly changed for 6 D/W cyclic sample (e_{Mi}=0.058). This implies that the micropores remained unchanged (or changed reversibly) when samples being subjected to repeated hydraulic loads.

Mesopores are associated with pores having size radius between 150 and 6094 A for the as-compacted sample. This dominant peak in PSD function of 6 D/W sample shifted toward larger pores where it took place at pore size radius of 9173 A. The mesopores are also believed to take place inside the peds. The meso-void ratio (e_{Me}) of the as-compacted sample was obtained to be 0.361. The effect of

repeated hydraulic loads on the microstructure of the as-compacted sample showed two types of structural change in the mesopores, as can be realised comparing the PSD functions of the as-compacted and 6 D/W cyclic samples. Although e_{Me} decreased to 0.325, but the pore size radius corresponding to the dominant peak increased to 9173 A. This implies that the porosity of the mesopores decreased, whereas individual larger pores were formed due to repeated hydraulic loads. The corresponding water ratios of the as-compacted and 6 D/W cyclic sample, obtained from the MIP analysis, are 0.415 and 0.34, respectively. This reduction is consistent with the decrease in threshold water ratios separating macropores and mesopores (zone I and II), which is 0.33 for drying path of the as-compacted sample and 0.2 for the one of the 6 D/W cyclic sample.

Macropores are related to the pores having size greater than 6094 A, where the pore size radius corresponding to the macropores dominant peak of the as-compacted sample is 50136 A. The macropores are related to the water ratio greater than 0.33 for drying water retention curve of the as-compacted sample. The macro-void ratio (e_{Ma}) of the as-compacted sample was found to be 0.235, which increased to 0.274 due to repeated hydraulic loads. This increase resulted from the expansion of the macropores itself (its dominant peak shifted toward larger pores) in addition to the change in the mesopores resulting in the formation of larger pores.

The comparison between the PSD function of the as-compacted and 6 D/W cyclic samples showed that the fabric of such samples is sensitive to changes in the water content resulting from repeated hydraulic loads, and the fabric changes can take place even without any significant changes in the global volumetric strain of the soil sample. The macropores increased in volume and size after being subjected to repeated hydraulic loads. This may induce by the reduction in the volume of the mesopores while the pore size corresponding to the dominant peak of the mesopores shifted to the larger pore size. However, the micropores experienced no significant alteration due to repeated hydraulic loads. The present experimental results suggest a sort irreversible volumetric change of the peds resulting from the response of the mesopores regions to repeated hydraulic loads. This resulted in the soil fabric quite different from the one of the as-compacted sample. On the contrary, the part of intra-peds voids associated with the micropores was not influenced when subjected to such loads. The observed structural change in soil fabric can describe the evolution of the water retention behaviour induced by repeated hydraulic loads. The expansion of the macropores and also the increase in the size of mesopores resulted in the increase in the rate of desorption and absorption of water in drying and wetting paths (zone I), respectively. However, corresponding rates became smaller at water ratio smaller

than 0.2 the increase in the rate of desorption and absorption of water in drying and wetting paths (zone II) since the volume of the mesopores decreased.

It has to be pointed out that the difference between the maximum intruded void ratio and the global void ratio was measured to be 0.057 and 0.123 for the as-compacted and 6 D/W cyclic samples, respectively. In the present work, the pore size of micropores are very small (smaller than 150 A), and a huge volume of micropores must take place with pore size radius smaller than 34 A, if the entire non-intruded void ratio assumed to be micropores. Moreover, intruded void ratios remained relatively constant at pore size radius smaller than 100 A, implying that micropores might be relatively filled with mercury. The residual water ratio was 0.039 and 0.041 for the as-compacted and 6 D/W cyclic samples, respectively. The same amounts of non-intruded void ratios were assumed to be associated with micrpores whereas the rests were attributed to the macropores. This portion of the macropores has very large diameters and is possibly filled by mercury even before starting actual injection.

5.4.1.2 MIP-WRC relationship

MIP data and water retention are related to pore sizes and pore network interconnections of porous media. MIP data has been exploited to quantitatively determine the water retention behaviour of geomaterials. The capillary equation defines the relationship between suction (s) and water surface tension (σ), contact angle of water-solid interface (θ_w) and apparent pore diameter (d),

$$s = \frac{4\sigma cos\theta_w}{d} \tag{5.1}$$

The relationship between the intrusion pressure (p) and mercury surface tension (σ_{Hg}), contact angle of mercury-solid interface (θ_{nw}) and apparent pore diameter (d) represented by Washburn equation (1921) for ideal pores of cylindrical shape or parallel infinite plates,

$$p = -\frac{4\sigma_{Hg} cos\theta_{nw}}{d} \tag{5.2}$$

The relationship between suction and mercury intrusion pressure can be obtained considering equations (5.1) and (5.2),

$$s = -\frac{\sigma cos\theta_w}{\sigma_{Hg} cos\theta_{nw}} p \tag{5.3}$$

Assuming the water surface tension (σ) of 0.072 N/m at 20 ℃, the mercury surface tension (σ_{Hg}) of 0.484 at 25 ℃, the contact angle of water-solid interface (θ_w) of zero and the contact angle of mercury-solid interface (θ_{nw}) of 140°, suction can be estimated by,

$$s \approx -0.196p \tag{5.4}$$

The non-wetting degree of saturation (Sr_{nw}) is defined as the ratio of the volume of intruded mercury to the total volume of pores, and it can be obtained by integrating pore size distribution function ($f(r)$) over unsaturated pores,

$$Sr_{nw}(r) = \int_r^{\infty} f(r)dr \tag{5.5}$$

The volume of pores not intruded by mercury –assuming a non-deformable soil– is used to evaluate the degree of saturation, $Sr = 1 - Sr_{nw}$, and the water content (w) can be obtained,

$$w = w_{sat}(1 - Sr_{nw}) = \frac{e}{G_s}(1 - Sr_{nw}) \tag{5.6}$$

where w_{sat} is saturated water content.

5.4.1.3 Comparing WR obtained from MIP and experimental WRC

Since in the solid-water-mercury mixture, mercury is the non-wetting fluid; mercury intrusion is equivalent to a drying process. MIP data were interpreted in terms of water retention curves according to equation (5.4) and (5.5).The predicted MIP WRCs were plotted in Figure 5.11 in terms of Sr-$\log(s)$ and e_w-$\log(s)$, and compared to the experimental water retention behaviour detected for drying path. The measured degree of saturation for suction values smaller than 4 MPa was well predicted by MIP data for both samples, as shown in Figure 5.11 (a). In fact, the effects of repeated hydraulic loads on water retention behaviour of the as-compacted sample were correctly reproduced by the predicted MIP WRC since such loading induced consistent changes in pore size distributions of the corresponding sample. The good agreement between MIP WRCs and the

experimental one was also detected when the stored water represented in terms of water ratio (5.11 (b)). Although the WRCs obtained from the MIP data were based on ignoring any volume change during suction changes, they were consistent with the experimental data. This resulted from the fact that experimental water retention was detected at relatively constant volume.

The inconsistency between the MIP and experimental WRCs at suction values greater than 4 MPa may be resulted from the fact that the water retention curve obtained from MIP results should be more relevant to the suction levels lower than 2 MPa, in which capillarity dominates water retention. Principally, water is generally held due to capillarity at low suctions, and by adsorption on particle surfaces and in clay inter-layers at higher suctions (Romero et al., 2012).

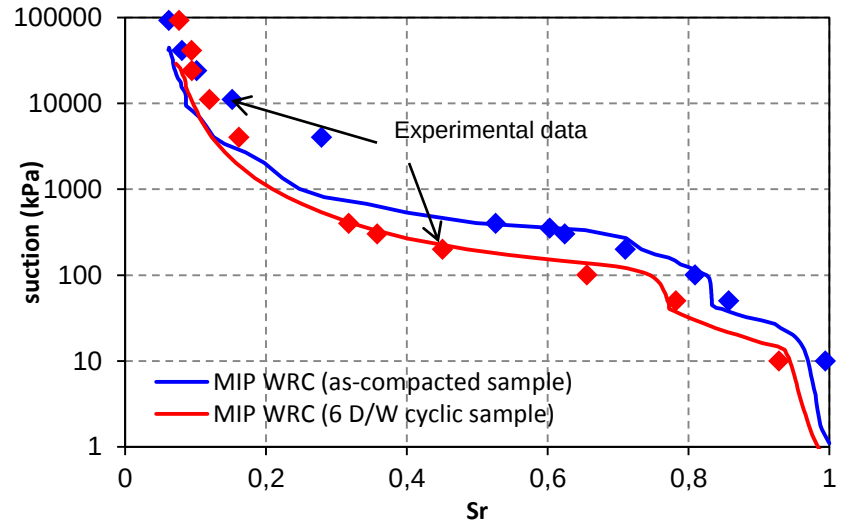

(a)

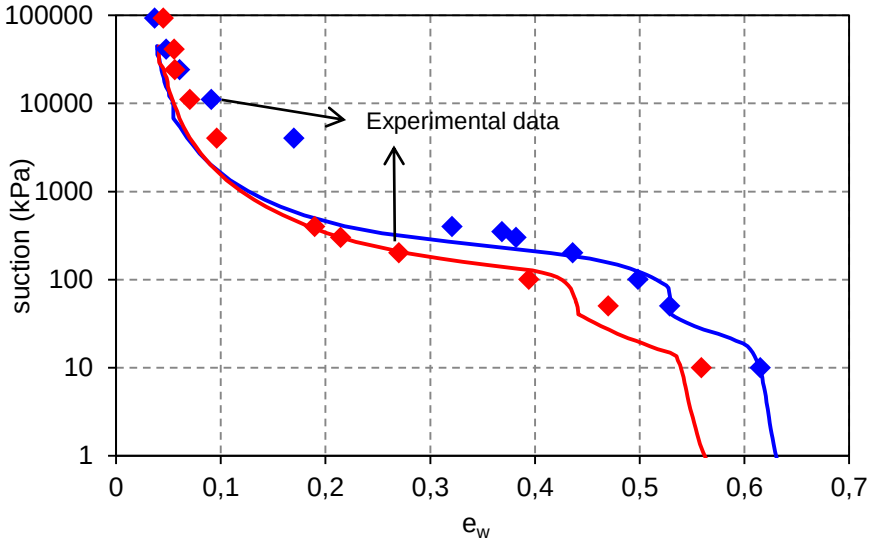

(b)

Figure 5.11. Comparing WRC predicted by MIP and experimental WRC: a) Sr-log(s) b) e_w-log(s)

5.4.2 Interpretation of ESEM analysis of the as-compacted sample

The soil sample with the dry density of 16.3 KN/m^3 was compacted at the water content of 19.8%. It was then used to study the fabric of the as-compacted sample at its natural water content by the ESEM analysis. The resulting photomicrographs at different magnifications are presented in Figure 5.12.

The tested material was clayey silt (Viadana silt) with the clay fraction of 20.4%, as it was characterized in chapter 2. The activity (A) of the tested material was measured to be 0.4, which indicates an inactive soil with typical Kaolinite behaviour. Figure 5.12 (a) may provide a general picture of the fabric of the as-compacted sample. It can be observed that the clay fraction composed of solid particles, whose size is of the order of 10 μm, as well as the peds. This might be consistent with the grain size distribution (presented in chapter 2, Figure 2.2) that shows a clay fraction of about 20%, whereas the remaining larger particles are mainly silt. The silt particles can be clearly detected regarding their size and shape, as some of them are denoted by "S" in Figure 5.12 (a). The arrangement of silt particles can form large pores (e.g. the pore space "Ma" formed between silt particles indicated by "S"). Individual clay particles (denoted by "C") and clay peds (denoted by "CA") are also identified in the soil structure. It is believed that the macropores associated with the pores formed between large particles, or between large particles and peds, as shown in Figure 5.12 (b). In Figure 5.12 (b), the pore size diameter of macropores mostly ranges from 1.5 to 20 μm, which is relatively consistent with the range of pore size identified for macropores regarding the MIP result and corresponding PSD function. The clay ped can also be detected (denoted by "CA") in Figure 5.12 (b). It is worth noting that the shape of the aggregate of the tested material may not take a typical form of the aggregate in the classic frame, but it seemed to possess a ped structure. Accordingly, some larger intra-ped pores can take place inside the peds, particularly around the planar clay particles, as shown in Figure 5.12 (c). Being the pore size diameter smaller than 1.2 μm, such pores are associated with the mesopores classification of the PSD function obtained from the MIP analysis. The changes in the pore size distribution resulted from drying-wetting cycles might then be associated with an irreversible behavior of the peds since the reduction in meso-porosity may be justified by the fact that the suction corresponding to air entering the peds was on the order of 100–200 kPa. Therefore, the fabric changes also resulted from the rearrangement of larger particles. The pore size diameter of the micropores was obtained to be smaller than 0.03 μm regarding the corresponding PSD function. In fact, the micropores associated with a small portion of intra-ped pore structure of the as-compacted sample, which cannot be easily visualized in photomicrographs represented in Figure 5.12.

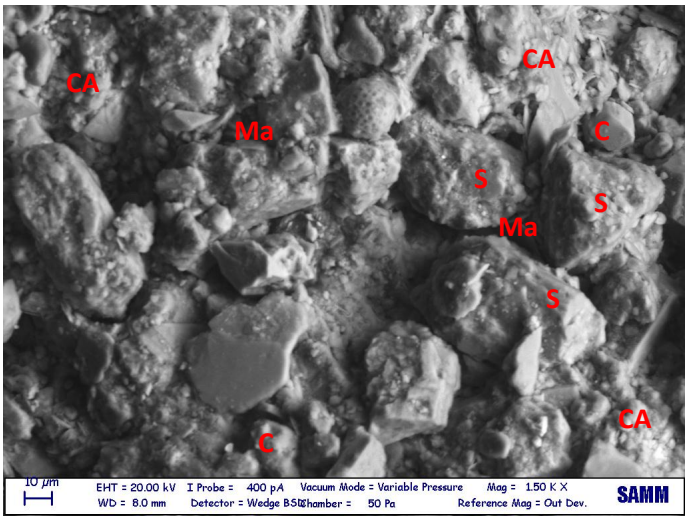

(a)

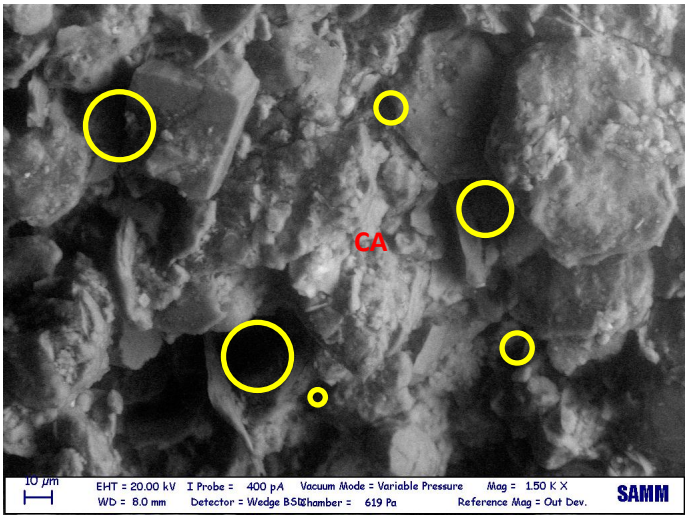

(b)

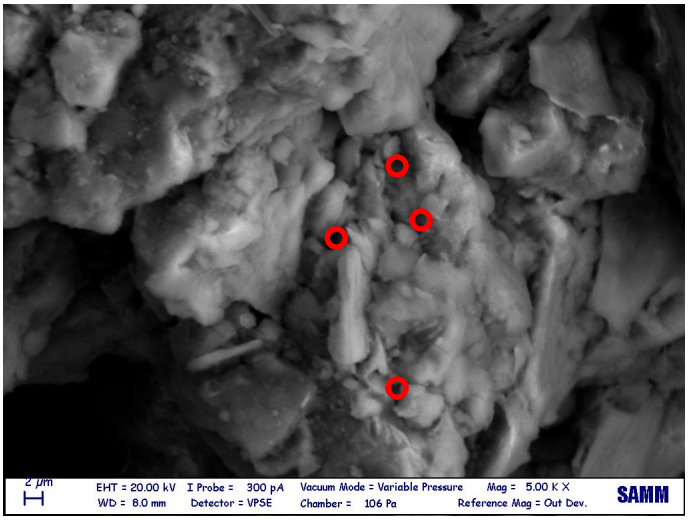

(c)

Figure 5.12. ESEM photomicrographs of as-compacted sample a) Soil particles and peds b) Macropores c) Mesopores.

5.5 WRC model accounting microstructural properties

5.5.1 The link between the pore size density function and water retention properties

The pore size distribution of the porous media $f(r)$ can be measured as a derivative of the cumulative function $F(r)$ with respect to pore radius r, where $F(r)$ defined as the volume of pores with radius equal or greater than any arbitrary value (r),

$$f(r) = \frac{dF(r)}{dr} \tag{5.7}$$

Assuming the pores network of soil can take form as a bundle of different sized cylindrical tubes without interconnections (Millington and Quirk, 1961; Mualem, 1976), the wetting process of soil sequentially fills the pores network from the smallest class of pores to largest ones in sequence. Accordingly, the current degree of saturation $Sr(R)$ can be defined as the volume of the pores filled with water whose radius sizes take place between the minimum value R_{min} and arbitrary one R. This allows introducing the current degree of saturation regarding the cumulative function, and in turn the integration of pore size distribution,

$$Sr(R) = F(R) = \int_{R_{min}}^{R} f(r)dr \tag{5.8}$$

Figure 5.13 represents the relationship between the pore size distribution and cumulative function, and the corresponding degree of saturation while the variable r was replaced by equivalent suction (s).

As proposed by Della Vecchia et al. (2015), $F^e(R)$ can also be introduced as a product of cumulative function and total void ratio (e), representing the contribution of pores having a size smaller than R,

$$F^e(R) = eF(R) \tag{5.9}$$

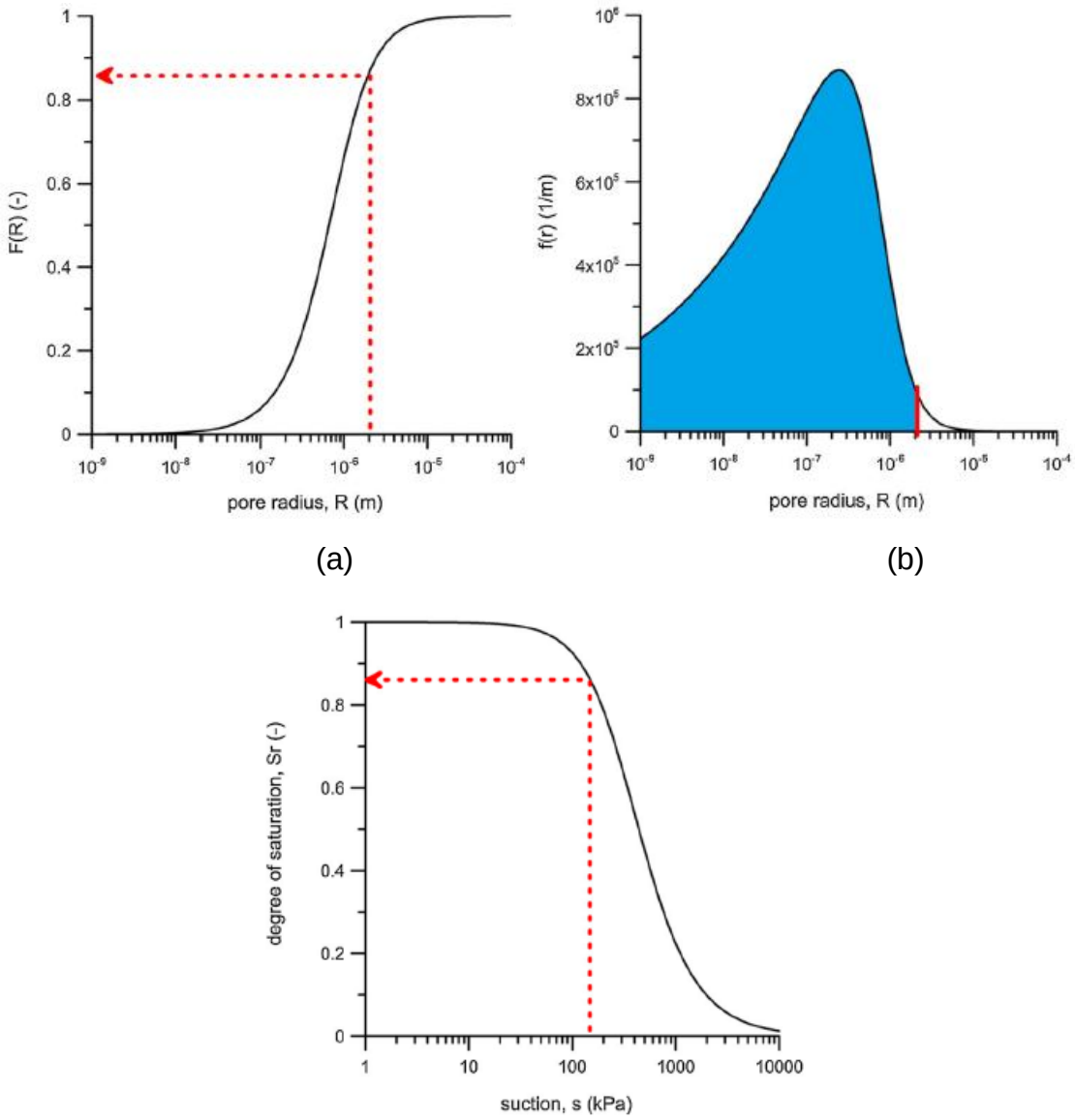

Figure 5.13. a) Cumulative function b) Pore size distribution function c) degree of saturation (Della Vecchia et al., 2015).

Therefore, the derivative of $F^e(R)$ with respect to logarithmic of r give the pore size density function ($PSD(r)$) which is an alternative function to represent pore size distribution,

$$PSD(r) = \frac{dF^e(r)}{dlog(r)} \tag{5.10}$$

Figure 5.14 (a) represents the PSD varies with pore size radius. In fact, the contribution of different pore radii to the total void ratio can be more effectively visualised and the link between the water retention properties and pore size distribution can be justified. The current water ratio $e_w(R)$ can be then obtained as,

$$e_w(R) = eSr(R) = eF(R) = F^e(R) \tag{5.11}$$

which measures the volume of saturated pores with respect to the volume of solids. Figure 5.14 (a) and (b) display the link between the water retention properties and the PSD.

5.5.2 Water retention curve model accounting for Multi-porosity evolving pore size density function

The bimodal water retention model was previously formulated by Dieudonné et al. (2013) and further developed by Della Vecchia et al. (2015) to reproduce the water retention behaviour of compacted clay subjected to hydraulic and mechanical loading. A similar framework is introduced in the following, accounting for required modifications to reproduce the corresponding fabric change observed in experimental results due to repeated hydraulic loads.

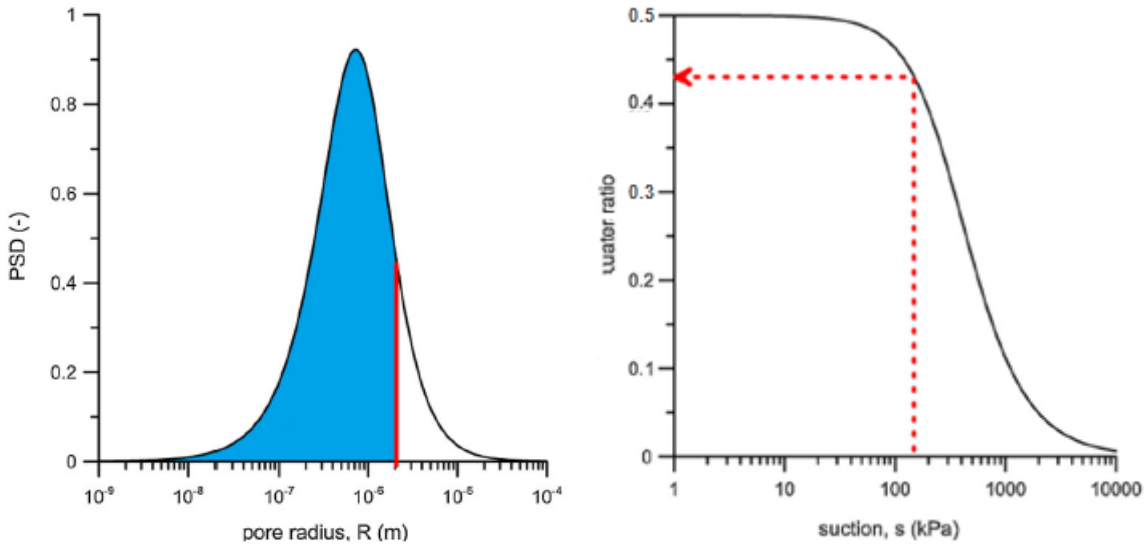

(a) (b)

Figure 5.14. a) Pore size density function b) water ratio.

The present framework lies on the fact that different classes of pores can individually respond to the water retention mechanism although the general concept linking the pore size distribution and water retention properties are preserved. This allows identifying different cumulative distribution functions responsible for different classes of pores. As previously discussed, three types of water retention trends correspond to three pore modes were detected in the as-compacted sample of Viadana silt. The cumulative distribution functions associated with these pore modes can be classified as,

$$F^e(R) = F^e(R)_{Ma} + F^e(R)_{Me} + F^e(R)_{Mi} \tag{5.12}$$

where $F^e(R)_{Ma}$, $F^e(R)_{Me}$ and $F^e(R)_{Mi}$ are cumulative distribution functions for macropores, mesopores and micropores, respectively.

As previously explained, micropores are characterized as intra-ped pores and possess a minor portion of overall porosity of the as-compacted sample. The water retention behaviour associated with micropores was not significantly influenced due to repeated hydraulic loads. Therefore, micropores were assumed to be part of mesopores for the aim of simplifying the modeling formulations. The double porosity structure were then assumed for the as-compacted sample and the cumulative distribution function can be formulated as,

$$F^e(R) = F^e(R)_{Ma} + F^e(R)_{Me} = e_{Ma}F(R)_{Ma} + e_{Me}F(R)_{Me} \tag{5.13}$$

where e_{Ma} is macro-void ratio, and e_{Me} is meso-void ratio.

Accordingly, the water ratio can be obtained as an amalgamation of water ratio of macropores $e_{w_{Ma}}$ and meso-pores $e_{w_{Ma}}$.

$$e_w(R) = e_{w_{Ma}}(R) + e_{w_{Me}}(R) = e_{Ma}Sr(R)_{Ma} + e_{Me}Sr(R)_{Me} \tag{5.14}$$

The equation (5.14) implies that the different analytical models can be employed to reproduce water retention behaviour associated with different pore modes regarding their equivalent PSD function. The water retention curve model proposed by van Genuchten (1980) was adopted in the present work,

$$Sr(s) = \left[\frac{1}{1+(\alpha s)^n}\right]^m \tag{5.15}$$

where n, m and α are model parameters.

Finally, the formulation of the water retention curve in terms of water ratio $e_w(s)$ can be expressed as,

$$e_w(s) = e_{w-Ma} + e_{w-Me} \tag{5.16}$$

hence,

$$e_w(s) = e_{Ma}\left[\frac{1}{1+(\alpha_{Ma}s)^{n_{Ma}}}\right]^{m_{Ma}} + e_{Me}\left[\frac{1}{1+(\alpha_{Me}s)^{n_{Me}}}\right]^{m_{Me}} \tag{5.17}$$

where n_{Ma}, m_{Ma}, α_{Ma} and n_{Me}, m_{Me}, α_{Me} are the parameters of van Genuchten model for macropores and mesopores, respectively.

The equation (5.17) implies that the bimodal water retention curve can be obtained as a superposition of two structure levels, i.e. the mesostructure and macrostructure.

5.5.3 Comparison between model predictions and experimental data

By means of the proposed model, the Bimodal water retention curve can be obtained for any soil sample, whose PSD is bimodal. For the tested material, the water retention curve was predicted resulted from the superposition of two different retention trends, one for the macropores and one for the mesopores. For the aim of simplicity, the micropores was assumed to be part of the mesopores since they were associated with the small range of water ratio and their retention behaviour can be predicted as a tail of the water retention curve of the mesopores.

The water ratio was calculated by summing the water ratio of the macropores and mesopores ($e_{w-Ma} + e_{w-Me}$) whereas the degree of saturation was obtained by the sum of the meso and macro degree of saturation, weighted by the corresponding volumetric fractions.

Figure 5.15 (a) and (b) shows predictions of the proposed model comparing to the experimental retention data of the as-compacted sample during drying and

wetting, as represented in terms of Sr-$\log(s)$ and e_w-$\log(s)$. The parameters of the model used in the present study are listed in Table 5.2.

Table 5.2. Parameters of the model

sample	Applied load	$1/\alpha_{Ma}$	n_{Ma}	m_{Ma}	$1/\alpha_{Me}$	n_{Me}	m_{Me}
As-compacted sample	Drying	76	2.67	0.83	554	1.71	0.29
	Wetting	9	2.66	0.78	48	1.92	0.164
6 D/W cyclic sample	Drying	57	3.24	0.54	273	1.64	0.37
	Wetting	7	2.79	0.41	23	1.26	0.19

As shown in Figure 5.15 (a) and (b), the bimodal predicted curves are evident. The degree of saturation of the macropores and mesopores are represented where each structure level possesses its own air-entry value. The predicted water retention curve associated with macropores shows that the saturated macropores at the beginning of drying path possess the water ratio of 0.2, which began to decrease at suction values of 76 kPa. Obviously, the air-entry value of mesopores is greater than this value due to their smaller pore size. The air-entry value for mesopores is measured to be 554 kPa at the drying path. This caused that macropores can be unsaturated for a certain value of suction whereas the mesopores are still filled with water.

Figure 5.15 (a) shows that the water ratio of the macropores and mesopores are 0.2 and 0.41 at the beginning of the drying curve when the as-compacted sample is saturated. In fact, these values were adopted with reference to the corresponding water ratios obtained from the MIP analysis of the as-compacted sample while the meso-void ratio involved also the micro-one ($e_{Me} + e_{Mi}$).

As previously discussed, the macro-void ratio increased to 0.27 and the meso-void ratio decreased to 0.32 after being subjected to the 6 cycles of drying-wetting. The corresponding void ratios at the end of the wetting path of water retention test were estimated by interpolating the evolution of the relevant void ratios in the first cycle. Therefore, it can be understood that the volume of the macropores increased while the one of the mesopores decreased after being subjected to drying and wetting.

It has to be pointed out that the samples subjected to 50 kPa axial net stress at the beginning of the water retention tests, where their void ratio decreased from 0.657 to 0.621. This volume reduction is believed to take place in macropores. The same amount of the volume reduction was considered in the computation of the macro-void ratio.

Figure 5.16 (a) and (b) shows the comparison between the model predictions and the experimental water retention detected for the 6 D/W cyclic sample. As the pore size of the dominant peak of the macropores and mesopores increased due to

repeated hydraulic loads, the air-entry value of each structure level decreased accordingly. Consequently, the macropores and mesopores are saturated at very low suction levels, as shown in Figure 5.16 (a). The volumetric components of each structure level assumed to change reversibly as they are equal at the beginning of drying and at the end of wetting. It was justified by the fact that the fabric changes took place in the preliminary drying-wetting cycles and it remained unchanged for following cycles. The proposed bimodal water retention curve was able to consistently predict the water retention behaviour of the as-compacted sample as well as the 6 D/W cyclic one, in which the inflections of the predicted curves were associated with the threshold water ratios detected in the water retention behaviour of these samples.

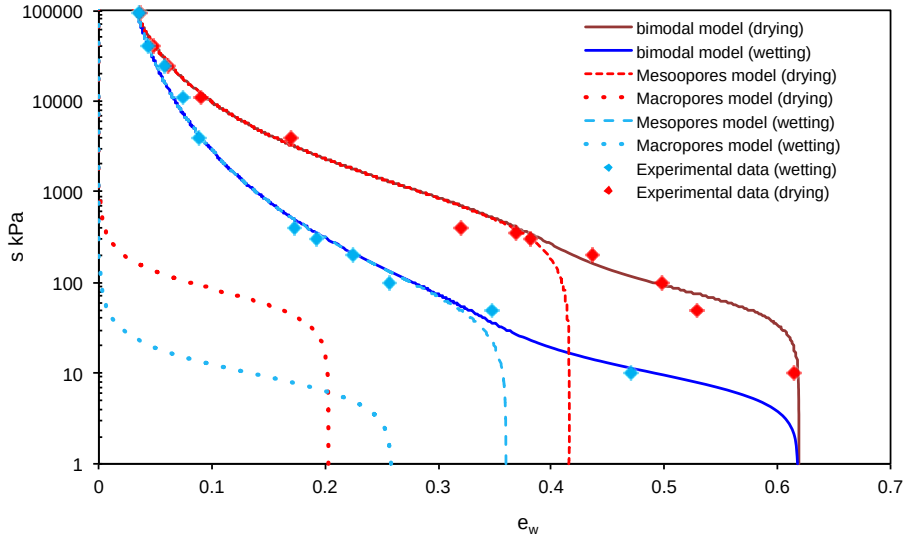

(a)

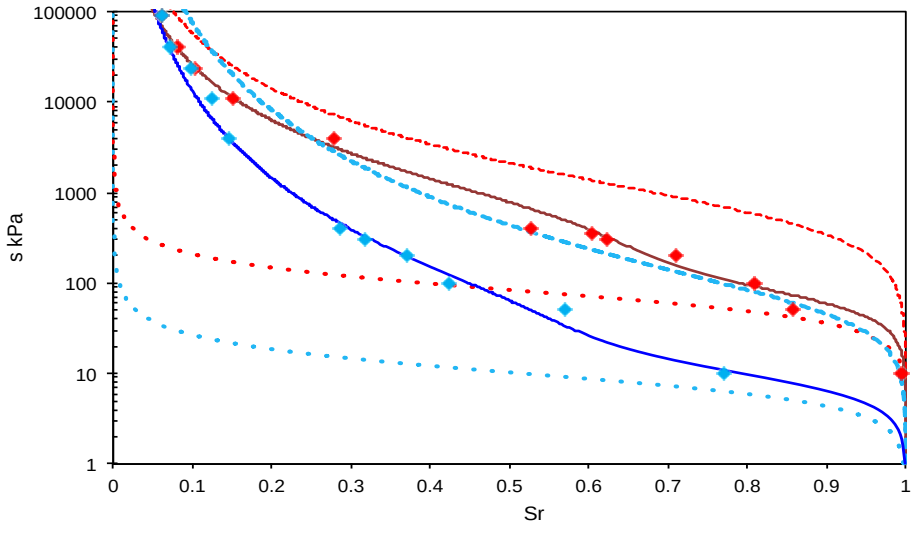

(b)

Figure 5.15. Comparing model predictions and experimental data for the as-compacted sample a) e_w-log(s) b) Sr-log(s)

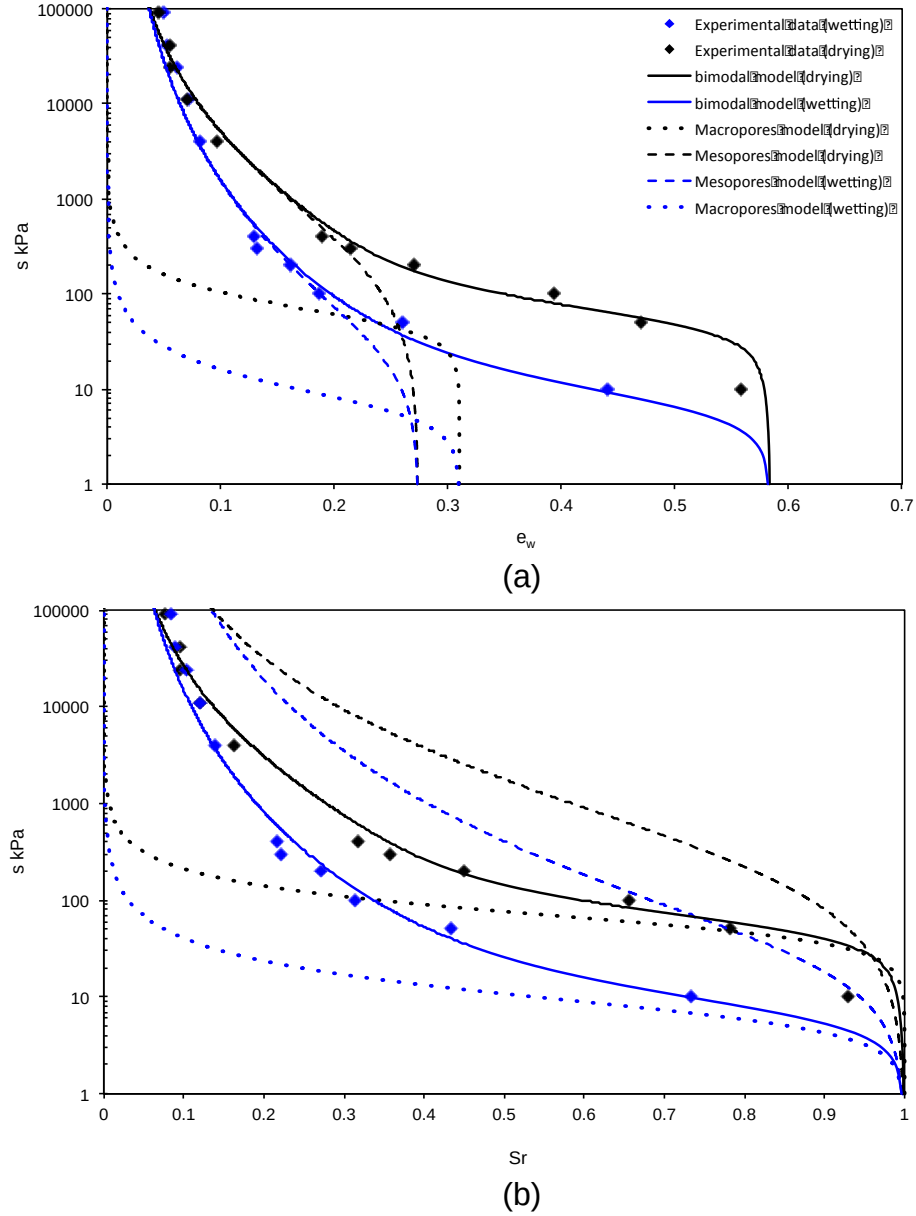

Figure 5.16. Comparing model predictions and experimental data for 6 D/W cyclic sample a) e_w-log(s) b) Sr-log(s)

5.6 Conclusion

In the present research, effects of repeated hydraulic loads on hydraulic properties of compacted clayey silt were studied. The water retention behaviour of the as-compacted sample was detected for drying and wetting path, and it was then compared to those obtained for the as-compacted samples subjected to 3 and 6 drying-wetting cycles (named as 3 and 6 D/W cyclic sample, respectively). The 3

and 6 D/W cyclic samples exhibited mainly the same water retention behaviour but different from the as-compacted one. It was observed that both main drying and main wetting water retention curves of the as-compacted sample shifted toward lower values of water content after being subjected to cycles of drying-wetting, although all wetting and drying curves were converged to the same value of water ratio at the suction level greater than 10 MPa.

Moreover, 3 types of water retention trend were identified for all drying and wetting branches, which were associated with contribution of different pore modes in the soil microstructure. It is believed that fabric changes took place in the soil structure of the as-compacted sample when being subjected to drying-wetting cycles, in which such fabric changes established after 2 or 3 cycles and no further alteration occurred due to the subsequent drying-wetting cycles.

The effects of repeated hydraulic loads in the microstructural level were also studied using the mercury intrusion porosimetry (MIP) analysis of the as-compacted and 6 D/W cyclic samples. The PSD functions of these samples were classified to 3 types of pore modes, namely, micropores, mesopores and macropores. These pore modes are believed to be responsible for different trends observed in water retention behaviour of the corresponding samples. The micropores and mesopores were identified as intra-ped, considering that the ped structure observed in micrograph (ESEM) of the tested material was different from a typical ped in the classical frame. The micropores were found to remain unchanged during drying and wetting whereas the volume of the mesopores decreased, leading to the irreversible volume change of the peds in response to drying-wetting cycle. Besides the reduction of mesoporosity, some individual larger pores were formed. On the other hand, macropores experienced the increase in the size and volume.

As a result, the effect of repeated hydraulic loads may be referred to the “fabric destruction” as they develop larger pores in the pore network of the as-compacted sample. It is worth noting that no significant global volumetric strain changes in the as-compacted sample was detected after being subjected to drying-wetting cycles, implying that the fabric changes took place due to interaction between different pore modes. The observed fabric changes resulted in the change of the rate of water absorption and desorption of the as-compacted sample, leading to the different water retention behaviours during wetting and drying paths.

The new water retention curve model was then proposed accounting for different pore modes detected in the soil fabric of the tested material. The proposed model allows evolving pore size distribution, in which different analytical formulation can be employed to reproduce water retention behaviour of different pore modes regarding their equivalent pore size density (PSD) functions. The bimodal water retention curve can be then predicted as a superposition of water ratios associated

with different structure levels. The formulation of the model was drived regarding the mesopores and macropores in the present research work (the micropores was neglected in the model for the aim of simplicity). Therefore, the proposed model wwas employed to quantify the effect of repeated hydraulic loads on the water retention behaviour regarding the corresponding changes in the PSD functions.

References

[1] Ahmed S, Lovell G, Diamond S. Pore sizes and strength of compacted clay. ASCE, Journal of Geotechnical Engineering Division 1974; 100:407–425.

[2] Al Mukhtar G, Belanteur N, Tessier D, Vanapalli S. The fabric of a clay soil under controlled mechanical and hydraulic stress states. Applied Clay Sciences 1996; 11:99–115.

[3] Alonso, E.E., Romero, E., Hoffmann, C., García-Escudero, E., 2005. Expansive bentonite–sand mixtures in cyclic controlled-suction drying and wetting. Eng. Geol. 81, 213–226.

[4] Alonso E, Vaunat J, Gens A. Modelling the mechanical behaviour of expansive clay. Engineering Geology 1999; 54:173–183.

[5] Alshihabi, O., Shahrour, I., Mieussens, C., 2002. Experimental study of the influence of suction and drying/wetting cycles on the compressibility of a compacted soil. Proceedings of 1st International Conference on Unsaturated Soils, Balkema, Rotterdam, The Netherlands, pp. 541–545.

[6] Aubertin, M., Mbonimpa, M., Bussière, B., and Chapuis, R. (2003). A model to predict the water retention curve from basic geotechnical properties. Canadian Geotechnical Journal, 40:1104–1122. 4.1.

[7] Benson, C. H., Sawangsuriya, A., Trzebiatowski, B., and Albright, W. H. (2007). Postconstruction changes in the hydraulic properties of water balance cover soils. Journal of Geotechnical and Geoenvironmental Engineering, 133(4):349–359. 4.1.

[8] Brooks RH, Corey AT. Hydraulic properties of porous media. Hydrological Papers (Colorado State University) 1964; 3.

[9] Calabresi G., Colleselli F., Danese D., Giani G.P., Mancuso C., Montrasio L., Nocilla A., Pagano L., Reali E., Sciotti A. (2013). A research study of the hydraulic behaviour of the Po river embankments. CANADIAN GEOTECHNICAL JOURNAL. Volume 50, Issue 9, Sep-tember 2013, Pages 947-960. ISSN: 00083674.

[10] Casini F, Vaunat J, Romero E, Desideri A. Consequences on water retention properties of double-porosity features in a compacted silt. Acta Geotechnica 2012; 7(2):139–150.

[11] Colombo, P. 1965. I materiali dei rilevati arginali. Studio delle caratteristiche dell'argilla limosa degli argini del Po. La ricerca scientifica. Anno 35, Serie 2, No. 8(4), 863–880.

[13] Cuisinier O, Laloui L. Fabric evolution during hydromechanical loading of a compacted silt. International Journal for Numerical and Analytical Methods in Geomechanics 2004; 28:483–499.

[14] Cuisinier, O., Masrouri, F., 2005. Hydromechanical behavior of a compacted swelling soil over a wide suction range. Eng. Geol. 81, 204–212.

[15] Delage P. A microstructure approach to the sensitivity and compressibility of some Eastern Canada sensitive clays. Geotechnique 2010; 60(5):353–368.

[16] Delage, P., Audiguier, M., Cui, Y., and Howat, M. (1996). Miscrostructure of a compacted silt. Canadian Geotechnical Journal, 33:150–158. 3.1.2, 3.2, 4.1.

[17] Delage P, Lefebvre G. Study of the structure of a sensitive Champlain clay and its evolution during consolidation. Canadian Geotechnical Journal 1984; 21:21–35.

[18] Della Vecchia G. Coupled hydro-mechanical behaviour of compacted clayey soils. Phd Thesis, Politecnico di Milano, 2009.

[19] Della Vecchia, G., A.C. Dieudonne, C. Jommi, R. Charlier, 2015. Accounting for evolving pore size distribution in water retention models for compacted clays. International Journal for Numerical and Analytical Methods in Geomechanics 39 (7), 702-723. DOI: 10.1002/nag.2326.

[20] Della Vecchia G, Jommi C, Romero E. A fully coupled elastic–plastic hydromechanical model for compacted soils accounting for clay activity. International Journal for Numerical and Analytical Methods in Geomechanics 2013; 37 (5):503–535.

[21] Diamond S. Pore size distributions in clays. Clays and Clay Minerals 1970; 18:7–23.

[22] Dieudonné AC, Levasseur S, Charlier R, Della Vecchia G, Jommi C. A water retention model for compacted clayey soils. In Computational Geomechanics COMGEO III, Proceedings of the 3rd International Symposium on Computational Geomechanics, Krakow, Poland, Pietruszczak S, Pande GN (eds.). International Centre for Computational Engineering: Rhodes, Greece & Swansea, UK, 2013; 23–31.

[23] Fredlund DG, Xing A. Equations for the soil-water characteristic curve. Canadian Geotechnical Journal 1994; 31 (3):521–532.

[24] Garcia-Bengochea, I., Lovell, C., and Altschaeffl, G. (1979). Pore distribution and permeability of silty clays. ASCE, Journal of Geotechnical Engineering Division, 105:839–856. 4.1

[25] Griffiths, F. and Joshi, R. (1989). Change in pore size distribution due to consolidation of clays. Géotechnique, 39 (1):159–167.

[26] Hu R, Chen YF, Liu HH, Zhou CB. A water retention curve and unsaturated hydraulic conductivity model for deformable soils: consideration of the change in pore-size distribution. Geotechnique 2013; 63(16):1389–1405.

[27] Kawai K, Kato S, Karube D. The model of water retention curve considering effects of void ratio. Proceedings of the Asian Conference on Unsaturated Soils, UNSAT-ASIA 2000, Singapore, 18–19 May, 2000. In Unsaturated Soils for Asia. Rahardjo H, Toll DG, Leong EG (eds.). AA. Balkema, Rotterdam, 2000; 329–334.

[28] Koliji A, Laloui L, Cusinier O, Vulliet L. Suction induced effects on the fabric of a structured soil. Transport in Porous Media 2006; 64:261–278.

[29] LIoret A, Khalili N (2000) A three phase model for unsaturated soils. Int J Numer Anal Method Geomech 24(11):983–927

[30] Lloret, A., Villar, M.V., Sanchez, M., Gens, A., Pintado, X., Alonso, E.E., 2003. Mechanical behaviour of heavily compacted bentonite under high suction changes. Geotechnique 53 (1), 27–40.

[31] Millington RJ, Quirk JP. Permeability of porous media. Nature 1961; 1983:387–388.

[32] Monroy R, Zdravkovic L, Ridley A. Evolution of microstructure in compacted London clay during wetting and loading. Géotechnique 2010; 60(2):105–119.

[33] Mualem Y. A new model for predicting the hydraulic conductivity of unsaturated porous media. Water Resources Research 1976; 12(3):513–522.

[34] Ng CW, Pang YW. Influence of stress state on soil-water characteristics and slope stability. Journal of Geotechnical and Geoenvironmental Engineering 2000; 126(2):157–166.

[35] Nowamooz, H., Masrouri, F., 2009. Density-dependent hydromechanical behaviour of a compacted expansive soil. Eng. Geol. 106, 105–115.

[36] Romero E. A microstructural insight into compacted clayey soils and their hydraulic properties. Engineering Geology 2013; 165:3–19.

[37] Romero E, Della Vecchia G, Jommi C. An insight into the water retention properties of compacted clayey soils. Geotechnique 2011; 61(4):313–328.

[38] Romero E, Simms P. Microstructure investigation in unsaturated soils: a review with special attention to contribution of mercury intrusion porosimetry and environmental scanning electron microscopy. Geotechnical and Geological Engineering 2008; 26:705–722.

[39] Romero, E. and Vaunat, J. (2000). Retention curves of deformable clays. proc. int. workshop on unsaturated soils. In Tarantino, A. and Mancuso, C., editors, Experimental Evidence and Theoretical Approaches in Unsaturated Soils, pages 91–106, Trento, Italy. AA. Balkema, Rotterdam.

[40] Sharma, R. S. (1998). Mechanical behavior of unsaturated highly expansive clays. PhD Thesis, Oxford University.

[41] Simms PH, Yanful EK. Estimation of soil-water characteristic curve of clayey till using measured pore-size distribution. Journal of Environmental Engineering 2004; 130(8):847–854.

[42] Sivakumar, V., Tan, W.C., Murray, E.J., McKinley, J.D., 2006. Wetting, drying and compression characteristics of compacted clay. Geotechnique 56 (1), 57–62

[43] Sridharan A, Altschaeffl A, Diamond S. Pore size distribution studies. ASCE, Journal of the Soil Mechanics and Foundation Division 1971; 97(5):771–787.

[44] Tarantino A, De Col E. Compaction behaviour of clay. Geotechnique 2008; 58(3):199–213.

[45] Van Genuchten MT. A closed-form equation for predicting the hydraulic conductivity of unsaturated soils. Soil Sci- ence Society of America Journal 1980; 44:892–898.

[46] Vanapalli SK, Fredlund DG, Pufahl DE. The influence of soil structure and stress history on the soil-water charac- teristics of a compacted till. Geotechnique 1999; 49(2):143–159.

[47] Wang Q, Tang AM, Cui YJ, Delage P, Barnichon JD, Ye WM. The effects of technological voids on the hydromechanical behaviour of compacted bentonite-sand mixture. Soils and Foundations 2013; 53(2):232–245.

[48] Wang Q, Tang AM, Cui YJ, Delage P, Gatmiri B. Experimental study on the swelling behaviour of bentonite/claystone mixture. Engineering Geology 2012; 124(4):59–66.

6

EFFECT OF REPEATED HYDRAULIC LOADS ON THE HYDROMECHANICAL BEHAVIOUR OF A SILTY SOIL

6.1 Introduction

6.1.1 Coupling hydromechanical behaviour

Effects of hydraulic history on the mechanical behaviour and volumetric response of unsaturated soils upon drying-wetting processes have been discussed by many authors during past years. Behaviour of unsaturated clayey soils with high activity has been commonly studied as they experienced much larger volumetric change upon drying-wetting compared with unsaturated soils with low activity. However, unsaturated soils with low activity also exhibited some particular features.

Alonso et al. (1987) suggested that an unsaturated soil may either swell or collapse upon wetting if the confining pressure is sufficiently low or high. The volumetric response does not depend only on confining pressures but also on initial density at which samples are prepared (Sivakumar et al., 2006). Principally, the results showed that compacted clayey soils swelled with a high initial dry density and collapsed at a low initial dry density. During drying, unsaturated soils generally experienced volumetric contractions, which observed to be irreversible if suction increased above the yield suction value (Alonso et al., 1990; Chen et al, 1999; Sivakumar et al., 2006).

Many researchers, such as Wheeler et al. (2003), Alonso et al. (2005), Nowamooz and Masrouri (2008), have studied the behaviour of expansive soils during wetting and drying cycles, in which the hydraulic loads were applied by controlling the imposed suction. Significant irreversible accumulation of strain for expansive clayey soil was reported during drying-wetting cycles at constant applied stress (e.g. Alonso et al., 1995; Sharma, 1998; Romero, 1999). Cui et al. (2002) presented similar reversible volumetric changes in dense compacted clays being subjected to drying-wetting cycles. Wheeler et al. (2003) showed the irreversible volumetric strain occurred in non-active kaolin when subjected to drying-wetting cycles at constant isotropic stress. This implied that the irreversible strains are not solely induced by active clay minerals but it can take place due to changes in the degree of saturation and resulting hydraulic hysteresis. The influence of chemical properties on the behaviour of expansive soils was also studied by some researchers (Alawaji, 1999; Musso et al., 2003; Di Maio et al., 2004; Rao and Shivananda, 2005; Casttellanos et al., 2008; Siddiqua et al., 2011).

Many researchers presented experimental results with reference to the effects of suction history on the stress-strain response, shear strength, volumetric strain and water content changes of unsaturated soils.

The compressibility of an unsaturated soil may increase with decreasing suction as reported by Alonso et al. (1990). However, the experimental work of Wheeler & Sivakumar (1995) and Chiu & Ng (2003) showed that the compressibility under saturated conditions is smaller than the one under unsaturated conditions. Some researchers (e.g. Sharma, 1998; Alshibabi et al., 2002; Sivakumar et al., 2006) compared isotropic compression curves at a given suction after wetting and after drying. It was found that a drying-wetting cycle resulted in a decrease in pre-consolidation stress in both non-expansive (Sivakumar et al., 2006) and expansive soils (Sharma, 1998). In the contrary, a drying-wetting cycle caused an increase in the pre-consolidation stress of the compacted clay (Alshibabi et al., 2002).

Besides the effect of suction and stress, the degree of saturation and void ratio were also reported to affect the shear behaviour of unsaturated soils. Recently, effects of hydraulic history on the hydromechanical behaviour of unsaturated soils, with reference to the role of water retention hysteresis, were studied by Nuth and Laloui (2008). Romero and Jommi (2008) also discussed the anisotropy of the strain response induced by repeated hydraulic loads.

Besides the effects of the hydraulic state on the mechanical behaviour, the retention behaviour is also coupled with the mechanical history. Experimental results justified the effects of mechanical variables on the water retention properties of unsaturated soil, e.g. Tarantino and De Col E. (2008), Vanapalli et al. (2000), Ng and Pang (2000) and Benson et al. (2007) among others.

Figure 6.1 shows the experimental results on Barcelona clayey silt presented by Barrera (2002), in which the hydromechanical stress path was applied and the coupling hydraulic and mechanical behaviour of unsaturated soil was reported. The effect of hydraulic state on the compressibility of the soil behaviour can be clearly recognised by comparing the changes in the void ratio during compression loading at different suction levels in BC, EF and HI stress paths (Figure 6.1 (a), and (c)). On the other hand, the drying paths CD and GH were applied while the sample was experienced different void ratios. The different water ratios observed in these two paths resulted from the effect of mechanical variable (void ratio) on the water retention curve (Figure 6.1 (b)). The irreversible changes in the degree of saturation (e_w/e) during loading-unloading cycles (EFG and HIJ) also justified the coupling between the hydraulic and mechanical behaviour of unsaturated soil (Figure 6.1 (d)).

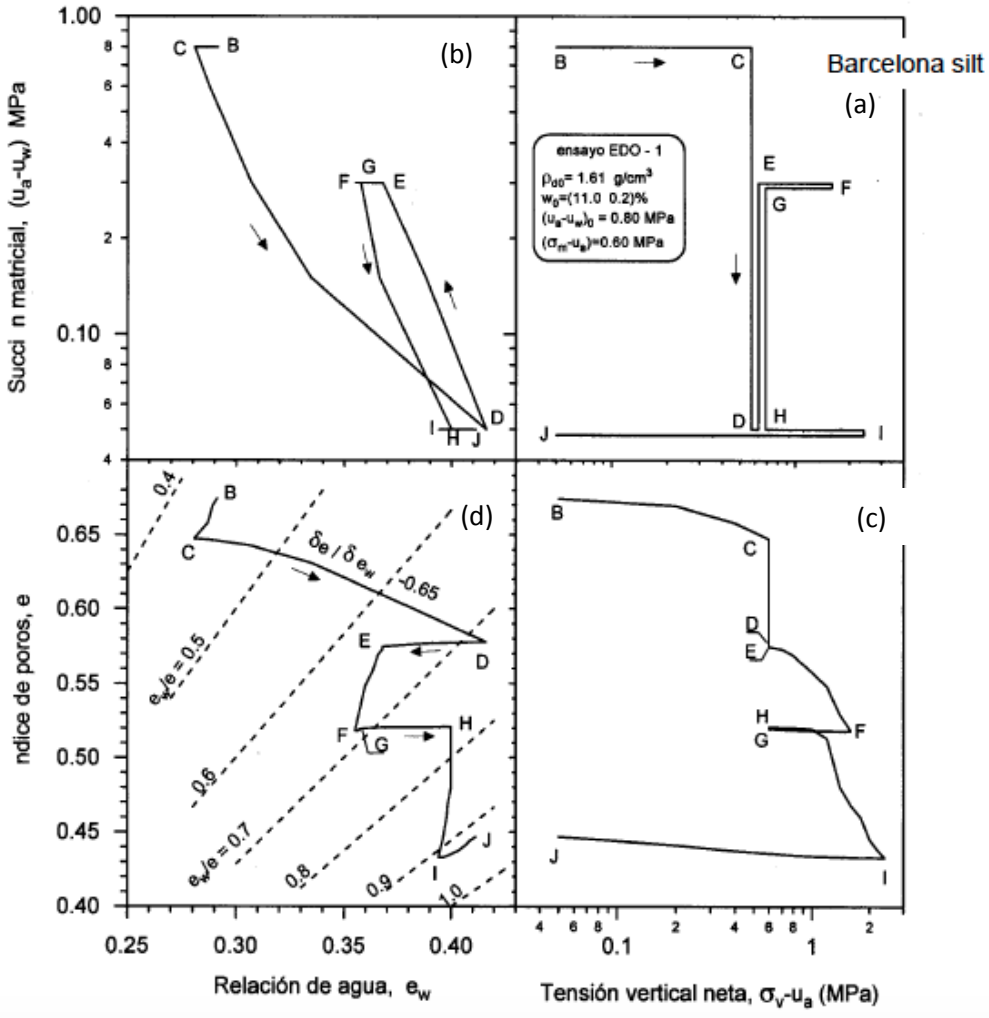

Figure 6.1. Hydromechanical paths applied to Barcelona silt compacted at the dry side of optimum. (a) Stress path followed in suction-axial net stress plane (b) water retention behaviour in terms of suction-water ratio (c) volume change response (d) water retention behaviour in terms of void ratio-water ratio (Barrera 2002).

6.1.2 Hydromechanical behaviour evolving microstructural features

The link between the hydromechanical response and microstructural features of unsaturated soils was addressed to be an important approach justifying many hydromechanical properties of unsaturated soils, such as the compressibility, shear strength, water retention and hydraulic conductivity. Microstructural experimental results allow studying the distinct response of microstructural levels as well as an understanding of their interactions upon hydromechanical loading paths. Such experimental results were employed to build up a framework for constitutive modelling of unsaturated soil behaviour considering multi-structural features. Some of research studies considering microsrtructural aspects of unsaturated soil behaviour were briefly discussed in chapter 5.

Figure 6.2 represents PSD functions of 3 different soils including illitic-kaolinitic clay (Figure 2 (a)), clayey silt (Figure 2 (b) and sand-bentonite mixture with a dominant sandy skeleton (Figure 2 (c)). As reported by Romero (2014), all samples were first freeze-dried and then used for MIP analysis. The initial and final PSD functions during compression at constant water ratios are represented in Figure 6.2. The bimodal PSD functions are evident for illitic-kaolinitic clay and clayey silt whereas the PSD function of sand-bentonite mixture exhibits multimodal form. The dominant peaks corresponding to the maximum pore size were classified as the macrovoid (inter-aggregate pores formed between aggregates). The macrovoid of illitic-kaolinitic clay was experienced a significant decrease in the volume and gentle reduction in the pore size due to the compression, where the void ratio decreased from 0.93 to 0.65. However, the volume of macrovoid of clayey silt decreased as well as a clear shift of dominant peak of macrovoid toward lower pore sizes, where the void ratio decreased from 0.82 to 0.55. The sand-bentonite mixture displayed the minimum reduction in the void ratio as the volume of the macrovoid decreased less than the other two cases. On the contrary, the microvoid volume (intra-aggregate pores inside aggregates) and their associated dominant pore sizes are not affected, at least in the void ratio range covered in these 3 cases. The results showed changes in inter-aggregate porosity are dominant during loading at constant water content while the amount such changes in volume and size depends on the initial void ratio, water content and amount of loading.

The effects of hydraulic loading on PSD functions of the same compacted soils are presented in Figure 6.3, in which illitic-kaolinitic clay is shown in Figure 6.3 (a), clayey silt in Figure 6.3 (b) and sand-bentonite mixture in Figure 6.3 (c). The bimodal fabric of the illitic-kaolinitic clay restructured to form a single mode PSD after saturation at constant volume. The microvoid expanded due to saturation, resulted in the decrease in the volume of macrovoid. The sample was dried after being saturated at constant volume. The bimodal PSD was partially recovered.

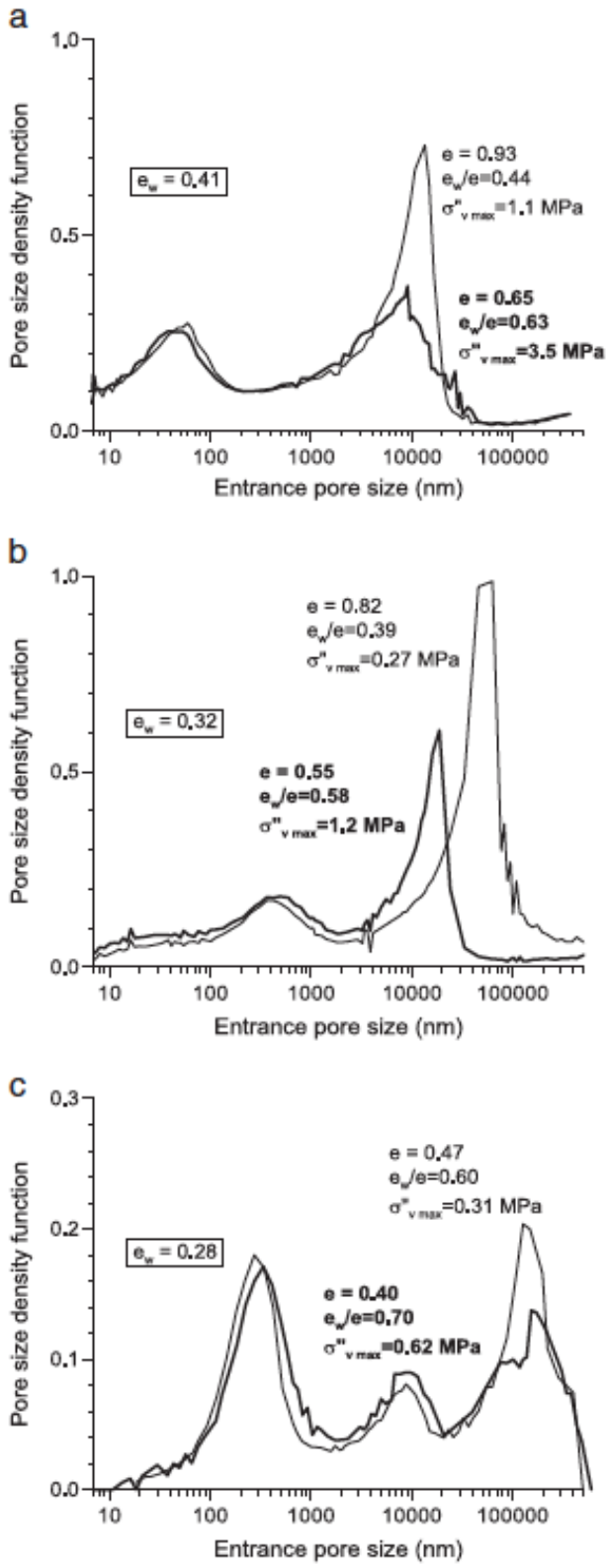

Figure 6.2. Response of different soils subjected to loading at constant water ratio and the evolution of the corresponding PSD function a) illitic-kaolinite clay b) clayey silt c) sand-bentonite (Romero, 2014).

The saturated microvoid was experienced volume shrinkage during drying and the initial dominant peak and corresponding pore size was recovered. However, macrovoid was partially recovered but substantial volume reduction can be detected since the global volume of the material decreased during drying. The PSDs of clayey silt presented in Figure 6.3 (b) showed that its response to the same hydraulic loading was similar to illitic-kaolinitic clay. Samples were moistened under constant volume in two steps, where suction decreased to 6 kPa at the first step and to 0 kPa at the second one. The single mode PSD was generated due to the increase in the volume and size of microvoid. The macrovoid was experienced volume reductions as a consequence of changes in microvoid. On the contrary, the volume of microvoid reduced during drying resulting in the volume expansion of the macrovoid. The resulting PSD at the end of drying was very close to the one detected before applying the hydraulic loads.

The PSD of sand–bentonite mixture possesses two dominant peaks of microvoid (pore size smaller than 20 μm), which exhibited volume expansion during wetting whereas the dominant peak of macrovoid vanished. This implied that the volume expansion of microvoid (bentonite fraction) was filled all the inter-grain porosity. During the drying path with no global volume changes, the microvoid volume reduced (bentonite shrinkage), which induced the re-emergence of the macrovoid volume. This re-emergence of macroporosity is associated with the pores of the shielding skeleton of the sand fraction that do not significantly shrink on drying. The results presented show that clay fabric is sensitive to water content changes and that important microstructural changes may occur even at a constant void ratio. In addition, it appears as a first approximation that the aggregates created by compaction on the dry side of optimum tend to swell and shrink almost reversibly and that they may be considered a permanent feature of the compacted soil microstructure.

The results showed changes in inter-aggregate porosity are dominant during loading at constant water content while the amount such changes in volume and size depends on the initial void ratio, water content and amount of loading. On the other hand, changes in microvoid volume of clayey soils are important during water content changes. Nevertheless, macrovoid volume is also affected as a consequence of two main phenomena: one, the multiphase coupling provided by the mutual interaction between the mechanical and hydraulic states (for instance, collapse on wetting) and the other, the multiscale coupling which originated from the interaction between different structural levels (for instance, invasion/retreat of macrovoids due to expanding/shrinking microvoids and irreversible macrovoid expansion on wetting of highly expansive clay minerals).

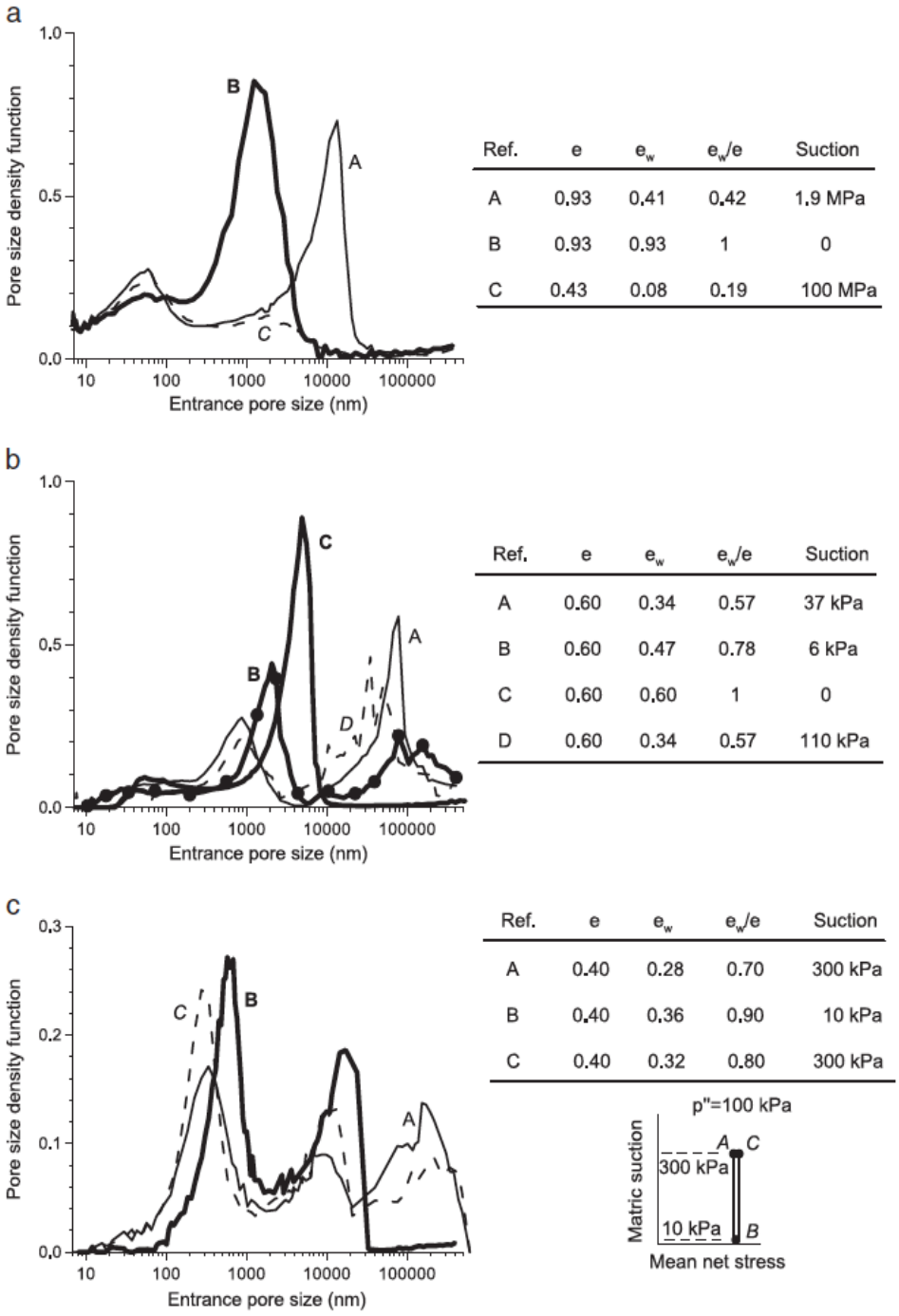

Ref.	e	e_w	e_w/e	Suction
A	0.93	0.41	0.42	1.9 MPa
B	0.93	0.93	1	0
C	0.43	0.08	0.19	100 MPa

Ref.	e	e_w	e_w/e	Suction
A	0.60	0.34	0.57	37 kPa
B	0.60	0.47	0.78	6 kPa
C	0.60	0.60	1	0
D	0.60	0.34	0.57	110 kPa

Ref.	e	e_w	e_w/e	Suction
A	0.40	0.28	0.70	300 kPa
B	0.40	0.36	0.90	10 kPa
C	0.40	0.32	0.80	300 kPa

Figure 6.3. Response of different soils subjected to hydraulic loads and the evolution of the corresponding PSD function a) illitic-kaolinite clay b) clayey silt c) sand-bentonite (Romero, 2014).

6.2 Sample preparation

6.2.1 As-compacted samples

The experimental study presented in this chapter carried out using 11 samples with 76 mm of height and 38 mm of diameter (triaxial sample) and 5 samples with 20 mm of height and 50 mm of diameter (oedometer sample). All samples were prepared with the dry density of 16.5 KN/m^3 and statically compacted at the water content of 20 %, which was the same as those of samples tested to studying the hydraulic behaviour (presented in chapter 5).

The properties of as-compacted samples are summarised in table 6.1, where γ_d is the dry unit weight, e_0 is the corresponding initial void ratio, w_0 and Sr_0 are the compaction water content and initial degree of saturation, respectively.

Such samples presented some features, which were relevant to the aim of the present study. First, the material used to construct the embankment might compact at the optimum water content and the experimental samples used in the present research could possess soil fabrics analogous to in-situ ones. Moreover, having the dry density on the dry side of the optimum, samples produced bimodal pore size distributions, which were of interest to study the interactions between different modes of pores upon hydromechanical stress paths. Finally, such samples did not show excessive accumulation of deformations or significant irreversible volume changes during drying-wetting. This allowed studying the behaviour mainly due to interactions between different pore modes.

Table 6.1. Properties of as-compacted samples.

Type of tests	γ_d (gr/cm^3)	e_0	w_0 (%)	Sr_0
Triaxial and MIP tests	1.65±0.009	0.657	20±0.5	0.83

6.2.2 Pre-consolidation stress of as-compacted samples

One-dimensional oedometer test was carried out to define the pre-consolidation stress of the as-compacted sample. All samples were prepared with the same properties using the same static compaction technique. Therefore, it can be expected that pre-consolidation stress of all as-compacted samples could be relatively the same. The as-compacted sample was placed in conventional oedometer but it was kept under unsaturated condition. It was then compressed applying vertical stress starting from 0 to 6276 kPa while the drainage was

permitted at both end-sides of the samples through porous discs. The loading steps began by applying 12.3 kPa of vertical stress and followed by doubling the previous vertical stress. After applying the maximum axial stress (6276 kPa), the sample was unloaded to 98 kPa. The sample was compacted when the effective stress being increased, which in turn required that the volume of the soil decreases by the expulsion of the pore water. The vertical displacement was being recorded using the precise dial gauge. The volumetric strain corresponding to each loading step was plotted with vertical effective stress (logarithmic scale) in Figure 6.4. The yielding axial stress of the as-compacted sample was found to be 657 kPa. The coefficient of lateral pressure can be estimated with respect to the plastic index (PI) of Viadana silt ($K = 0.4 + 0.007(PI)$). The pre-consolidation mean pressure was then obtained to be 420 kPa. The post-compaction suction of the as-compacted samples was measured to be about 33 kPa, whereas these samples were subjected to suction levels of 50 and 300 kPa at suction equalisation phase of triaxial tests. Being subjected to the greater values of suction than the post-compaction one, the pre-consolidation stress of these samples expected to be greater than 420 kPa. As-compacted samples were subjected to 100, 200 and 400 kPa, which are smaller than the obtained pre-consolidation pressure.

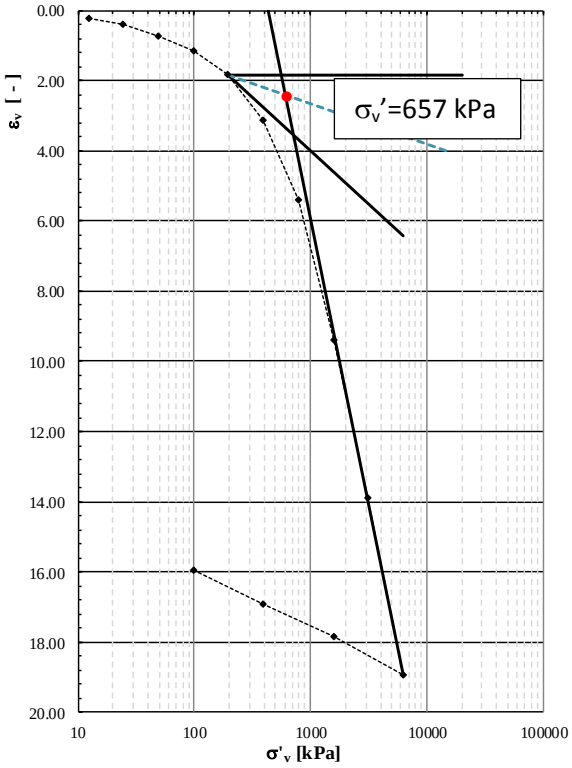

Figure 6.4. Results of Oedometer Compression test in terms of volumetric strain and axial effective stress

6.2.3 Applying repeated hydraulic loads

In order to study the effects of repeated hydraulic loads on the hydromechanical behaviour of as-compacted samples, repeated hydraulic loads were applied to 8 triaxial samples and 2 oedometer samples. The procedure used to dry and wet the oedometer samples was explained in chapter 5. Triaxial samples prepared at 76 mm of height and 38 mm of diameter. The techniques used to wet and dry the samples were similar to the ones of oedometer sample (having 20 mm in height and 50 mm in diameter), but different types of equipment were employed due to their different sizes. 3 samples were subjected to 3 cycles of drying-wetting whereas the rest (7 samples) experienced 6 cycles. The repeated hydraulic loads were applied to samples by controlling their water content.

Dying process was applied similarly by placing the sample in the temperature controlled room while samples being exposed to the temperature of 21℃ and relative humidity of 38.5%, as shown in Figure 6.5 (a). Such atmospheric conditions implied that samples experienced about 128.8 MPa of suction during the drying process. The drying process was last about 90 hours. A dead weight was placed above the samples to apply 10 kPa of axial stress during the drying phase while radial stress is null. Under this condition, the shrinkage of the samples occurred mostly by means of axial deformation, and excessive decrease of diameter of the sample was prevented. The weight of the samples was sequentially monitored to track the water volume change of the samples. At the end of drying, the height and diameter of the samples were directly measured.

The hydraulic connections of a “table”-triaxial cell were used to wet the sample. As shown in Figure 6.5 (b), the dry sample was mounted in the “table”-triaxial while the plastic porous disk, consisting of several plastic rings, was placed between the sample and the pedestal. The top lightweight cap was positioned above the sample. All parts including the pedestal, plastic disk, sample and top cap were closed with two-pieces of steel mould formerly used for preparing compacted sample. The “table”-triaxial cell chamber was then mounted preventing the evaporation during wetting of the sample.

The water was injected in to the sample through the pedestal and plastic disc with injection rate of about 0.5 cm^3/h. This low injection rate ensured the water flow did not apply significant pressure to the soil fabric. The presence of the plastic disk ensured that the injected water was well distributed at the basement of the sample. The water gradually filled the pores of the sample while the air was leaving the pores through a tiny passage hole in the top cap. The amount of injected water was continuously measured using a water volume meter with 50cc capacity, as shown in Figure 6.5 (b). The wetting process was stopped when the initial water content of the as-compacted sample was achieved.

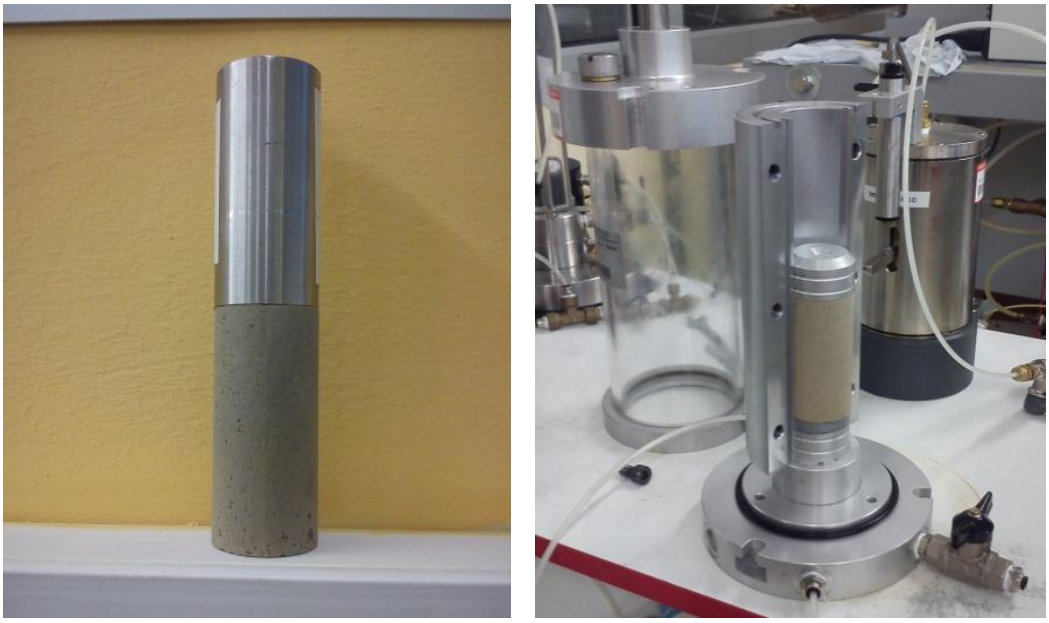

(a) (b)

Figure 6.5. Schematic plot of equipment and technique used to apply repeated hydraulic loads (triaxial sample) a) Drying process b) Wetting process.

The diameter of dry samples was slightly smaller than the internal diameter of the mould. Therefore, the radial deformation was constrained after small volume expansion, and further deformation was obliged to occur along the height of the sample during the wetting. At the end of wetting, the sample was dismantled and wrapped up in a plastic cover and held in a sealed humid container for at least 5 days to ensure equalisation of the water within the entire volume of the sample. The size of the sample was directly measured at the end of wetting process and the end of equalisation phase.

Figure 6.6 shows the water volume change of samples subjected to repeated hydraulic loads for one cycle of wetting and one cycle of drying. The water volume changes were plotted for both samples prepared for oedometer and triaxial tests. The water content of all samples was 20%, but the water volume of samples was obviously different since their size and volume were not the same. During wetting, water was injected at the same rate while the water volume changes required to achieve 20% of water content were 13 and 28 cm3 for oedometer and triaxial samples, respectively. The drying process of the triaxial sample was faster since it was laterally free for the evaporation whereas oedometer sample was placed in a steel holder ring and the evaporation occurred through reticular sheet placed in the basement of the sample.

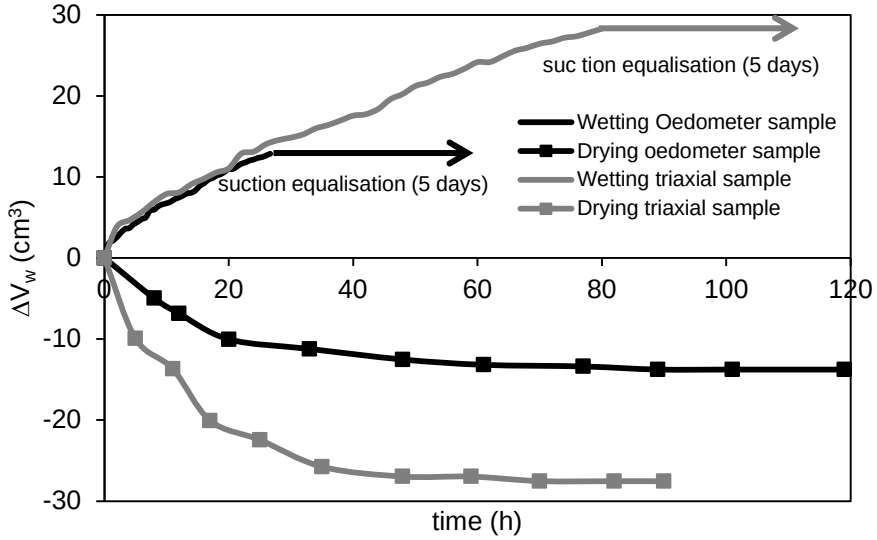

Figure 6.6. Water volume change of samples during wetting and drying.

It has to be pointed out that the proposed technique accelerates the process of the drying and wetting of the sample, in which the sample can be subjected to numbers of cycles within few weeks. Moreover, the variation of the moist content of the sample in the laboratory scale can be a more realistic reproduction of the variation of the moist content of the unsaturated soil in geotechnical engineering practice, when it is subjected to drying-wetting cycles due to seasonal variation.

6.3 Volumetric change of as-compacted samples due to repeated hydraulic loads

Figure 6.7 (a) shows the evolution of suction with water contents for one of the as-compacted sample (it is named as “Tx6D/WS50P200” in the following sections) when 6 cycles of drying-wetting were applied. It is believed that the post-compaction suction of the as-compacted sample was about 33 kPa, whereas it decreased to about 5 kPa after being subjected to 6 cycles of drying-wetting. These suction values were measured using the filter paper technique as explained in chapter 2. Although the filter paper technique is not precise for measuring very low suction, but suction obtained from the calibration curve proposed by Caruso et al. 2011 was consistent to the corresponding water retention curves of these samples.

It is assumed that suction established at the end of each wetting and drying process remained at 5 KPa and 208 MPa, respectively. The evolution of the water content with suction is represented in Figure 6.7 (a). The average residual water content of samples was measured to be 0.4 % at the end of drying processes

while the initial water content (~20%) was recovered at the end of wetting processes. Suction acting within the samples took the same value at the end of drying processes since the relative humidity of the room was kept constant, but its initial value decreased at the end of the first wetting path and assumed to be the same at the end of the subsequent wetting paths. The volumetric strains developed during 6 cycles of drying-wetting for this sample were represented in Figure 6.7 (b). The compression volumetric strains developed at the end of drying process took a place between 1.5 and 2.5 %. However, it was found that gentle swelling occurred due to wetting. The maximum swelling volumetric strain of this sample was measured to be -0.31%.

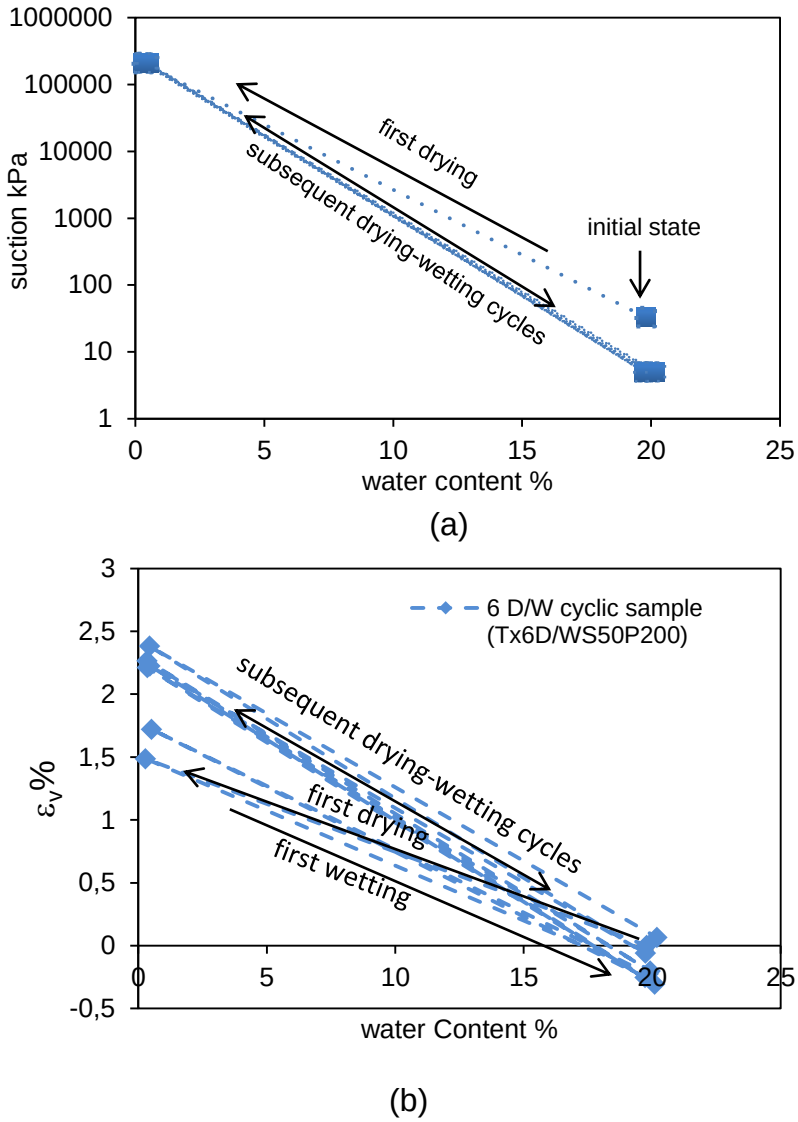

Figure 6.7 Behaviour of triaxial samples subjected to repeated hydraulic loads: (a) suction-water content (b) volumetric strain-water content (Positive value means volumetric compression).

Figure 6.8 (a) shows the volumetric strain (ε_v) measured for the same sample at the end of wetting and drying cycles with respect to the number of applied hydraulic cycles. The volumetric behaviour implied that this samples experienced the minimum compression and maximum expansion volumetric strains at the end of drying and wetting paths, respectively. The minimum compression volumetric strain at the end of first drying was 1.49%, which increased to 2.5% after being subjected to the 3rd drying path. The volumetric strain obtained at the end of drying remained relatively constant in subsequent hydraulic cycles. On the other hand, the maximum swelling (-0.31%) was observed at the end of first wetting and no significant changes in the value of ε_v, obtained at the end of wetting, was observed in the following cycles. This may result from the fact that these samples experienced a smaller value of suction at the end of wetting process comparing to one equilibrated after preparation as their hydraulic state moved from scanning domain to main wetting branch.

Figure 6.8 (b) shows volumetric strain changes ($\Delta\varepsilon_v$) obtained at the end of drying process of each cycle for samples subjected to 3 and 6 cycles of drying-wetting. The volumetric strain changes were measured to mainly increase at preliminary cycles, and it remained relatively constant after 3 cycles. It has to be pointed out that the volumetric responses of triaxial samples due to repeated hydraulic loads were similar to the response of oedometer samples as discussed in chapter 5. This may justify that the resulting behaviour stemmed from the natural response of material to repeated hydraulic loads.

It is believed that some sort of structural alteration took place in the fabric of as-compacted samples due to being subjected to repeated hydraulic loads. Such fabric changes established after initial drying-wetting cycles (up to 3 cycles) and no further alteration occurred for the subsequent cycles. Although no important changes in the global volumetric strain were measured after drying and wetting, but the as-compacted samples experienced irreversible volumetric change upon 2 or 3 cycles of drying-wetting, followed by sort of reversible volume changes for subsequent cycles of hydraulic loads.

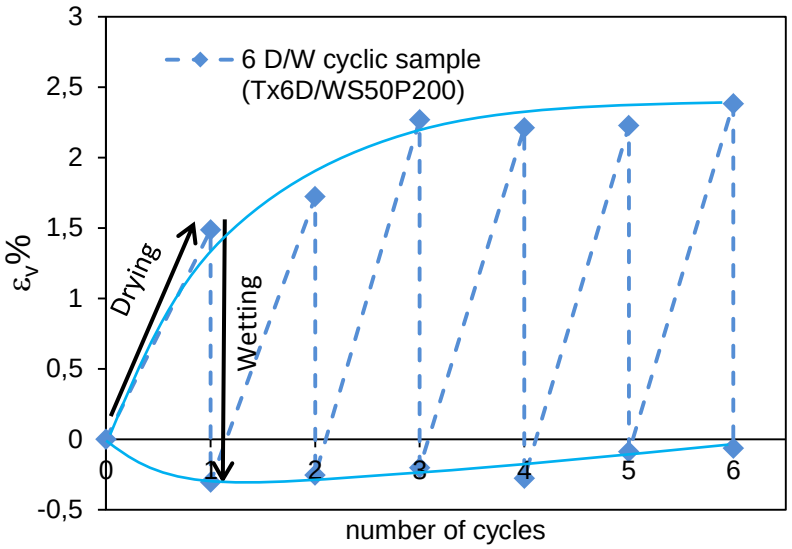

(a)

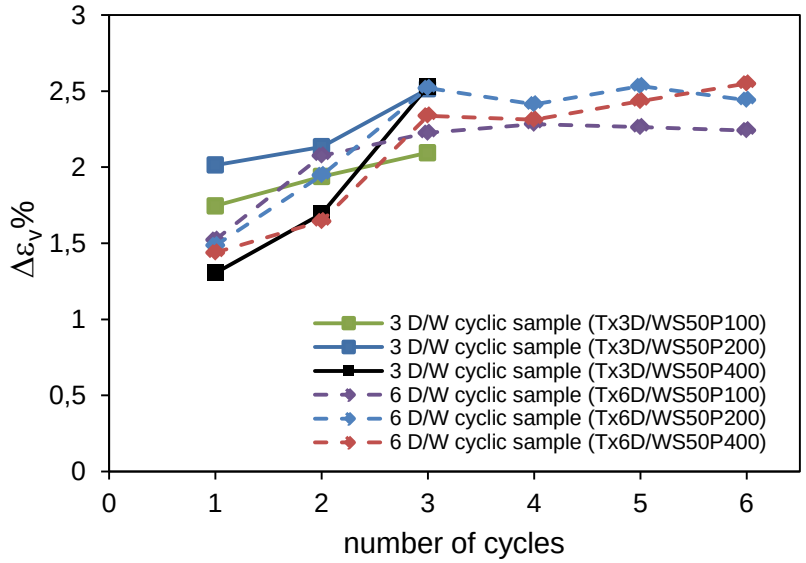

(b)

Figure 6.8. Volumetric behaviour of samples subjected to repeated hydraulic loads: (a) Volumetric strain with number of cycles (b) Volumetric strain change at the end of drying processes with number of cycles. (Positive value means volumetric compression).

6.4 Triaxial tests procedure

All units of triaxial apparatus involving water circuits were thoroughly saturated before performing each test. These units included the axial loading piston and ram chamber, the water volume change measuring system (burette), the separation cell transferring the pneumatic pressure to hydraulic one and all water conduits.

The soil sample was then mounted by placing on the triaxial pedestal, where a thin layer of water was previously held at the top of the porous stone to ensure a perfect transient between water phase of porous stone and sample. The sample was encased in the rubber latex membrane and the top cap was placed. The membrane was closed at its contact with the top cap and the bottom pedestal by using the O-rings. The air drainages were maintained closed until the application of the pressures to minimize the evaporation of water within the soil mass and porous stone. Two lasers placed at two sides of the samples and two local LVDTS were mounted at two other sides (see details in chapter 2). Triaxial cell chamber was placed and the cell pressure of 15-20 kPa and air pressure of 10 kPa were applied to the sample before starting the main test. This small net pressure (5-10 kPa) was applied to ensure that the air pressure does not exceed the cell pressure during the gradual increase of pressures while the test is being carried out. Finally, the main test began by simultaneously increasing the three pressures until the predefined initial values.

Triaxial tests consisted of three phases including the suction equalisation, compression and shearing. These phases are schematically presented in terms of deviatoric stress, net mean stress and suction in Figure 6.9.

The suction equalization phase was carried out by applying the desired suction while the net mean pressure was kept constant at 5-10 kPa. The sample was being held at suction equalisation phase until the suction was homogenously equalised within the soil mass, where it increased from the value established at the post-compaction to the given value during the first phase of the test. This was justified as the measured volume and water content change of the sample reached to the steady state. The net mean pressure increased to a predefined value at a free drainage condition during the compression phase of triaxial tests while the suction was kept constant at its initial value. The pressures gradually increased at the rate of 50 kPa/h while the deviatoric stress was maintained smaller than 5 kPa providing the isotropic consolidation.

The constant water content (CW) condition was imposed during the shearing phase. The water drainage was closed at the end of the compression phase and the water pressure acting on the sample was measured during shearing, while the air pressure was kept constant. The shearing phase of tests was carried out under the strain-controlled condition, in which the strain rate of 0.25%/h was applied. The cell pressure remained constant and the axial force was measured during the shearing phase. Triaxial tests performed in the present research are described in Table 6.2. It has to be pointed out that the behaviour of unsaturated soil was studied using triaxial constant water content tests by different authors, e.g. Bishop et al. 1960, Bishop and Donald 1961, Blight 1961, Satija 1978, Sivakumar 1993, Rahardjo et al. 2004 and Thu et al. 2006.

As-compacted samples were tested by applying 2 suction values (50 and 300 kPa), 3 compression pressures (100, 200 and 400 kPa) and shearing under the constant water content condition. The same tests were also carried out on 3 and 6 D/W cyclic samples to study the effect of repeated hydraulic loads on their hydromechanical behaviour.

Table 6.3 also summarizes the initial properties (specific volume, degree of saturation and water ratio) of the samples at the beginning of the triaxial tests, as well as their values at the end of suction equalisation and compression phases. As formerly explained, samples were compacted at the same dry density and water content. Specific volume and water ratio of as-compacted samples detected after being subjected to 3 and 6 cycles of drying-wetting were not significantly different from the initial values.

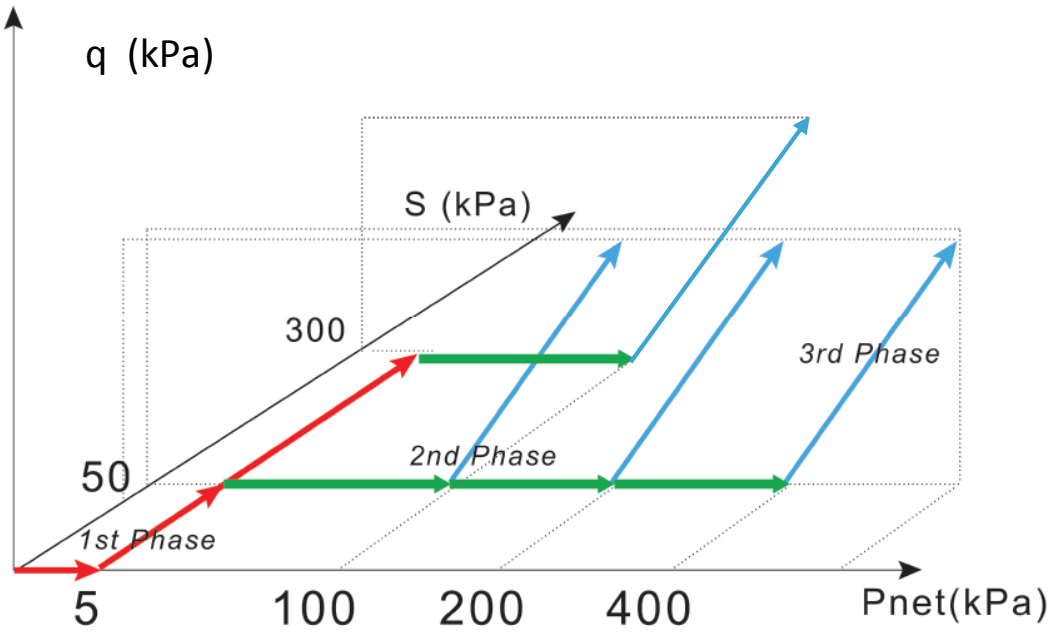

Figure 6.9. Applied stress paths in triaxial tests.

Table 6.2. Program of applied stress paths in triaxial tests

Type of tests	sample	Initial s kPa	Initial P_{net} kPa	Suction equalisation kPa	Compression kPa	Shearing
TxS50P100	As-compacted	50	5-10	Cons.	100	StrainCon. CW
TxS50P200	As-compacted	50	5-10	Cons.	200	StrainCon. CW
TxS50P400	As-compacted	50	5-10	Cons.	400	StrainCon. CW
TxS300P100	As-compacted	300	5-10	Cons.	100	StrainCon. CW
Tx3D/WS50P100	As-compacted+ 3 D/W	50	5-10	Cons.	100	StrainCon. CW
Tx3D/WS50P200	As-compacted+ 3 D/W	50	5-10	Cons.	200	StrainCon. CW
Tx3D/WS50P400	As-compacted+ 3 D/W	50	5-10	Cons.	400	StrainCon. CW
Tx6D/WS50P100	As-compacted+ 6 D/W	50	5-10	Cons.	100	StrainCon. CW
Tx6D/WS50P200	As-compacted+ 6 D/W	50	5-10	Cons.	200	StrainCon. CW
Tx6D/WS50P400	As-compacted+ 6 D/W	50	5-10	Cons.	400	StrainCon. CW
Tx6D/WS300P100	As-compacted+ 6 D/W	300	5-10	Cons.	100	StrainCon. CW

Table 6.3. Properties of samples at different stage of triaxial tests

Type of tests	Initial value			End of Suction equalisation			End of compression		
	ν	S_r	e_w	ν	S_r	e_w	ν	S_r	e_w
TxS50P100	1.660	0.826	0.545	1.657	0.772	0.507	1.619	0.775	0.480
TxS50P200	1.661	0.834	0.551	1.652	0.775	0.505	1.606	0.787	0.477
TxS50P400	1.659	0.839	0.553	1.657	0.769	0.505	1.587	0.794	0.466
TxS300P100	1.662	0.817	0.541	1.642	0.575	0.369	1.627	0.571	0.358
TxS50P400D/WS50P100	1.666	0.821	0.547	1.654	0.638	0.417	1.597	0.673	0.402
TxS50P400D/WS50P200	1.667	0.822	0.548	1.648	0.648	0.42	1.589	0.689	0.406
TxS50P400D/WS50P400	1.664	0.828	0.550	1.653	0.643	0.42	1.587	0.659	0.387
Tx6D/WS50P100	1.659	0.838	0.552	1.651	0.644	0.419	1.596	0.676	0.403
Tx6D/WS50P200	1.658	0.842	0.554	1.653	0.663	0.433	1.595	0.687	0.409
Tx6D/WS50P400	1.662	0.828	0.548	1.652	0.655	0.427	1.586	0.683	0.40
Tx6D/WS300P100	1.663	0.799	0.530	1.636	0.412	0.262	1.612	0.410	0.251

6.4.1 Constant water content (CW) triaxial tests (as-compacted samples)

The triaxial experimental results of the 4 as-compacted samples of Viadana silt are represented in the following.

6.4.1.1 Suction equalisation

The behaviour of as-compacted samples during the suction equalisation phase are represented in Figure 6.10. As-compacted samples were subjected to suction values of 50 kPa while the net mean stress was kept constant at 5 kPa as shown in Figure 6.10 (a). These values were higher than post-compaction suction (33 kPa), implying that suction acting on soil increased during the suction equalisation phase. If suction changes, the soil sample can exhibit contraction or swelling depending on the microstructure, stress history, level of stress and amount of current variation. However, the volume change caused by increasing suction is commonly contraction. The volumetric behaviour is represented in terms of specific volume and time in Figure 6.10 (b). The volumetric contraction was measured for all samples as they were subjected to the greater level of suction and their water contents decreased during the equalisation phase. Since the amount of increase in suction was small, no significant volumetric change was detected. However, sample TxS50P100 experienced more contraction which may result from more inhomogeneity of such a sample.

Figure 6.10 (c) shows the variation of the water ratio (e_w) with time (min). The water ratio decreased from 0.55 to 0.51 (average values) as water expelled from the samples due to the increase in suction. The water ratios of these samples obtained at the equilibrium were quite the same. The equilibrium was established after about 800 minutes for these tests. However, the suction equalisation phase was carried out a bit longer than the required equilibrium time to detect the effect of evaporation and diffusion on water volume change, which was needed to calibrate the measurements as it was explained in chapter 2.

Figure 6.10 (d) shows the decrease in the degree of saturation during the suction equalisation phase, where these samples experienced about -0.06 of reduction in the degree of saturation (ΔS_r).

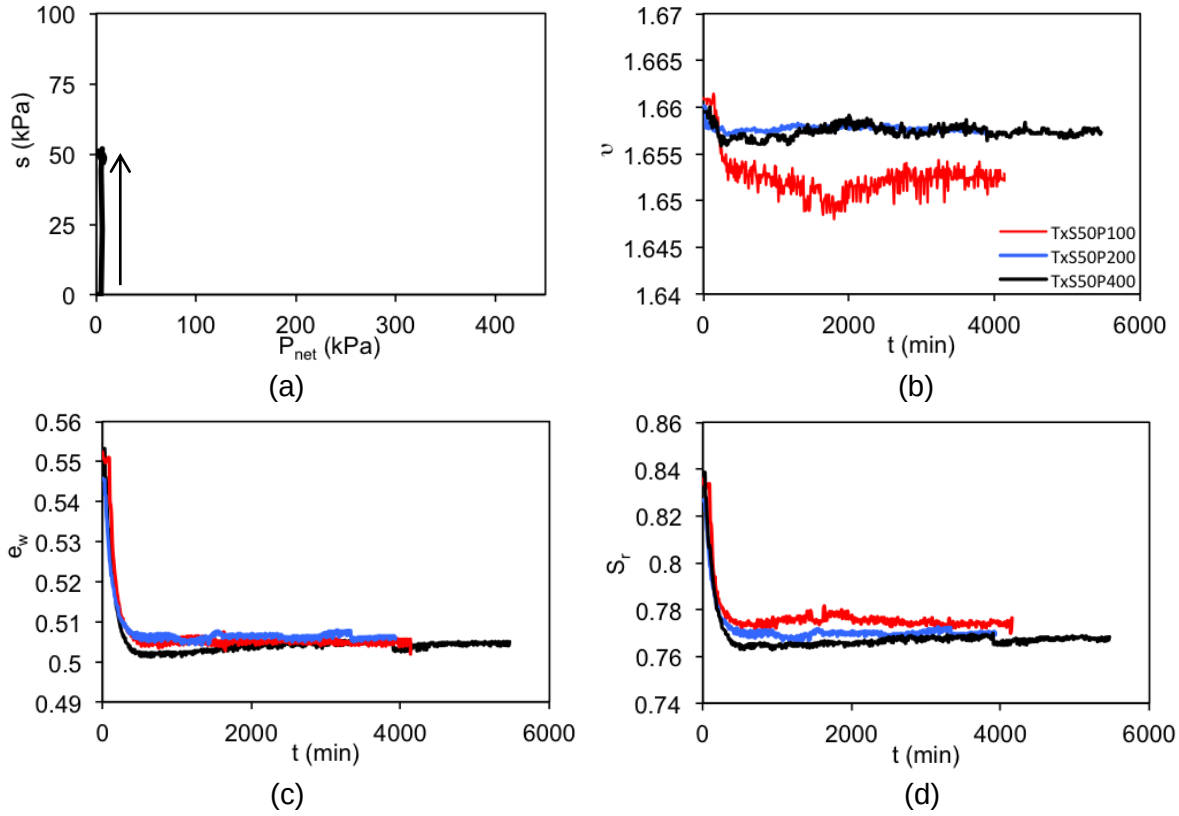

Figure 6.10. Behaviour of as-compacted samples subjected to 50 kPa of suction: a) suction-p_{net} b) specific volume-time c) water ratio- time d) degree of saturation-time.

Figure 6.11 shows the comparison between behaviours of sample TxS50P100 and TxS300P100, where they were subjected to 50 and 300 kPa of suction, respectively (Figure 6.11 (a)). As shown in Figure 6.11 (b), sample TxS300P100 contracted more ($\varepsilon_v = 1.2\%$) than sample TxS50P100 ($\varepsilon_v = 0.2\%$) as it was subjected to greater suction, implying that the difference between the imposed and initial suction levels for these test was significantly higher, and in turn, more amount of water was expelled. Accordingly, the time required to reach the equilibrium for test TxS300P100 was longer than the one of sample TxS50P100. As shown in Figure 6.11 (c) and (d), the water ratio and degree of saturation of sample TxS300P100 decreased to the lower values comparing to the ones of sample TxS50P100. Its water ratio and degree decreased to 0.37 and 0.57, respectively.

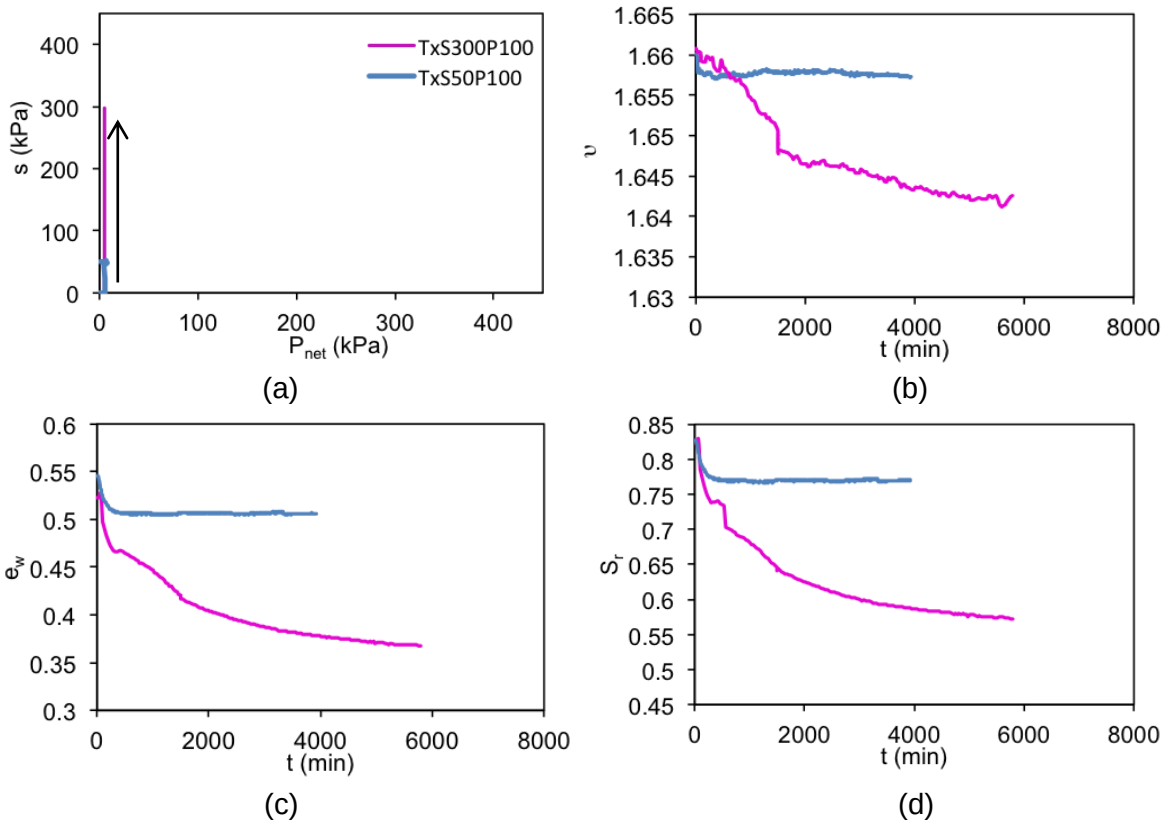

Figure 6.11. Behaviour of as-compoacted samples subjected to 50 and 300 kPa of suction: a) suction-p_{net} b) specific volume-time c) water ratio- time d) degree of saturation-time

As it was explained in chapter 2, post-compaction suction of 2 as-compacted samples was measured using the filter paper method. The average suction value measured for these samples, which were compacted at the same dry density and water content of samples used in triaxial tests, were 33 kPa. It was assumed that initial suction (post-compaction) of all as-compacted samples was the same. Figure 6.12 (a) shows the results of the suction equalisation phase of tests TxS50P100, TxS50P200, TxS50P400 and TxS300P100 in terms of void ratio and water ratio. It can be understood that behaviour of samples subjected to 50 kPa were almost hydraulic one as changes in water ratio (or degree of saturation) were significantly greater than changes in void ratio. Although the void ratio of sample TxS300P100 slightly decreased, the reduction in the water ratio was clearly evident.

The same results with the main drying and main wetting water retention curves of Viadana silt were also plotted in Figure 6.12 (b) and (c) in terms of S_r-s and e_w-s, respectively. The water retention curves were obtained for the as-compacted sample with the same initial properties using the axis translation (suction-controlled oedometer) and vapor equilibrium (desiccator) tests, as explained in

chapter 5. The suction values were represented in natural scale as it was easier to follow the water retention behaviour of these samples at this scale when they were subjected to suction values of 50 and 300 kPa. The hydraulic states were presented with reference to the initial state (post-compaction) and final state obtained at the end of suction equalisation phase. The initial states of samples implied that the post-compaction suction were placed in scanning domain but very close to the main drying curve. Therefore, when these samples were subjected to the greater level of suction (50 or 300 kPa) comparing to the initial one, the variation of their water content mainly occurred close to the main drying curve. This can be observed considering S_r or e_w values at the end of suction equilibrium phases. Particularly, it is more evident for sample TxS300P100 because it was subjected to the greater suction and the variation of water content was sufficient to reach to the main drying curve.

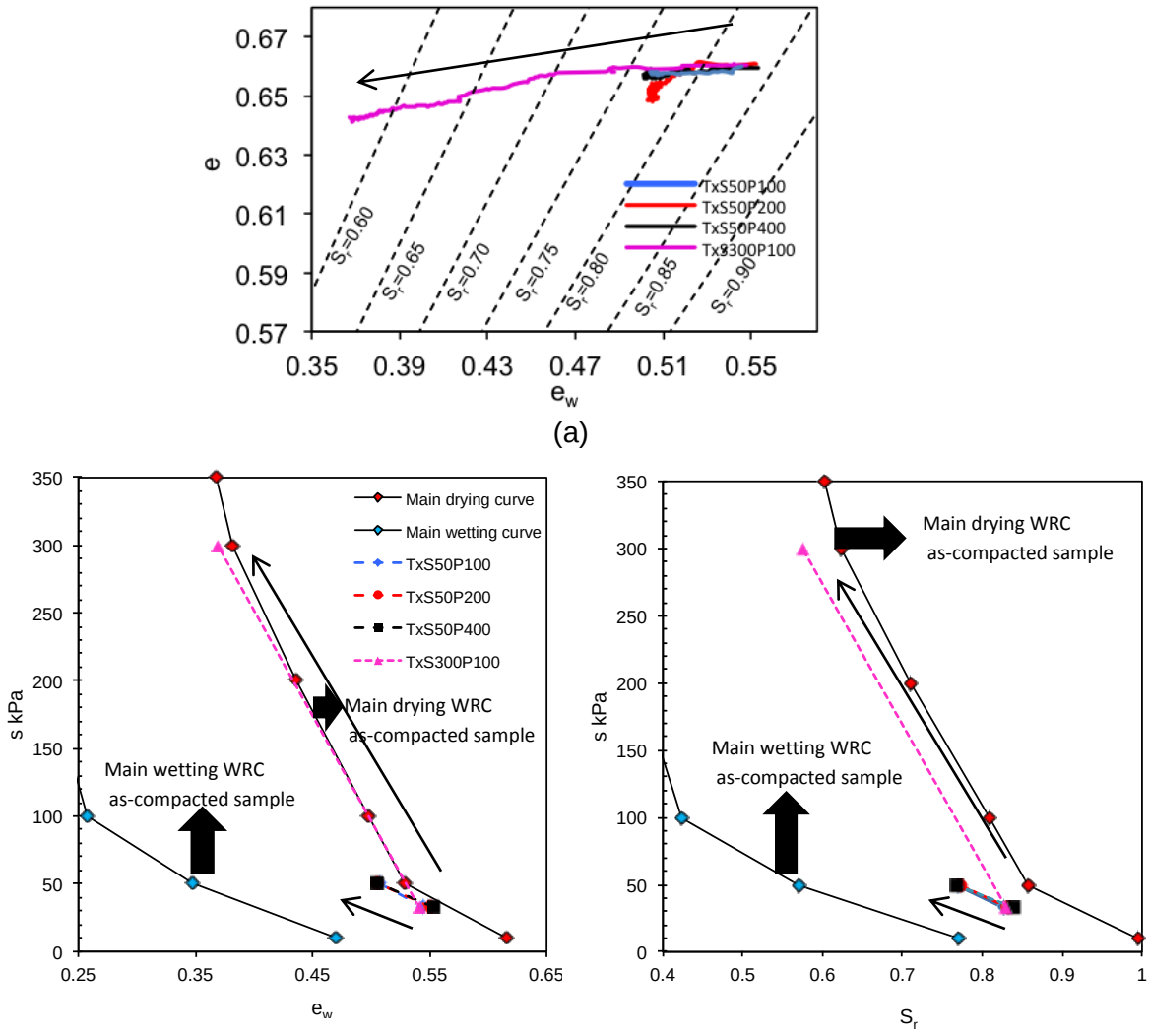

Figure 6.12. Behaviour of as-compacted samples subjected to 50 and 300 kPa of suction: a) void ratio-water ratio b) suction-water ratio c) suction-degree of saturation.

6.4.1.2 Compression behaviour

The compressibility of the as-compacted samples was studied when they were subjected to the mean net pressures of 100, 200 and 400 kPa. Figure 6.13 shows the compression behaviour of tests TxS50P100, TxS50P200 and TxS50P400 while imposed suction was kept constant at the same value previously applied at suction equilibrium phase (50 kPa), as shown in Figure 6.13 (a). The compression pressures increased to desired values at the rate of 40 kPa/h. The samples were then being subjected to the compression pressures until they were fully consolidated.

The pre-consolidation net pressure of sample compacted at the same properties was measured to be 420 kPa, as it was explained in section 6.2. Therefore, all samples were subjected to compression pressures smaller than their pre-consolidation one, implying that the compression behaviours were studied in the unloading-reloading region. Figure 6.13 (b) shows the change in the specific volume with the net mean stress. The highly nonlinear behaviour is possibly due to the relatively high stress rate imposed, which allowed full water drainage only after the desired net stress was applied.

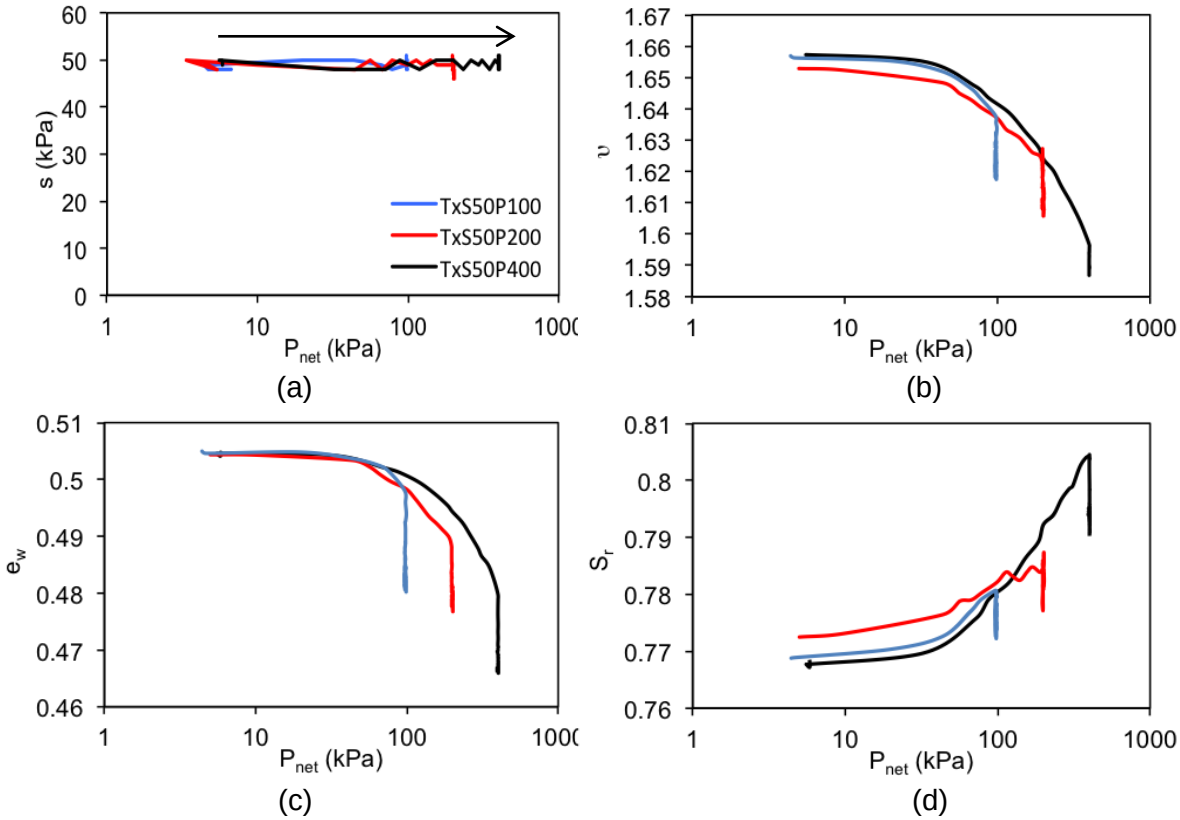

Figure 6.13. Behaviour of as-compoacted samples (s=50 kPa) subjected to isotropic compression to 100, 200 and 400 kPa: a) suction-p_{net} b) specific volume- p_{net} c) water ratio- p_{net} d) degree of saturation- p_{net}

The unloading-reloading slopes, regarding the initial and ending volume during the compression phase, were obtained to be 0.015, 0.014 and 0.017 ($k = -\frac{\Delta e}{\Delta \log(p_{net})}$) for samples TxS50P100, TxS50P200 and TxS50P400, respectively. The amount of water expelled from the samples increased as they were subjected to the greater net mean stress, where their water ratios decreased from 0.51 to 0.48, 0.477 and 0.466 for TxS50P100, TxS50P200 and TxS50P400 (Fig 6.13 (c)).

The degree of saturation decreases with the water content whereas it increases with the volume contraction. The degree of saturation increased in these samples at the beginning of the compression phases since samples were initially experienced mostly the volume contraction. However, it decreased as the water expelled from the samples. Generally, the degree of saturation increased in all tests, as the volume contraction was the dominant effect in compression phases. The degree of saturation of sample TxS50P100 increased to 0.772 whereas the one of sample TxS50P400 reached to 0.791 since it subjected to greater net mean stress (400 kPa), as shown in Fig 6.13 (d).

After the equilibrium was established due to the application of 300 kPa of suction, sample TxS300P100 was subjected to 100 kPa of mean net stress while suction remained at 300 of kPa. The compression behaviour of this sample is presented in Figure 6.14 and its trend was compared to the behaviour of sample TxS50P100, which was subjected to the same net mean stress but different suction (50 kPa).

At the beginning of the compression phase, the specific volume of sample TxS300P100 was smaller since it experienced more contraction and became stiffer when being subjected to the suction of 300 kPa. This caused that its volumetric contraction during compression phase was smaller ($\varepsilon_v = 0.9\ \%$) than sample TxS50P100 ($\varepsilon_v = 2.3\ \%$). As shown in Figure 6.14 (c), the change in water ratio of sample TxS300P100 was 0.01, which corresponds to 0.37% of changes in the water content. The change of the degree of saturation was also negligible in the compression phase as the effects of changes in volume and water content were counterpart (Figure 6.14 (d)).

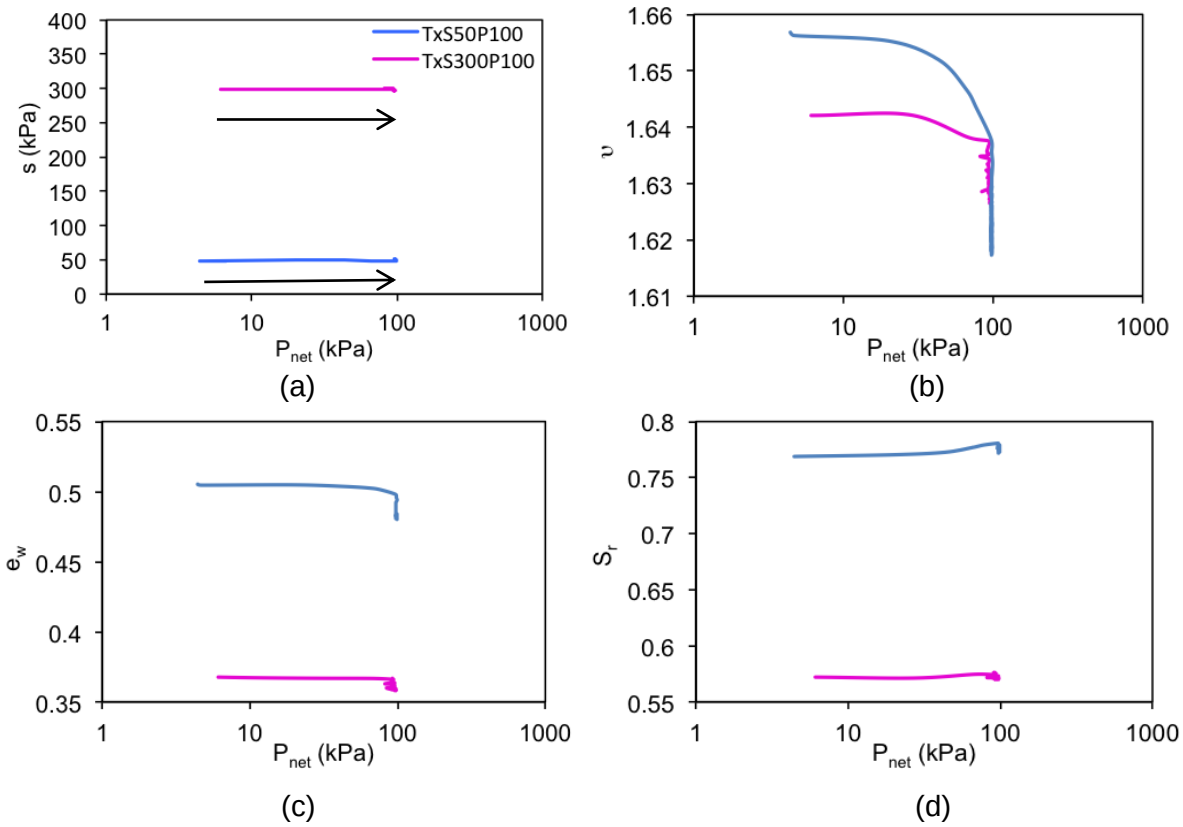

Figure 6.14. Behaviour of as-compated samples (s=50 and 300 kPa) subjected to isotropic compression to 100 kPa: a) suction-p_{net} b) specific volume- p_{net} c) water ratio- p_{net} d) degree of saturation- p_{net}

Figure 6.15 (a) shows changes in void ratio and water ratio of samples TxS50P100, TxS50P200, TxS50P400 and TxS300P100 during the compression phase. The initial behaviour associated with the loading stage of the compression phase where the rate of decrease in the void ratio in all samples was greater than the one of the water ratio. However, the water ratio and void ratio decreased at about a similar rate in the following as the loading stage was completed and the rate of volume change decreased and water began to expel faster from the samples. Also, it can be understood that the water ratio and void ratio of sample TxS300P100 decreased less than the other samples. The degree of saturation at the beginning and at the end of compression phase can also be detected with respect to contours lines presented in Figure 6.15 (a). Obviously, the degree of saturation of sample TxS300P100 is smaller as it was subjected to the greater value of suction (300 kPa).

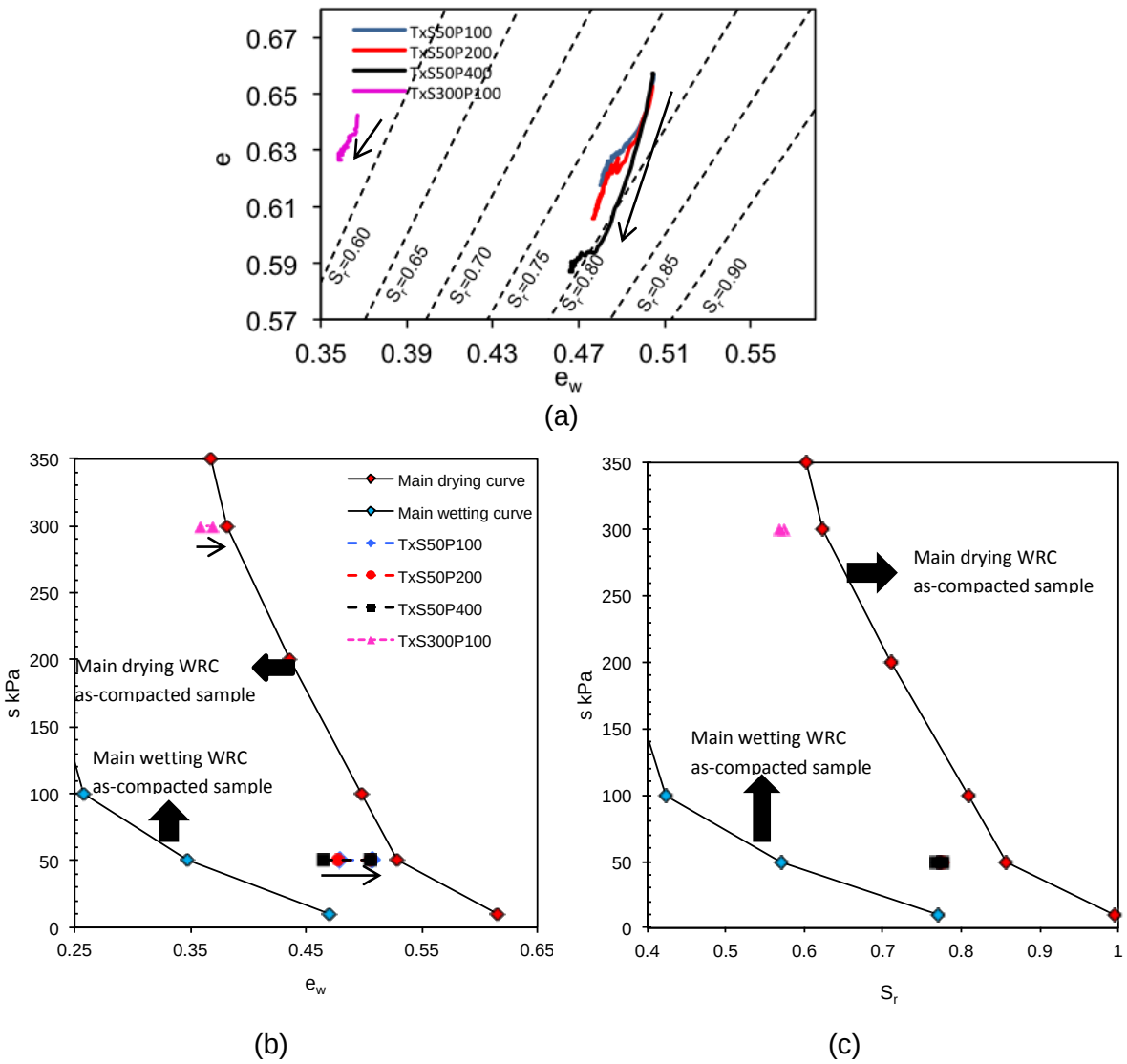

Figure 6.15. Behaviour of as-compacted samples subjected to 50 and 300 kPa of suction: a) void ratio-water ratio b) suction-water ratio c) suction-degree of saturation

Figure 6.15 (b) and (c) represents the results in terms of S_r-s and e_w-s, where the states of the soil at the beginning and at the end of the suction equilibrium phases and compression phase were plotted. As shown in Figure 6.15 (b), the water ratio decreased in all tests as the samples were allowed to be drained during the compression phase. It is believed that the water retention states of these tests still remains close to the main drying curve at the end of the compression phase. It has to be pointed out that the main water retention curves in Figure 6.15 (b) and (c) were detected for the sample at relatively constant volume. Therefore, it can be expected that the main curves slightly changed due to the volume change of the samples during the compression phase. In fact, the main drying curves can move to the upper levels of degree of saturation inS_r-s plane and it can shift to the lower level of water ratio in e_w-s plane. As it was described, the degree of saturation of

these samples increased insignificantly and its increments cannot be clearly detected in Figure 6.15 (c).

6.4.1.3 Shearing

After the compression phase, all samples were subjected to the loading (shearing) under the strain-controlled condition. The shearing phase was applied at constant water content condition as the water drainage was closed. Therefore, the water pressure was measured and the air pressure was kept constant. This allowed computing changes in suction with respect to the measured water pressure during the shearing. The results of the shearing phase of tests TxS50P100, TxS50P200, TxS50P400 and TxS300P100 are plotted in Figure 6.16 and represented in terms of deviatoric stress, volumetric strain, degree of saturation and suction with respect to deviatoric strain.

As shown in Figure 6.16 (a), the deviatoric stress increased with increasing net confining pressures as it can be understood by comparing the deviatoric behaviour of samples TxS50P100, TxS50P200 and TxS50P400. They exhibited a sharp increase in the deviatoric stress at very small deviatoric strain followed by the smooth increase for further loading. The deviatoric stress of tests TxS50P200 and TxS50P400 increased smoothly during the shearing phase where they approached the steady state at the end of the loading process. The maximum deviatoric stress was 848 and 442 kPa for tests TxS50P200 and TxS50P400, respectively. The deviatoric behaviour of test TxS50P100 showed the increase in deviatoric stress, followed by a gentle softening associated with the decrease in the deviatoric stress. This may be consistent with results presented by Thu et al. (2006) where the soil sample showed more tendency for softening behaviour at lower confining pressures although the deviatoric stress of such samples was reported to decrease significantly after the peak. In the present research, the post-peak decrease in the deviatoric stress of the sample with 50 kPa of suction and 100 kPa of net mean stress was gentle. The softening post-peak began at about 6.3% of deviatoric strain, where the peak of the deviatoric stress of test TxS50P100 was 281 kPa. The softening behaviour was more evident for sample TxS300P100, which was subjected to the same mean net stress of sample TxS50P100 (100 kPa), but it experienced greater suction. The sample TxS300P100 showed more strength comparing to sample TxS50P100 as it was being subjected to the greater level of suction. The deviatoric stress increased to the maximum value of 492 kPa at 5.1% of deviatoric strain and then it decreased sharply to 310 kPa for further loading as it may be more brittle comparing to the sample TxS50P100.

The samples TxS50P200 and TxS50P400 experienced volume contractions, as shown in Figure 6.16 (b). Sample TxS50P400 showed 3.9% of volume contraction which was greater than the volumetric contraction of TxS50P200 (2.2%). The sample TxS50P100 showed a gentle dilation after having the constant value of volume contraction (1%) over a relatively large deviatoric strain. The dilatant behaviour was clearly evident in the volumetric behaviour of sample TxS300P100, which was subjected to the minimum net mean stress (100 kPA) and maximum suction (300 kPa). Sample TxS300P100 experienced the volumetric strain value of 1.23% which decreased to -0.65% during the dilation.

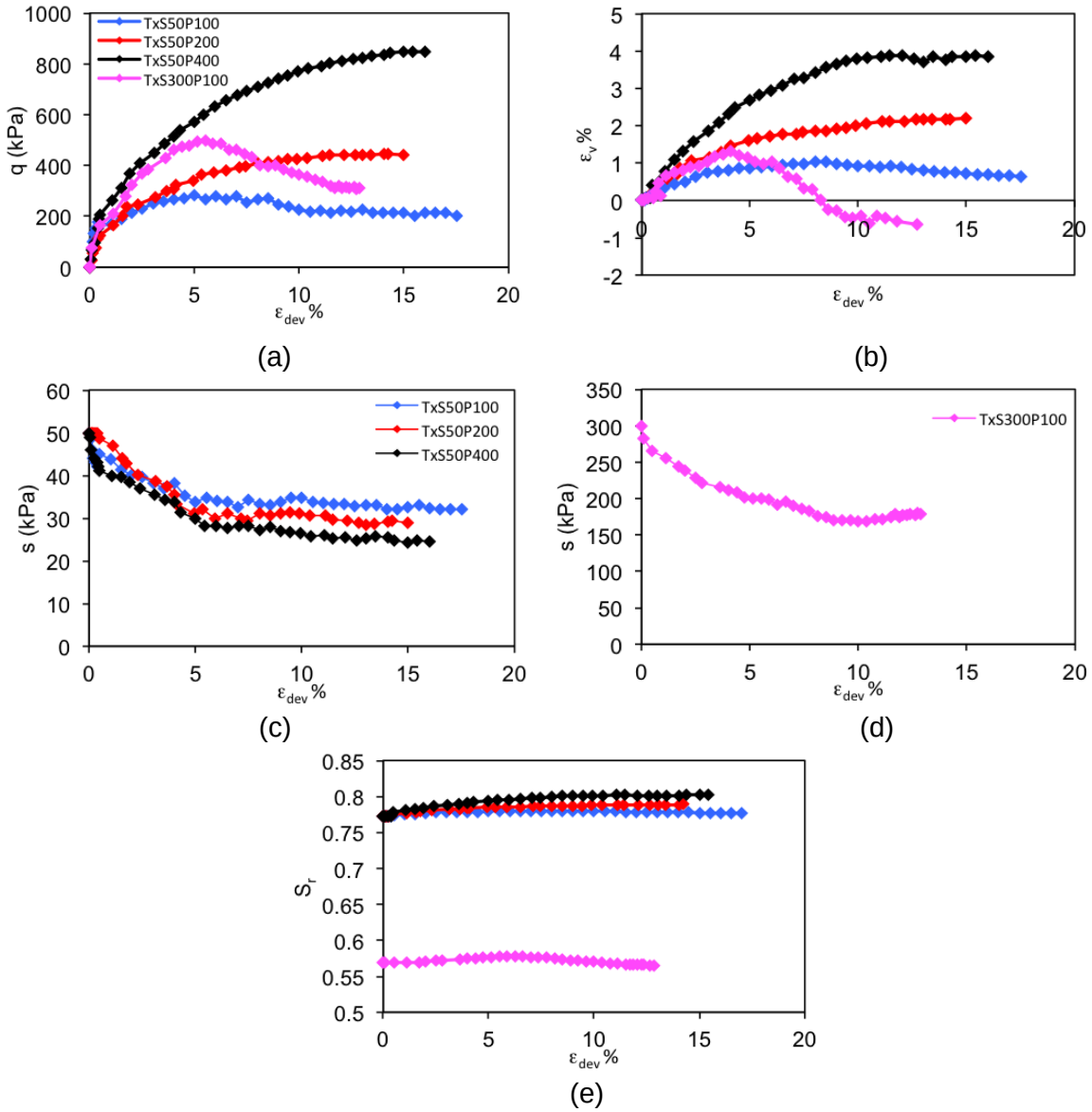

Figure 6.16. Behaviour of tested samples (s=50 and 300 kPa) during the shearing phase

a) q- ε_{dev} b) ε_v- ε_{dev} c) s (s_0=50 kPa) - ε_{dev} d) s (s_0=300 kPa) - ε_{dev} e) S_r- ε_{dev}

The deviatoric and volumetric behaviour of these samples showed that the softening in the deviatoric stress and the dilatancy in volumetric behaviour increases if a sample is subjected to the lower net confining stress and greater suction.

Figure 6.16 (d) shows the suction values measured during shearing. Samples previously subjected to 50 kPa of suction experienced suction reduction. The suction measured for sample TxS50P100, TxS50P200 and TxS50P400 decreased to 32, 29 and 25 kPa, respectively. The suction measured for sample TxS300P100 also displayed the decrease in suction from 300 to 169 kPa. However, the suction measured for sample TxS300P100 slightly increased at the end of the shearing phase.

Since tests were carried out under constant water content condition, the degree of saturation was computed corresponding to the volume change of samples and represented in Figure 6.16 (e). The degree of saturation increased as the volume of the samples decreased. Sample TxS300P100 showed dilative behaviour, and in turn, its degree of saturation decreased.

Figure 6.17 shows the hydraulic behaviour of aforementioned samples during the shearing phase in terms of e_w-e, e_w-s and S_r-s. The water ratio remained unchanged as the shearing was carried out under constant water content condition as shown in Figure 6.17 (a). It was pointed out that the main water retention curves in Figure 6.17 (b) and (c) were detected for the sample at relatively constant volume using the water retention tests. Hence, it was expected that the main curves slightly changed due to the volume change of these samples during the compression phase. However, they can be assumed to remain unchanged as the volume change of these samples were small and cannot change the main retention curves in this range of suction. This implied that the water retention state of the samples at the beginning of shearing phase was mainly close to main drying curve. Generally, the degree of saturation of all samples mainly increased due the volume reduction of samples, and in turn, the suction decreased during the shearing. This results in changing the hydraulic state of these samples in scanning domain. The amount of change in suction measured for sample TxS300P100 was greater than the others because it was subjected to the greater value of suction and the water retention at the greater level of suction are more influenced by volumetric changes.

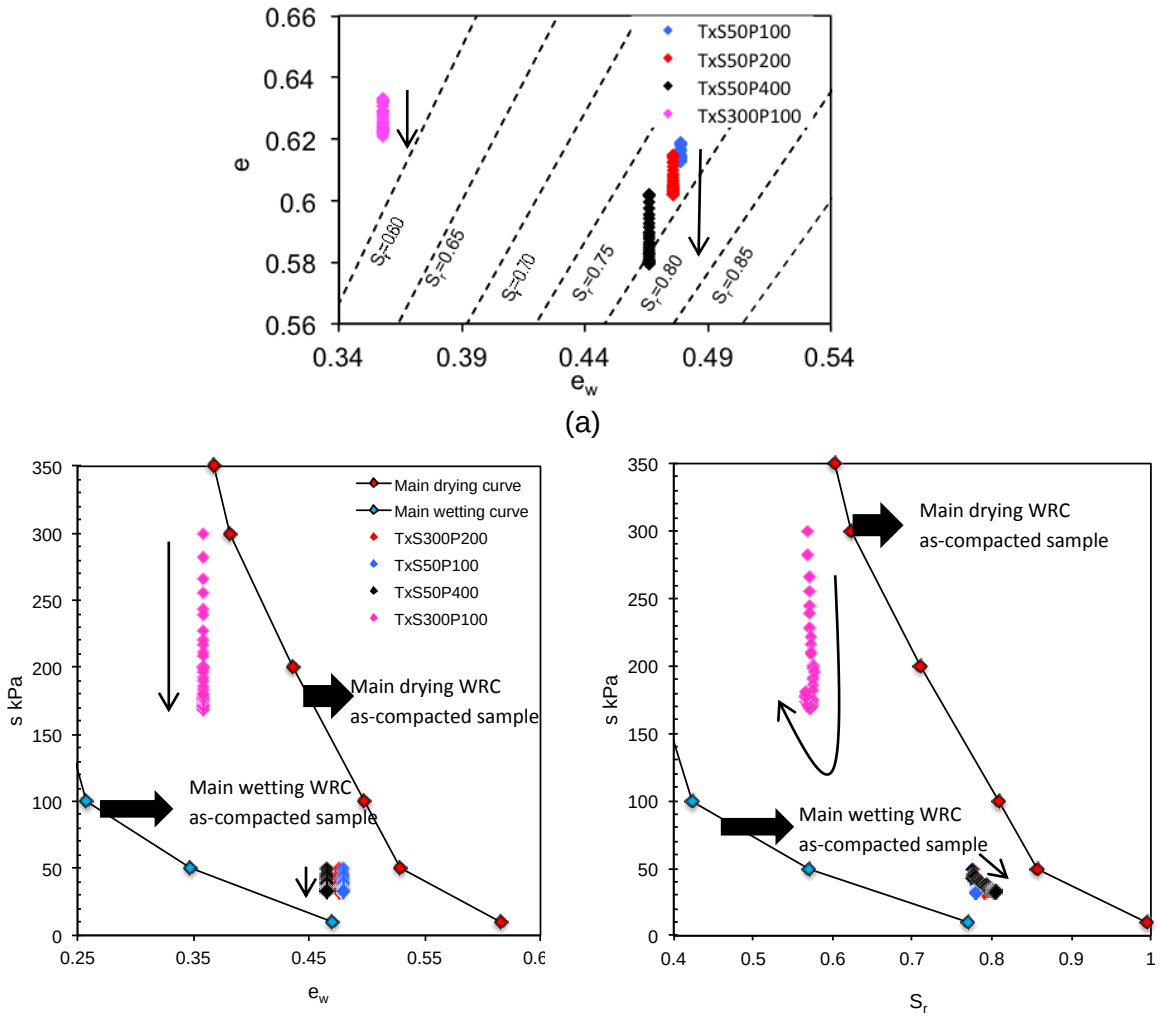

Figure 6.17. Behaviour of tested samples subjected to 50 and 300 kPa of suction: a) void ratio-water ratio b) suction-water ratio c) suction-degree of saturation

6.4.2 Constant water content (CW) triaxial tests (D/W cyclic samples)

Similar stress path including suction equalisation, compression and shearing at constant water content were applied to the as-compacted samples subjected to 3 or 6 drying-wetting cycles (3 and 6 D/W cyclic samples). The results are represented in the following where the effects of repeated hydraulic loads on the hydromechanical behaviour of Viadana samples is discussed by comparing the behaviour of 3 and 6 D/W cyclic samples and as-compacted samples.

6.4.2.1 Effect of repeated hydraulic loads on the suction equalisation

The experimental results of suction equalisation phase for 3 and 6 D/W cyclic sample are represented in Figure 6.18 and compared to the behaviour of as-compacted samples. Samples Tx3D/WS50P100, Tx3D/WS50P200, Tx3D/WS50P400, Tx6D/WS50P100, Tx6D/WS50P200 and Tx6D/WS50P400 were subjected to 50 kPa of suction (Figure 6.18 (a)). Similar to the as-compacted samples being subjected to 50 kPa of suction, water was expelled from 3 and 6 D/W cyclic samples where they experienced small volume contractions as shown in Figure 6.18 (b). This implied that imposed suction (50 kPa) was greater than suction acting on soil after being subjected to 3 or 6 cycles of drying-wetting. The amount of water desorption of 3 and 6 D/W cyclic samples was relatively the same. The water ratio of these samples decreased to 0.43, which is smaller than the one obtained for the as-compacted sample (TxS50P100, TxS50P200 and TxS50P400) at the end of suction equalisation phase (Figure 6.18 (c)).

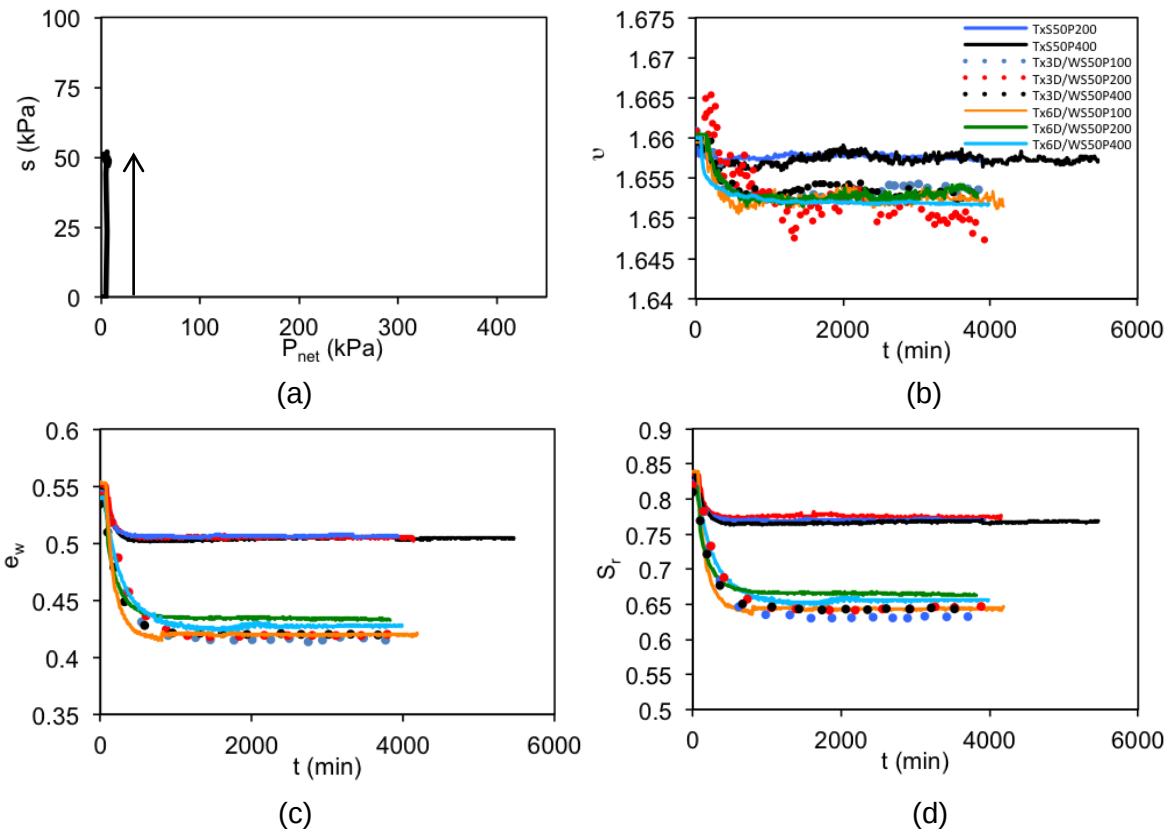

Figure 6.18. Effect repeated hydraulic loads on the behaviour of tested samples subjected to 50 kPa of suction: a) suction-p_{net} b) specific volume-time c) water ratio- time d) degree of saturation-time

Also, the volume of D/W cyclic samples decreased more than the as-compacted samples since they expelled more water during suction equalisation phase as shown in Figure 6.18 (b). Accordingly, the degree of saturation of D/W cyclic samples decreased to 0.66 (average value), which was smaller than the one of the as-compacted samples obtained at the equilibrium (0.76).

It can be pointed out that the repeated hydraulic loads affected the behaviour of the as-compacted samples in such a way that their water ratio was established at a lower level during the suction equalisation phase. However, the influence of 3 or 6 cycles of drying-wetting was found to be similar since their corresponding water ratio decreased to the same value.

Similar results can be drawn by comparing the behaviours of sample TxS300P100 and Tx6D/WS300P100, where both samples subjected to 300 kPa of suction (Figure 6.19 (a)). The latter one, which experienced 6 cycles of drying-wetting, expelled more water and exhibited more volume contraction during the suction equalisation phase, as shown in Figure 6.19 (b) and (c). The degree of saturation of samples TxS300P100 and Tx6D/WS300P100 decreased to 0.57 and 0.41, respectively (Figure 6.19 (d)).

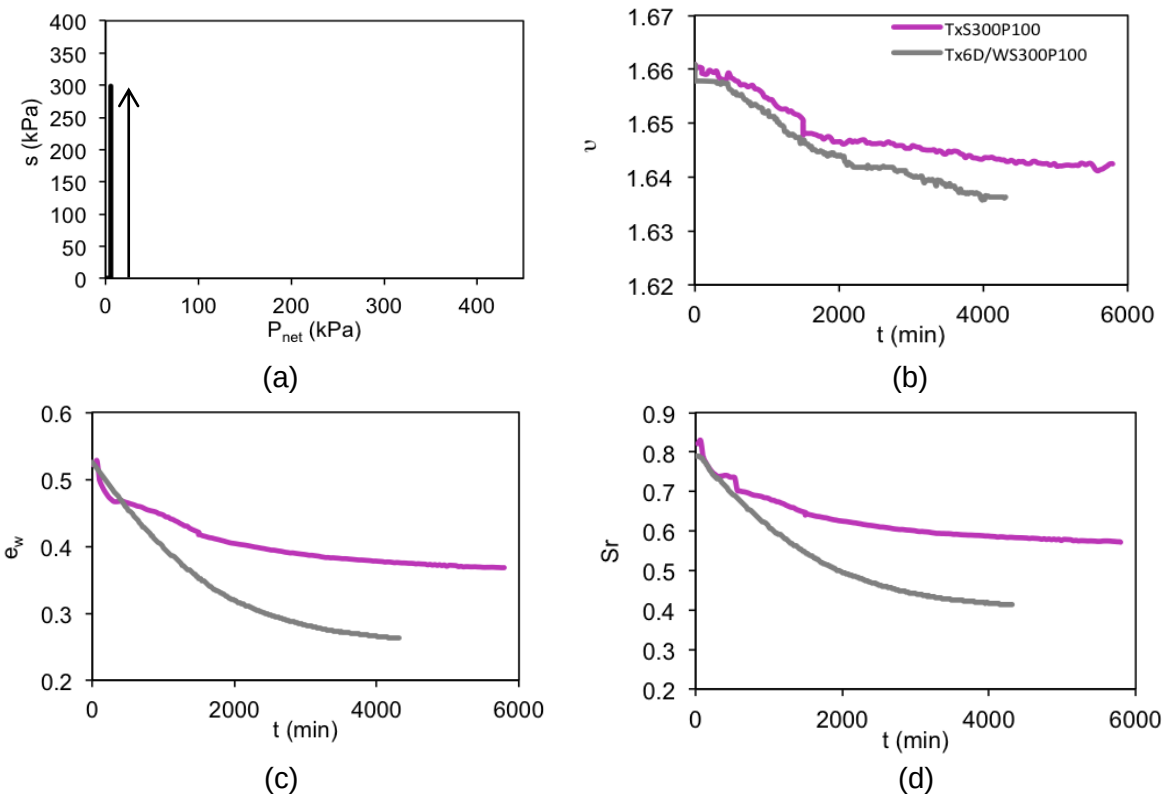

Figure 6.19. Effect repeated hydraulic loads on the behaviour of tested samples subjected to 50 kPa of suction: a) suction-p_{net} b) specific volume-time c) water ratio- time d) degree of saturation-time

Figure 6.20 (a) shows the behaviour of the as-compacted and 6 D/W cyclic sample when subjected to 50 kPa of suction in terms of e-e_w It can be clearly understood that the water ratio and degree of saturation of 6 D/W cyclic samples decreased more than the as-compacted samples. Similar trend can be observed in the behaviour of the as-compacted and 6 D/W cyclic samples when subjected to 300 kPa of suction, as shown in Figure 6.20 (b).

Post-compaction suction of the as-compacted samples was measured to be 33 kPa, and after being subjected to 6 drying-wetting cycles, suction acting on soil was found to be 5 kPa. It was assumed that suction established after 3 and 6 cycles of drying-wetting were mainly the same since 3 and 6 D/W cyclic samples showed similar behaviour during the suction equalisation phase. This may justified by the fact that the water retention behaviour of samples subjected to 3 and 6 drying-wetting cycles was detected to be the same as presented in chapter 5. The initial state and the one established at the end of the suction equalisation phase were represented in Figure 6.20 (c) and (d) in terms of S_r-s and e_w-s. The main drying water retention curves obtained for as-compacted and 6 D/W cyclic samples (represented in chapter 5) were also plotted. The initial states of the as-compacted samples are positioned at scanning domain but very close to their main drying curve. However, the initial states of 6 D/W cyclic samples were positioned more close to the main corresponding wetting curve. This was reasonable as the 6 D/W cyclic sample was being subjected to the wetting process over a wide range of suction at the last stage of applying repeated hydraulic loads.

The 6 D/W cyclic sample expelled more water and their water ratio and degree of saturation obtained at the end of the suction equalisation phase was smaller than the as-compacted samples, as represented in Figure 6.20 (c) and (d). The observed trends are consistent with the corresponding main water retention curves. The water retention curves obtained for 6 D/W cyclic samples were steeper and placed at the lower level of water ratio (and degree of saturation), implying that during the drying process the 6 D/W cycles samples expelled more water than the as-compacted samples, complied with corresponding main drying water retention curve. It can be pointed out that the water retention states of these samples were very close to their main drying curve at the end of the suction equalisation phase.

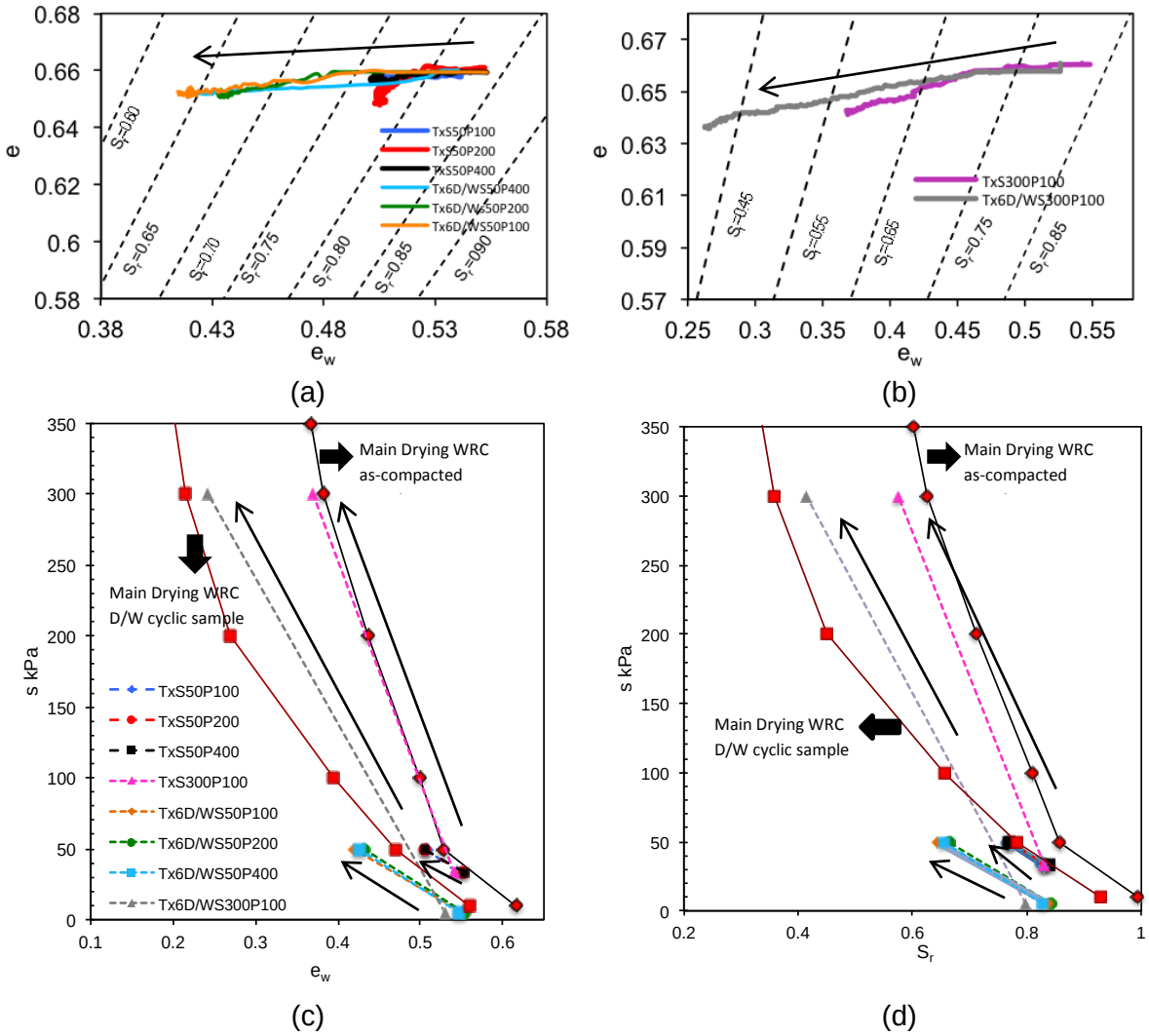

Figure 6.20. Behaviour of D/W cyclic and as-compacted samples subjected to 50 and 300 kPa of suction:
a) void ratio-water ratio (samples subjected to 50 kPa of suction)
b) void ratio-water ratio (samples subjected to 300 kPa of suction)
c) suction-water ratio d) suction-degree of saturation

6.4.2.2 Effect of repeated hydraulic loads on the compression behaviour

Samples that experienced hydraulic repeated loads (D/W cyclic samples) were isotropically compressed subjected to 100, 200 and 400 kPa of confining net pressures as well as the as-compacted samples. Figure 6.21 shows experimental results of the compression phase of samples Tx6D/WS50P100, Tx6D/WS50P200 and Tx6D/WS50P400. The compression pressures were applied to these samples while imposed suction was kept constant at 50 kPa (Figure 6.21 (a)). Figure 6.15 (b) shows the volumetric behaviour of these samples in terms the volumetric strain and mean net stress, which is compared to the volumetric behaviour of as-compacted samples subjected to the same mean net stresses. The amount of the volumetric contractions (positive value) of D/W cyclic samples was greater than as-compacted samples when the net mean stresses were 100 and 200 kPa.

The volumetric strain increased to 3.4 and 3.6% for samples Tx6D/WS50P100 and Tx6D/WS50P200 whereas it was measured to be to 2.4 and 2.8% for samples TxS50P100 and TxS50P200, respectively. However, samples Tx6D/WS50P400 and TxS50P400 experienced the same amount of contractive volumetric strain (4.2%). Figure 6.21 (c) shows the volumetric behaviour in terms of specific volume and mean net stress where the specific volume of D/W cyclic samples reached to the smaller value comparing to the one of the as-compacted samples when subjected to 100 and 200 kPa whereas the specific volume of samples subjected to 400 kPa was the same. The volumetric response of samples subjected to 400 kPa showed that the compressibility of the D/W cyclic sample was higher than the one of the as-compacted sample up to the mean net stress of 200 kPa, but it decreased as the net mean stress increased to the greater values than 200 kPa and it became smaller than the compressibility of the as-compacted sample.

Changes in the water ratio of these samples are represented in Figure 6.21 (d). The water ratio of all samples decreased as water expelled from these samples during the compression phase. The water ratio of samples TxS50P100 and Tx6D/WS50P100 decreased from 0.507 and 0.42 to 0.482 and 0.403, respectively. Although 6 D/W cyclic sample were found to be more compressible than the as-compacted one but no significant difference was observed in the amount of water expelled from these samples. The degree of saturations of these samples increased as shown in Figure 6.21 (e).

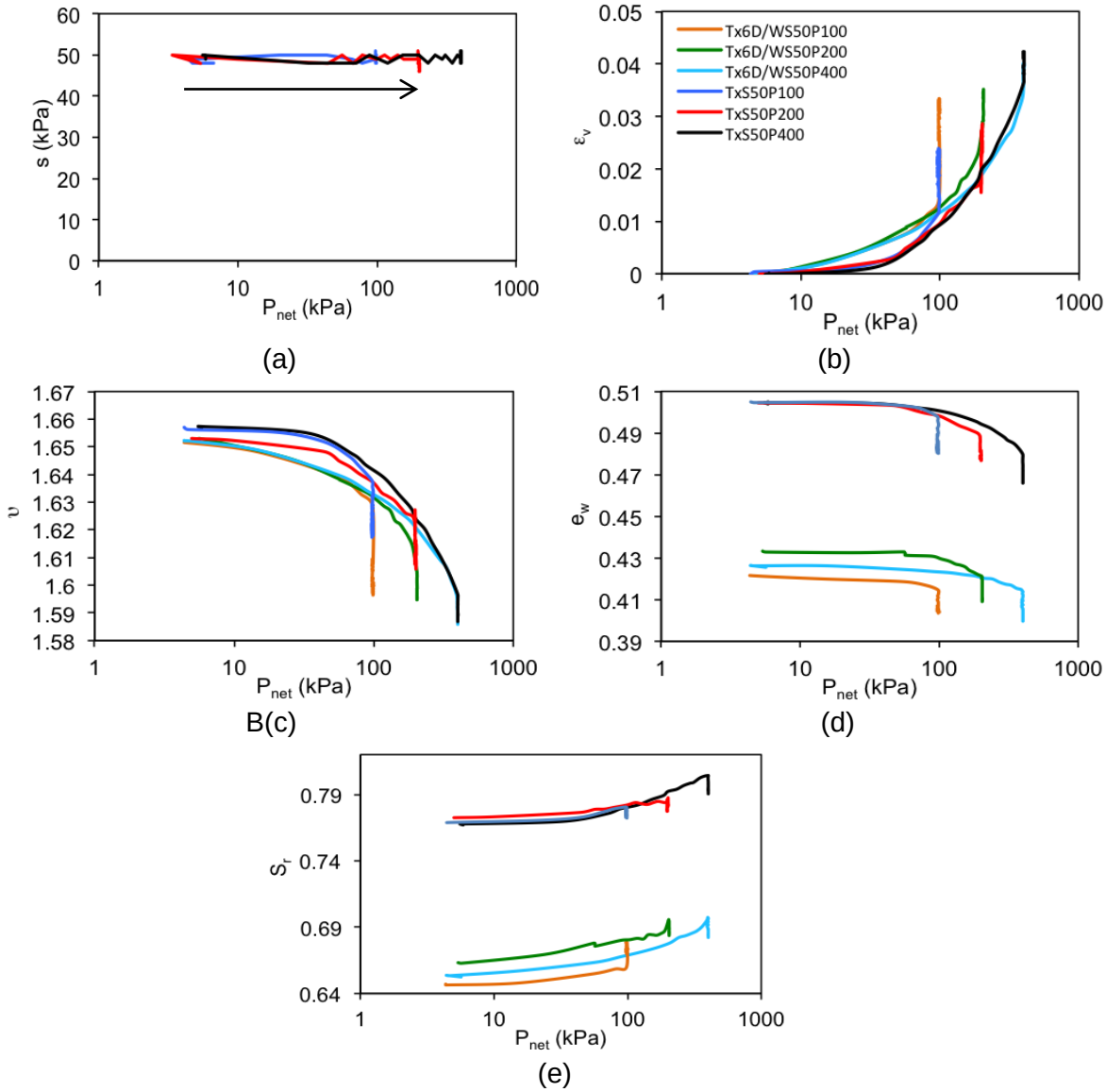

Figure 6.21. Behaviour of D/W cyclic and as-compacted sample (s=50 kPa) subjected to isotropic compression to 100, 200 and 400 kPa:
a) suction-p_{net} b) volumetric strain- p_{net}
c) specific volume- p_{net} d) water ratio- p_{net} e) degree of saturation- p_{net}

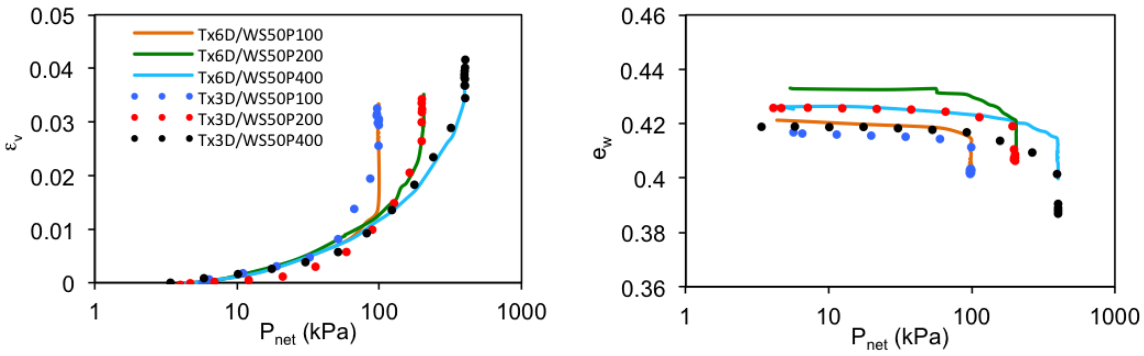

(a) (b)

Figure 6.22. Comparison between compression behaviours of samples subjected to 3 and 6 cycles of drying-wetting
a) volumetric strain- p_{net} b) water ratio- p_{net}

The volumetric compression behaviour of samples formerly subjected to 3 and 6 cycles of drying-wetting was relatively similar as shown in Figure 6.22 (a) and (b) in terms of volumetric strain-p_{net} and water ratio- p_{net}.

Figure 6.23 shows the compression behaviour of samples TxS300P100 and Tx6D/WS300P100 subjected to 100 kPa of mean net stress while suction was kept constant at 300 kPa (Figure 6.23 (a)). As shown in Figure 6.23 (b), the sample subjected to drying-wetting cycles exhibited more compressibility even though its void ratio and water ratio at the beginning of compression phase were smaller and it is expected to be stiffer than the as-compacted sample (Figure 6.23 (c)). The decrease in the water ratios of these samples was smaller comparing to the others since they were stiffer as being subjected to a higher suction. As a result, the degree of saturations of these samples did not change importantly, as shown in Figure 6.23 (d).

Figure 6.24 (a) and (b) shows the changes in void ratio and water ratio of aforementioned samples during the compression phase. It can be understood that the void ratio of these samples decreased more than the water ratio. Moreover, 6 D/W cyclic samples positioned close to contours of the degree of saturation with lower values since they expelled more water in the suction equalisation phase. Although they possess less water content comparing to the as-compacted samples, but their void ratio decreased more except for samples TX6D/WS50P100.

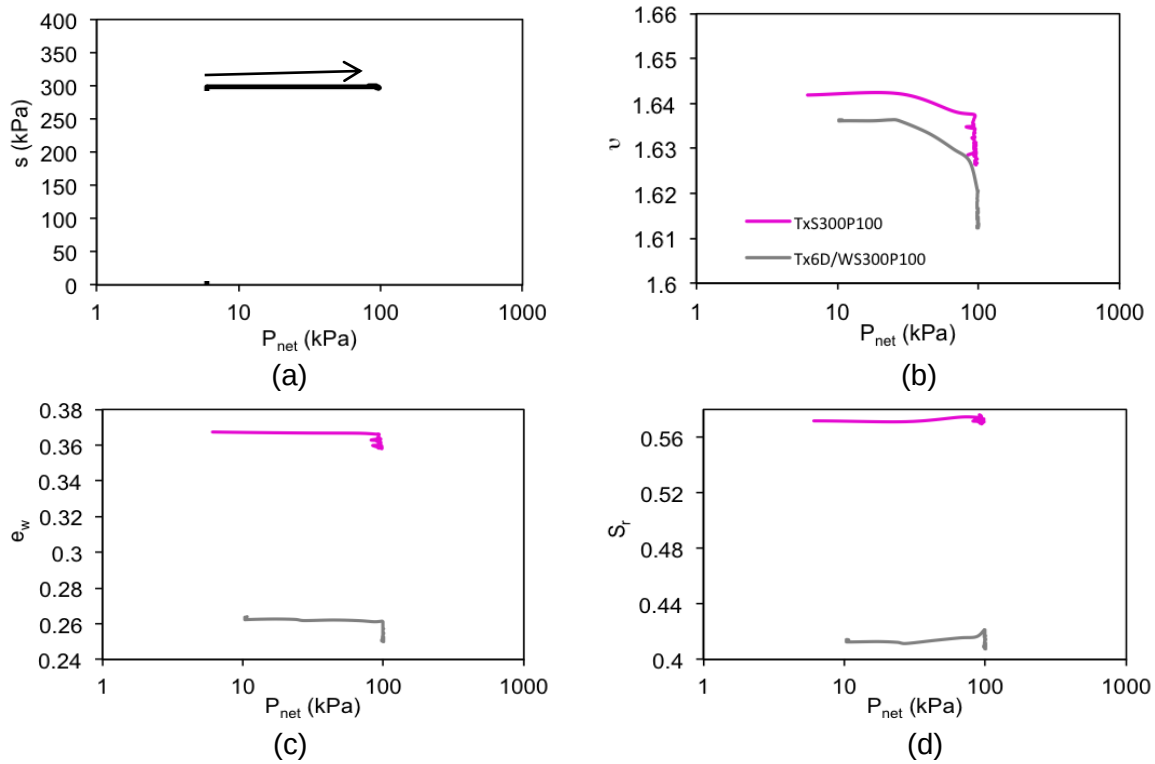

Figure 6.23. Behaviour of as-compacted and D/W cyclic samples (s=300 kPa) subjected to isotropic compression to 100 kPa:
a) suction-p_{net} b) specific volume- p_{net} c) water ratio- p_{net} d) degree of saturation- p_{net}

As the samples were being fully drained during the compression phase, the water ratio changed slightly and samples volume contractions were more evident. The degree of saturation at the beginning and at the end of compression phase can also be detected with respect to contours lines presented in Figure 6.18 (b). Obviously, the degree of saturation of sample TxS300P100 and TxS50P100 (6D/W) were placed in lower levels as it was subjected to the greater value of suction.

Figure 6.24 (c) and (d) shows the results in terms of S_r-s and e_w-s, where the hydraulic states of the samples at the end of suction equalisation and compression phases were plotted. The water ratio samples being subjected to 50 kPa of suction decreased more evidently whereas no significant changes in the degree of saturation were detected. This implied the hydraulic states of this samples remained very close to the main drying curve during the compression phase.

In conclusion, repeated hydraulic loads resulted in the increase in compressibility of as-compacted Viadana silt at low-stress levels up to the certain value of confining pressures. For greater value of confining stress, the compressibility decreased and become similar to the as-compacted one. The fundamental fabric changes induced by drying-wetting cycles may be vanished as the confining pressure increased. Moreover, samples subjected to 3 and 6 cycles exhibited the

same volumetric behaviour during the compression phase. It may be consistent with the volumetric behaviour of such samples when being subjected to drying-wetting cycles, in which their volume changes became reversible after 3 cycles. This may imply that the fabric changes took place upon 3 cycles and no further modification occurred in the following cycles.

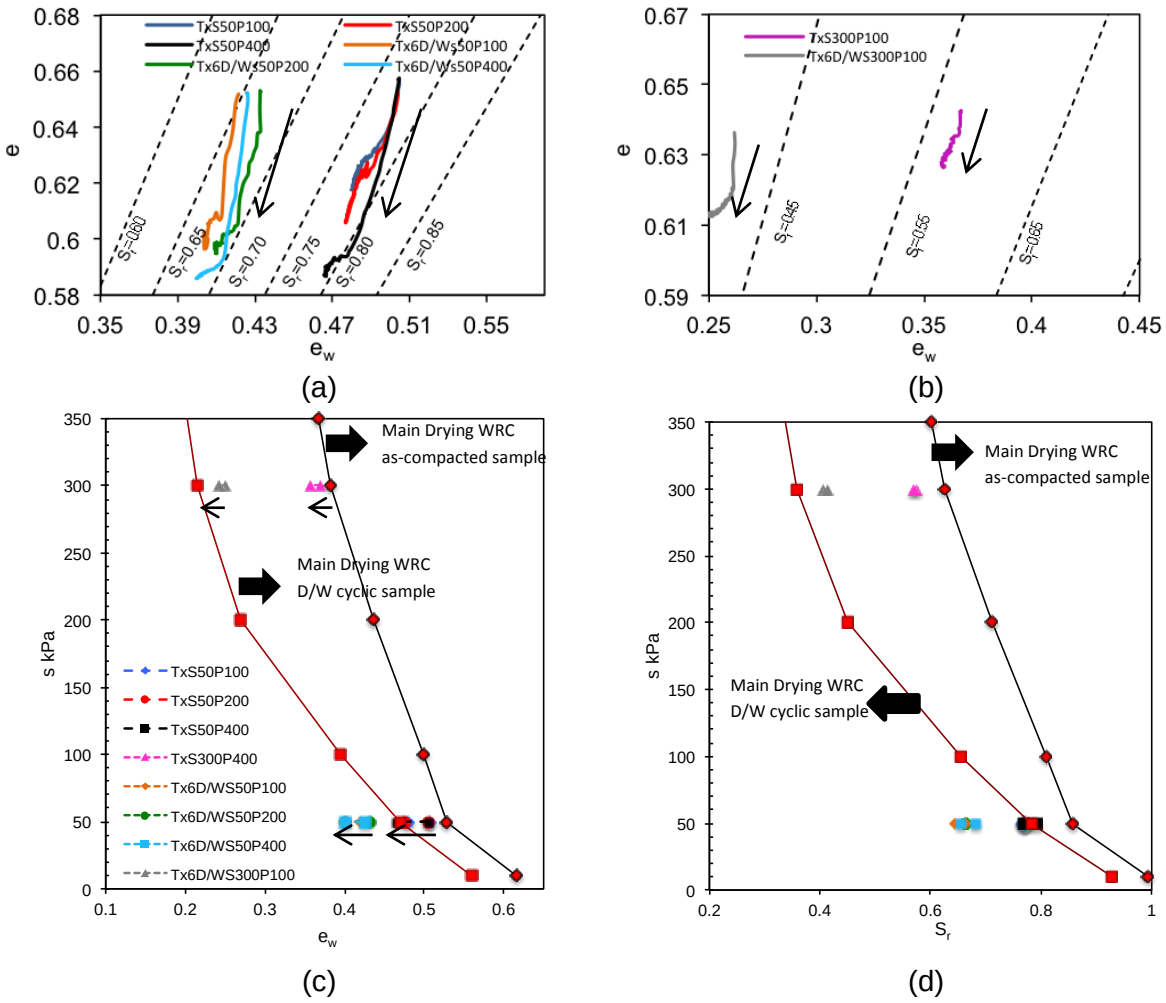

Figure 6.24. Behaviour of as-compacted and D/W cyclic samples subjected to 50 and 300 kPa of suction:
a) void ratio-water ratio (samples subjected to 50 kPa of suction)
b) void ratio-water ratio (samples subjected to 300 kPa of suction)
c) suction-water ratio d) suction-degree of saturation

6.4.2.3 Effect of repeated hydraulic loads on the shearing behaviour

When the equilibrium was established at the end of the compression phase, samples subjected to repeated hydraulic loads (D/W cyclic samples) were also sheared by applying an axial load at constant strain rate while the water drainage was closed. The behaviour of D/W cyclic samples during the shearing is presented in the following and it is compared to the behaviour of the as-compacted samples.

The results of the shearing phase of tests TxS50P200, Tx3D/WS50P200 and Tx6D/WS50P200 are represented in Figure 6.25, where the as-compacted, 3 D/W cyclic and 6 D/W cyclic samples were subjected to the confining pressure of 200 kPa and suction of 50 kPa during the compression phase. The results of similar samples but subjected to 400 kPa of the confining pressure are also presented in Figure 6.25 (TxS50P400, Tx3D/WS50P400 and Tx6D/WS50P400).

The effects of 3 and 6 cycles of wetting and drying were still analogous, similar to previous phases. As shown in Figure 6.25 (a), the deviatoric stress of D/W cyclic samples increased slightly more than the as-compacted samples. The maximum deviatoric stress of Tx3D/WS50P400 and Tx6D/WS50P400 was 933 and 896 kPa while the deviatoric stress of the as-compacted sample TxS50P400 increased to 847 kPa. The deviatoric stress of D/W cyclic samples when the confining pressure was 200 kPa also showed a small increase comparing to the one of the as-compacted sample with the same confining pressure. Moreover, samples Tx3D/WS50P200 and Tx6D/WS50P200 experienced a gentle softening at the end of the shearing phase.

Accordingly, contractive volumetric strains of D/W cyclic samples with 400 kPa of mean net stress were greater than the as-compacted sample, as shown in Figure 6.25 (b). The volumetric strain of the as-compacted sample TxS50P400 reached to 3.87% while the cyclic ones experienced 4.56% of contractive volumetric strains. The dilation of D/W cyclic sample with the confining pressure of 200 kPa was consistent with the observed softening. However, such a dilation trend was not evident in the volumetric behaviour of sample Tx3D/WS50P200.

Figure 6.25 (c) shows suction acting on both as-compacted and D/W cyclic samples measured during the shearing phase. The imposed suction of these samples before starting the shearing phase was 50 kPa, while it was observed to decrease upon shearing. The measured suction of D/W cyclic samples decreased less than the as-compacted ones. The suction acting on samples TxS50P200, and TxS50P400 decreased from 50 kPa to 29 and 25 kPa, respectively, whereas D/W cyclic samples experienced the minimum suction of 42 kPa (average value).

Principally, measured suction declared that the suction decreased more if samples being subjected to the greater value of the net mean stress. Moreover, the effect of repeated hydraulic loads on the as-compacted samples caused that such samples experienced less reduction in suction during the shearing phase under constant water content condition.

As shown in Figure 6.25 (d), the degree of saturation of these samples mainly increased due to the decrease in their volumes during the shearing phase except the degree of saturation of sample Tx6D/WS50P200, where a small decrease in its degree of saturation can be observed.

The results of the shearing phase of tests TxS50P100, TxS300P100, Tx6D/WS50P100 and Tx6D/WS300P100 are represented in Figure 6.26, where samples were subjected to the confining pressure of 100 kPa and suction of 300 kPa during the compression phase. The behaviour of samples subjected to 6 cycles of drying-wetting (6 D/W) was only represented since no significant differences were detected between the behaviour of 3 and 6 D/W cyclic samples.

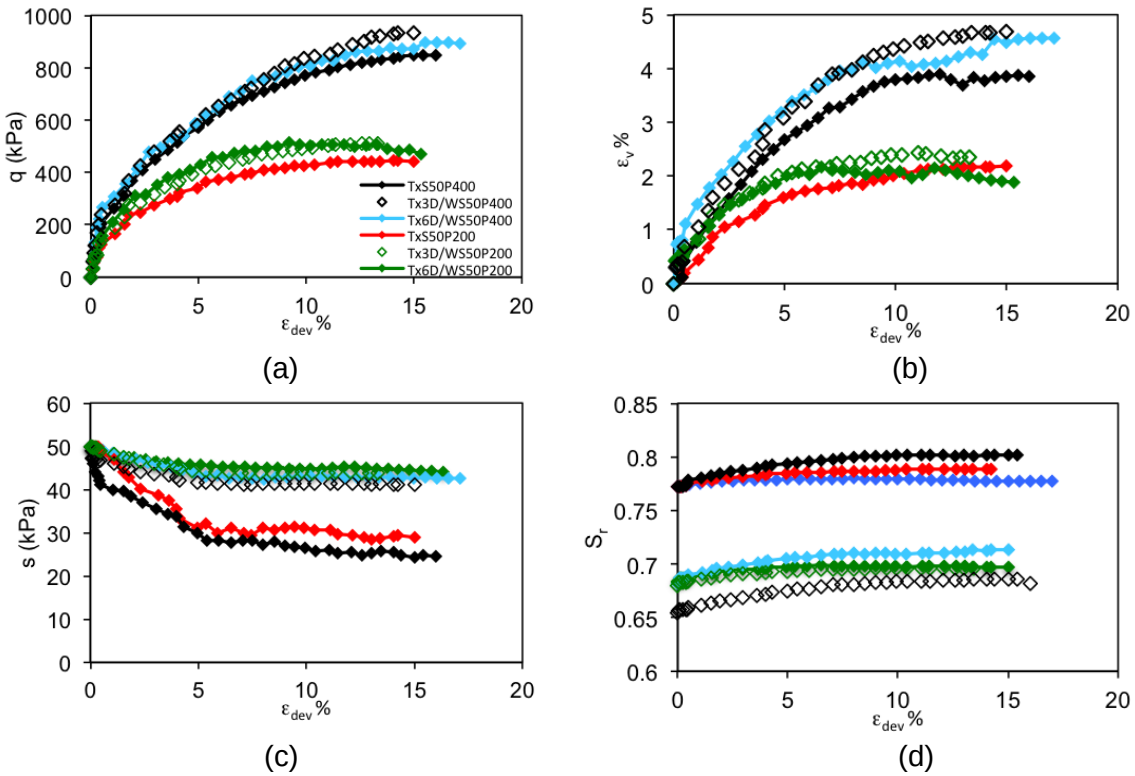

Figure 6.25. Behaviour of as-compacted and D/W cyclic samples (s=50 kPa, P_{net}=200 and 400 kPa) during the shearing phase
a) q- ε_{dev} b) ε_v- ε_{dev} c) s - ε_{dev} d) s - ε_{dev} e) S_r- ε_{dev}

The peak of the deviatoric stress of Tx6D/WS50P100 cyclic sample found to be 376 kPa whereas the as-compacted sample TxS500P100 experienced the maximum deviatoric stress of 281 kPa. Both samples exhibited the softening behaviour after the peak of the deviatoric stress although it is more evident in the behaviour of the 6 D/W cyclic sample, where the deviatoric stress of sample TxS50P100 (6D/W) decreased to 247 kPa. Sample Tx6D/WS300P100 showed the similar increase in the deviatoric stress and more softening comparing to the behaviour of as-compacted sample TxS300P100 while the deviatoric stress after the peak decreased sharply in both samples (Figure 6.26 (a)). It has to be pointed out the samples Tx6D/WS50P100 and Tx6D/WS300P100 possessed smaller void ratios comparing to samples TxS50P100 and TxS300P100, respectively, since they experienced more compressive volumetric strains during the compression phase.

As shown in Figure 6.26 (b), D/W cyclic samples showed more dilative behaviour comparing to the corresponding as-compacted samples. The volumetric strain of sample Tx6D/WS50P100 decreased to zero at the end of the shearing phase while the dilation in sample TxS50P100 was very small. Samples TxS300P100 and Tx6D/WS300P100 shows more dilation comparing to the sample subjected to suction of 50 kPa (at the beginning of the shearing phase), although 6 D/W cyclic sample experienced more swelling as the volumetric strain reached to -1.36%. The resulting volumetric behaviours were consistent with the existence and severity of the softening behaviours observed in the deviatoric stress behaviour of the corresponding samples.

Figure 6.26 (c) shows suction of these samples measured during the shearing phase. The suction of as-compacted sample being subjected to 50 kPa decreased to 32 kPa, and the one being subjected to 300 kPa decreased to 178 kPa. Sample subjected to repeated hydraulic loads (6 D/W cyclic samples) being subjected to 50 kPa decreased to of 45 kPa, and the one being subjected to 300 kPa decreased to 232 kPa. This implied that the repeated hydraulic loads resulted in less decrease of suction during the shearing phase.

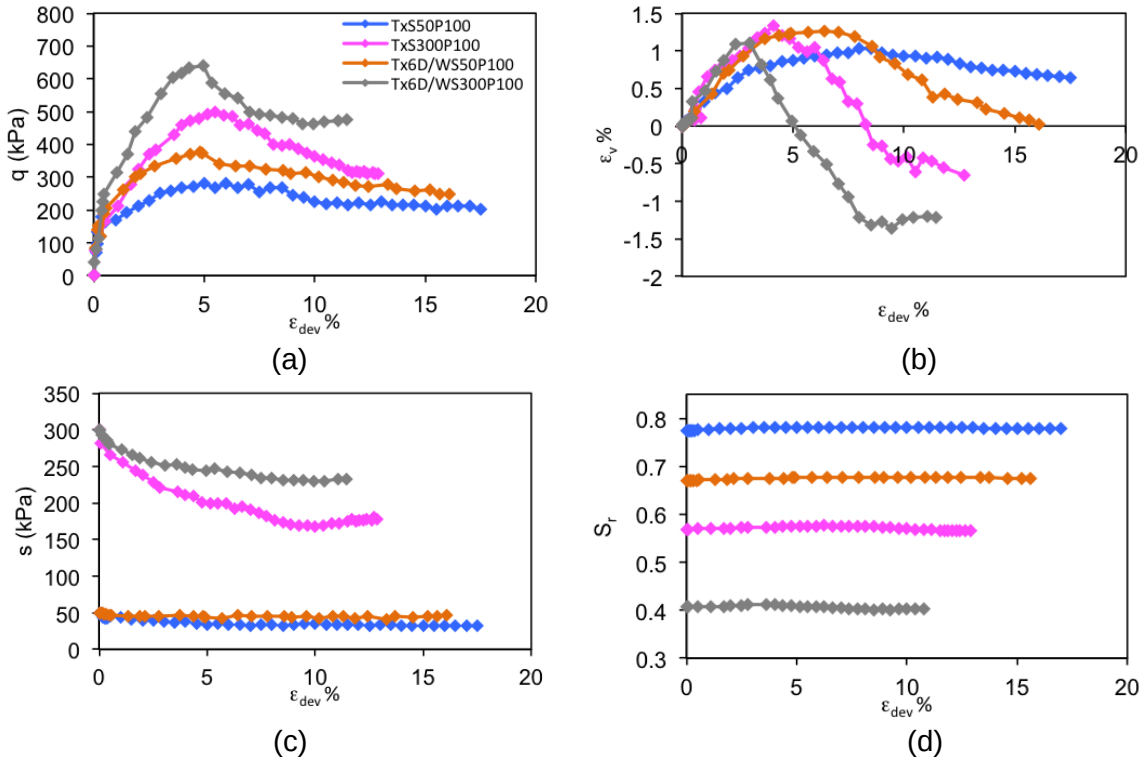

Figure 6.26. Behaviour of as-compacted and D/W cyclic samples (s=50 and 300 kPa, P_{net}=100 kPa) during the shearing phase

a) q- ε_{dev} b) ε_v- ε_{dev} c) s (s_0=50 kPa) - ε_{dev} d) s (s_0=300 kPa) - ε_{dev} e) S_r- ε_{dev}

The water content of samples was kept constant as the shearing phase was carried out under constant water condition. The variation of the degree of saturations resulted from the volume changes of samples, as represented in Figure 6.26 (d). The decrease in the degree of saturation of samples TxS300P100 and Tx6D/WS300P100 at the end of the shearing phase are evident due to the observed swelling volumetric behaviour.

It is believed that the effect of repeated hydraulic loads on the behaviour of as-compacted sample vanished at the higher value of net mean stress as it was discussed for the behaviour of 400 kPa of net mean stress.

The more softening behaviour observed in samples being subjected to the greater value of suction was also obtained in experimental results of constant water content tests, as reported by Sivakumar (2009). Repeated hydraulic loads resulted in the more evident softening behaviour of the as-compacted samples, besides the increase of the peak of the deviatoric stress.

Figure 6.27 (a) shows the variation of the void ratio of the as-compacted and 6 D/W cyclic samples during the shearing phase while the water ratio was constant as the tests were carried out under constant water content condition. Comparing

the void ratio and water ratio of the as-compacted and corresponding 6 D/W cyclic samples showed that the void ratio of the 6 W/D cyclic samples at the beginning of the shearing is smaller than the one of the as-compacted sample as they experienced more contraction during the compression phase. Moreover, the water ratio of 6 D/W cyclic samples subjected to 50 kPa of suction at the beginning of the shearing phase was smaller than the one of the as-compacted samples. This was also observed for water ratio of 6D/W cyclic sample when subjected to 300 kPa.

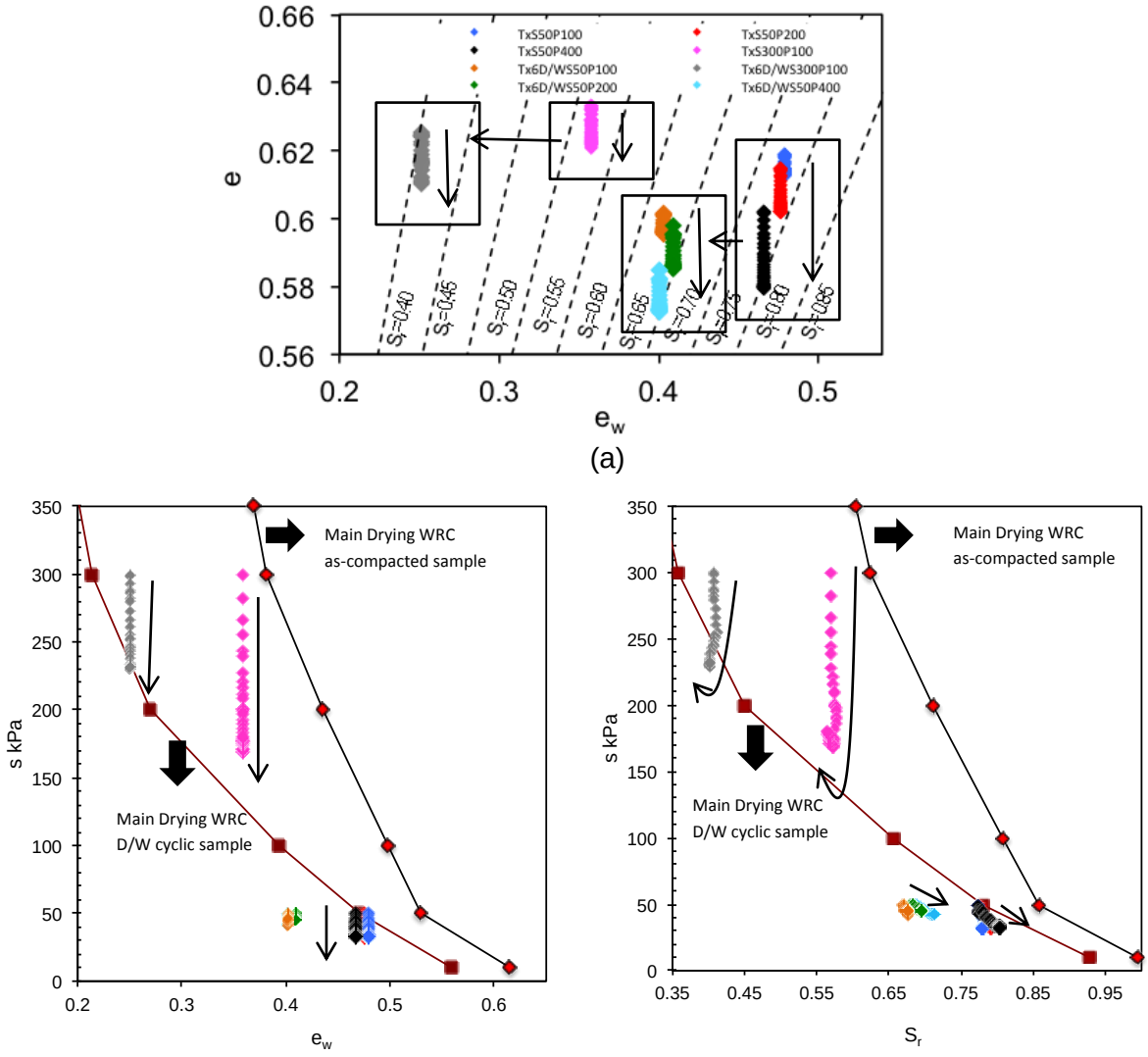

Figure 6.27. Behaviour of as-compacted and D/W cyclic samples (s=50 and 300 kPa, P_{net}=100, 200 and 400 kPa) during the shearing phase

a) void ratio-water ratio c) suction-water ratio d) suction-degree of saturation b)

Figure 6.27 (b) and (c) show the water retention behaviour represented in terms of e_w-s and S_r-s. It was expected that the water retention state of the samples at the beginning of shearing phase was mainly close to main drying curve. The water ratio remained constant whereas the degree of saturation of most samples was mainly increased due the volume reduction of the samples, and in turn, the suction decreased during the shearing (Figure 6.27 (c)).

In conclusion, two main effects of repeated hydraulic loads on the shearing behaviour of the as-compacted sample were detected. The strength of material increased slightly and also more evident softening associated with dilative volumetric behaviour were observed. Since samples subjected to repeated hydraulic loads experienced more volumetric contraction during compression, they were slightly denser than the as-compacted one. Moreover, they followed their corresponding water retention curves, where D/W cyclic samples expelled more water than the as-compacted one, particularly during the suction equalisation phase. Therefore, the water content of the 6 D/W cyclic samples was smaller and suction measured during the shearing phase remained at higher levels than the one of the as-compacted samples. The resulting increase in strength of D/W cyclic sample may be justified due to having smaller void ratio and water content in the beginning of the shearing phase. The increase in softening and dilation may be resulted from the greater suction acting on 6 D/W cyclic samples during the shearing phase.

6.5 Microstructural study

The effect of repeated hydraulic loads on the fabric of soil samples of Viadana silt were studied by the comparison between the pore size density functions of the as-compacted and 6 D/W cyclic samples obtained from MIP analysis, and the results were discussed in chapter 5. In order to study the response of similar samples to the mechanical loadings, four samples of Viadana silt (50 mm diameter and 20 mm height) were prepared with the same dry density (16.5 KN/m^3) and compacted at 20% of water content. Two of them were subjected to 6 cycles of drying-wetting (similar to 6D/W cyclic sample). As-compacted and 6 D/W cyclic samples were then placed in conventional oedometer apparatus and subjected to 98 and 1596 kPa of net axial stress. At the end of oedometer tests, samples were removed and trimmed into small cylindrical samples, having sizes appropriate for MIP apparatus. They were then dehydrated using the freeze-drying technique to preserve the fabric of samples at their natural water content.

6.5.1 Interpretation of MIP results

Figure 6.28 (a) shows the effect of the repeated hydraulic loads on the PSD of the as-compacted sample. The evolution of PSD showed that the as-compacted samples of Viadana silt in the microstructural level were sensitive to changes in moisture content, and the fabric changes can take place even without significant changes in the global volumetric strain of the soil sample. In fact, the volumetric strain of these samples was measured and found to be mainly reversible although fabric changes can take place regarding the interaction between different classes of pores. 3 classes of pores were identified for as-compacted samples of Viadana silt considering the PSD and WRC obtained in the experimental work. They were named as macropores, mesopores and micropores.

As shown in Figure 6.28 (a), macropores increased in the volume and size after being subjected to repeated hydraulic loads. However, the volume of the mesopores decreased while larger pores formed in the pore network of as-compacted sample. This was justified as pore size corresponding to the dominant peak of mesopores shifted to the larger pore size. However, the micropores of Viadana silt experienced no significant alteration due to repeated hydraulic loads. The experimental results suggest sort of irreversible changes in the macropores and mesopores regions due to repeated hydraulic loads, resulted in changes of the soil fabric.

Figure 6.28 (b) shows the PSDs of the as-compacted sample, and as-compacted samples after being subjected to the load of 98 and 1596 kPa. The pore size radius and PSD of the dominant peak of macropores of as-compacted sample was 50316 A and 0.3, respectively. The PSD decreased to 0.09 when the sample was subjected to the load of 98 kPa. This implied that the volume of macropores decreased due to the loading (98 kPa).

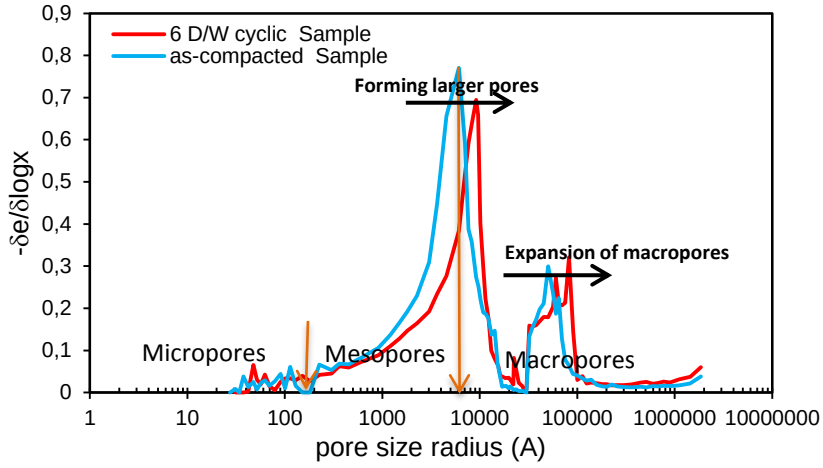

(a)

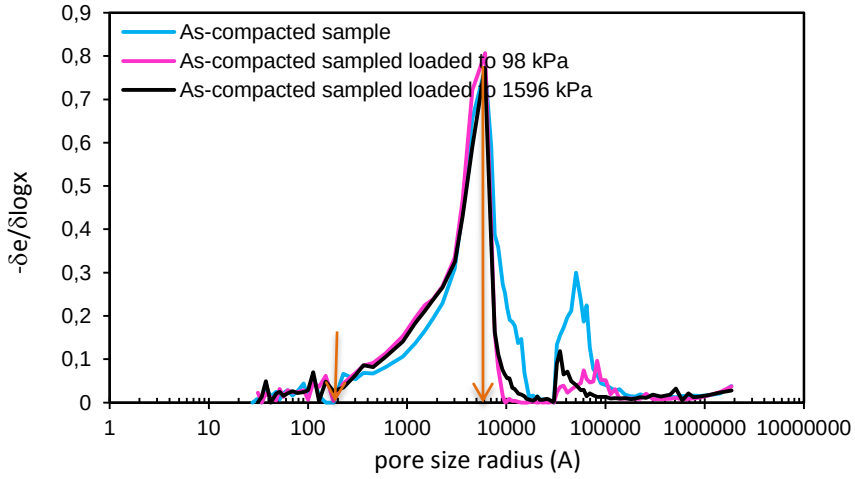

(b)

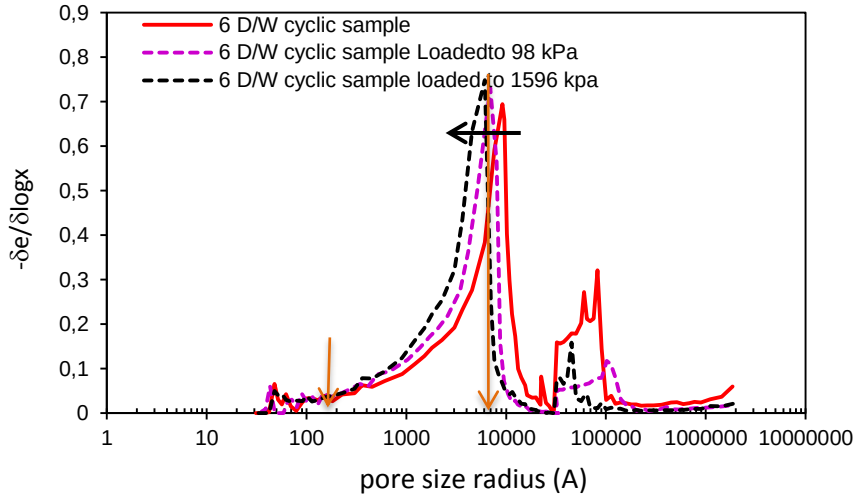

(c)

Figure 6.28. PSD functions of as-compacted and 6 D/W cyclic samples: a) as-compacted and 6 D/W cyclic samples b) as-compacted samples loaded to 98 and 1596 kPa c) 6 D/W cyclic samples loaded to 98 and 1596 kPa kPa

On the other hand, the pore size radius and PSD of the dominant peak for mesopores of the as-compacted sample exhibited no important alteration and their value remained constant at about 6029 A and 0.8, respectively. However, it can be understood that the PSD function at the right side of the dominant peak of mesopores became sharper. This may further justify the choice of the threshold pore size that separates the macropores and mesopores. In other words, the fact that the pores, having the radius size between 6029 and 20000 A, are influenced by the loading, imply that the domain with pore size radius greater than 6029 A (peak of the dominant mesopores) has to associate with macropores. As a result, macropores with size radius between 6029 and 20000 A also vanished when as-compacted sample subjected to the load of 98 kPa. The PSD of the as-compacted sample subjected to the load of 1596 kPa showed that the portion of the macropores and mesopores with pore size radius smaller than 20000 A did not experience further changes, whereas the portion of macropores with radius size greater than 20000 A was clearly affected as the corresponding PSD function moved to the left due to the reduction in the pore size radius. Consequently, the volume of macropores decreased by means of changes in the size of pores due to being loaded with the greater load.

The PSDs were also plotted for 6 D/W cyclic sample, 6 D/W cyclic sample being subjected to loads of 98 and 1596 kPa, as represented in Figure 6.28 (c). The macropores with radius size greater than 20000 A changed in the same manner that the ones of the as-compacted sample subjected to the same load. The dominant peak of PSD of macropores decreased from 0.32 to 0.14 due to the loading of 98 kPa. The size of the peak of the dominant macropores was then decreased as the PSD of this region shifted to the left side when subjected to the load of 1596 kPa. Moreover, the portion of macropores and mesopores with size radius smaller than 20000 A were also influenced by the loading process. As the right side of the dominant peak of the PSD became steeper, the volume of the macropores decreased. Moreover, the pore size radius corresponding to the dominant peak decreased from 9173 A to 6936 and 6091 A being subjected to loads of 98 and 1596 kPa, respectively. The comparison between the response of the as-compacted and 6 D/W cyclic samples with reference to the obtained PSDs declared that the macropores were not the only pore mode of the as-compacted sample influenced by loading but mesopores of 6 D/W cyclic sample were experienced changes mainly in size upon loading.

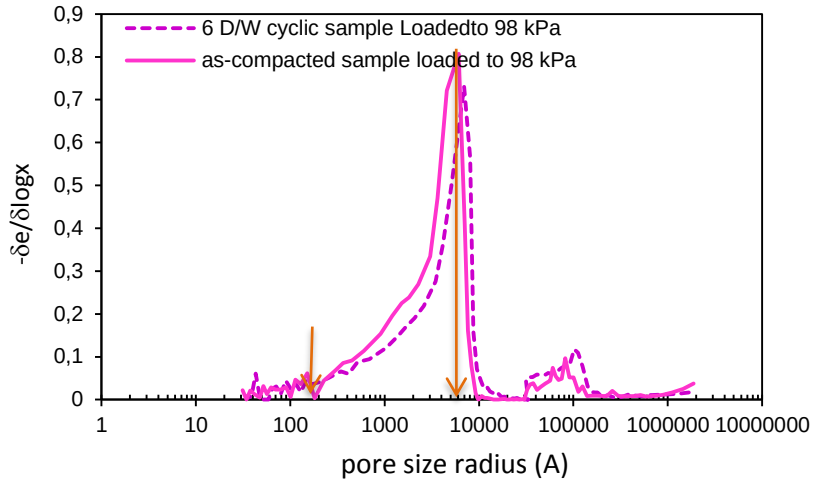

(a)

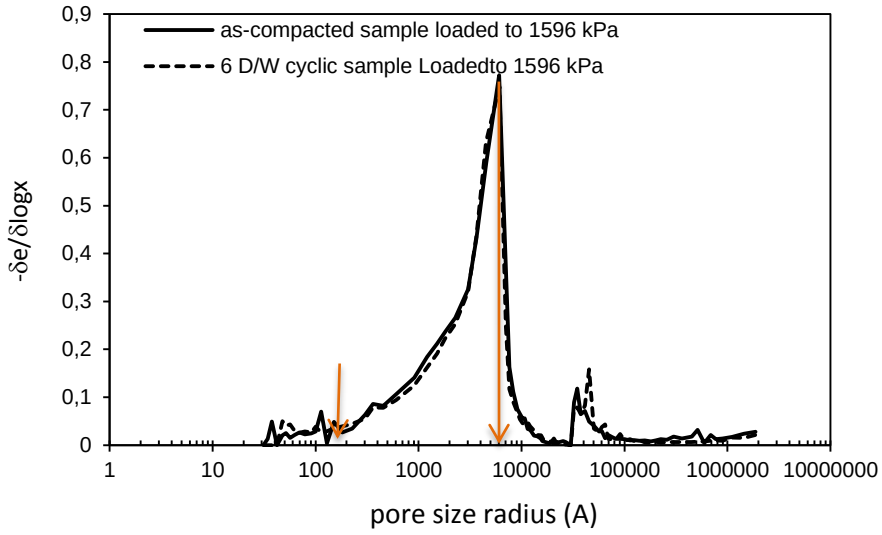

(b)

Figure 6.29. PSD functions of as-compacted and 6 D/W cyclic samples: a) subjected to the load of 98 kPa b) subjected to the load of 1596 kPa.

As it was pointed out, repeated hydraulic loads increased the macro-void ratio whereas the meso-void ratio decreased after being subjected to cycles of drying-wetting. Micro-void ratio, which was associated with the small portion of the pore structure of tested samples, was not influenced by repeated hydraulic loads. When as-compacted and 6 D/W cyclic samples were subjected to 98 kPa (as represented in Figure 6.29 (a)), the volume of the 6 D/W cyclic samples decreased more than the as-compacted sample. This may be consistent with compression volumetric strains measured for similar samples during the compression phase of triaxial tests at 100 and 200 kPa of net mean stress, where the volumetric strain of 6 D/W cyclic sample was found to be greater than the one of the as-compacted sample. On the other hand, the compressibility of the 6 D/W cyclic sample

decreased with the increase of the net mean stress resulted in the as-compacted and 6 D/W cyclic samples possess relatively the same volumetric strain when subjected to 400 kPa of net mean stress. This can be justified by comparing the PSDs of such samples being subjected to the high value of loads, as represented in Figure 6.29 (b). The PSDs of the as-compacted and 6 D/W cyclic samples overlapped implying that the pore structures of these samples took a similar form when being subjected to high value of stresses..

6.6 Conclusion

In this chapter, the hydromechanical behaviour of unsaturated silty soil was discussed accounting for the effects of hydraulic loads on the microstructure of as-compacted sample. As-compacted samples of Viadana silt were subjected to drying-wetting cycles, in which these samples experienced irreversible volumetric change upon 2 or 3 cycles of drying-wetting, followed by sort of reversible volume changes for subsequent cycles of hydraulic loads. It is believed that some sort of structural alteration took place in the fabric of as-compacted samples due to being subjected to repeated hydraulic loads while no significant global volumetric changes were observed. Such fabric changes established after initial drying-wetting cycles (up to 3 cycles) and no further alteration occurred for the subsequent cycles.

When such samples subjected to the different suction levels, the variation of their water content was different from the as-compacted samples. In fact, the hydraulic behaviour of these samples was consistent with the water retention curve detected for samples similarly subjected to hydraulic repeated loads. The water retention of the as-compacted sample found to be shifted toward lower levels of water content when they experienced drying-wetting cycles. When the equilibrium was established, different net mean pressures were applied to the samples. The compression behaviour declared that repeated hydraulic loads resulted in the increase in compressibility of the as-compacted Viadana silt at low-stress levels up to the certain value of net mean pressures. For the greater value of net mean stress, the compressibility decreased and become similar to the as-compacted one. The fundamental fabric changes induced by drying-wetting cycles vanished as the confining pressure increased. Moreover, samples subjected to 3 and 6 cycles exhibited the same volumetric behaviour during the compression phase. It may be consistent with the volumetric behaviour of such samples when being subjected to drying-wetting cycles, in which their volume changes became reversible after 3 cycles. This may imply that the fabric changes took place upon 3 cycles and no further modification occurred in the following cycles.

Finally, the hydromechanical behaviour of such samples was studied when subjected to shear loading under constant water content condition. The results showed that the strength of the material increased slightly associated with more softening. The volumetric behaviour was also consistent as more dilative behaviour was observed. Moreover, suction measured and mainly decreased during the shearing. However, samples subjected to repeated hydraulic loads experienced less reduction in suction comparing to the as-compacted samples.

Since samples subjected to repeated hydraulic loads experienced more volumetric contraction during compression, they were slightly denser than the as-compacted one at the beginning of the shear loading. Moreover, they followed their corresponding water retention curves, where they expelled more water than the as-compacted one, particularly during the suction equalisation phase. Therefore, the water content of such samples was lower and suction measured during the shearing phase remained at higher levels than the one of the as-compacted samples. The resulting increase in strength may be justified due to having lower void ratio and water content in the beginning of the shearing phase and the increase in softening and dilation may result from the greater suction acting on these samples during the shearing phase.

References

[1] Alawaji, H.,1999.Swell and compressibility characteristics of sand bentonite mixtures inundated with liquids.Applied Clay Science13(3–4), 411–430.

[2] Alonso EE, Gens A, Josa A. A constitutive model for partially saturated soils. Géotechnique 1990; 40:405**–**430.

[3] Alonso, E., Lloret, A., Gens, A., and Yang, D. (1995). Experimental behaviour of highly expansive double-structure clay. In Proc. 1st Int. Conf. Unsaturated Soils, pages 11–16, Paris, France.

[4] Alonso, E., Romero, E., Arnedo, D., and Olivella, S. (2005). Geotechnical properties of low density unsaturated carbonated clayey silts and impact on the foundation of canal embankments. In Proc. 16th Int. Conf. on Soil Mechanics and Geotechnical Engineering, pages 1823–1826. Millpress, Rotterdam, Netherlands.

[5] Alshihabi, O., Shahrour, I., Mieussens, C., 2002. Experimental study of the influence of suction and drying/wetting cycles on the compressibility of a compacted soil. Proceedings of 1st International Conference on Unsaturated Soils, Balkema, Rotterdam, The Netherlands, pp. 541–545.

[6] Benson, C. H., Sawangsuriya, A., Trzebiatowski, B., and Albright, W. H. (2007). Post construction changes in the hydraulic properties of water balance cover soils. Journal of Geotechnical and Geoenvironmental Engineering, 133(4):349–359. 4.1

[7] Bishop, A. W., Alpan, I., Blight, G. E., and Donald, I. B. _1960_. “Factors controlling the shear strength of partly saturated cohesive soil.” Proc., ASCE Research Conf. on Shear Strength of Cohesive Soils, Univ. of Colorado, Boulder, Colo., 503–532.

[8] Bishop, A. W., and Donald, I. B. _1961_. “The experimental study of partly saturated soil in the triaxial apparatus.” Proc., 5th Int. Conf. on Soil Mechanics and Foundation Engineering, Paris, Vol. 1, 13–21.

[9] Blight, G. E. 1961. “Strength and consolidation characteristics of compacted soil.” PhD dissertation, Univ. of London, London.

[10] Casttellanos, E., Villar, M.V., Romero, E., Lloret, A., Gens, A., 2008. Chemical impact on the hydro-mechanical behaviour of high density FEBEX bentonite. Physics and Chemistry of the Earth 33,516–526.

[11] Chen, F.H., 1988. Foundationon Expansive Soils, 2nded. Elsevier Science Publishing Co., New York, USA.

[12] Chen, Z. H., Fredlund, D. G., and Gan, J. K.-M. 1999. Overall volume change, water volume change and yield associated with an unsaturated compacted loess, Canadian Geotechnical Journal, Vol. 36, No. 2, pp. 321–329.

[13] Chiu, C. F., and Ng, C. W. W. 2003. A state-dependent elastoplastic model for saturated and unsaturated soils, Geotechnique, Vol. 53, No. 9, pp. 809–829.

[14] Cui, Y., Yahia Aissa, M., and Delage, P. (2002). A model for the volume change behaviour of heavily compacted swelling clays. Engineering Geology, 64:233–250. 4.1.5

[15] Della Vecchia G. Coupled hydro-mechanical behaviour of compacted clayey soil. PhD Thesis, Politecnico diMilano 2009.

[16] Di Maio, C., Santoli, L., Schiavine, P., 2004. Volume change behaviour of clays: the influence of mineral composition, pore fluid composition and stress state. Mechanics of Materials 36(5–6), 435–451.

[17] Musso, G., Romero, E., Gens, A., Castellanos, E., 2003. The role of structure in the chemically induced deformations of FEBEX bentonite. Applied Clay Science 23 (1–4), 229–237.

[18] Ng, C. and Pang, Y. (2000). Influence of stress state on soil-water characteristics and slope stability. Journal of Geotechnical and Geoenvironmental Engineering, 126(2):157–166. 4.1

[19] Nowamooz, H., Masrouri, F., 2009. Density-dependent hydromechanical behaviour of a compacted expansive soil. Eng. Geol. 106, 105–115.

[20] Nuth, M. & Laloui, L. (2008). Advances in modelling hysteretic water retention curve in deformable soils. Comput. Geotech. 35, No. 6, 835–844.

[21] Rahardjo, H., Heng, O. B., and Leong, E. C. _2004_. “Shear strength of a compacted residual soil from consolidated drained and the constant water content triaxial tests.” Can. Geotech. J. 41, 1–16.

[22] Rao, S.M., Shivananda, P., 2005. Role of osmotic suction in swelling of salt-amended clays. Canadian Geotechnical Journal 42(1), 307–315.

[23] Romero, E. (1999). Thermo-hydro-mechanical behaviour of unsaturated Boom clay: an experimental study. PhD thesis, Universidad Politècnica de Catalunya, Barcelona, Spain.

[24] Romero E. A microstructural insight into compacted clayey soils and their hydraulic properties. Engineering Geology 2013; 165:3–19.

[25] Romero E, Della Vecchia G, Jommi C. An insight into the water retention properties of compacted clayey soils. Geotechnique 2011; 61(4):313–328.

[26] Satija, B. S. _1978_. “Shear behaviour of partly saturated soil.” PhD thesis, Indian Institute of Technology, Delhi, India.

[27] Sharma, R. S. (1998). Mechanical behaviour of unsaturated highly expansive clays. PhD Thesis, Oxford University.

[28] Siddiqua, S., Blatz, J., Slemens, G., 2011. Evaluation of the impact of pore fluid chemistry on the hyromechanical behaviour of clay-based sealing material. Canadian Geotechnical Journal 48, 199–213.

[29] Sivakumar, V. _1993_. “A critical state framework for unsaturated soil.” PhD thesis, Univ. of Sheffield, Sheffield, U.K.

[30] Sivakumar, V., Tan, W.C., Murray, E.J., McKinley, J.D., 2006. Wetting, drying and compression characteristics of compacted clay. Geotechnique 56 (1), 57–62

[31] Tarantino A, De Col E. Compaction behaviour of clay. Geotechnique 2008; 58(3):199–213.

[32] Thu, T. M., Rahardjo, H., and Leong, E. C. 2006b. Shear strength and pore-water pressure characteristics during constant water content triaxial tests, Journal of Geotechnical and Geoenvironmental Engineering, ASCE, Vol. 132, No. 3, pp. 411–419.

[33] Vanapalli, S., Fredlund, D., and Pufahl, D. (1999). The influence of soil structure and stress history on the soil-water characteristics of a compacted till. Gèotechnique, 49(2):143–159. 4.1, 5.1

[34] Wheeler, S.J., Sharma, R.S., Buisson, M.S.R., 2003. Coupling of hydraulic hysteresis and stress–strain behaviour in unsaturated soils. Geotechnique 53 (1), 41–54.

[35] Wheeler, S. and Sivakumar, V. (1995). An elasto-plastic critical state framework for unsaturated soil. Gèotechnique, 45:35–53. 5.1

7

SUMMARY AND FUTURE PROSPECTIVES

In the present research, the coupled hydromechanical behaviour of a silt, typically used in the construction of dykes, with the aim of providing a better understanding of the consequences of wetting-drying cycles in the field on the overall response of the material. The results showed that the hydraulic repeated loads changed the soil fabric, resulting in fundamental changes in their hydromechanical response. Repeated hydraulic loads were applied to the as-compacted soil samples using different procedures: 1) changing suction acting on soil samples, and 2) wetting and drying the sample (controlling the water content).

The first series of tests involved wetting-drying and loading-unloading stress paths applied in suction-controlled oedometer. Irreversible changes in the degree of saturation implied that hysteresis of water retention is induced by changes in the suction and volume of soil samples. The nonlinearity and irreversibility of the soil behaviour in an unsaturated state are more evident which may result from the contribution of two fluids in response to mechanical and hydraulic loading. In the present work, the mechanical model was developed under the hypoplastic framework incorporating the hydraulic state of the soil by means of employing average soil skeleton stress and new compression law, and also introducing a new mechanism accounting for coupling between hydraulic and mechanical model. On the other hand, a new water retention curve model was proposed accounting for the mechanical effect on the water retention behaviour and also hysteresis

induced by both loading-unloading and wetting-drying cycles, in which the contact angle was used to express the dependence of the response on non-monotonic changes in suction and void ratio. The proposed constitutive hypo-plastic model was then coupled with the contact angle-WRC model to account for the coupling between the hydraulic and the mechanical behaviours. The proposed coupled hydromechanical hypoplastic model was then validated comparing the predictions of the model and experimental behaviour of Viadana silt. The model was able to capture the effect of hydraulic state on the compressibility of the soil upon loading as well as the effect of changing void ratio on the water retention behaviour. The proposed framework is open to improve by introducing a different mechanical and hydraulic functions accounting for the hysteresis of WRC which can be obtained by geomechanical and geometrical features of soil-liquid interface relationships. In addition, the formulation of the mechanical model was limited to the isotropic stress states and, therefore, an extension for the three-dimensional case is needed. They can also be adopted for practical engineering purposes provided their efficient implementation in finite element codes.

The second series of experimental tests was performed to study the impact of wetting-drying cycles on microstructural features and hydraulic properties of as-compacted samples. The water retention behaviour of the as-compacted sample was detected for drying and wetting path, and it was then compared to those obtained for the as-compacted samples subjected to 3 and 6 drying-wetting cycles. The samples subjected to drying-wetting cycles exhibited mainly the same water retention behaviour but different from the as-compacted one. It was observed that both main drying and main wetting water retention curves of the as-compacted sample shifted toward lower values of water content after being subjected to cycles of drying-wetting, although all wetting and drying curves were converged to the same value of water ratio at the suction level higher than 10 MPa. The repeated hydraulic loads developed larger pores in the pore network of the as-compacted sample. It is worth noting that no significant overall volumetric strain changes in the as-compacted sample were detected after being subjected to drying-wetting cycles, implying that the fabric changes took place due to the interaction between different pore modes. The new water retention curve model was then proposed accounting for different pore modes identified with reference to the pore size distribution of the tested material. The proposed model allows evolving pore size distribution, in which different analytical formulation can be employed to reproduce the water retention behaviour of different pore modes regarding their corresponding pore size density (PSD) functions. Although the parameters of the model and their calibration for in situ compacted soils, whose physical properties and the previous history may not be known, could become difficult. An effort is needed to try to provide clear indications of the possible range of the parameters for different soils and define a relationship between the parameters of the model and characteristic properties of the material. The task

may be pursued by trying to verify the model capabilities against experimental data from different compacted soils.

Finally, the hydromechanical behaviour of such samples was studied when subjected to shear loading under constant water content condition. The results showed that the strength of the material increased slightly associated with more softening and dilation. Since samples subjected to repeated hydraulic loads experienced more volumetric contraction during compression, they were slightly denser than the as-compacted one at the beginning of shear loading. Moreover, they followed their corresponding water retention curves, where they expelled more water than the as-compacted one, particularly during the suction equalisation phase. Therefore, the water content of such samples was lower and suction measured during the shearing phase remained at higher levels than the one of the as-compacted samples. The resulting increase in strength may be justified due to having lower void ratio and water content at the beginning of the shearing phase and the increase in softening and dilation may result from higher suction acting on these samples during the shearing phase. A better understanding of the evolution of the yield surface, shear strength and volumetric responses of soil subjected to repeated hydraulic loads may be provided by performing supplementary triaxial tests in which such samples subjected to different stress paths, such as shearing followed by wetting at constant deviatoric stress, loading at constant stress ratio and etc.

“Science never solves a problem without creating ten more.”

George Bernard Shaw